From recognition to reaction: Mechanistic analysis of the interactions of the HECT ligase E6AP with ubiquitin

Von der Erkennung bis zur Reaktion: Mechanistische Analyse der Wechselwirkungen der HECT-Ligase E6AP mit Ubiquitin

Doctoral Thesis

for a doctoral degree at the Graduate School of Life Sciences,
Julius-Maximilians-Universität Würzburg,
Section Biomedicine

submitted by

Lena Kerstin Ries

from Aschaffenburg, Germany

Würzburg 2019

Submitted on: ……
(office stamp)

Members of the *Promotionskomitee*:

Chairperson:	Prof. Dr. Utz Fischer
Primary Supervisor:	Dr. Sonja Lorenz
Supervisor (Second):	Prof. Dr. Franz Xaver Schmid
Supervisor (Third):	Prof. Dr. Hermann Schindelin
Supervisor (Fourth):	Prof. Dr. Martin Eilers

Date of Public Defense: ……

Date of Receipt of Certificates: ……

„The greatest glory in living
lies not in never falling,
but in rising every time we fall. “

(Nelson Mandela)

Table of Contents

Table of Contents

Summary

The ubiquitination of proteins controls a multitude of physiological processes. This versatility of ubiquitin as a molecular signal arises from the diverse ways by which it can be attached to target proteins. Different ubiquitination patterns are then translated into different downstream consequences. Due to the enormous complexity of possible ubiquitin modifications, the ubiquitination machinery must be highly specific and tightly controlled. Ubiquitination proceeds through an enzymatic cascade, the last step of which is catalyzed by the E3 enzyme family. E3 enzymes are the crucial regulators since they dictate the specificity of substrate selection and modification.

Deregulation of the HECT-type ubiquitin ligase E6AP (UBE3A) is implicated in human papilloma virus-induced cervical tumorigenesis and several neurodevelopmental disorders. Yet the structural underpinnings of activity, regulation and specificity in this crucial ligase are incompletely understood.

One aim of this study was to unravel the role of the α1'-helix N-terminal to the HECT domain that was found to be a key element mediating regulation and oligomerization in other HECT ligases. I found that most N-terminally extended HECT domain constructs were insoluble when expressed in *E. coli*, indicating that additional regions N-terminal to the tested fragments may be essential to protect this highly hydrophobic helix from causing aggregation.

Another question addressed in this study was how E6AP builds ubiquitin chains. Using single-turnover experiments, I showed that ubiquitin-loaded E6AP is unable to transfer an additional ubiquitin molecule onto a stably linked ubiquitin-E6AP complex. This indicates that E6AP cannot assemble chains on its active site and may instead follow a sequential addition mechanism in which one ubiquitin molecule is transferred at a time to the target protein.

Using NMR spectroscopy and extensive mutational analyses, the determinants of ubiquitin recognition by the C-lobe of E6AP were unraveled and assigned to particular steps in the catalytic cycle. A functionally critical interface was identified that is specifically required during thioester formation between the C-terminus of ubiquitin and the ligase active site. This interface resembles the one utilized by NEDD4-type enzymes, suggesting a conserved ubiquitin binding mode across HECT ligases, independent of their linkage specificities. Moreover, I identified critical surface patches on ubiquitin and in the N- and C-terminal portions of the catalytic domain of E6AP that are important for the subsequent step of isopeptide bond formation. I also uncovered key determinants of the Lys48-linkage specificity of E6AP, both in the E6AP HECT domain and ubiquitin itself. This includes the C-terminal tail of E6AP and a hydrophilic surface region of ubiquitin in proximity to the acceptor site, Lys48.

It is thus tempting to speculate that ubiquitin linkage formation by E6AP is substrate-assisted. Taken together, my results improve our mechanistic understanding of the structure-function relationship between E6AP and ubiquitin, thus providing a basis for ultimately manipulating the functions of this HECT ligase for therapeutic applications.

Zusammenfassung

Die Ubiquitinierung von Proteinen ist an nahezu jedem physiologischen Prozess beteiligt. Die Vielseitigkeit mit der Ubiquitin als molekulares Signal fungiert, rührt von den vielfältigen Möglichkeiten her, wie es an Zielproteine gebunden werden kann. Verschiedene Ubiquitinierungsmuster rufen unterschiedliche biologische Ereignisse hervor. Angesichts der enormen Komplexität möglicher Ubiquitinierungsmodifikationen muss die Ubiquitinierungsmaschinerie hochspezifisch und streng kontrolliert sein. Die Ubiquitinierung erfolgt über eine enzymatische Kaskade. Der letzte Schritt wird hierbei durch die Enzymfamilie der Ubiquitin-Ligasen katalysiert. Ubiquitin-Ligasen sind primär für die Spezifität in Substraterkennung und Ubiquitin-Kettenbildung verantwortlich.

Misregulation der HECT-Ligase E6AP fördert die durch humane Papillomaviren induzierte Tumorentwicklung im Gebärmutterhals und ist mit zwei schweren neurologischen Krankheiten verbunden. Strukturelle Einzelheiten über den Mechanismus, die Regulation und die Spezifität dieser wichtigen Ligase sind jedoch weitgehend unbekannt.

Für verschiedene HECT-Ligasen wurde gezeigt, dass die α1'-Helix N-terminal zur HECT-Domäne ein Schlüsselelement für die Regulation und den Oligomerisierungszustand der Enzyme darstellt. In dieser Arbeit konnte gezeigt werden, dass die Helix eine wichtige Funktion für die Stabilität von E6AP erfüllt. Der Großteil N-terminal verlängerter, in *E. coli* exprimierter HECT-Domänen-Konstrukte war unlöslich, was darauf hindeutet, dass N-terminal gelegene Regionen hydrophobe Bereiche des Proteins vor Aggregation schützen.

Eine weitere Fragestellung dieser Arbeit befasste sich mit dem Mechanismus der Ubiquitin-Kettenbildung durch E6AP. Mit '*single-turnover*'-Experimenten konnte gezeigt werden, dass ein über einen Thioester gebundenes Ubiquitin von E6AP nicht auf einen stabil verknüpften Ubiquitin-E6AP-Komplex übertragen werden kann. Dies deutet daraufhin, dass E6AP keine Ketten auf dem katalytischen Cystein aufbauen kann und stattdessen einem sequentiellen Additionsmechanismus der Ubiquitin-Kettenbildung folgt.

Mithilfe von NMR Spektroskopie und umfangreicher Mutagenese-Studien wurde eine Interaktion zwischen dem C-Lobe von E6AP und Ubiquitin gefunden, die während der Thioesterbildung zwischen dem C-Terminus von Ubiquitin und dem aktiven Zentrum von E6AP gebraucht wird. Diese Interaktionsfläche ähnelt derer der NEDD4-Familie, was auf einen konservierten Bindungsmodus der HECT-Ligasen an Ubiquitin im ersten Reaktionsschritt hindeutet, ungeachtet der jeweiligen Kettenspezifitäten. Verschiedene Oberflächen auf Ubiquitin und E6AP, sowohl auf dem C-Lobe als auch auf dem N-Lobe, konnten identifiziert werden, die für die Bildung einer Isopeptidbindung zwischen zwei

Ubiquitin-Molekülen von Bedeutung sind. Neben dem C-Terminus von E6AP wurde eine hydrophile Oberfläche auf Ubiquitin in unmittelbarer Nähe zum Akzeptor Lys48 gefunden, die wichtig für die Lys48-spezifische Ubiquitin-Kettenbildung ist. Der Gedanke liegt nahe, dass die Ubiquitin-Kettenbildung durch E6AP über Substratunterstützte Katalyse verläuft.

Zusammenfassend erweitern diese Ergebnisse maßgeblich unser Verständnis der Erkennung von Ubiquitin durch die HECT-Ligase E6AP und können möglicherweise dazu beitragen Wirkstoffe zu entwickeln, welche eine Fehlregulierung von E6AP ausgleichen können.

1 Introduction

1.1 The ubiquitin conjugation system

"The ubiquitin system – basic biological platform on which so many cellular processes are arising, and then pathology and diseases, drug development. It's a whole world"

(taken from an interview with **Aaron Ciechanover**, Nobel Laureate in Chemistry for "the discovery of ubiquitin-mediated protein degradation" at the 57th Meeting of Nobel Laureates in Lindau, Germany, July 2007).

Ubiquitination, the posttranslational modification of target proteins with ubiquitin (Ub), plays an eminent role in physiology and diseases. It controls the lifetimes, conformational dynamics, as well as the localization and interaction patterns of eukaryotic proteins [112]. The extraordinary versatility of ubiquitin as a molecular signal originates from the many ways by which it can be attached to its targets. Proteins can be tagged with individual ubiquitin molecules or with polyubiquitin chains of variable length and topology **(Figure 1)**.

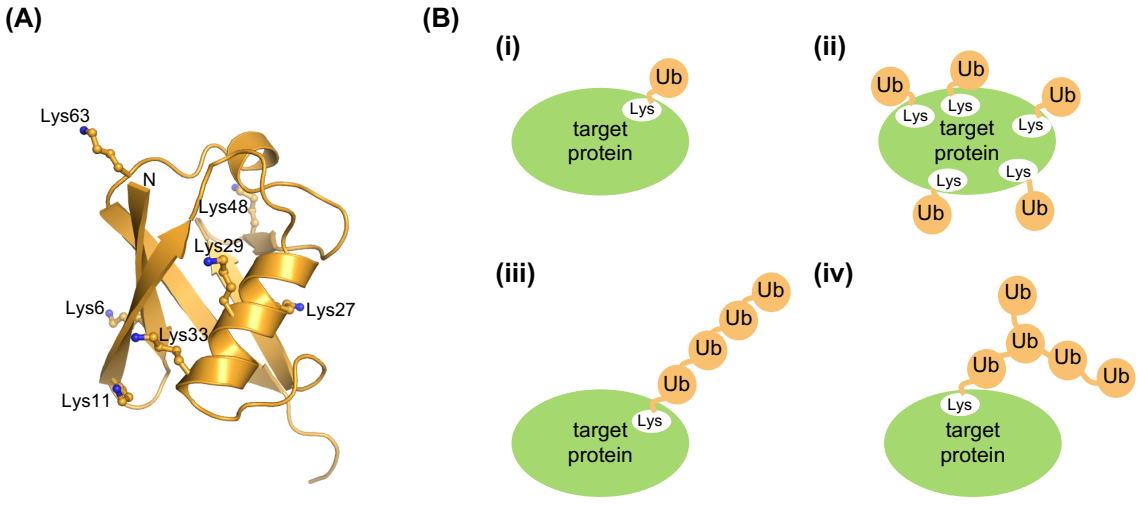

Figure 1: Different modes of ubiquitination. (A) Crystal structure of ubiquitin shown in ribbon representation (PDB ID: 1UBQ [221]). The lysine side chains (shown in balls and sticks) and the N-terminus represent potential linkage sites. **(B)** A single ubiquitin (Ub) molecule can be attached at one **(i)** or several sites **(ii)** of a target protein. In addition substrates can be modified with homotypic **(iii)** or branched **(iv)** ubiquitin chains.

Ubiquitin chains are composed of (iso)peptide-linked moieties, with the C-terminus of one ubiquitin molecule being bound to a primary amino group of the next molecule. Since ubiquitin has seven lysine residues and a free N-terminus, a total of eight different

(iso)peptide linkage types can be formed **(Figure 1A)**. Moreover, ubiquitin chains can contain more than one linkage type and/or branches **(Figure 1B)** [118]. Importantly, all of these types of ubiquitin modifications are found in the cell and are used as platforms for different protein-protein interactions, thereby eliciting distinct signaling functions [112]. It is thus critical that ubiquitination reactions occur in a highly specific and tightly controlled manner. However, the underlying mechanisms encoding the specificity of ubiquitination are incompletely understood. Lys48-linked ubiquitin chains are the best characterized and usually target proteins for proteasomal degradation [27], whereas mono-ubiquitination is involved in DNA repair [82] and chromatin remodeling [186]. Lys63-linked polyubiquitinated chains can direct substrates to the endocytotic pathway [76] or regulate NF-κB signaling [222].

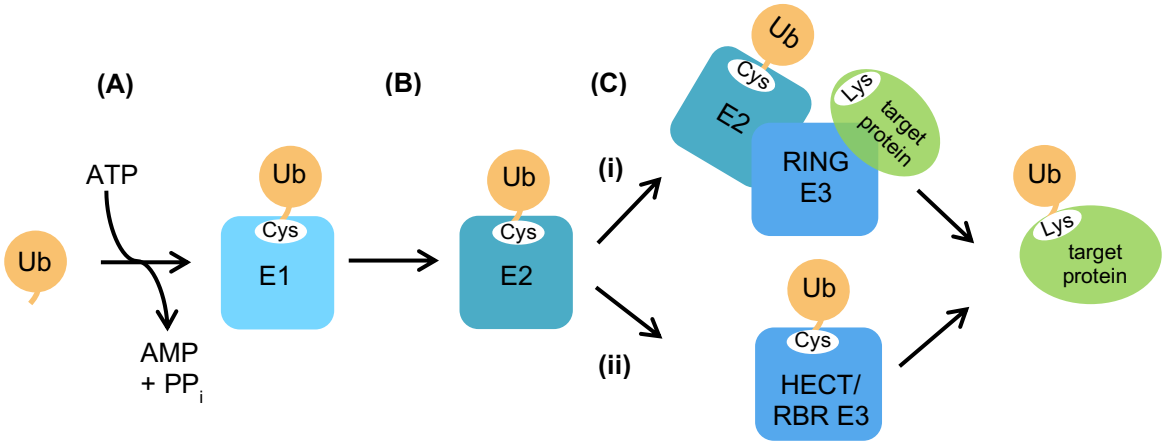

Figure 2: The ubiquitin conjugation system. Ubiquitination is accomplished through the sequential actions of ubiqutin-activating enzymes (E1), ubiquitin-conjugating enzymes (E2) and ubiquitin ligases (E3). **(A)** In the initial ATP-consuming step the E1 enzyme catalyzes the formation of a thioester between its catalytic cysteine and the C-terminus of ubiquitin. **(B)** Ubiquitin is then passed to the catalytic cysteine of the E2 enzyme. **(C)** Finally, the E3 facilitates the transfer of ubiquitin from the E2 to a substrate either directly (in case of Really Interesting New Gene (RING) ligases) **(i)** or through an E3-ubiquitin intermediate (in case of Homologous to E6AP C-Terminus (HECT) or RING-between-RING (RBR) ligases) **(ii)**.

Ubiquitination is carried out by an enzymatic cascade that involves three enzymes **(Figure 2)** [79]: a ubiquitin-activating enzyme (E1) that uses ATP to form a thioester bond between the C-terminus of ubiquitin and its active site cysteine residue; a ubiquitin-conjugating enzyme (E2) that also contains a catalytic cysteine and takes over ubiquitin from the E1 in a trans-thioesterification reaction; and, finally, a ubiquitin ligase (E3) that transfers ubiquitin from the E2 to a particular lysine residue on the target protein or on the second ubiquitin, thus forming ubiquitin chains [80, 176]. Ubiquitination of proteins is finely tuned through an interplay of ubiquitinating and deubiquitinating activities (encoded by deubiquitinases (DUBs)), while the liberated ubiquitin is recycled [236].

The human genome encodes two E1 enzymes [34, 77, 96, 171], approximately 40 E2 enzymes [152] and more than 600 putative E3 enzymes. E3 enzymes are thus the most

diverse group among the classes of ubiquitination enzymes [128] and account for the specificity in target protein selection and, in many cases, the specificity in ubiquitin linkage formation. Hence, E3 enzymes determine the fates of thousands of substrates. Consistently, the deregulation of E3 enzymes is tightly linked to many pathologies, such as cancer, autoimmune diseases, and neurodegenerative disorders [68, 200]. It is, therefore, not surprising that E3 enzymes are considered prime targets for drug discovery. Yet key steps in their catalytic actions and the molecular determinants of their specificity have remained elusive.

Components of the ubiquitination cascade have emerged as targets in the treatment of human diseases [30, 86]. The potential of exploiting the ubiquitin system for therapeutic use has been demonstrated by the outstanding clinical effectiveness of the proteasome inhibitor Bortezomib (tradename: Velcade) in the treatment of multiple myeloma [1]. While Bortezomib acts at the very bottom of the ubiquitination cascade and shuts down protein degradation globally, drugs targeting E3 enzymes are expected to have much higher specificity and, therefore, smaller side effects.

1.2 HECT ligases

1.2.1 Domain organization

E3 enzymes are typically divided into three classes based on the E2-ubiquitin binding domain and the ubiquitin transfer mechanism: E3 enzymes of the RING (Really Interesting New Gene)-type represent the largest subfamily. They act as scaffolds that bring together ubiquitin-loaded E2 enzymes and their target proteins simultaneously. Some facilitate the direct transfer of ubiquitin from the E2 enzyme to the target through the stabilization of a particular 'closed' orientation of ubiquitin with respect to the E2 enzyme [48, 52, 178, 180, 210].

In contrast, HECT (Homologous to E6AP C-Terminus)-type ligases follow a two-step mechanism [87, 201]. Like E2 enzymes, HECT-type ligases contain a catalytic cysteine residue and form a thioester-linked intermediate with ubiquitin (donated by the E2 enzyme) before passing it on to the target. Finally, the RING-between-RING (RBR) class of E3 enzymes have both RING-like and HECT-like features [232]. They also contain a catalytic cysteine residue to form a thioester-linked intermediate with ubiquitin prior to target ubiquitination, but they utilize a canonical RING domain to recruit the E2-ubiquitin intermediate [231].

Subject of this thesis is the class of HECT-type ligases, key players in an array of biological processes and thus not surprisingly associated with diseases such as cancers, neurological disorders and autoimmunity [191, 200]. They encode specificity for ubiquitination reactions as they recruit specific target proteins and determine the type of ubiquitin chains to be formed. Key steps in their catalytic actions and the molecular determinants of their specificities in ubiquitin linkage formation have remained elusive.

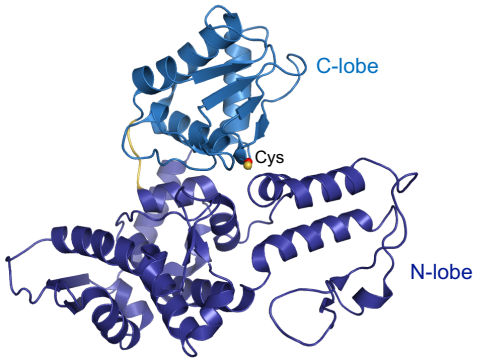

Figure 3: Architecture of the catalytic HECT domain. The crystal structure of the catalytic HECT domain of WWP1 is displayed in ribbon representation, revealing a bilobal organization; both lobes are connected by a short linker (yellow). The active site cysteine residue is shown in ball-and-stick mode. (PDB ID: 1ND7 [220]).

The human genome encodes 28 HECT ligases varying in length between 700 and 4800 amino acids. HECT E3 enzymes share a conserved catalytic HECT domain (~40 kDa) of two-lobe structure invariably positioned at the C-terminus **(Figure 3)** [85]. The N-terminal lobe (N-lobe) interacts with E2 enzymes [57, 85, 99, 188] and, at least in some cases, with a regulatory ubiquitin molecule [8, 66, 67, 108, 143, 144, 167, 250] (see **1.2.5**); the smaller C-terminal lobe (C-lobe) bears the catalytic cysteine and interacts both with the donor and the acceptor during the catalytic cycle [85, 94, 98, 99, 107, 144, 188]. The two lobes are connected by a short hinge region. Flexibility around this hinge and thereby conformational rearrangements of the lobes with respect to each other was found to be important for target ubiquitination [220]. Substrate binding, localization in the cell and regulation are primarily determined by the extended regions located next to the catalytic HECT domain. Based on the type of domains predicted in this region, HECT ligases have been grouped into three subfamilies **(Figure 4)**: the HERC family, the NEDD4 family and HECTs with diverse protein-protein interaction domains.

The HERC family members contain one or more regulator of chromosome condensation 1 (RCC1)-like domains (RLDs), which act as guanine nucleotide-exchange factor (GEF) for the GTPase Ran and interact with chromatin through histones H2A and H2AB. This family is further subdivided into small HERCs (~100 kDa) containing a single RLD and large HERCs (>500 kDa) with multiple RLDs and additional domains, such as SPRY and WD40 [72].

The NEDD4 family is characterized by a unique domain architecture encompassing an N-terminal, Ca^{2+}-dependent phospholipid-binding C2 domain for regulation of cellular localization and two to four WW domains, which bind to short proline-rich (PY) motifs in substrates [91]. NEDD4-type ligases are involved in the regulation of transcription, neuronal development, immune response and trafficking [13].

The remaining 13 HECT proteins contain diverse domains, such as ubiquitin-associated (UBA) domain, mademoiselle (MLLE or poly(A)-binding protein C-terminus (PABC)) domains, ankyrin repeats (AR), zinc fingers, and others. However, only a small portion of the N-terminal region comprises structurally defined domains and/or motifs, the remainder is made up of extended regions of predicted disorders and low sequence complexity. The functional properties of the N-terminal regions – likely evolved as interaction platforms for the assembly of signaling complexes [132] – remain largely unclear.

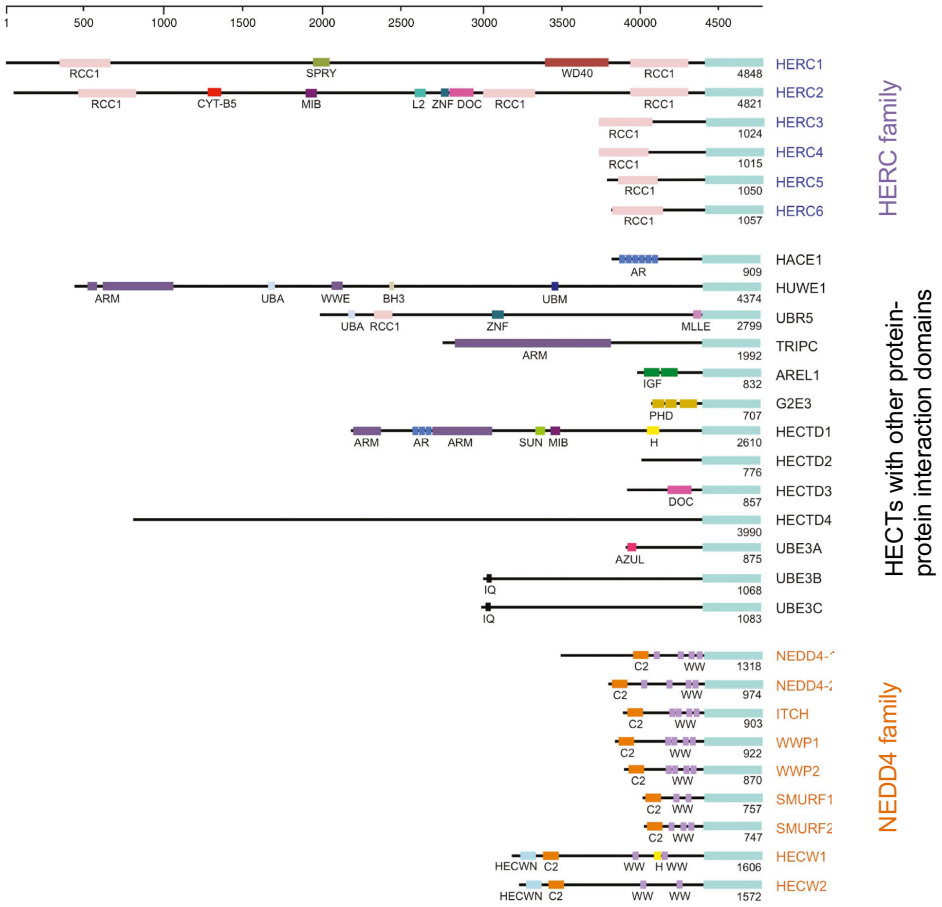

Figure 4: Domain organization of the 28 human HECT-type ligases. Shown here is an overview of the domain architecture of HECT ligases taken from the review "Structural Mechanisms of HECT-Type Ubiquitin Ligases" by S. Lorenz [132]. The top scale depicts approximate domain sizes and the localization within the respective full-length protein with the total number of amino acids being provided below. The catalytic HECT domain is located in all cases at the C-terminus of the protein. Substrate binding, localization in the cell and regulation is mediated by domains or motifs N-terminal to the HECT domain. Based on these motifs, HECT ligases are subdivided into the HERC subfamily (top section), "other HECTs" (middle section) and the NEDD4 family (on the bottom).

1.2.2 Catalytic mechanism

The conserved HECT domain was shown to be necessary and sufficient for ligase activity. Ubiquitination by HECT ligases occurs through a two-step reaction; it involves the formation of an isopeptide bond between the C-terminus of one ubiquitin molecule that is thioester-linked to the catalytic cysteine of the ligase, known as the 'donor', and the ε-amino group of a lysine residue on either another ubiquitin molecule, known as the 'acceptor', or on a substrate. The basic steps in the catalytic cycle of HECT-type ligases are shown in **Figure 5**. After recruiting a ubiquitin-loaded E2 enzyme **(Figure 5B)**, the HECT C-lobe engages in a thioester linkage between its catalytic cysteine and the C-terminus of the donor ubiquitin **(Figure 5C)**. Subsequently, the activated carbonyl function of the donor is attacked in a nucleophilic substitution reaction by the primary amino group of a lysine residue of the

acceptor ubiquitin **(Figure 5D)** or a target protein **(Figure 5E)**, giving rise to an isopeptide linkage. For the reaction to be linkage specific, the C-lobe needs to orient the acceptor ubiquitin or the substrate in a specific manner with respect to the donor, such that one particular lysine residue (out of eight potential primary amino groups of ubiquitin and probably even more of a respective substrate) points to the active site [107]. This orientation holds the key to specificity in linkage formation and associated signaling responses. Yet, how this mechanism is structurally implemented in HECT ligases is not entirely clear. The specificity of substrate recognition is achieved by the HECT E3 enzyme through direct interactions with the substrate via its N-terminally located target binding regions (as discussed later, **1.2.3**).

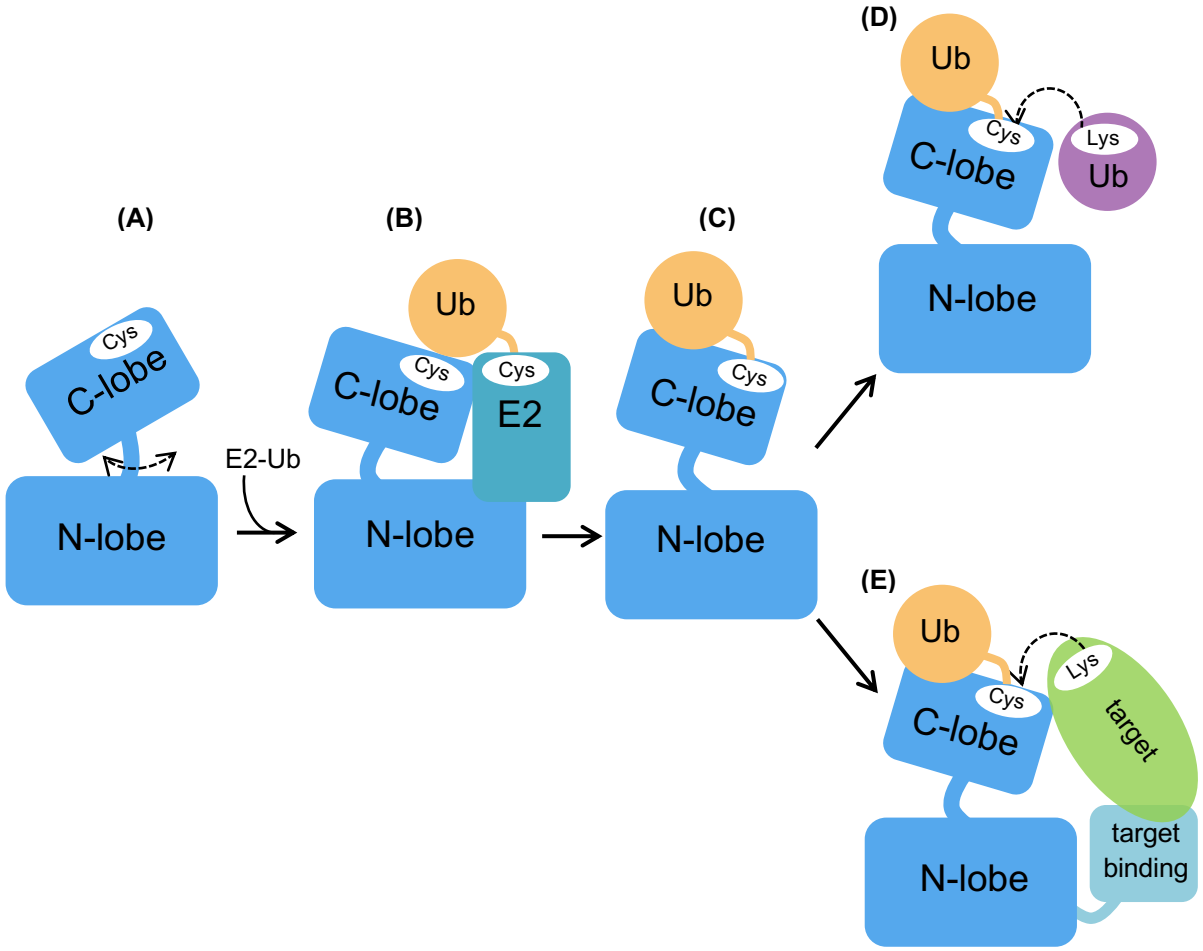

Figure 5: Schematic of the basic steps in ubiquitin chain formation by HECT ligases. (A) Shown here is the HECT domain (blue) in the apo state in which the N-lobe and C-lobe are flexible to each other. **(B)** After trans-thioesterification with the E2 (cyan)-ubiquitin (orange) complex, **(C)** the catalytic cysteine residue on the C-lobe of the HECT E3 enzyme is loaded with ubiquitin. Subsequently, a lysine on a second ubiquitin (acceptor, purple) **(D)** or a lysine on a substrate (green) **(E)** attacks the C-terminal carbonyl group of the donor to form an isopeptide-linked di-ubiquitin or – through iterations of this process – ubiquitin chains. Step **(D)** determines linkage specificity, yet no structural information is available on how HECT ligases interact with acceptor ubiquitin.

Several crystal structures of the HECT domain in the *apo* state or in complex with the E2 enzyme and/or ubiquitin show fundamental variations in the relative orientation of both lobes

with respect to each other **(Figure 6)** [134]. Conformational rearrangements of both lobes are likely required to juxtapose the actives sites of the E2 and the E3 enzymes to allow for the trans-thioesterification reaction. They might also be needed to search for accessible lysine residues on the target protein and to orient ubiquitin moieties for ubiquitin chain formation, thus enabling specificity [98, 144]. However, a structural rationale for this phenomenon and a detailed understanding of how these rearrangements are involved in ubiquitin chain formation by HECT ligases are lacking.

In a crystal structure of the HECT domain of E6AP bound to the E2 UBE2L3 the active site cysteine residues of the E2 and the E3 enzyme are separated by 41 Å **(Figure 6A)** [85]. The two lobes were found to adopt an L-shaped conformation. The interaction with the E2 enzyme is established through the N-lobe. It involves the L1 and L2 loops and the N-terminal α1-helix of the E2 enzyme which binds to a concave hydrophobic groove on the N-lobe subdomain [85]. The primary contact involves a phenylalanine residue (Phe63 for UBE2L3; conserved among members of the HECT-specific E2 subfamily) in the L1 loop. This residue is buried in the center of the hydrophobic groove. Also, a region encompassing the active site cysteine is an essential determinant for the interaction with the HECT domain [85]. The hydrophobic residues that line the E2-binding groove on the HECT domain are only moderately conserved in HECT ligases. The dissociation constants of the E2-E3 complexes are in the micromolar range *in vitro* [56, 57], but in the cell the interaction might be stronger, mediated by co-localization or by adaptor proteins. The presence of ubiquitin bound to UBE2D2 was also shown to strengthen the binding to E6AP [156], yet, this could not be observed for UBE2L3 [181]. The identification of combinatorial preferences of E2-HECT E3 pairs has proven challenging in the cellular context. So far, only few physiological pairs could be defined [5, 44, 119, 239]. Further studies are required to elucidate the structural underpinnings of how specific E2 enzymes interact with specific E3 enzymes.

The transition from the L-shaped arrangement to a T-shaped state was shown to reduce the distance between the active site cysteine residues of the E2 and the E3 enzymes **(Figure 6B, C)** [99, 220], indicating that a major structural reorganization occurs upon trans-thioesterifcation. In the absence of ubiquitin, the orientation of the N- and C-lobe is not fixed, and both can rather freely rotate relative to each other. It could be that the L- and T-shaped conformations represent the endpoints along a dynamic pathway involving the rotation of both lobes to allow the C-lobe to participate in distinct phases of ubiquitin transfer, in chain formation and in the subsequent transfer of ubiquitin to target proteins.

To position the donor ubiquitin on the HECT C-lobe, further rotation about the hinge must be involved to bring the two catalytic cysteine residues into a position that allows for the

formation of the HECT E3~ubiquitin ('~' denotes a thioester bond) intermediate. A crystal structure of NEDD4L in complex with UBE2D2~ubiquitin reveals interactions between individual components of the E2~ubiquitin intermediate with both lobes of the E3 enzyme, and they were shown to be important for ubiquitin transfer **(Figure 6C)** [99]. In this structure, ubiquitin is sandwiched between the catalytic centers of the E2 enzyme and the HECT domain of the E3 enzyme. Hydrophobic interactions between the C-lobe and ubiquitin bring the C-lobe into proximity of the E2 enzyme and thus facilitate the trans-thioesterification [99]. These hydrophobic residues are conserved for NEDD4 family members, but, only for a few other HECT ligases indicating that alternative modes must also exist for engaging the encountering ubiquitin in the complex with the E2 enzyme.

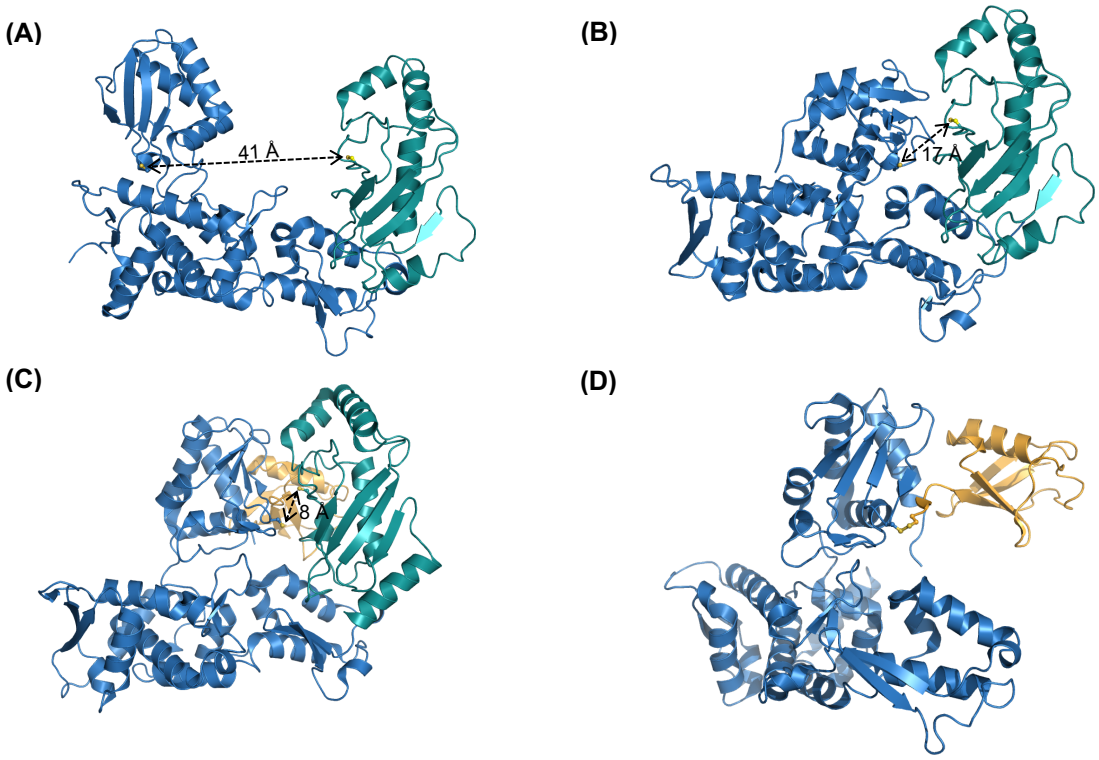

Figure 6: Crystal structures of different states during the catalytic mechanism of HECT ligases. Ribbon representation of **(A)** the L-shaped conformation of the HECT domain of E6AP in complex with UBE2L3 (PDB ID: 1C4Z [85]); **(B)** the T-shaped conformation of WWP1 (PDB ID: 1ND7 [220]) with modelled UBE2L3 according to the E6AP HECT domain-UBE2L3 structure (PDB ID: 1C4Z [85]); **(C)** Pre-trans-thioesterification state of the HECT domain of NEDD4L in complex with UBE2D2 C85S linked to ubiquitin via a stable oxyester (PDB ID: 3JVZ [99]); **(D)** Trans-thioesterification state of the HECT domain of NEDD4 linked via a disulfide bridge to donor ubiquitin (PDB ID: 4BBN [144]). The HECT domain is shown in blue, the E2 enzyme in cyan, donor ubiquitin in orange. The active site cysteine residue is displayed as balls and sticks.

The replacement of the labile thioester bond between the donor ubiquitin and the HECT domain by a stable oxyester or disulfide-bridge enabled several groups to solve crystal structures that reveal how the donor ubiquitin might be position in the absence of the E2 on the HECT C-lobe of NEDD4-type enzymes **(Figure 6D)** [94, 98, 99, 144]. These studies

illustrated a conserved hydrophobic interface between Ile36, Leu71 and Leu73 of ubiquitin and the C-lobe. The C-terminus of ubiquitin adopts an extended conformation, which was shown to prime ubiquitin for catalysis [99, 144]. Although recent structural studies have shown that HUWE1, whose HECT domain is closely related to the NEDD4-type subfamily, use a common binding mode for the donor ubiquitin [94], it is unknown whether this mode is conserved across evolutionarily more distant members of the HECT family.

Attempts to characterize the structure of a HECT domain with ubiquitin located in an acceptor position facing the active site have been unsuccessful so far. Biochemical studies indicate that linkage specificity is independent of the HECT N-lobe or the cooperating E2 enzyme. It seems to be governed exclusively by the last 60 amino acids of the C-lobe of HECT E3 enzymes [107]. This suggests that the last three β-strands, the active-site loop and terminal α-helix of the C-lobe have to interact in an unknown fashion with the acceptor ubiquitin. A major challenge in unraveling how the C-lobes of HECT ligases recognize their ubiquitin substrates lies in the fact that functionally critical interactions are rather weak and might thus have escaped experimental detection [67, 99, 107, 146].

The mechanism by which the attacking primary amino group of the acceptor lysine becomes deprotonated is also still largely unclear. The chemical environment of individual lysine residues might play a role to stimulate isopeptide bond formation. Several properties of the C-lobe were suggested to be important. For NEDD4, the negatively charged side chain of Asp900 was proposed to approach the active site during catalysis and thus be crucial for lysine deprotonation and the subsequent ligation reaction [144]. In addition, a conserved histidine residue, two residues away from the catalytic cysteine, might impact the chemical environment at the active site and thereby facilitates the deprotonation of the attacking primary amino group of the acceptor [98, 99].

For RSP5 and WWP1, the C-terminal region was proposed to be involved in the formation of isopeptide bonds [98, 220]. In this region, a conserved phenylalanine residue four amino acids from the C-terminus (-4 Phe) was also reported to be a key requirement for substrate ubiquitination and polyubiquitin chain formation [190, 197]. Maspero and colleagues showed that the last four residues determine ubiquitin chain type specificity in NEDD4 [144]. While the -4 Phe residue is not resolved in most crystal structures of HECT domains, it was found to contact the N-lobe in yeast RSP5 HECT ligase to anchor both lobes in an orientation that is productive for substrate ubiquitination [98]. The flexible tail around the -4 Phe might also stabilize the HECT~ubiquitin thioester intermediate by interacting with the extended C-terminal tail of the bound ubiquitin [94]. Still, understanding the role of the C-terminal tail requires further investigation.

Following ubiquitin ligation, the HECT domain must be reloaded with ubiquitin, requiring the C-lobe to rotate again to receive another ubiquitin molecule from the E2 enzyme and to start the next ubiquitination cycle. Major aspects of the highly dynamic process of ubiquitin chain formation still remain speculative and more structural and functional investigations are needed to arrive at a molecular understanding of ubiquitin chain formation by HECT ligases.

1.2.3 Substrate selection

It has been a long-standing question, how HECT ligases specifically recognize their target proteins and the correct sites for the modification with ubiquitin. Trapping physiological E3/substrate pairs remains challenging, since the affinities between the components are weak and many target proteins are rapidly degraded by the proteasome after ubiquitination [78]. An additional obstacle lies in the architecture of HECT ligases, where substrate specificity is determined by binding modules that are separated from the catalytic HECT domain by extended, presumably disordered regions.

Still, crosslinking studies indicate that HECT ligases orient target proteins in such a manner that the lysine residue to be ubiquitinated is close to the E3 active site [170]. Recently the crystal structure of a complex mimicking the catalytic intermediate of the HECT domain of RSP5 with ubiquitin and a substrate peptide was solved [98]. In this complex, donor ubiquitin G75C was crosslinked to the N-terminus of a peptide derived from the substrate SNA3. This structure provided first insights into how the correct acceptor lysine might be selected [98]. It revealed that the C-lobe of the HECT domain undergoes a 130° rotation about the flexible hinge region generating new inter-lobe contacts with the N-lobe primed for catalysis. The binding of the donor ubiquitin remains unaltered, yet the C-terminal tail with Arg74 is anchored to both lobes, thereby bringing critical N-lobe residues into the vicinity of the thioester linkage with the catalytic cysteine residue. In this arrangement the thioester would be optimally primed for the nucleophilic attack of the preferred substrate lysine residue. In this structure, the -4 Phe approaches the N-lobe, which points to a critical function of the tail/-4 Phe in the ligation reaction by anchoring the two lobes.

Another example for target protein selection is UBR5 which harbors a target-binding region, known as the MLLE (or PABC) domain located adjacent to the HECT domain. The MLLE domain mediates the interaction with a conserved sequence motif of PAIP2 [113]. However, it is unclear how the MLLE/substrate complex is oriented [159].

Modification of substrates may require a large degree of flexibility in the linkage between the HECT domain and the remainder of the protein in such a way that different surfaces of the substrate can be presented towards the active site. Several proteins have been identified as

substrates of HECT ligases [90, 124, 227]. The physiological relevance of most of these interactions is often unclear, in particular with respect to their role in the development of many human diseases. It will remain of major importance to elucidate the structural basis of how specific lysine residues of target proteins are selected for ubiquitination and to delineate the conformational changes of the HECT domain in the course of this process.

1.2.4 Mechanisms of ubiquitin chain formation

Once ubiquitin is primed in the HECT E3~ubiquitin thioester intermediate, the ligase may catalyze consecutive ubiquitin transfers resulting in polyubiquitin chains with a selective linkage. Yet the mechanism by which HECT E3 enzymes assemble polyubiquitin chains remains poorly understood. Several models for the mechanism of ubiquitin chain formation have been proposed [81]. One model posits that HECT ligases build ubiquitin chains by elongating chains at the *distal* ubiquitin of the growing chain in a sequential fashion, transferring one ubiquitin molecule at a time **(Figure 7A)** [107, 225]. An alternative model ('indexation' model) posits that ubiquitin chains are pre-assembled on the E3 active site and then transferred *en bloc* to the target in a single step **(Figure 7B)** [225]. Such a model may involve the successive transfer of ubiquitin from the E2 to the E3 catalytic cysteine. A more complicated mechanism may involve E2 or E3 oligomers, at least dimers, in which multiple chain transfer events occur between the E2 and the E3 to build a thioester-tethered chain ('seasaw'). Discriminating between these models has historically been difficult, due to the instability of the native thioester linkage between donor ubiquitin and E3 enzyme.

Initial data based on single-turnover pulse-chase assays with E6AP suggested that ubiquitin chains are built on the active site **(Figure 7B)** [224, 225]. More recently, two functionally distinct E2~ubiquitin binding sites have been reported. In this model, thioester formation was proposed to arise from binding of the E2~ubiquitin complex at a cryptic site on the HECT domain, whereas the canonical E2 binding site was proposed to be responsible for the subsequent ubiquitin chain elongation step [188, 190]. In this model both sites function in tandem to assemble ubiquitin chains from the *proximal* end prior to *en bloc* transfer of the chain to the substrate [188, 190].

At present, there is evidence for both mechanisms in NEDD4-type enzymes [66, 213, 214], and it is unclear how cellular factors, such as macromolecular complexes, influence chain formation mechanistically. A non-covalent ubiquitin-binding site, the 'exosite' on the N-lobe (see **1.2.5**), was shown to be required for processive chain elongation and was suggested to tether a growing ubiquitin chain to the E3 enzyme [66, 67, 108, 143, 167]. However, structural evidence of key catalytic intermediates in support of one or the other model are still lacking.

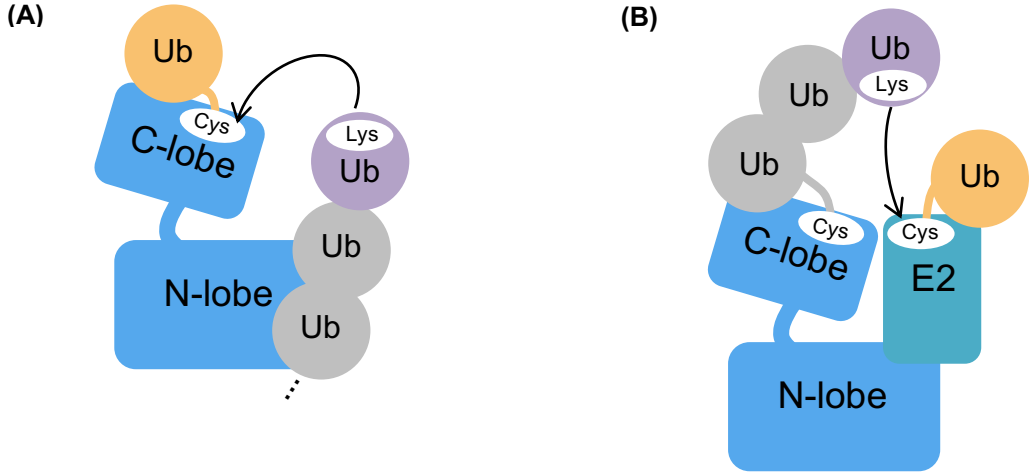

Figure 7: Models for ubiquitin chain formation by HECT ligases. (A) In the 'sequential' addition model a single ubiquitin is conjugated to a substrate protein, and the chain is elongated by conjugation of additional ubiquitin molecules to the growing end of the chain. **(B)** For the 'indexation' model a thioester-linked polyubiquitin chain is built on the E3 active site with ubiquitin being delivered by the E2 enzyme.

1.2.5 Regulation

A precise control of the activity of E3 enzymes is urgently required to ensure that their functions are restricted to the correct time and place. Insights regarding the mechanism of HECT E3 regulation are emerging. HECT ligases can catalyze their own ubiquitination, which might serve as a mechanism for autoregulation, and/or trigger degradation [21, 46, 164]. In addition, numerous mechanisms have been proposed for how HECT ligases can be regulated in a precise manner [208].

Mechanisms controlling the catalytic properties of HECT ligases involve macromolecular interactions of the HECT domain, binding of adaptors to domains in the N-terminal region, posttranslational modifications, as well as the recruitment of the respective E2 enzyme. The C2 or WW domains were shown to interact with the HECT domain of some NEDD4 family members and thus inhibit the catalytic activity of these enzymes [32, 60, 139, 158, 173, 185, 223, 235, 250, 253]. Also numerous post-translational modifications such as ubiquitination and/or phosphorylation were found to regulate the activity of NEDD4-type ligases [70, 130].

The E3 enzyme ITCH, for example, is negatively regulated through interactions of its catalytic domain with the preceding WW domain. Phosphorylation in the N-terminal part of ITCH triggers, conformational changes and relieve auto-ubiquitination [70]. In WWP2, a helical linker segment between the second and third WW domain (2,3-linker) was delineated as an additional tunable regulatory element of the NEDD4 family **(Figure 8A)** [32]. The interaction between the 2,3-linker and the HECT domain traps this ligase in an inactive state which can be relieved by phosphorylation of the linker [32]. In SMURF2, intramolecular interactions between the C2 domain and HECT domain were shown to exert an inhibitory effect by

restricting the flexibility of the C- and N-lobe with respect to each other [235]. The auto-inhibitory interaction can be released by binding to the adaptor protein SMAD7 which displaces the C2 domain. The N-terminal domain of SMAD7 was also reported to bind to both the HECT domain of SMURF2 and the E2 UBE2L3 [166]. By tethering both enzymes their ability to interact with each other would be enhanced and thus SMURF2 is activated.

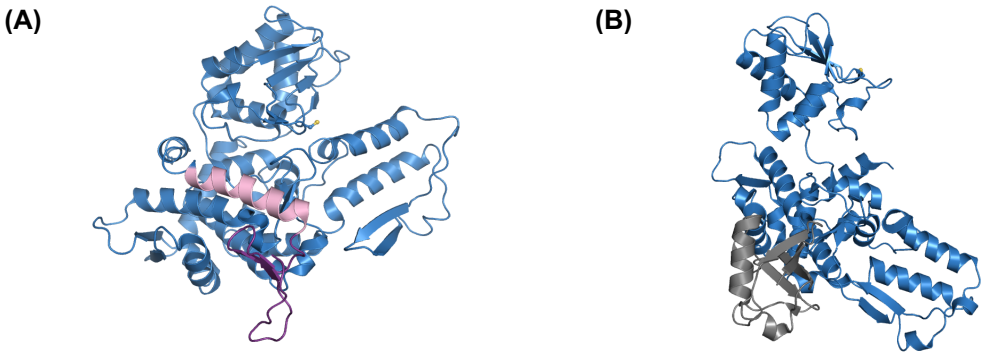

Figure 8: Regulatory mechanisms of HECT ligases. (A) 2,3-linker mediated auto-inhibition of WWP2 as seen in a crystal structure of a WW-2-(2,3-linker)-HECT fusion construct (PDB ID: 5TJ7 [32]). The 2,3-linker is depicted in light pink and the WW-2 domain in purple. **(B)** NEDD4 family members contain a ubiquitin (grey)-binding exosite on the N-lobe (PDB ID: 2XBB [108, 143]). The proteins are shown in ribbon representation (the HECT domain is shown in blue, the active site cysteine residue as balls and sticks).

In addition to intramolecular interactions, it was shown, that NEDD4-type ligases harbor a second, non-covalent ubiquitin-binding site, the so-called exosite, on their N-lobe [66, 67, 101, 110, 143, 167, 250], which enhances the processivity of ubiquitin chain elongation **(Figure 8B)**, possibly by stabilizing and orienting a growing ubiquitin chain. Polyubiquitin chain formation is impaired by the disruption of this interface [167], but the E2-E3 trans-thioesterification and the conjugation of the first ubiquitin to a target are not affected [108, 143]. Since the exosite-bound ubiquitin is removed from the E3~donor ubiquitin complex, it is unlikely that it reflects a donor or acceptor ubiquitin. But a precise function of the exosite needs further investigation.

A study with yeast RSP5 showed that the E3 activity could be modulated by the association with a ubiquitin-specific protease (USP) which reverses the ubiquitination reaction of the E3 enzyme [103]. The interplay between an E3 enzyme and a DUB has emerged as a common mechanism of modulating the activity of ubiquitin ligases [24].

Emerging evidence suggests that HECT ligases are regulated through changes in the oligomeric state. Attali and colleagues investigated functional implications of auto-ubiquitination-dependent oligomerization of RSP5 and found that the α1′-helix next to the HECT domain acts as a structural switch [8]. The activity of HUWE1 has recently been shown to underlie oligomerization driven control through a unique conformational switch between an active monomeric state and an auto-inhibited dimer [198]. A conserved segment in the N-

terminal region can counteract dimer formation *in cis*, thus holding the protein in an active state. Binding of p14ARF to this segment releases the dimerization region from its intramolecular engagement, thus promoting dimerization [198]. Oligomerization of E6AP has been reported to modulate the ligase activity and will be discussed in section **1.3.3**.

Besides all these different regulatory principles, a tight control of intracellular levels of HECT ligases contributes to the required specificity of the ubiquitin-conjugation system. Collectively, it will be of great importance to expand knowledge on how the activities of HECT ligases can be turned on and off in the cellular context by posttranslational modifications, intra- and intermolecular interactions or oligomerization.

1.2.6 Roles as therapeutic targets

The importance of HECT ligases in biological processes is emphasized by the fact that their genetic alteration, aberrant expression or dysfunction drives the development of many pathological diseases, including cancer, inflammation and neurodegenerative disorders [200]. Since HECT ligases have emerged as crucial regulators of disease-related proteins, they present promising, yet unexploited therapeutic targets.

Several NEDD4 family members affect key signaling pathways that regulate cellular growth and proliferation, with important implications for development and cancer. Besides its role in regulating T cell function [242], NEDD4 was shown to ubiquitinate and to degrade N- and C-MYC oncoproteins, as well as the tumor suppressor protein PTEN, emphasizing the role of NEDD4 in cancer development [131, 226]. *Itchy* mutant mice were shown to develop severe inflammatory diseases [172], whereas WWP1 gene amplification has been found to play a critical role in the progression of several tumors, including breast and prostate cancers [252]. Many of the identified SMURF substrates are involved in signaling pathways that participate in tumor progression or suppression [45]. Mutations of genes of HERC E3 subfamily members are also associated to a subset of human diseases, like tuberous sclerosis [35], the Prader-Willi syndrome and Angelman Syndrome (AS) [162]. HUWE1 has been implicated in many processes, like cell proliferation, apoptosis, DNA repair or neuronal differentiation and was shown to have pro-oncogenic and tumor-suppressor functions in different setups [3, 29, 39, 92, 161].

HECT ligases have attracted attention as possible pharmaceutical targets for the modulation of biological signaling and the treatment of many diseases [30]. To date, several small molecules targeting HECT ligases by attacking a cysteine residue in the exosite or by blocking interactions with substrates have been reported, but are mostly unsuitable for *in vivo* studies, yet [62].

1.3 E6AP: the founding member of the HECT ligase family

1.3.1 Structure, catalytic mechanism, substrates and localization

E6AP (E6-associated protein or UBE3A), was the first E3 enzyme shown to function through a thioester intermediate [201] and the first HECT ligase to be structurally characterized [85]. It mediates the human papillomavirus (HPV) E6 protein-induced ubiquitination of p53 [87] and also targets substrates in an E6-independent manner. There are three isoforms arising from differential splicing that differ in their amino-terminal region, but it is still unclear whether or how they differ in function [241].

In a yeast two hybrid assay, it was shown that E6AP cooperates with UBE2L3 and UBE2L6, two E2 enzymes that do not modify lysine residues per se [119, 232]. Other E2 enzymes were also shown to support E6AP catalysis *in vitro*, albeit with reduced efficacy, due to impaired binding [163].

The crystal structure of the E6AP HECT domain reveals a common bilobal structure with a conserved cleft containing the catalytic cysteine at the junction of the two lobes **(Figure 6A)**. The N-lobe portion of the cleft is primarily lined by polar and charged residues with a lysine residue (Lys549) close to the active site cysteine. The C-lobe portion of the cleft contains a hydrophobic patch that is partially exposed to solvent [85]. The catalytic cysteine is part of a four-residue loop comprising Thr819, Cys820, Phe821 and Asn822. Thr819 and Asn822 being most conserved among the HECT family, Phe822 and His818 preceding the loop are moderately conserved. A hydrophobic patch on the C-lobe formed by Phe785, Leu814, Pro815, Ala842 and Phe849 (-4 Phe) is highly conserved as well. The -4 Phe of E6AP was also shown to be involved in substrate ubiquitination and polyubiquitin chain formation [190, 197].

E6AP preferentially builds Lys48-linked ubiquitin chains that function as a proteasomal targeting signal for the modified substrate [107, 109, 225]. Wang and Pickart suggested that E6AP forms ubiquitin chains most likely through the ‘indexation’ mechanism [225]. Based on kinetic analyses, it was also shown that E6AP harbors two functionally distinct E2~ubiquitin binding sites to assemble ubiquitin chains before transferring them onto the substrate [188, 190]. In contrast to the NEDD4 family members, to date it is not proven that E6AP harbors the ubiquitin exosite, which might also affect the mode of ubiquitin chain type formation by E6AP [143].

E6AP functions as a cellular quality control caretaker by degrading cytoplasmic misfolded proteins. Several substrates of E6AP such as members of the Src (sarcoma) family of protein tyrosine kinases [165] and the promyelocytic leukemia (PML) tumor suppressor protein [135]

have been described. Other identified substrates are the DNA excision repair proteins HHR23A and B, MCM7, AIB1, annexin A1 and α-synuclein, as well as the core component ARNTL/BMAL1 of the circadian clock [73, 116, 120, 138]. E6AP temporally regulates the steady-state levels of p27 during mitotic progression, ablation of which leads to cell cycle arrest [154]. In a recent study, E6AP was shown to govern the stability of polycomb repressive complex (PRC) 1 protein RING1B through Lys48-linked ubiquitination and subsequent degradation [248]. E6AP ubiquitinates the tumor-suppressor protein p53 in complex with the high-risk human papilloma virus E6, which contributes to the neoplastic progression of cells infected by these viruses. E6AP catalyzes also non-proteolytic polyubiquitination of β-catenin, the key component of the Wnt (wingless-type MMTV integration site family member) signaling pathway, which is likely stabilized by this ubiquitin modification [37, 121].

Besides its role as ubiquitin ligase, E6AP was reported to act as transcriptional coactivator of the progesterone receptor PGR [49] and ARC (activity-regulated cytoskeleton-associated protein) [74]. It also induces the expression of the *INK4/ARF* locus which encodes key tumor suppressor proteins at the transcriptional level [71]. It is intriguing that several of the known E6AP substrates are associated with fundamental cellular pathways mediating cell cycle control, DNA replication, cell survival and cell development, thus matching the role of E6AP in viral oncogenesis, that is discussed in the next paragraph **(1.3.2)**.

In response to a variety of stress conditions such as reactive oxygen species (ROS), altered E6AP expression could be observed [154, 238]. E6AP was found to be distributed broadly in many subcellular compartments [23]. In mitochondria, E6AP helps to regulate oxidative stress; in axon terminals, E6AP is highly concentrated and might locally regulate individual synapses. It was also selectively found in euchromatin-rich nuclear domains where it might regulate gene transcription [23]. The prominent localization in neurons emphasizes the contribution of altered E6AP expression in the development of neurological disorders.

Since disease related phenotypes are thought to reflect the inhibition or the hyper-activation of E6AP catalysis, the identification of its substrates in the respective cellular environment is critical for therapeutic approaches.

1.3.2 Roles in human diseases

E6AP provides an impressive example for how deregulation of an E3 enzyme can severely impact human health. E6AP is encoded by the *UBE3A* gene on chromosome *15q11-13* playing an important role in brain development and function. The *UBE3A* gene is located in an imprinted region, which leads to maternal-specific expression in brain [51, 193]. The copy of paternal *UBE3A* is intact but silenced by a nuclear-localized long non-coding RNA, *UBE3A* antisense transcript (*UBE3A-ATS*) [150, 192]. Maternal loss or mutations of E6AP in the brain, for example, in cerebellar Purkinje cells and the hippocampus, give rise to the neurodevelopmental disorder Angelman syndrome (AS). AS is characterized by mental retardation, motor difficulties and epileptic seizures, ataxia, abnormal behavior, sleep disorders and speech deficits [111]. The genetic abnormalities associated with AS are caused by deletion of the *15q11–13* region of the maternal chromosome (in 70% of patients), uniparental paternal disomy (where both *UBE3A* alleles derive from the father and are thus inactive), imprinting defects or single point mutations in the *UBE3A* gene. It is noteworthy that similar abnormalities were also observed in *UBE3A* transgenic mice upon disruption of the maternal allele [38, 95].

A *Drosophila melanogaster* null mutant of this gene exhibits some of the mammalian symptoms connected to AS, including abnormal circadian rhythmicity and locomotive behavior and defective long-term memory. In AS mouse models, Shi et al. found a unique link between neuronal imprinted *UBE3A* and circadian rhythms [205]. Inactivation of E6AP expression elevated the levels of ARNTL/BMAL1, which alters circadian-clock behavior and metabolism, underlying the sleep disorders that characterize AS [205].

Not surprisingly, most of the AS-associated mutations are located within the catalytic cleft of E6AP correlating with a loss of the ligase activity [63] and thus deregulation of E6AP substrates. The deregulation of the neuronal protein ARC, which regulates endocytic trafficking of proteins required for synaptic plasticity and long term memory [36], was shown to contribute to the manifestation of AS. E6AP negatively affects ARC expression at the estradiol-mediated transcriptional level rather than at the posttranslational level [74].

Quite recently a potential therapeutic intervention for AS was developed by reducing *UBE3A-ATS* with antisense oligonucleotides (ASOs), thus reverse silencing of paternal *UBE3A* in neurons. The partial restoration of E6AP was shown to ameliorate some cognitive deficits in an AS mouse model [150]. ASO therapy has been tested already in human clinical trials with no serious adverse events [209].

In contrast, duplications or triplications of the chromosomal region *15q11-13* and the corresponding over-expression of *UBE3A* are implicated in some forms of autism spectrum disorders (ASD) [40, 83]. However, besides altering the ARC level, so far, it is largely unknown, which substrates of E6AP and which pathways downstream of E6AP are critical for these neurological diseases.

An unscheduled activation of E6AP was found in cervical cancer. E6AP is hijacked through a region N-terminal to the HECT domain by the viral E6 oncoprotein upon infection of cells with high-risk human papillomavirus (HPV) which represents the causative agent of most cervical cancers [16, 88]. This provides an example of how viral pathogens can overtake the ubiquitin proteasome system of their host and exploit the ubiquitin-conjugation system for viral purposes. The interaction with E6 extends the E6AP substrate spectrum to include the tumor suppressor p53 and other proteins in infected cells. Thus, E6AP ubiquitinates and targets them for proteasomal degradation, which, in turn, promotes HPV-induced cervical carcinogenesis [11, 168, 199].

The interaction with the E6 protein is mediated by acidic leucine-rich motifs containing the 'LxxLL' consensus sequence in the N-terminal region of E6AP [6, 89, 249]. A recently published structure containing the ternary complex of the 'LxxLL'-E6AP-derived peptide, E6, and the core domain of p53 explains why E6AP-E6 complex, but not the E6 protein alone, can recruit p53 **(Figure 9)** [142]. The 'LxxLL' motif adopts an α-helical conformation inserting within a deep pocket formed by the two zinc-binding domains (E6N and E6C) and the linker helix of E6 [249], thereby rendering the conformation of E6 competent for interaction with p53. In addition E6 induces conformational changes in E6AP which brings E6 and p53 in close proximity to the catalytic center of E6AP facilitating ubiquitin transfer onto p53 [196].

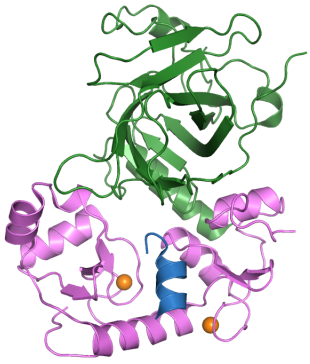

Figure 9: Structure of the ternary complex of HPV-16 E6, p53 and a E6AP-derived peptide. The ternary complex is displayed in ribbon representation with the two zinc-binding domains E6N and E6C shown in purple, p53 in green and the E6AP-derived peptide in blue, Zn^{2+}ions are shown in orange (PDB ID: 4XR8 [142]).

In addition, other E6 target substrates including PDZ domain-containing proteins, the E6 targeted protein 1 (E6TP1), protein tyrosine phosphatase H1 (PTPH1) and the telomerase reverse transcriptase transcription repressor NFX1 [202] were identified as substrates for the E6-E6AP complex. The extensive association between E6 and E6AP also triggers the recruitment of E6 to different protein complexes through binding to E6AP. This, in turn, might promote cellular proliferation and transformation and might increase the contribution to a number of the cellular phenotypes that have been attributed to the high-risk HPV E6 proteins.
Thus, an increase (in ASD and cervical cancer) or decrease (in AS) in the activity of E6AP contribute to several severe pathologic outcomes, indicating that at least in certain tissues E6AP activity and levels must be tightly controlled. However, the underlying molecular mechanisms remain elusive. It is important to study them in order to design effective therapies for HPV-associated cervical cancer, ASD and AS.

1.3.3 Regulation

Besides the control of the transcription level of the *UBE3A* gene [43, 150] and auto-ubiquitination followed by degradation of E6AP, there is a long-standing question on whether the activity of E6AP is regulated through oligomerization. Previous studies have found that the active state of E6AP is a trimer [189]. Available crystal structures of the E6AP HECT domain in its *apo* and the E2-bound state contain a trimeric arrangement through N-lobe-N-lobe interactions **(Figure 10A)** [85]. Whether this trimer presents a functionally relevant state in solution is not clear. Alanine substitution of Phe727, a key contact at the trimeric interface, had little effect on trans-thioesterification, which originally led to the conclusion that the trimer may be a consequence of crystal packing [85]. In gel filtration experiments of mammalian cell lysates full-length E6AP eluted mainly as a monomer [88, 140]. In contrast, Ronchi and colleagues showed that the substitution of Phe727 to an aspartate led to a decrease in the size of recombinantly expressed full-length E6AP, in line with the disruption of an oligomer [189]. Also mutational studies referring to the crystallographic trimer were found to diminish the catalytic activity of E6AP, which would support the hypothesis that a trimer represents an activated state of E6AP [26, 156, 189]. However, Yi and colleagues found that E6AP self-association only occurs upon mutation of a physiological phosphorylation site linked to autism and could not be observed for the wild-type protein [243].
E6AP can also target itself for ubiquitination resulting in degradation to control the half-life of E6AP and, thus its intracellular levels [164]. It is assumed that auto-ubiquitination of E6AP is mediated predominantly by inter- rather than intramolecular transfer of ubiquitin. This scenario implies that E6AP exists at least transiently in an oligomeric form [100, 164].

However, a trimeric arrangement as seen in the original crystal structure is incompatible with the position of a predicted α-helical region, when modelled upon NEDD4-type enzymes, that flanks the HECT domain N-terminally (denoted as 'α1′-helix') and which was omitted from the crystallization construct of E6AP. Yet this region is structurally important for the stability and the activity in other HECT ligases [169]. All other HECT domain structures were crystallized in the presence of the α1'-helix. In those cases the helix adopts a conserved position with respect to the HECT domain [220] and this position is incompatible with the crystallographic trimer of E6AP. Modelling the α1'-helix at the same position as observed for NEDD4-type enzymes into the trimeric arrangement of E6AP **(Figure 10B)**, shows that it would clash with the oligomerization interface. But it has to be mentioned, that the sequence of the helix of E6AP diverges from other HECT domains and contains additional seven amino acids. Thus, it is unclear whether it would adopt a similar confirmation and position as the corresponding helix in other ligases. In the studies of Ronchi et al., the addition of an α1'-helix-derived peptide to full-length E6AP led to the dissociation of an oligomer to a monomer as measured by static light scattering [189]. In line with this finding, the α1'-helix of E6AP might be structurally shielded in the context of the full-length protein, and hence, would not interfere with trimerization *in cis*. As mentioned above, a mechanism of RSP5 regulation through auto-ubiquitination-dependent oligomerization through the α1'-helix was proposed [8]. In contrast to a trimer formed by E6AP that is mostly thought to be associated with enhanced activity [26, 189], the RSP5 trimer confers auto-inhibition.

An alternative mechanism for the regulation of oligomerization of E6AP is provided by phosphorylation of residue Tyr636 in the HECT domain of E6AP by c-ABL (Abelson murine leukemia) or Thr485 within the α1'-helix by protein kinase A (PKA) [26, 243]. Tyrosine phosphorylation at residue 636 controls the activity of E6AP in a substrate-specific manner by deterring the ability of E6AP to oligomerize [26]. Phosphorylation of Thr485 was shown to downregulate the activity of E6AP [243]. The disruption of this phosphorylation site (T485A, an autism-linked mutation [93]) led to E6AP self-association and hyper-activation and caused the excessive dendritic spine development in the brain and has been associated with autism. Since self-association was not detected by a phospho-mimetic variant (T485E), phosphorylation may have a crucial role in inhibiting oligomerization in the cell. Regardless of the exact oligomeric state of functional E6AP, the full-length protein has the ability to self-associate in the cell and this process is modulated by phosphorylation.

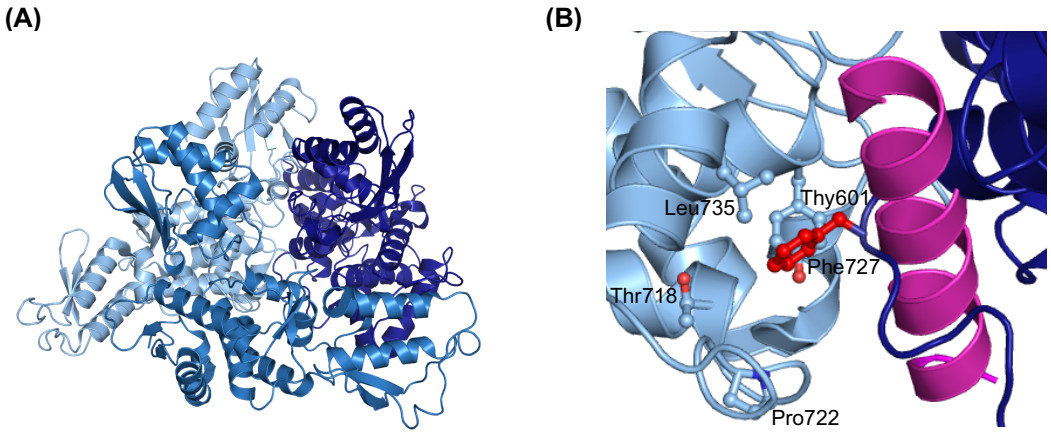

Figure 10: Crystallographic trimer formed by the E6AP HECT domain with a modelled α1'-helix of HUWE1. **(A)** The trimeric arrangement of E6AP HECT domain is shown in ribbon representation (PDB ID: 1C4Z [85]). **(B)** Close-up view of the N-lobe-N-lobe interface. The α1'-helix of HUWE1 (purple) was modelled by structural superposition of the HUWE1 HECT domain (PDB ID: 3H1D [169]) with one N-lobe of the E6AP crystallographic trimer. Important residues in the trimeric interface are shown as balls and sticks. Note that the α1'-helix of HUWE1 clashes with the N-lobe-N-lobe interface.

E6AP also provides a good example for the complex interplay between several E3 enzymes. E6AP is a target protein for several other HECT ligases and thus can regulate E6AP in an antagonistic fashion. For instance, UBR5 polyubiquitinates E6AP and thus targets it for proteasomal degradation [215]. Furthermore it was reported, that HERC2 acts in an ubiquitin-independent manner as an allosteric activator of the activity of E6AP [117] by forming a high-molecular weight complex which might be involved in mTORC1 signaling [141].

The oncoprotein E6 not only alters the substrate spectrum of E6AP, but it also functions as an allosteric activator and stimulates significantly E6AP-mediated ubiquitination – both towards itself and towards its associated proteins – likely by inducing conformational changes in E6AP that convert it to a fully active state [156]. It appears that the E6-induced self-ubiquitination of E6AP is primarily, but not exclusively the result of intramolecular transfer of ubiquitin from the active site to one or more lysine residues on the same E6AP molecule that become accessible through the E6-mediated conformational rearrangement [100].

1.4 Objectives

To date, no structural data on how the E6AP HECT domain interacts with ubiquitin are available. It is thus unknown how the donor ubiquitin is positioned and how the acceptor ubiquitin or target proteins are presented to the catalytic center with respect to the bound donor ubiquitin. Not much is known on how E6AP produces polyubiquitin chains that are specifically linked via Lys48. The N-terminal part next to the HECT domain is of central importance as a platform for substrate recruitment and as a molecular scaffold to assemble signaling complexes. Structural insight into how these functions are achieved is missing; this has precluded rational approaches to target this ligase therapeutically [30].

The objectives of this thesis are to provide a structural basis for the above-mentioned functions of E6AP. One aim was to reveal how E6AP recognizes ubiquitin during ubiquitin chain formation in comparison to the well-characterized NEDD4 family. This study also aimed to identify the determinants in E6AP that confer linkage specificity in the assembly of polyubiquitin chains. In addition, this study addressed a long-standing question regarding the mechanism of ubiquitin chain formation by E6AP: are ubiquitin chains assembled on substrates sequentially or pre-assembled on the catalytic site of E6AP before being transferred *en bloc* to a substrate? The structural mechanism of how oligomerization of E6AP is involved in chain formation and how the oligomeric state modulates the activity of E6AP is poorly understood and was part of my studies. To reach these goals high-resolution structural analyses by X-ray crystallography and NMR in combination with extensive mutational analyses and biochemical and biophysical investigations and absolute quantification (AQUA) mass spectrometry were applied.

More insights into how the HECT ligase E6AP is regulated through potential changes in the oligomeric state, posttranslational modifications or intra- and intermolecular interactions, would greatly aid the development of E6AP inhibitors, and thus open up avenues towards rational, therapeutic manipulation of E6AP in cervical cancer, ASD and AS therapy.

2 Materials

2.1 Primers

Oligonucleotides for restriction free (RF) cloning, site-directed mutagenesis and sequencing were purchased from Sigma-Aldrich in high purity salt free (HPSF) quality and in lyophilized form. The table with all primers can be found in **Table 14**.

2.2 Bacterial strains and expression constructs

Table 1: Vectors used for protein expression

Vector	Host	Affinity Tag	Cleavage site	Resistance	Supplier
pET-24d	Bacterial	C-terminal His_6	none	Kan	EMBL
pET-28a	Bacterial	N-/ C-terminal His_6	Thrombin	Kan	Merck
**pET-28a*	Bacterial	N-/ C-terminal His_6	3C	Kan	
***pET-28a*	Bacterial	N-/C-terminal His_6	TEV	Kan	
****pET-28a*	Bacterial	N-/C-terminal His_6	ULP1	Amp	
pET-30a	Bacterial	N-/C-terminal His_6	Thrombin	Kan	Merck
**pCDF-1a/b*	Bacterial	N-terminal His_6-TXN/SMT3	3C	Spec	EMBL
pRK793	Bacterial	N-terminal His_6	TEV	Amp	Addgene
pFGET19	Bacterial	N-terminal His_6		Kan	Addgene

Table 1: *pET-28a and *pCDF-1b were modified to encode an N-terminal 3C protease-cleavable His_6-tag. **pET-28a was modified with a N-terminal TEV-cleavage site after its His_6-tag. ***pET-28a was modified with a N-terminal ULP1-cleavable His_6-tag.

Table 2: Expression constructs

Insert	Residues	Vector	Gene source
E6AP N-terminal extended HECT domains	398/432/451/462/ 471-852	**pET-28a*/ **pCDF-1a/b*	ATCC
E6AP HECT domain	495-852	**pET-28a*	
E6AP C-lobe	741-852	**pET-28a*	
E6AP N-lobe	495-740	**pET-28a*	
NEDD4 HECT domain	514-900	**pET-28a*	Sino Biological Inc.
NEDD4 C-lobe	782-900	**pET-28a*	
Ubiquitin	1-76	*pET-28a/30a*	Sonja Lorenz
UBE2D3	1-147	***pET-28a*	Michael Rape

UBE2L3	1-154	**pET-28a*	Michael Rape
CDC34A	1-236	****pET-28a*	Nikita Popov
3C Protease	1-401	*pET-24d*	Florian Sauer
TEV Protease	1-303	*pRK793*	John Kuriyan
ULP1 Protease	403-621	*pFGET19*	John Kuriyan

Table 2: All protein sequences were those of *Homo sapiens* besides the three proteases. The numbering of E6AP-derived sequences refers to isoform 1. NEDD4-derived sequences are numbered according to isoform 4. All full-length sequences for wild-type proteins are found in the **Appendix** – supplementary data.

Table 3: Bacterial strains

Organism	Strain	Genotype	Supplier
E. coli	Top10	F^- *mcr*A Δ(*mrr-hsd*RMS-*mcr*BC) Φ80*lacZ*ΔM15 Δ*lac*X74 *rec*A1 *ara*D139 Δ(*ara leu*) 7697 *gal*U *gal*K *rps*L (StrR) *end*A1 *nup*G	Invitrogen
E.coli	DH5α	F^- φ80*lacZ*ΔM15 Δ(*lac*ZYA-*arg*F)U169 *rec*A1 *end*A1 *hsd*R17(r_k^-, m_k^+) *pho*A *sup*E44 *thi*-1 *gyr*A96 *rel*A1 λ^-	Invitrogen
E. coli	BL21 (DE3)	F^- *ompT hsdS*(r_B^- m_B^-) *dcm*$^+$ gal *I* (DE3)	Invitrogen
E. coli	Rosetta (DE3) pLysS	F^- *ompT hsdS*(r_B^- m_B^-) *dcm*$^+$ gal *I* (DE3) [pLysS Cam^R]	Novagen
E. coli	SoluBL21 (DE3)	F^- *ompT hsdS*(r_B^- m_B^-) *dcm*$^+$ gal *I* (DE3)	Genlantis
E. coli	JM109 (DE3)	*end*A1, *rec*A1, *gyr*A96, *thi, hsd*R17 (r_k^-, m_k^+), *rel*A1, *sup*E44, λ–, Δ(*lac-pro*AB), [F´, *tra*D36, *pro*AB, *lac*I^qZΔM15] / (DE3)	Promega
E. coli	ArcticExpression (DE3)	*F^- ompT hsdS*(r_B^- m_B^-) *dcm*$^+$ *Tet^r gal λ(DE3) endA Hte [cpn10 cpn60 Gent^r]*	Agilent

2.3 Bioreagents, kits and enzymes

Table 4: Manufactured compounds, kits and enzymes

Designation	Supplier
5x Q5 reaction buffer	New England Biolabs
5x Q5 High GC Enhancer	New England Biolabs
10x Standard *Taq* Reaction Buffer	New England Biolabs
Albumin Fraktion V (BSA)	Roth
anti-E6AP (D10D3) Rabbit mAb antibody (RRID:AB_10971637)	Cell Signaling Technology, Danvers/MA
anti-His Tag (27E8) Mouse mAb antibody (RRID: AB_10828092)	Cell Signaling Technology, Danvers/MA
anti-K48 linkage (D9D5) Rabbit mA antibody (RRID:AB_2490534)	BostonBiochem
anti-ubiquitin (P4D1) SC-8017 Mouse mAb antibody (RRID:AB_2315523)	Santa Cruz Biotechnology, Dallas/TX
anti-UBE2L3 (D5G1) Rabbit mAb antibody (RRID:AB_10829170)	Cell Signaling Technology, Danvers/MA
anti-mouse HRP-linked antibody (RRID:AB_330924)	Cell Signaling Technology, Danvers/MA
anti-rabbit HRP-linked antibody (RRID:AB_2099233)	Cell Signaling Technology, Danvers/MA
BugBuster® 10x Protein Extraction Reagent	Merck
cOmplete EDTA-free protease inhibitor tablets	Roche
DNaseI	Invitrogen
Dpn1	New England Biolabs
GC buffer (PCR)	New England Biolabs
Gel Filtration Standard	Bio-Rad
GeneRuler™ 1 kb DNA Ladder	Thermo Fisher Scientific
Lysogeny broth (LB) medium	Carl Roth
Lysozyme	Carl Roth
Midori Green Advance DNA stain	Biozym Scientific
NucleoSpin Gel and PRC cleanup kit	Macherey&Nagel
NucleoSpin Plasmid kit	Macherey&Nagel
PageRuler™ Prestained Protein Ladder	Thermo Fisher Scientific

Pierce® Silver Stain Kit	Thermo Fisher Scientific
Q5® high fidelity DNA Polymerase	New England Biolabs
SignalFire™ ECL Reagent	Cell Signalling Technology
SYPRO® Orange	Invitrogen
Taq DNA Polymerase	New England Biolabs
Terrific Broth (TB) medium	Carl Roth
Trypsin	Sigma-Aldrich

2.4 Chemicals

All chemicals listed below were of highest available purity.

Table 5: List of chemicals and reagents

Substance	Supplier
2'-Deoxyadenosine 5'-triphosphate (dATP), sodium salt solution	New England Biolabs
2'-Deoxycytidine 5'-triphosphate (dCTP), sodium salt solution	New England Biolabs
2'-Deoxyguanosine 5'-triphosphate (dGTP), sodium salt solution	New England Biolabs
2'-Deoxythymidine 5'-triphosphate (dTTP), sodium salt solution	New England Biolabs
2-Propanol (Isopropanol)	Carl Roth
3-(Cyclohexylamino)-2-hydroxy-1-propanesulfonic acid (CAPSO)	Sigma-Aldrich
3-morpholinopropane-1-sulfonic acid (MOPS)	Sigma-Aldrich
4-(2-hydroxyethyl)-1-piperazineethanesulfonic acid (HEPES)	Carl Roth
5,5′-Dithiobis-2-nitrobenzoic acid (DTNB)	Carl Roth
Acetic acid	Carl Roth
Agarose NEEO ultra quality	Carl Roth
Ammonium persulfate (APS)	Carl Roth
Ammonium acetate (NH_4COOH)	Carl Roth
^{15}N-labeled Ammonium chloride ($^{15}NH_4Cl$)	Sigma-Aldrich
Ampicillin sodium salt	Carl Roth
Benzamidin hydrochloride monohydrate	Carl Roth
Beta-mercapthoethanol (β-ME)	Sigma-Aldrich
Bis-Acrylamid 29:1	Fisher Bioreagents
Bromphenol blue	Carl Roth
Calcium chloride dihydrate ($CaCl_2$)	Carl Roth
Chloramphenicol	Carl Roth
Coomassie Brilliant Blue G-250	Carl Roth

Coomassie Brilliant Blue R-250	Carl Roth
Deuteriumoxid (D_2O)	Sigma-Aldrich
Dichloroacetone (DCA)	Sigma-Aldrich
Dimethylformamide (DMF)	Sigma-Aldrich
Dimethylsulfoxide (DMSO)	Carl Roth
Disodium hydrogen phosphate (Na_2HPO_4)	Car Roth
Dithiothreitol (DTT)	Carl Roth
Ethanol (EtOH)	Carl Roth
Ethylenediaminetetraacetic acid (EDTA)	Carl Roth
Ethylene glycol	Sigma-Aldrich
Glucose	Carl Roth
Glycerol	Carl Roth
Glycine	Carl Roth
Hydrochloric acid (HCl)	Carl Roth
Imidazole	Carl Roth
Iron(II) sulfate heptahydrate ($FeSO_4$)	Sigma-Aldrich
Isopropyl-β-D-thiogalactopyranoside (IPTG)	Carl Roth
Kanamycin sulfate	Carl Roth
Lysozyme	Sigma-Aldrich
Magnesium chloride hexahydrate	Carl Roth
Magensium sulfate heptahydrate (Mg_2SO_4)	Sigma-Aldrich
Manganese(II) chloride tetrahydrate ($MnCl_2 \cdot 4\ H_2O$)	Sigma-Aldrich
Methanol	Carl Roth
N-Ethylmaleimide (NEM)	Carl Roth
Nickel(II) sulfate hexahydrate	Carl Roth
Perchloric acid	Sigma-Aldrich
Phospho(enol)pyruvic acid trisodium salt hydrate	Sigma-Aldrich
Potassium dihydrogen phosphate	Carl Roth
Potassium formate (KOOH)	Carl Roth
Rubidium chloride (RbCl)	Sigma-Aldrich
Sodium acetate	Carl Roth
Sodium borate	Carl Roth
Sodium chloride (NaCl)	Carl Roth
Sodium dodecyl sulfate (SDS)	Sigma-Aldrich
Sodium dihydrogenphosphate dihydrate (NaH_2PO_4)	Carl Roth

Sodium hydroxide (NaOH)	Carl Roth
Spectomycin	Sigma-Aldrich
Tetramethylethylenediamin (TEMED)	Carl Roth
Thiamine hydrochloride	Sigma-Aldrich
Tris-(2-carboxyethyl)-phosphine (TCEP)	Carl Roth
Tris-(hydroxymethyl)-aminoethane (Tris)	Carl Roth
Triton™ X-100	Sigma-Aldrich
Tween® 20	Sigma-Aldrich
Urea	Carl Roth
Yeast nitrogen base	Sigma-Aldrich
Zinc chloride ($ZnCl_2$)	FlukaBioChemica

2.5 Crystallization screens

Table 6: Commercially available crystallization screens

Name	Supplier
Additive Screen™	Hampton Research
Crystal Screen, Crystal Screen 2	Hampton Research
Index Screen HT	Hampton Research
JCSG+	Molecular Dimensions
Nextal PEG Suite	Qiagen
Nucleix Suite	Qiagen
Optimix™ 3	Fluidigm
Optimix™ PEG	Fluidigm
PEGs Suite, PEGs II Suite	Qiagen
pH Clear Suite, pH Clear II Suite	Qiagen
Protein Complex Suite	Qiagen
Silver Bullets Bio™	Hampton Research
Wizard 1+2, Wizard 3+4	Emerald BioSystems

2.6 Special consumables

Table 7: List of special consumables

Type	Model	Supplier
24-well hanging-drop crystallization plates	Crystalgen SuperClear™ Plate	Jena Bioscience
96-well sitting-drop crystallization plates	Crystalquick™ 1 square well, flat bottom, low profile	Greiner Bio-One
96-well half area microplates	Microplate 96 well	Greiner Bio-One
Cuvettes	Rotilabo®-single-use	Carl Roth
Cover slides (22 mm)	Siliconised	Jena Bioscience
Dialysis membranes	Spectra/Por®	Spectrum Laboratories
Disposable cuvettes	UVette®	Eppendorf
Filter paper	Whatman® Blotting Paper	Sigma-Aldrich
Nickel-beads	Ni-NTA agarose	Machery&Nagel
Needles	0.90x40 mm Gr.1	Braun
Optical quality sealing foil	VIEWseal™	Greiner Bio-One
Pipette tips	10 µl, 200 µl, 1000 µl	StarLab
PVDF membrane	Roti®-PVDF	Carl Roth
SDS gels	10-20% Tris-Glycine Mini Gels, WedgeWell™; 12% NuPAGE Bis-Tris gels	Thermo Fisher Scientific
Syringe	30 ml, 12 ml, 5 ml, 3 ml, 1 ml	Braun
Syringe attachment filter	0.22 µm or 0.45 µm	Carl Roth
Syringe attachment filter for SEC	0.22 µm	Merck Millipore
Ultrafiltration units	Amicon® MWCO 3-30 kDa, 0.5-20 ml	Merck Millipore

2.7 Equipment and instrumentation

Table 8: Scientific equipment

Device	Model	Company
Affinity chromatography column	HisTrap HP 1 ml/5 ml	GE Healthcare
Agarose gel electrophoresis system	Mini-Sub® Cell GT System	Bio-Rad Laboratories
Anion exchange chromatography column	Mono Q 10/100 GL Mono Q 4.6/100 PE	GE Healthcare
Autoclave	V-150	Systec
Balances	LE225D TE412	Sartorius
Bottle for JLA 8.100 rotor	Bottle J-Lite 1000 ml	Beckmann Coulter
Casting frame	Mini-PROTEAN Casting Frame	Bio-Rad
Casting stand (for pouring single gels)	Mini-PROTEAN Tetra Cell Casting Module	Bio-Rad
Cation exchange chromatography column	Mono S 4.6/100 PE HiTrap SP 5 ml	GE Healthcare
CD cuvette	QS-110	Hellma
CD spectropolarimeter	J-810	Jasco
Centrifuge	Avanti J-26 XP 5415R and 5804R	Beckmann Coulter Eppendorf
Chemiluminescence imaging	FluorchemQ Multi image	Alpha Innotech
Crystallization tools (sample holder, sample vial, handling tool, loops)	CrystalCap™ Magnetic, CryoVial, CrystalWand™ Magnetic, CryoLoop	Hampton Research
Crystallization robot	Analytic Honey Bee 963	Digilab
Crystal storage pucks	SPINE Puck	Jena Bioscience
Differential refractometer	Optilab T-rEX	Wyatt Technologies
FPLC column	HiLoad 16/600 Superdex (SD) 75/200 pg HiLoad 26/600 Superdex 75 Superdex 75/200 10/300 GL	GE Healthcare
FPLC system	ÄKTA pure 25 ÄKTA purifier (MALS)	GE Healthcare

Gel electrophoresis chamber	Mini-Protean® 3-cell	Bio-Rad
(SDS-PAGE)	XCell SureLock™ Mini-Cell	Invitrogen
Ice machine	Eismaschine 94774	Ziegra Eismaschinen
Illumination table	Leuchtplatte Größe 2E	Carl Roth
Liquid handling robot	Lissy	Zinsser Analytik
Magnetic stirrer	VS-C7	VWR
MALS detector	DAWN® 8 + HELEOS® II	Wyatt
Microplate Reader	CLARIOstar®	BMG LABTECH
Microscope	SteREO Discovery.V12	Zeiss
	STEMI 2000	
Microscope: Camera	AxioCam MRC	Zeiss
Microscope: Light source	KL 2500 LCD	Zeiss
NMR	DRX 700 MHz spectrometer	Bruker
PCR Cycler	C1000 Touch Thermal Cycler	Bio-Rad
pH meter	FE20/EL20	Mettler Toledo
Pipet boy	Heathrow Scientific™ RF3000™ Li-Ion Battery Pipet Controller	Heathrow Scientific™
Pipettes	PIPETMAN®	Gilson
Power supply (for gel electrophoresis chambers)	PowerPac Basic	Bio-Rad
Robotic sealing unit for microplates	RoboSeal	HJ-BIOANALYTIC
Rotor for Avanti J-26 XP	JA 25.50	Beckmann Coulter
	JLA 8.1000	Beckmann Coulter
Scanner	Odyssey	LI-COR
Shaker	LabTherm & LabTherm LT-X	Kühner
	ISF-1-W	Kühner
	ISF-1-X	Kühner
Sonicator	Labsonic®	B. Braun Biotech International
Spectrophotometer	Bio-Photometer Plus	Eppendorf
	Nanodrop ND 2000c	Terhmo Fisher, PEQLAB
Stirrer	VS-C7	VWR
Thermo block	Rotilabo-Block Heater250	Carl Roth

Thermomixer	Comfort	Eppendorf
Tube for JA 25.50 rotor	Polypropylene bottle, screw-cap (29 x 104 mm, 50 mL)	Beckmann Coulter
UV imaging system	Gel Doc™ XR System	Bio-Rad
Western blot	Trans-Blot® Turbo™ Transfer-System	Bio-Rad
Water bath	1092	GFL
X-ray cryosystem	X-Stream™ 2000	Rigaku
X-ray detector	R-AXIS HTC	Rigaku
X-ray generator	MicroMax™-007 HF	Rigaku
X-ray optics	VariMax™ HF	Osmic Inc.

2.8 Software, servers and databases

Software, server-based tools and databases were used in the latest version published at the time.

Table 9: Software, servers and databases

Program	Description	Supplier/Reference
AIMLESS	Scaling and merging of diffraction data capturing, analyzing, and annotating	[61]
AlphaView	Images of the FluorchemQ system	Alpha Innotech
Astra VI	MALS control and data analysis	Wyatt
AxioVision	Microscopy image recording software	ZEISS
blastp/ blastn	Sequence search	[206]
Biological Magnetic Resonance Bank	A Repository for Data from NMR Spectroscopy on Proteins, Peptides, Nucleic Acids, and other Biomolecules	[218]
CCP4	Software suite for macromolecular X-ray crystallography	[237]
COOT	Model-building software	[59]
Clustal Omega	Sequence alignments	[129, 149, 207]
CrystalClear	X-ray data collection and basic processing	Rigaku
DrawCoil 1.0	Creating helical wheel diagrams for coiled coils	[75]

ExPASy ProtParam tool	Computation of physical and chemical properties of proteins	[7]
ExPASy Translate tool	Translation tool of nucleotide sequences to protein sequences	[7]
Geneious Basic	Sequence alignment editor	[102]
GraFit	Graphics and data analysis software, 5.0	Erithacus Software Ltd.
ImageJ	image processing program, 1.48v	[137]
Interactive Tree of Life v3 server	Generation of phylogenetic trees	[126]
MARS	Clariostar data analysis software	BMG LABTECH
Microsoft Excel	Spreadsheet software	Microsoft Corporation
Microsoft Word	Generation of documents	Microsoft Corporation
MolProbity	Structure validation for macromolecular crystallography	[31]
MXCube2	X-ray data collection GUI	[69]
Multalin	Multiple sequence alignment tool	[41]
NMRviewJ	Software for visualization and analysis of NMR Spectra	One Moon Scientific
ODYSSEY	Infra-red imaging software	LI-COR
OriginPro	Graphics and data analysis software, V 8.6	OriginLab
PDB Databank	Protein Data Bank	[12]
PHASER	Phasing software	[148]
Phenix	Software suite for macromolecular X-ray crystallography	[2]
Phyre^2	Biosequence analysis; protein 3D-structure prediction	[104]
PISA	Bioinformatic characterization of interfaces	[114]
PrimerX	Automated design of mutagenic primers for site-directed mutagenesis	Lapid, 2003
PROPKA	Estimation of isoelectric points	[9]
PyMOL	3-dimensional visualisation and	DeLano Scientific LLC

	graphical illustration software	
Pubmed	Literature search	[136]
RF-cloning.org	automated primer design process for RF cloning	[15]
Quantity One®	UV imaging system control; UV image recording and analysis	Bio-Rad
Spectra Manager	CD data acquisition and analysis	Jasco
UNICORN	FPLC instrument control; recording, analysis and management of chromatograms	GE Healthcare
XDS	Indexing, and integration of diffraction images	[97]

3 Methods

Several of the listed methods in this chapter have been originally described in the thesis-associated publication by Ries et al. [184] and represent an original excerpt from the manuscript, extended or adapted to account for the additional methods that have been exclusively presented here.

3.1 Protein production

3.1.1 Cloning and mutagenesis

3.1.1.1 Preparation and transformation of chemically competent *E. coli* cells with plasmid DNA

TFB1	30 mM KCOOH, pH 5.8, 75 mM $CaCl_2$, 10 mM RbCl, 15% gylcerol
TFB2	10 mM MOPS, pH 6.5, 75 mM $CaCl_2$, 10 mM RbCl, 15% gylcerol

Competent cells were prepared typically by the lab technician using an adapted protocol of the QIAexpressionist. Therefore, 2.5 ml of LB medium supplemented with the appropriate antibiotic were inoculated with a single colony from a LB plate and incubated at 37 °C overnight. 1 ml of the overnight culture was sub-cultured into 100 ml pre-warmed LB medium supplemented with antibiotic and was shaken at 37 °C until the OD_{600} reached 0.4-0.6. Thereafter, the cells were cooled on ice for 5 min and then pelleted for 5 min at 4000 rpm. The cell pellet was then re-suspended in 30 ml ice-cold TFB1 (transformation buffer). After 90 min on ice, cells were pelleted as before. Finally, the cells were re-suspended in 4 ml of ice-cold TFB2 and after 60 min incubation on ice, 100 µl aliquots were flash-frozen in liquid nitrogen and stored at -80 °C. During the preparation, the cells had to be stored on ice all the time and the solutions used must be sufficiently cooled.

For the transformation of chemical competent cells, an aliquot of the frozen competent cells was thawed on ice for 5 min. 10-100 ng of the desired plasmid DNA was added and the mixture was incubated for 15 min on ice. Then, cells were subjected to a 45 sec heat shock at 42 °C in a Thermomixer (Eppendorf), immediately taken up in 700 µl LB medium and shook for 1 h at 37 °C. Afterwards, cells were pelleted, re-suspended in 100 µl LB and plated on a LB-agar plate supplemented with the appropriate selection antibiotics at 37 °C overnight.

3.1.1.2 Isolation and purification of plasmid DNA from bacteria

Single colonies obtained after transformation carrying the desired target DNA were transferred to 5 ml LB-medium supplemented with the appropriate antibiotics. The cultures were shaken for at least 6 h at 37 °C and pelleted at 5000 rpm for 5-10 min at 4 °C, before

the double-stranded DNA was isolated with the NucleoSpin Plasmid Kit (Macherey&Nagel) according to the manufacturer's instructions.

3.1.1.3 Cloning techniques

3.1.1.3.1 Site-directed mutagenesis

Single amino acid substitutions or small insertions/deletions were introduced using the standard QuickChange™ site-directed mutagenesis protocol (Stratagene). Therefore, the template plasmid was amplified with the appropriate primer pairs carrying the mutation of interest using Q5® high fidelity DNA polymerase (New England Biolabs) according to the manufacturer's protocol. Primers were designed using the online program PrimerX (Carlo Lapid, 2003). The mutation was introduced in the middle of the primer with at least 16 bp overhang on each site, so that the mismatch between the primer and the gene was compensated by the surrounding bases. According to the size of the plasmid the amplification duration was adapted. To reduce the number of false positive clones methylated template DNA was digested afterwards by addition of DpnI for at least 4 h at 37 °C. The mixture was then transformed into chemical competent *E. coli* cells (**3.1.1.1**). Colonies were then screened for the presence of the mutated gene. The correct nucleotide sequence of all variants was finally verified by DNA sequencing (Eurofins Genomics or Microsynth Seqlab).

3.1.1.3.2 Restriction free cloning

Restriction free cloning (RF-cloning) was used to insert a longer DNA fragment (or even a whole gene) into a desired location within a circular plasmid, independent of restriction sites and ligation [219]. Primer design was performed with the web service tool RF-Cloning.org [15]. In a first PCR reaction, the DNA fragment to be inserted was amplified with unique overhangs at either site, which are complementary to sequences flanking the site of insertion in the vector. The PCR was carried out as described above with the amplification duration being adapted to the size of the DNA insertion length (**3.1.1.3.1**). The resulting PCR products were then detected by 1% agarose gel electrophoresis (**3.1.4.1**) and purified according to the manufacturer's instructions using the NucleoSpin Gel and PRC cleanup kit (Machery&Nagel). The gene of interest functioning as the primer pair was then incorporated into the desired vector in a second PCR. Hereby, the polymerase extended the primer over the entire length of the plasmid. The original plasmid was subsequently digested with DpnI (New England Biolabs) and screened for correct insertion of the DNA fragment as described above.

3.1.1.3.3 Colony PCR

Colony PCR was performed to screen for gene insertion with T7 promotor and terminator. In this case, cell material from individual colonies was used directly from the plate for a PCR reaction. This enabled the detection of the correct insert of a plasmid to be cloned. In 50 µl 33 µl ddH_2O, 5 µl 10x standard Taq reaction buffer, 2 µl 10 mM dNTPs, 2 µl 10 µM T7 terminator and T7 promoter and 2 U Taq polymerase were mixed. The mixture was distributed to five tubes of 10 µl each and inoculated with cell material of a single colony. 50 µl of LB medium was inoculated with the remaining cell material for an overnight culture. The PCR was carried out as in **3.1.1.3.1** (amplification time: 2 min). The resulting PCR product was detected by 1.6% agarose gel electrophoresis (**3.1.4.1**). 5 ml LB medium were inoculated with single insertion-positive clones and incubated at 37 °C overnight. The amplified plasmids were sequenced (Eurofins Genomics or Microsynth Seqlab). The chemical competent *E. coli* cells were then transformed by the plasmids with the desired mutation, plated on LB plates supplemented with the appropriate antibiotics and incubated at 37 °C overnight (**3.1.1.1**).

3.1.2 Protein expression and purification

All buffers were prepared with ultrapure H_2O (ddH_2O) derived from a TKA GenPure water system, using at least analytical grade chemicals. All buffers were filtered and, where needed, degassed prior to usage. Buffers were stored at 4 °C.

3.1.2.1 Protein expression in *E. coli*

The plasmid coding for a particular protein variant was transformed into one of the *E. coli* expression strains via heat-shock as described in **3.1.1.1**. A single colony of the respective variant from the plate was then used to inoculate an overnight starter culture (100 LB medium supplemented with the appropriate antibiotics), which was shaken at 37 °C.

3.1.2.1.1 Test expression

The expression of the N-terminal extended HECT domain constructs of E6AP was first tested in small scale. Therefore, a 10 ml overnight starter was used to inoculate 50 ml TB medium to an OD_{600} ~0.05. After shaking at 37 °C, recombinant protein expression was initiated by adding IPTG (0.1-1.0 mM) after the OD_{600} reached values of 0.8-1.0. The culture flasks were then transferred to the desired expression temperature. Expression lasted 4 h at 37 °C, 8 h at 30 °C or overnight at 18-20 °C. Using BugBuster® Protein Extraction Reagent (Merck) to disrupt the cell wall of *E. coli* and to release soluble protein, the expression and solubility of

the tested constructs were analyzed by SDS-PAGE (**3.1.4.2**) and the best expression conditions for the large-scale expression were determined.

3.1.2.1.2 Large-scale protein expression

Besides UBA1, all proteins described here were recombinantly produced by T7 promotor driven [212], *lac*-repressor [54] controlled expression in *E. coli* (DE3) in either TB or LB medium supplemented with the appropriate antibiotics. Cultures in volumes of 1 or 2 l in 5 l Erlenmeyer flasks were inoculated to an OD_{600} of ~0.05 with a 100 ml overnight pre-culture and were shaken at 37 °C until the OD_{600} reached values of 0.6-0.8 for LB medium or 1.0-1.2 for TB medium, respectively. Protein overexpression was then induced by the addition of 0.5 mM IPTG. For the different constructs the shaker temperature and expression time were adapted. Finally, cells were harvested by centrifugation at 5000 rpm for 15 min at 4 °C and either re-suspended immediately in lysis buffer for protein purification or the pellets were stored at -80 °C.

^{15}N-enriched proteins for NMR experiments were expressed in M9 medium supplemented with filtrated 0.4% (w/v) (^{13}C) glucose, 2 mM $MgSO_4$, 0.1 mM $CaCl_2$, 2 mg/l thiamine, 10 mM $FeSO_4$, 10 mM $ZnCl_2$, 0.17% (w/v) yeast nitrogen base (YNB) and 0.1% (w/v) ^{15}N-enriched ammonium chloride ($^{15}NH_4Cl$). The expression and purification of the different ^{15}N-enriched proteins were performed as described below.

3.1.2.2 Recombinant protein purification

3.1.2.2.1 Cell lysis

Cell pellets were re-suspended in 10 volumes of the respective lysis puffer on ice while stirring and lysed afterwards by sonication using Labsonic® Sonicator (B. Braun Biotech International) on ice. Through 1 min persisting ultrasonic frequencies (>20 kHz) followed by 1 min lasting breaks to avoid heating of the solution, cell membranes were disrupted, and cellular content was released. The resulting crude extract was afterwards cleared by centrifugation for 45 min at 25.000 rpm at 4 °C in a Beckmann JA 25.50 rotor.

3.1.2.2.2 Nickel-affinity chromatography and tag cleavage

Soluble proteins in the supernatant were separated from host proteins using immobilized metal-affinity chromatography [246] (IMAC; with exception of untagged ubiquitin). Hereby, proteins with a recombinantly poly-histidine tag can be separated from untagged proteins by adsorbance on a solid phase exposing to divalent metal cations (in this case Ni^{2+}). By application of increasing imidazole concentrations, the protein elutes competitively.

Therefore, the supernatant of the centrifuged crude extract was applied to a 5 ml HisTrap HP column (GE Healthcare) equilibrated in a respective non-imidazole containing buffer using an ÄKTA pure system (GE Healthcare). The column was then washed with 5 CV (column volume) of a buffer supplemented with 25 mM imidazole to remove nonspecifically bound proteins from the column. Elution of the tagged protein was carried out subsequently using a linear gradient over 6 CV from 25 mM to 300 mM imidazole. Protein containing fractions (determined by their A_{280} and verified by SDS-PAGE (**3.1.4.2**)) were pooled and the His_6-tag was removed through proteolysis by incubation with the respective protease at 4 °C overnight while dialyzing into the appropriate size exclusion chromatography buffer. By reapplication of the dialysate to a HisTrap HP column, the cleaved target protein in the flow-through was separated from the His_6-tag, the His_6-protease and residual non-cleaved protein that bound to the affinity matrix.

3.1.2.2.3 Ion exchange chromatography

Proteins with sufficiently different net charges can be separated from each other using ion exchange chromatography depending on the pI (isolelectric point) of the protein [216]. The pI is defined as the pH value at which the net charge of the protein is zero. The pI values were estimated using the ExPASy ProtParam or PROPKA servers [7, 9]. Negatively charged proteins bind to anion exchange chromatography (AIEX) columns, positively charged ones to cation exchange chromatography (CIEX) columns. After washing, the bound proteins could be eluted using a salt gradient up to 500 mM NaCl over 10 to 20 CV. In this study, CIEX was conducted for purification purposes only in case of untagged ubiquitin (**3.1.7**).

3.1.2.2.4 Size-exclusion chromatography

The final purification step was size exclusion chromatography (SEC) [179]. This allows for the separation of components according to their hydrodynamic radius. Based on different speed of molecules with different size to traverse a porous bead shaped column material protein are separated.

For SEC the protein suspension was concentrated to 2-5 ml according to the protein yield and applied through a 0.22 µm syringe attachment filter to an appropriate pre-equilibrated HiLoad Superdex (SD) pg column (connected to an ÄKTA pure system) using the respective SEC buffer and eluted from the column at a constant flow rate. Peak fractions from the size exclusion chromatography were analyzed via SDS-PAGE (**3.1.4.2**), pooled, concentrated and flash-frozen in liquid nitrogen and stored at -80 °C.

3.1.3 Protein concentration determination

Protein concentrations in solution were generally estimated by the light absorbance at wavelength 280 nm using a Nanodrop ND 2000c spectrophotometer (Peqlab). The protein samples were measured in their folded and reduced state three times and values were averaged. The protein concentration based on the absorption at 280 nm which is dominated by the aromatic amino acids was then determined according to the Lambert-Beer law **(Equation 1)**. Extinction coefficients for the different constructs were calculated by the ExPASy ProtParam tool [7].

$$c = \frac{A_{280}}{\varepsilon \cdot d}$$

Equation 1: Lambert-Beer law. c is the protein concentration [mol·l^{-1}], A_{280} is the measured absorption at 280 nm, ε the molar extinction coefficient [l·mol^{-1}·cm^{-1}] and d [cm] the path length of the light through the sample.

3.1.4 Electrophoretic methods

3.1.4.1 Agarose gel electrophoresis

TAE puffer (1x)	40 mM Tris/HCl, pH 8.0, 20 mM acetic acid, 1 mM EDTA
DNA Loading Dye (6x)	4 M urea, 10 mM EDTA, 50% (v/v) glycerol, 0.1% (w/v) bromphenol blue

DNA fragments were separated according to their size by horizontal agarose gel electrophoresis. Depending on the size of the fragments to be analyzed, the concentration of agarose was chosen (from 1.0% (w/v) for plasmids and DNA fragments >1 kb to 1.6% (w/v) for DNA fragments <1 kb). Agarose was solved in 1x TAE supplemented with Midori Green Advance and poured into an appropriate gel-caster. The samples were mixed with 6x of DNA loading dye. Electrophoresis was carried out for 30 min in TAE buffer at 120 V. DNA fragments were visualized through the intercalating Midori Green by exposing the agarose gel to UV light. DNA concentrations were determined by UV-VIS spectroscopy using a spectrophotometer (Nanodrop ND 2000c, Peqlab) equivalent to section **3.1.3**.

3.1.4.2 SDS-PAGE

Stacking gel	4% (w/v) Bis-Acrylamid 29:1, 125 mM Tris/HCl, pH 6.8, 0.1% (w/v) SDS, 0.1% APS, 0.025% TEMED
Separating gel	10-15% (w/v) Bis-Acrylamid 29:1, 375 mM Tris/HCl, pH 8.8, 0.1% (w/v) SDS, 0.1% APS, 0.025% TEMED
SDS sample buffer (4x)	62.5 mM Tris/HCl, pH 7.0, 40 mM EDTA, 15% (w/v) SDS, 48% (w/v) glycerol, 0.04% (w/v) bromphenol blue, ± 120 mM β-ME
Running buffer	25 mM Tris, 192 mM glycine, 0.1% SDS
Staining solution	0.1% (w/v) Coomassie Brilliant Blue G-250/R-250, 25% (v/v) Isopropanol, 10% (v/v) acetic acid
Destaining solution	10% (v/v) acetic acid

Sodium dodecyl sulfate poly-acrylamide gel electrophoresis (SDS-PAGE) allows separation of proteins between 5 and 200 kDa and therefore the estimation of a protein's molecular weight and purity [122]. Gels (thickness 0.75 cm) were prepared in casting frames and casting stands purchased from Bio-Rad. Protein samples were mixed with ¼ volume of SDS sample buffer and then heated for 3 min at 95 °C. Samples were loaded next to a protein standard marker (PageRuler protein ladder, Thermo Fisher Scientific) and electrophoresis was carried out at room temperature (RT) in a Mini-Protean® electrophoresis chamber (Bio-Rad) filled with running buffer for typically 45 min at 230 V. After electrophoresis, the stacking gel was removed, and the separating gel stained for 10 min in Coomassie G-250 or R-250 containing staining solution after brief heating in a microwave, followed by destaining in destaining solution. For documentation, the gels were scanned using the Odyssey system (LI-COR).

To visualize lower protein concentrations and to achieve higher sensitivity silver staining of the gels was performed using Pierce Silver Stain kit (Thermo Fisher Scientific) according to the manufacturer's protocol.

In some cases precasted gels (Novex™ 10-20% Tris-Glycine Mini Gels, Thermo Fisher Scientific) were used according to the manufacturer's protocol.

3.1.5 E6AP constructs

Lysis buffer	50 mM Tris/HCl, pH 8.0, 500 mM NaCl, 5 mM benzamidine, 1 tablets protease inhibitor cocktail per 250 ml, 3% glycerol, 0.4% Triton X-100, 8 mM β-ME
Buffer A	50 mM Tris/HCl, pH 8.0, 400 mM NaCl, 8 mM β-ME, 25 mM imidazole
Buffer B	50 mM Tris/HCl, pH 8.0, 400 mM NaCl, 8 mM β-ME, 500 mM imidazole
SEC buffer	50 mM Tris/HCl, pH 7.5, 75 mM NaCl, 2 mM DTT

The following expression and purification protocol was applied to all different E6AP constructs: isolated HECT domain, HECT domain with a N-terminal extended α1'-helix, N-lobe and C-lobe. The proteins were expressed in 2 l TB medium (supplemented with an appropriate antibiotic) of *E. coli* BL21 (DE3) cells at 18 °C overnight after induction with IPTG. Cells were harvested by centrifugation and lysed in lysis buffer. After cell disruption by sonication and centrifugation the supernatant was applied to a 5 ml HisTrap HP column, washed with buffer A and eluted through a linear gradient with buffer B. Cleavage of the His_6-tag by 3C protease was performed for the isolated HECT domain, N-lobe and C-lobe in SEC buffer at 4 °C overnight. To remove the tag and the protease a second Ni-NTA chromatography was performed, followed by gel filtration (HiLoad 16/600 or 26/600 SD 75

pg) in SEC buffer. N-terminal extended HECT domain constructs were concentrated after elution from the first HisTrap column and directly subjected to SEC (HiLoad 16/600 SD 200 pg). Pure E6AP constructs were concentrated if possible up to 500 µM and flash-frozen for storage at -80 °C.

3.1.6 NEDD4 HECT domain and C-lobe

SEC buffer 100 mM HEPES, pH 7.5, 300 mM NaCl

The expression and purification protocol of NEDD4 HECT domain and C-lobe were identical to that described above for the respective E6AP constructs. Only the dialysis and the SEC were performed in another buffer.

3.1.7 Ubiquitin

The expression and purification of untagged ubiquitin were modified from the protocol described in Methods on Enzymology – Ubiquitin and Protein Degradation [47].

Lysis buffer	50 mM Tris/HCl, pH 7.5, 50 mM NaCl
Buffer A	50 mM NH_4COOH, pH 4.5
Buffer B	50 mM NH_4COOH, pH 4.5, 500 mM NaCl
SEC buffer	50 mM Tris/HCl, pH 7.5, 100 mM NaCl

Ubiquitin was produced recombinantly in *E. coli* BL21 (DE3) cells from 2 l LB media supplemented with Kan. After induction with IPTG, cells were harvested after 4 h at 37 °C and re-suspended in 40 ml lysis buffer and lysed by sonication. After centrifugation for 35 min at 25.000 rpm 0.4 ml of 60% perchloric acid were slowly added while stirring on ice. After 10 min stirring, precipitated proteins were spun down at 8000 rpm for 30 min. The supernatant was then dialyzed into buffer A at 4 °C overnight. With a pI of 6.56 (calculated by ExPasy ProtParam [7]) ubiquitin is positively charged at pH 4.5 and could bind to a negatively charged cation exchange matrix. After filtration, the solution was therefore subjected to a 5 ml HP SP column (GE Healthcare) equilibrated in buffer A. Protein elution was achieved by a linear gradient of buffer B (ubiquitin eluted at concentration of 200 mM NaCl). While concentrating the protein, buffer exchange in SEC buffer was performed. After gel filtration with a HiLoad 16/600 or 26/600 SD 75 pg column in SEC buffer, the protein was concentrated to ~3 mM and flash-frozen for storage at -80 °C.

His-tagged ubiquitin variants were expressed, harvested, lysed and sonicated as the untagged version. The supernatant was then subjected to a HisTrap HP 5 ml column (same buffers as used in **3.1.5**). Immobilized His-tagged protein was eluted by 200 mM imidazole,

concentrated while buffer exchange in SEC buffer was performed and gel filtrated as described above for the untagged version.

3.1.8 UBA1

UBA1 was prepared by Dr. Sonja Lorenz as described previously [233].

3.1.9 E2 enzymes

The expression of the different E2 conjugation enzymes (UBE2D3, UBE2L3 and CDC34A) was performed in 1 l TB medium of *E. coli* BL21 (DE3) cells at 18 °C overnight through the addition of 0.5 mM IPTG. The purification procedure of these proteins was analogue to the purification protocol of E6AP HECT domain using the same buffers (**3.1.5**). Only His_6-tag removal during dialysis was performed using a suitable protease for the respective tag.

3.1.10 Proteases

All the proteases were typically prepared by a lab technician.

3.1.10.1 3C Protease

Lysis buffer	25 mM Tris/HCl, pH 8.0, 500 mM NaCl, 10 mM $MgCl_2$, DNase, Lysozyme, 8 mM β-ME
Buffer A	50 mM Tris/HCl, pH 8.0, 500 mM NaCl, 5 mM β-ME; 20 mM imidazole
Buffer B	50 mM Tris/HCl, pH 8.0, 500 mM NaCl, 8 mM β-ME, 500 mM imidazole
Buffer C	25 mM Tris/HCl, pH 8.0, 200 mM NaCl, 2 mM DTT

His_6-tagged rhinovirus 3C protease was expressed in *E. coli* BL21 (DE3) using pET-24d recombinant plasmid provided by Dr. Florian Sauer (University of Würzburg). After induction with IPTG, cells were grown at 18 °C overnight. Cell pellets were re-suspended in lysis buffer, disrupted by sonication and centrifuged. The supernatant was loaded on a 5 ml HisTrap HP column equilibrated with buffer A and eluted with buffer B. After dialysis against 2 l of buffer C at 4 °C overnight, pure 3C was concentrated to 8 mg/ml and flash-frozen for storage at -80 °C.

3.1.10.2 TEV Protease

Lysis buffer	25 mM Tris/HCl, pH 8.0, 500 mM NaCl, 20 mM imidazole, DNase, Lysozyme, 2 mM β-ME, 0.005% Triton X-100, 10% gylcerole
Buffer A	25 mM Tris/HCl, pH 8.0, 500 mM NaCl, 20 mM imidazole, 2 mM β-ME, 10% gylcerole
Buffer B	25 mM Tris/HCl, pH 8.0, 150 mM NaCl, 20 mM imidazole, 2 mM β-ME, 10% gylcerole
Buffer C	25 mM Tris/HCl, pH 8.0, 150 mM NaCl, 500 mM imidazole, 2 mM β-ME, 10% gylcerole
Buffer D	25 mM Tris/HCl, pH 8.0, 150 mM NaCl, 0.5 mM EDTA, 5 mM DTT, 10% gylcerole

His_6-tagged tobacco etch virus (TEV) protease (plasmid provided by Prof. John Kuriyan (UC Berkeley)) was expressed in *E. coli* Rosetta (DE3) in 6 l TB medium after induction with IPTG at 25 °C overnight. Cells were harvested and re-suspended in lysis buffer. Cell disruption was performed by sonication, cell depris were pelleted and the supernatant was subjected to a 5 ml HisTrap HP column equilibrated in buffer A. After washing with buffer B, the protein was eluted with a linear gradient of buffer C. The eluate was dialyzed against buffer D overnight and then concentrated to 2.5 mg/ml. 200 µl aliquots were flash-frozen for storage at -80 °C.

3.1.10.3 ULP1 Protease

Buffer A	50 mM Tris/HCl, pH 8.0, 500 mM NaCl, 20 mM imidazole, 10% glycerol, 5 mM β-ME
Buffer B	50 mM Tris/HCl, pH 8.0, 500 mM NaCl, 500 mM imidazole, 10% glycerol, 5 mM β-ME
Buffer C	50 mM Tris/HCl, pH 8.0, 250 mM NaCl, 10% glycerol, 5 mM β-ME

The expression of His_6-tagged ULP1 protease (provided by Prof. John Kuriyan) was done in 4 l TB medium inoculated with *E. coli* Rosetta (DE3) pLysS cells and protein expression was induced with IPTG. After overnight expression at 18 °C, cells were harvested, re-suspended in buffer A and disrupted by sonication. Lysate was spun down and the supernatant was loaded on a HisTrap HP column equilibrated in buffer A. The protein eluted with 50 ml buffer B. Desalting of the protein in buffer C was performed using Zeba™ Spin Desalting Columns (Thermo Fisher Scientific) and then concentrated to 2.5 mg/ml. 200 µl aliquots were flash-frozen for storage at -80 °C.

3.1.11 Lys48-linked ubiquitin chain synthesis

Reaction buffer	50 mM Tris/HCl, pH 8.0, 1 mM DTT, 2 mM ATP, 5 mM $MgSO_4$
Buffer A	50 mM NH_4COOH, pH 4.5
Buffer B	50 mM NH_4COOH, pH 4.5, 500 mM NaCl

Lys48-linked polyubiquitin chains can be synthesized *in vitro* using ubiquitin-activating UBA1 and ubiquitin-conjugating enzyme CDC34A. For Lys48-linked polyubiquitin chain synthesis 0.5 µM UBA1, 50.0 µM CDC34A, 0.6 mM ubiquitin wild-type (WT) were incubated in a total volume of 5 ml in reaction buffer at 37 °C overnight. The solution was then dialyzed for at least 4 h against buffer A and loaded on a 5 ml HP SP column (**3.1.7**) [33]. The polyubiquitin chains eluted with a linear gradient of 0 to 500 mM NaCl, with longer Lys48-linked chains eluting at higher salt concentration. Proteins were concentrated afterwards while the buffer was exchanged to 50 mM Tris/HCl, pH 7.5 and 100 mM NaCl and flash-frozen for storage at -80 °C.

3.2 Biochemical and biophysical methods

3.2.1 Native PAGE

Stacking gel	3% (w/v) Bis-Acrylamid 29:1, 125 mM Tris/HCl, pH 6.8, 50% glycerol, 0.1% APS, 0.025% TEMED
Separating gel	10% (w/v) Bis-Acrylamid 29:1, 375 mM Tris/HCl, pH 8.8, 0.1% APS, 0.025% TEMED
Sample buffer (4x)	0.2 M Tris/HCl, pH 6.8, 48% glycerol, 0.04% (w/v) bromphenol blue
Running buffer	12.5 mM Tris, 96 mM glycine

To analyze protein-protein interactions native PAGE was performed. Non-denaturating gels were poured using casting frames and casting stands (Bio-Rad) according to standard protocols. Gels were pre-run without samples for at least 20 min at 100 V at 4 °C. In the meantime, protein samples were mixed and incubated at 30 °C. Then, the samples are diluted with ¼ volume of sample buffer and loaded on the gel. Electrophoresis was performed in running buffer at 4 °C for around 3 h at 100 V. Gels are stained as described for SDS-PAGE (**3.1.4.2**).

3.2.2 Western Blot

Transfer buffer	25 mM Tris/HCl, pH 7.5, 192 mM glycine, 20% methanol (MeOH)
TBS-T	20 mM Tris/HCl, pH 7.5 150 mM NaCl, 0.1% Tween®20
Blocking buffer	5% BSA in TBS-T

Proteins can be specifically detected by immunoblot (Western blot) if respective antibodies are available [217]. For this, proteins are first separated via SDS-PAGE, electrophoretically transferred to a polyvinylidene difluoride (PVDF) membrane and visualized via immunostaining.

After SDS-PAGE (**3.1.4.2**), the gel was equilibrated in pre-cooled transfer buffer 3 times for 5 min. The PVDF membrane was activated by immersing it shortly in methanol and then in transfer buffer. The assembly of the transfer cell was performed directly on the cassette of the Trans-Blot® Turbo™ Transfer System (Bio-Rad). Hereby, the gel was put on top of the membrane sandwiched between a Whatman filter paper soaked in transfer buffer. The transfer was carried out at 25 V and 1 A for 30 min. Subsequently the membrane was blocked for 1 h in blocking buffer while shaking gently at RT. Then, the membrane was probed with a respective dilution of the primary antibody dissolved in blocking buffer at 4 °C overnight. The membrane was then washed 3 times for 10 min in TBS-T, followed by 1 h incubation with secondary antibody dissolved in blocking buffer. After washing the membrane again 3 times for 10 min in TBS-T, chemiluminescence detection with SignalFire™ ECL Reagent (Cell Signaling) was performed at a FluorchemQ Multi image system (Alpha Innotech). Hereby, the addition of HRP substrate luminol was oxidated by the HRP (horse-radish peroxidase) coupled to the secondary antibody, resulting in chemiluminescence.

3.2.3 Circular dichroism

Buffer 10 mM sodium phosphate, pH 7.4

To analyze the structural integrity and folding state of a protein and its variants far-UV circular dichroism spectra in the range of 180 to 260 nm were recorded at a Jasco J-810 spectropolarimeter in a temperature-controlled quartz cuvette with a layer thickness of 1 mm [203]. All measurements were conducted with a protein concentration of 4 or 8 µM in 10 mM sodium phosphate, pH 7.4 in 0.1 nm steps, at a scanning speed of 20 nm/min and a band width of 1 nm and a response of 2 s. The measuring temperatures were 10 °C or 80 °C. In order to improve the signal-to-noise ratio ten spectra were recorded and the signal averaged, corrected for the buffer signal and normalized to the molar ellipticity according to **Equation 2**.

$$[\theta] = \frac{\theta \cdot 100}{c \cdot d \cdot N_{AS}}$$

Equation 2: Calculation of the molare ellipticity. [Θ]: molare ellipticity in deg·cm^2·dmol^{-1}; Θ: measured ellipticity in mdeg; c: protein concentration in mM; d: thickness of the cuvette in cm; N_{AS}: number of amino acids of the protein.

The thermally induced unfolding transitions of different variants were monitored using the Jasco J-810 spectropolarimeter with PTC-348 WI peltier element through the change of the CD signal at 222 nm from 10 °C to 80 °C. The measurements were carried out with a protein concentration of 4 µM in a total volume of 300 µl in a 1 mm quartz cuvette. The heating rate was 60 K/h. The thermal unfolding transitions were evaluated with **Equation 3**. The change in thermal capacity ΔC_P was set to 4000 J^{-1}·mol^{-1}·K^{-1}.

$$y(T) = \frac{y_N^0 + m_N \cdot T + (y_U^0 + m_U \cdot T) \cdot e^{\left(\frac{\Delta H_D}{R} \cdot \left(\frac{1}{T} - \frac{1}{T_M}\right) - \frac{\Delta C_P}{R} \cdot \left(1 - \frac{T_M}{T} + \ln\frac{T_M}{T}\right)\right)}}{1 + e^{\left(\frac{\Delta H_D}{R} \cdot \left(\frac{1}{T} - \frac{1}{T_M}\right) - \frac{\Delta C_P}{R} \cdot \left(1 - \frac{T_M}{T} + \ln\frac{T_M}{T}\right)\right)}}$$

Equation 3: Evaluation of the thermal transition. $y(T)$: measured value at a particular temperature; y_N^0, y_U^0: theoretical value for native and denatured protein respectively at 0 K; m_N, m_U: slope of the base line of the native and denatured protein in K^{-1}; ΔH_D: van't Hoff enthalpy in $kJ \cdot mol^{-1}$; ΔC_P: change of molar thermic capacity in $J \cdot mol^{-1} \cdot K^{-1}$; R: general gas constant in $kJ \cdot mol^{-1} \cdot K^{-1}$; T: temperature in K; T_M: temperature at the transition in K.

3.2.4 Thermofluor assay

Fluorescence-based thermal shift analysis was performed on E6AP HECT domain C604S C737S, the disulfide-linked E6AP HECT domain C604S C737S~ubiquitin complex and the N-terminal extended HECT domain of E6AP in a high-throughput approach to identify buffer conditions in which the proteins are stable and aggregation is reduced [42]. To this end, thermally induced unfolding of the protein is followed by an increase in the fluorescence signal, arising from a fluorophore (SYPRO Orange), which binds to hydrophobic amino acids that become accessible to the dye upon unfolding of the protein. 1 µl of 1 mg/ml protein was incubated with 1 µl of 2.5% SYPRO Orange solution mixed with 18 µl of 96 different buffer conditions of the thermofluor advanced buffer screen (buffer composition **Table 15**) in a 96 PP-PCR-plate (Greiner Bio-One International AG). Through gradually heating from 25 °C to 95 °C in 1 °C per min steps using real-time PCR cycler (Stratagene Mx3005P), SYPRO Orange fluorescence could be monitored (excitation 492 nm/emission 610 nm). The obtained melting curves were analyzed using an Excel (Microsoft) sheet provided by the Structural Genomics Consortium (SGC) in Oxford. The melting temperature (T_M) for each buffer condition was deduced based on the inflection point.

3.2.5 Analytical size exclusion chromatography

SEC (**3.1.2.2.4**) can also be applied for the analytical separation of biomolecules to analyze non-covalent complex formation. Potential interactions partners were incubated on ice 30 min in advance and centrifuged prior to aSEC for at least 30 min at highest speed to remove aggregates. aSEC was performed using an ÄKTA pure system with a SD 75 or 200 10/300 GL column (GE Healthcare) in a respective buffer at 4 °C. 100 µl of sample passed through the column with a flow rate of 0.75 ml/min and complex formation was followed by the absorbance at 280 nm and verified by SDS-PAGE (**3.1.4.2**).

3.2.6 SEC-coupled multi-angle light scattering

For molecular mass determination of different proteins, size exclusion chromatography coupled multi-angle light scattering (SEC-MALS) was performed [230]. 3.5-10 mg/ml of pure

E6AP HECT domain or C-lobe were loaded onto an equilibrated SD 75/200 10/300 GL column, which was attached to an ÄKTA purifier FPLC system, equipped with a MALS detector and a refractive index (RI) monitor. Therefore, protein elution was not only detected by absorption at 280 nm, but also by light scattering (at multiple angles relative to the primary beam) and changes in the refractive index (differential RI or dRI). The intensity of scattered light at various angles was monitored using a Dawn 8^+ MALS detector (Wyatt) and the concentration could be obtained by RI measurements with an Optilab T-rEX refractometer (Wyatt). Using this information, the molecular mass could be calculated by analysis with the ASTRA 6.1 software (Wyatt) [251]. In contrast to conventional aSEC experiments, SEC-MALS was performed at RT without fractionation.

3.2.7 Crosslinking

3.2.7.1 Crosslinking of the active site cysteine of a HECT E3 enzyme and ubiquitin with Ellman's reagent

Reaction buffer 75 mM NaP, pH 7.5, 1 mM EDTA

Ubiquitin G75C/G76C was covalently linked to either E6AP or NEDD4 C-lobe or a single Cys-containing E6AP HECT domain (C604S C737S) via a disulfide bond, activated by the reaction with Ellman's reagent (DTNB: 5,5'-dithio-bis-nitrobenzoic acid) in reaction buffer. Ellman's reagent can be used to quantify the number or concentration of thiol groups in a sample [58]. In my case, the Cys75 or Cys76 of the ubiquitin variant (~1 mM), respectively, was activated by a 9-fold excess of DNTB to ubiquitin, and then excess of DNTB was removed through buffer exchange. Afterwards, a sub-stoichiometric amount of one of the single Cys-containing HECT E3 enzyme constructs (~300-500 µM) was added. DTNB released upon the disulfide exchange reaction was afterwards removed through buffer exchange, and the disulfide-linked protein complex was isolated from excess of non-crosslinked ubiquitin by anion or cation exchange chromatography using a Mono Q 10/100 GL or Mono S/Q 4.6/100 PE (GE Healthcare) with a gradient from 0 to 500 mM NaCl over 20 CV [133].

3.2.7.2 Crosslinking of E6AP C-lobe and ubiquitin with dichloroaceton

Reaction buffer	20 mM sodium borate buffer, pH 8.1, 1 mM TCEP
Buffer A	50 mM Tris/HCl, pH 7.5, 400 mM NaCl, 8 mM β-ME
Buffer B	50 mM Tri/HCl, pH 7.5, 400 mM NaCl, 8 mM β-ME, 500 mM imidazole
Buffer C	50 mM Tris/HCl, pH 7.5, 200 mM NaCl, 1 mM EDTA

Non-hydrolyzable ubiquitin and E6AP C-lobe conjugate was synthesized by crosslinking ubiquitin containing a terminal cysteine residue (G76C) to the active site cysteine of E6AP

according to the protocol of Wiener et al. [234, 245]. Purified His-tagged ubiquitin G76C and E6AP C-lobe were dialyzed against reaction buffer at 4 °C overnight. 100 µM C-lobe were incubated with 250 µM ubiquitin on ice for 15 min. A final concentration of 100 µM of a 5 mM stock of DCA in 10 ml DMF (dimethylformamide) was added to the mixture. After 1 h incubation on ice, the reaction was stopped by the addition of 10 mM β-ME for 30 min on ice. Via IMAC using a 1 ml HisTrap HP column equilibrated in buffer A, His_6-tagged conjugates were separated from non-crosslinked species with a linear gradient of 0 to 500 mM imidazole over 35 CV. Through a final aSEC with buffer C free ubiquitin was separated from the higher molecular weight conjugate.

3.2.7.4 Enzymatic generation of an isopeptide linkage between E6AP HECT domain and ubiquitin

Reaction buffer	50 mM Tris/HCl, pH 7.5, 200 mM NaCl, 2 mM DTT, 5 mM $MgCl_2$, 2 mM ATP
Buffer A	50 mM Tris/HCl, pH 6.5, 1 mM EDTA
Buffer B	50 mM Tris/HCl, pH 6.5, 500 mM NaCl, 1 mM EDTA
Buffer C	50 mM Tris/HCl, pH 7.5, 200 mM NaCl, 2 mM DTT

The enzymatic generation of an isopeptide bond in lieu of the native thioester has proven successful in linking ubiquitin to E2 enzymes [178] and was applied here to obtain a stable linkage between ubiquitin and E6AP HECT domain. This involved the mutation of the catalytic cysteine to lysine residue (C820K) via site-directed mutagenesis (**3.1.1.3.1**). 1 µM UBA1, 50 µM UBE2D3 and 500 µM ubiquitin were incubated with 50 µM E6AP HECT domain C820K in reaction buffer for 30 min at 30 °C. The complete approach was then applied to a HiLoad 16/600 SD 75 pg column equilibrated in reaction buffer without ATP and $MgCl_2$ (**3.1.2.2.4**). The isopeptide-linked containing fractions were pooled, dialyzed in buffer A at 4 °C overnight and subjected to a Mono Q 4.6/100 PE equilibrated in buffer A and eluted using increasing percentage of buffer B. The complex was finally loaded on a SD 75 10/300 GL equilibrated in buffer C and the purity was afterwards confirmed by SDS-PAGE (**3.1.4.2**).

3.2.8 *In vitro* activity assays

All reactions were analyzed by SDS-PAGE and Coomassie or silver staining (**3.1.4.2**) or by Western blotting (**3.2.2**). If needed, appropriate reaction products were quantified with ImageJ [137] and normalized to the amount of input enzyme (minus ATP). The means and standard deviations from three independent experiments were plotted.

3.2.8.1 Isopeptide bond formation assay

To monitor the formation of unattached ubiquitin chains and E6AP auto-ubiquitination *in vitro* activity assays were performed. Hereby, different ratios of UBA1, different E2 enzymes and ubiquitin variants were mixed in the absence or presence of the respective HECT E3 construct in reaction buffer of different pH values and different salt concentrations at various temperatures for 1 min up to 6 h (precise buffer and reaction conditions are listed in the respective figure legend). All reactions were quenched with reducing SDS loading dye.

3.2.8.2 Single-turnover assays from UBE2L3 to E6AP HECT domain

Thioester transfer of ubiquitin from the E1 (UBA1) to the E2 (UBE2L3) was monitored by incubating 1 µM UBA1, 10 µM UBE2L3, and 200 µM ubiquitin WT or variants thereof in 50 mM Tris/HCl, pH 7.0, 75 mM NaCl, 10 mM $MgCl_2$, and 2 mM ATP at 30 °C for 30 sec to 120 sec. All reactions were quenched by addition of non-reducing SDS loading dye.

3.2.8.3 Single-turnover assays from UBE2L3 to E6AP HECT domain

To monitor ubiquitin transfer from UBE2L3 to E6AP HECT domain single-turnover assays were performed [98]. 1 µM UBA1, 10 µM UBE2L3 and 200 µM ubiquitin variant were incubated in 50 mM Tris/HCl, pH 7.0, 75 mM NaCl, 10 mM $MgCl_2$ and 2 mM ATP at 30 °C for 30 min. The reactions were quenched by 4-fold dilution including 25 mM EDTA on ice and the UBE2L3~ubiquitin conjugate was then incubated with 5 µM of different E6AP HECT domain wild-type or variants for 15 sec to 60 sec. The reactions were quenched by addition of non-reducing SDS loading dye.

3.2.8.4 Single-turnover assays between two E6AP HECT domain molecules

Reaction buffer	50 mM HEPES, 7.5, 200 mM NaCl, 2 mM DTT, 5 mM $MgCl_2$, 2 mM ATP

To monitor if ubiquitin chains are pre-assembled on the active site of E6AP prior to substrate ubiquitination single-turnover assays were performed. Therefore, in one approach UBA1, UBE2D3 and E6AP HECT domain C820K/C820S were incubated with ubiquitin WT in reaction buffer for 30 min at 30 °C. In a second approach UBA1, UBE2L3 and E6AP HECT WT/K549R K688R K847R were mixed with ubiquitin K48R at 30 °C for 10 min, respectively. The reactions were quenched with 20 mM EDTA for 30 min on ice. Then, the corresponding approaches were mixed together and incubated at 30 °C for 1 h. All reactions were quenched by addition of reducing SDS loading dye.

3.2.8.5 ΔGG Assay

To test the effects of mutations in the donor and acceptor ubiquitin full-length ubiquitin and His_6- $Ub^{\Delta GG}$ variants were mixed at 100 µM concentration (each) with 0.2 µM UBA1, 2 µM UBE2L3, and 2 µM E6AP HECT domain in 50 mM Tris/HCl, pH 7.0, 75 mM NaCl, 10 mM $MgCl_2$, and 2 mM ATP at 30 °C for 60 min.

3.2.9 Nuclear magnetic resonance spectroscopy

Buffer	75 mM sodium phosphate, pH 7.4, 10% D_2O, ± 5 mM DTT /2 mM TCEP

All nuclear magnetic resonance spectroscopy (NMR) experiments were performed at 25 °C on a Bruker DRX 700 MHz spectrometer equipped with a triple-resonance z-axis gradient $^{1}H/^{15}N/^{13}C$ cryo-probe at the University of Bayreuth. All NMR spectra were recorded in the presence of 10% (v/v) D_2O. Data processing was performed using NMRPipe and chemical shifts were analyzed using the program NMRViewJ (One Moon Scientific). Backbone resonance assignments for the E6AP C-lobe and ubiquitin, respectively, were taken from the Biological Magnetic Resonance Bank (BMRB) [218] (BMRB accession number 5013 [240] and 17437 [233]). ^{15}N-enriched proteins were produced in M9 medium, and extensively dialyzed into exact the same buffer as the unlabelled protein (if required the pH-value was adjusted). Titration experiments were performed by mixing two stock solutions containing the same concentration of ^{15}N-enriched protein and either no ligand, or a maximum concentration thereof. The two stocks were mixed to yield the desired protein-ligand ratios. In case of ^{15}N-enriched E6AP C-lobe variants, 200 µM C-lobe variant was mixed with up to 12 mM unlabeled ubiquitin variant. 200 µM ^{15}N-enriched ubiquitin variant was mixed with a maximal concentration of 2.5 mM unlabeled C-lobe. Phase-sensitive gradient-enhanced ^{1}H-^{15}N HSQC [155] and BEST-TROSY [64] spectra were acquired for ubiquitin and E6AP, respectively. Weighted combined chemical shift perturbations, $\Delta\delta(^{1}H^{15}N)$, were calculated according to **Equation 4**.

$$\Delta\delta(\,^{1}\mathrm{H}^{15}\mathrm{N}) = \sqrt{(\delta(\,^{1}\mathrm{H}) - \delta(\,^{1}\mathrm{H})_0)^2 + 0.04 \cdot (\delta(^{15}\mathrm{N}) - \delta(^{15}\mathrm{N})_0)^2}$$

Equation 4: Calculation of weighted combined chemical shift perturbations. $\delta(^{1}H)/(^{15}N)$: $^{1}H/^{15}N$ chemical shift of the perturbed spectrum; $\delta(^{1}H)_0/(^{15}N)_0$: $^{1}H/^{15}N$ chemical shift of the unperturbed spectrum (without ligand).

In the case of the E6AP C-lobe, missing values are due to proline residues (793, 809, 815, 827) or missing assignments (820, 764) or broadening of peaks (801, 819). In the case of ubiquitin, gaps are due to proline residues (19, 37, 38).

The dissociation constant, K_D, in the case of a bimolecular binding reaction is defined by the law of mass-action **(Equation 5)**.

$$K_D = \frac{[P]\cdot[L]}{[PL]}$$

Equation 5: Definition of K_D. [P] denotes the concentration of the free protein (here: E6AP C-lobe), [L] the concentration of the free ligand (here: ubiquitin), and [PL] the concentration of the formed complex in equilibrium.

$[P_{tot}]$ denotes the total concentrations of protein and $[L_{tot}]$ the total concentrations of the ligand. They are composed of the respective free and bound concentrations. Thus, **Equation 5** can be restated to **Equation 6**.

$$K_D = \frac{([P_{tot}] - [PL]) \cdot ([L_{tot}] - [PL])}{[PL]}$$

Equation 6: Definition of K_D. With $[P_{tot}]$ denoting the total concentration of protein or $[L_{tot}]$ that of ligand.

$$[PL] = \frac{([P_{tot}] + [L_{tot}] + K_D) \pm \sqrt{([P_{tot}] + [L_{tot}] + K_D)^2 - 4 \cdot [P_{tot}] \cdot [L_{tot}]}}{2}$$

Equation 7: Solvation of Equation 6 for [PL].

Since in the case of my experiments bound and free states exchange fast on the NMR timescale for most resonances, the binding-induced chemical shift perturbations ($\Delta\delta(^1H^{15}N)$) are linearly dependent on the fraction of protein in the ligand bound state **(Equation 8)**.

$$\Delta\delta(^1H^{15}N) = \Delta\delta(^1H^{15}N)_0 + (\Delta\delta(^1H^{15}N)_{max} - \Delta\delta(^1H^{15}N)_0) \cdot \frac{[PL]}{[P_{tot}]}$$

Equation 8: Linear dependency of the binding-induced chemical shift perturbations on the C-lobe-ubiquitin complex. $\Delta\delta(^1H^{15}N)_{max}$ denotes the maximum experimental signal observed at 100% saturation of C-lobe with ubiquitin and $\Delta\delta(^1H^{15}N)_0$ denotes the signal from free C-lobe in the absence of ubiquitin.

K_D-values could be estimated by globally fitting the binding curves for individual resonances to a single-site model given by **Equation 9**.

$$\Delta\delta(^1H^{15}N) = \Delta\delta(^1H^{15}N)_{sat}(([P_{tot}] + [L_{tot}] + K_D) \pm \sqrt{([P_{tot}] + [L_{tot}] + K_D)^2 - 4 \cdot [P_{tot}] \cdot [L_{tot}]})/2 \cdot [P_{tot}]$$

Equation 9: Calculation of K_D-values. $\Delta\delta(^1H^{15}N)$ defines a weighted combined chemical shift perturbation. $[P_{tot}]$ and $[L_{tot}]$ denote the concentrations of ^{15}N-enriched protein and unlabeled protein, respectively.

In addition BEST-TROSY [64] spectra were acquired for the disulfide linked E6AP C-lobe~Ub complex by comparing the BEST-TROSY spectra of ^{15}N-labeled C-lobe (reference spectra) with those in complex with unlabeled ubiquitin G76C and in addition of 3 mM free ubiquitin WT, respectively.

3.2.10 Fluorescence polarization

Reaction buffer	20 mM HEPES, pH 7.2, 200 mM NaCl, 5% glycerol, 1 mM TCEP
FP buffer	20 mM HEPES, pH 7.2, 200 mM NaCl, 1 mM TCEP, 0.01% Triton-X 100

The fluorescence polarization (FP) assays were carried out by Dr. Bodo Sander according to Maspero et al. [143]. Thiol-reactive fluorescent probe BODIPY® TMR C5-maleimide (Thermo Fisher Scientific) was dissolved in DMSO and conjugated to ubiquitin G76C in reaction buffer at 4 °C. In the overnight reaction ubiquitin G76C was incubated with a 10-fold molar excess of the dye. Separation of the fluorophore was achieved by three rounds of dialysis and subsequent SEC performed with a HiLoad 16/600 SD 75 (GE Healthcare) equilibrated in reaction buffer.

FP assays were carried out at RT in FP buffer in 96-well flat-bottom microplates (Greiner Bio-One) using the Clariostar microplate reader (BMG LabtecH) at 540 nm excitation and 590 nm emission wavelengths. The peptide concentration was 50 nM, the protein concentrations varied from 0 to 500 µM. Polarization readings from three independent experiments were averaged and fitted as described in Sander et al. [198].

3.2.11 Trypsin digestion and high resolution and accurate mass spectrometry analysis

Reactions were separated by SDS-PAGE (12% NuPAGE Bis-Tris gels; Thermo Fisher Scientific) and in-gel trypsin digestion was performed by my collaboration partners Kirandeep Deol and Prof. Eric Strieter (University of Massachusetts, Amherst, MA/USA) [175]. Extracted peptides were frozen and dried to completion in a speed-vac. Samples were then spiked with ubiquitin AQUA peptides (Cell Signaling Technology) and oxidized with 0.15% TFA/0.3% hydrogen peroxide at 4 °C for 12 hours.

Peptides were separated using an Easy nLC 1000 UHPLC (Thermo Fisher Scientific) equipped with a homemade ProntonSIL C18 (75 µm x 15 cm) column. A linear gradient of 0% to 50% of solvent B over solvent A for 30 min, 50% to 95% of solvent B for 3 min, and 95% hold of solvent B for 7 min (solvent A: 0.1% formic acid (FA) in water; solvent B: 0.1% FA in acetonitrile (ACN) was applied with a flow rate of 300 nl/min. For HR/AM AQUA analysis the UHPLC system was coupled with an Orbitrap Fusion Tribid Mass Spectrometer (Thermo Fisher Scientific). The resolving power of the mass analyzer was set to 60000; spectra were recorded over a range of 300 to 1500 m/z. For data-dependent MS/MS, the top 4 most intense ions with charge states of 2 to 5 were selected using an isolation window of 2 m/z. Fragmentation was achieved by collision-induced dissociation (CID) at 35% nominal energy with product ion detection in the linear ion-trap. Ion chromatograms were extracted for each ubiquitin peptide of interest with a window of 5 ppm. Chromatograms were smoothed using

the Boxcar algorithm with a 7-point window. Integration was performed using default parameters with manual adjustment, as appropriate. Results were normalized to the total amount of ubiquitin for each linkage type detected and represented from three replicates.

3.3 X-ray crystallography

3.3.1 Protein crystallization and data collection

X-ray crystallography is a method to determine the three-dimensional structure of macromolecules to very high resolution [14, 28, 183, 194]. Therefore, pure protein samples were diluted to the desired concentration (2 to 60 mg/ml) using the respective purification buffer and centrifuged for 30 min at 20.000 rpm at 4 °C. In case of co-crystallization attempts, the components were mixed in a molar ratio of 1:1 and incubated for at least 30 min on ice before centrifugation. High-throughput crystallization screening was performed via the sitting drop vapor diffusion method in a sealed airtight 96 well crystallization plate (Greiner Bio-One). Using a crystallization robot (Analytic Honey Bee 963 (Genomic Solutions)), 0.3 µl protein solution were mixed automatically with 0.3 µl mother liquor of different commercially available sparse-matrix screens **(Table 6)** to generate the crystallization drop and equilibrated against 40 µl mother liquor. The plate was sealed with adhesive film and stored at 20 °C (or 4 °C). Crystal formation was examined on a daily basis within the first two weeks and then once a week using the microscope SteREO Discovery.V12 (Zeiss). Initial promising conditions were chosen for manual fine screening in a 24-well plate via the hanging drop method by varying the concentration of precipitant or pH. Therefore, the different protein-precipitant solutions (1 µl of each) were pipetted on a cover slide, which was then flipped and sealed the reservoir well containing 500 µl mother liquor. Crystallization attempts of N-terminal extended E6AP HECT domain constructs (3-25 mg/ml), the isolated HECT domain alone (5-10 mg/ml), in complex with ubiquitin/di-ubiquitin (5-10 mg/ml) or ubiquitin+UBE2L3 (10 mg/ml), as well as the conjugate of E6AP C-lobe disulfide linked to ubiquitin were unsuccessful (2-8 mg/ml). Only crystals for ubiquitin, E6AP C-lobe dimer (60 mg/ml) and the disulfide-linked NEDD4 C-lobe~ubiquitin G75C conjugate (10 mg/ml) were obtained. These crystals were harvested from the crystallization drop using a nylon loop, cryo-protected with mother liquor containing 10 to 25% ethylene glycole or glycerol and plunged in liquid nitrogen. Diffraction data were collected on BL14.1 at the BESSY II electron storage ring operated by the Helmholtz-Zentrum Berlin [157]. All data were collected at cryogenic temperature of 100 K using the single axis rotation method and a PILATUS detector. Two initial diffraction images were collected rotated by 1° one at the initial position (0°) and the other one after a 90° rotation. The crystal lattice

was indexed using MOSFLM and an appropriate collection strategy calculated to minimize exposure time and avoid radiation damage [10, 125, 237].

3.3.2 Structure determination and refinement

Individual reflections were indexed and integrated with XDS [97]. Crystallographic screw axes in a given space group were identified using POINTLESS (Collaborative Computational Project 1994 (CCP4 program suite)) [61]. Depending on the data quality indicators (R_{merge}: measure of internal consistency, R_{meas}: multiplicity weighted, $R_{p.i.m.}$: precision indicating merging R factor, $<I/\sigma(I)>$: signal-to-noise ratio at the cutoff level, $CC_{1/2}$: Pearson correlation coefficient between random half datasets). AIMLESS (CCP4 program suite) was used to reduce and scale the data [50, 228, 229]. The number of molecules in the asymmetric unit were estimated by calculation of the Matthews coefficient [147].

Initial phases for the different datasets were determined by molecular replacement (MR) using PHASER (CCP4 suite or Phenix module) [148] and the respective search models (PDB ID: 1UBQ, 1C4Z, 4BBN [85, 144, 221]). For complexes, MR was performed on the basis of an ensemble of structures. With the initial phase information, the resulting model was refined and manually completed using COOT [59]. Successive rounds of model building and automated refinement using REFMAC5 [160] or PHENIX.refine [2] were performed until the R_{free} and R_{work} values converged. MolProbity was used for structure validation [31]. Electron density maps were generated with the phenix.maps tool [2]. All images of crystal structures were created with PyMOL (Open source, V1.7.6; DeLano Scientific LLC).

4 Results and Discussion

4.1 Expression and purification of different E6AP constructs

According to the crystal structure of the E6AP HECT domain [85], the sequence of the equivalent gene was cloned in a vector with a N-terminal 3C-cleavable His_6-tag. The boundaries of the C-lobe and N-lobe constructs, respectively, were defined through their secondary structure within the bilobal arrangement of the HECT domain covering the complete HECT domain sequence.

The individual steps of the protein expression and purification were followed by SDS polyacrylamide gel electrophoresis (PAGE) as shown for the E6AP HECT domain WT in **Figure 11A**. The same procedure was used for all E6AP constructs, including the HECT domain, N-lobe and C-lobe, and all corresponding variants with amino acid substitutions or deletions. *E. coli* BL 21 (*DE3*) cells were transformed with the respective expression plasmids and recombinant protein production was induced with IPTG. After shaking overnight, a strong band appeared in lane 2 with a molecular weight of about 45 kDa compared to the sample 'before induction' (lane 1) indicating a successful overexpression of the His_6-tagged E6AP HECT domain.

After harvesting, 20-30 g of *E. coli* cell pellet was re-suspended in lysis buffer and cell lysis was performed by sonication. Cell fragments were pelleted (lane 4), while the overexpressed protein remained mainly in the soluble fraction (lane 3). The cleared supernatant was applied to a 5 ml HisTrap HP IMAC column. Thereby His_6-tagged protein was bound to the Ni^{2+}-chelate matrix, while endogenous *E. coli* proteins that do not bind to the column could be removed. There was only a weak band for the His_6-tagged protein in the flow-through indicating that the binding capacity of the HisTrap column was already at its limit (lane 5). During consecutive washing, steps small amounts of the fusion protein were removed (lane 6). The His_6-tagged protein was eluted with an imidazole gradient (lane 7), and the respective elution profile is shown in **Figure 11B**.

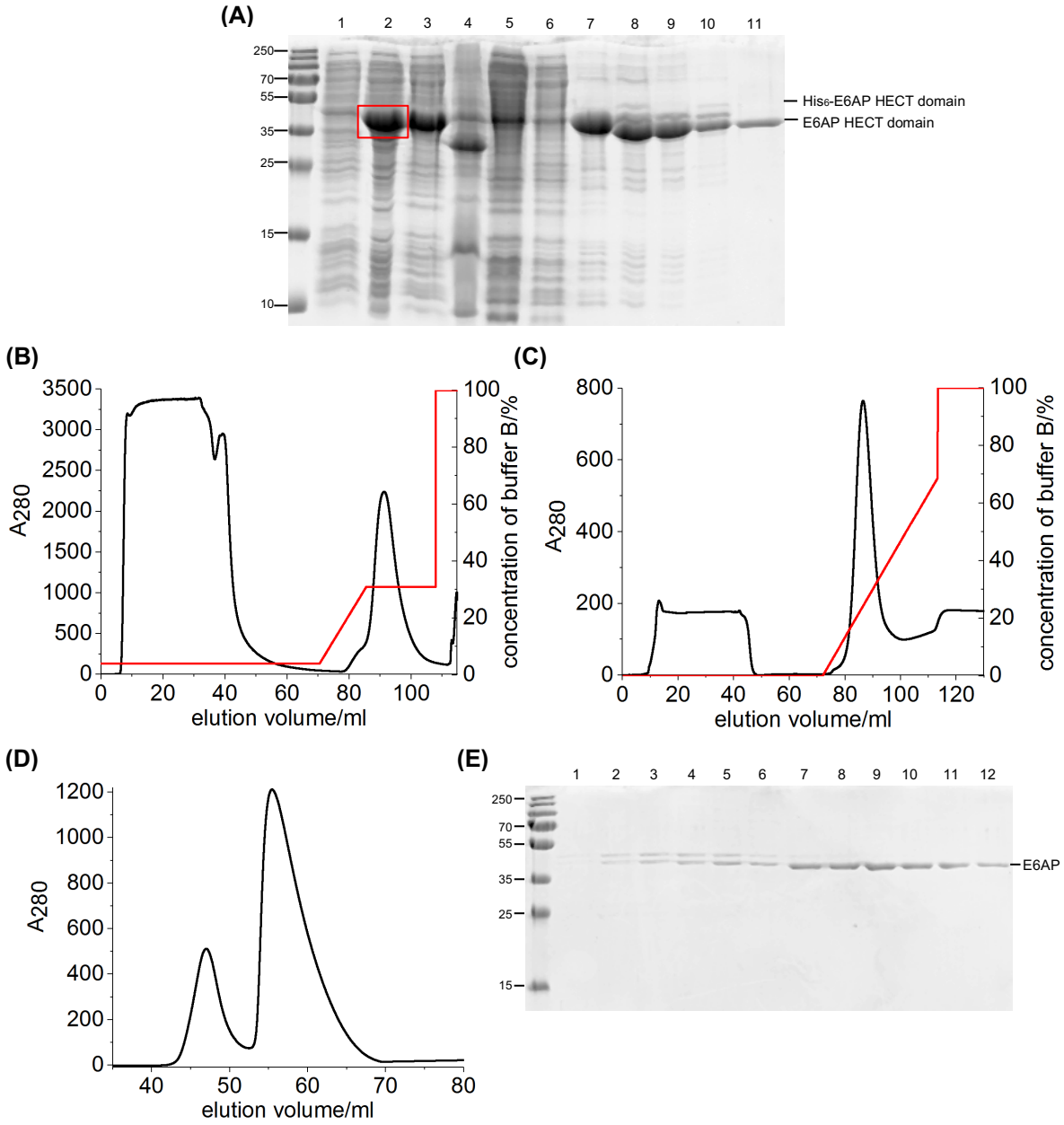

Figure 11: Purification of the HECT domain of E6AP. (A) SDS-PAGE of the purification of E6AP HECT domain WT. 1: before induction; 2: after induction (recombinantly expressed protein is highlighted); 3: supernatant; 4: pellet fraction; 5: flow-through of 1.Ni-NTA chromatography; 6: wash fraction of 1.Ni-NTA chromatography; 7: eluate of 1.Ni-NTA chromatography; 8: after dialysis; 9: flow-through of 2.Ni-NTA chromatography; 10: eluate of 2.Ni-NTA chromatography; 11: concentrated protein after SEC. **(B)**, **(C)** 1. and 2. Ni-NTA chromatography steps (black line: absorption at 280 nm; red line: concentration of buffer B in percent). **(B)** 1.Ni-NTA chromatography: E6AP HECT domain was eluted from the affinity matrix with 150 mM imidazole. **(C)** 2.Ni-NTA chromatography: the cleaved protein eluted in the flow-through. With increasing concentration of buffer B, the His_6-tagged-3C protease, the His_6-tag and non-cleaved protein eluted. **(D)** SEC with a HiLoad SD 16/600 75 pg in 50 mM Tris/HCl, pH 7.5, 75 mM NaCl, 2 mM DTT and **(E)** corresponding SDS-PAGE: every fraction from 48 ml to 72 ml.

The eluate was dialyzed overnight in the presence of the His_6-3C protease to remove the His_6-tag (lane 8). The dialysate was then subjected to a second Ni-NTA-column to separate the cleaved protein (~42 kDa; in the flow-through) from His_6-3C protease, cleaved His_6-tag

(not-visible) and remaining non-cleaved His_6-tag fusion protein (lane 9). Unfortunately, the separation of the cleaved and non-cleaved protein was incomplete as indicated by a slight band running above the main cleaved fraction. This might have occurred through a portion of the His_6-tagged protein being either folded in such a way that the tag is buried within the protein itself or by a transient oligomerization with another molecule of E6AP. Thus, the affinity tag might have been inaccessible for the affinity matrix, and the tagged protein eluted in the flow-through. Upon addition of imidazole (lane 10), three bands corresponding to His_6-3C (~50 kDa) and His_6-E6AP HECT domain (~45 kDa) as well as untagged E6AP HECT domain (~42 kDa) were present in the eluate of the second Ni-NTA column. This would also point to a transient interaction of untagged and tagged protein, resulting in co-elution of the complex **(Figure 11C)**.

Through the finale preparative size exclusion chromatography (SEC), untagged monomeric HECT domain (second peak) could be separated from the higher molecular weight His_6-tagged protein (first peak) as well as from minor contaminations (lane 11) **(Figure 11D, E)**. At an elution volume of 45 ml to 55 ml the His_6-tagged protein eluted (lane 1 to 6), whereas the desired untagged protein eluted at 55 ml (lane 2 to 12) **(Figure 11D, E)**. The elution volume of the second peak corresponds to a globular monomeric protein of ~40 kDa size. Therefore, only the protein containing fractions of the second peak were combined, concentrated up to 500 μM and aliquoted into 50 μl samples for analysis.

These protein batches were either used directly or stored after flash-freezing in liquid nitrogen at -80 °C. Proteins were prepared with a yield of around 50 mg per liter of bacterial culture. All E6AP HECT domain, C-lobe and N-lobe variants included in these studies expressed similar amounts of protein.

The phenomenon of two separate peaks eluting in the final SEC with a HiLoad SD 16/600 75 pg, could be observed for all HECT domain variants and for the isolated N- or C-lobe **(Figure 12A, B)**. This indicates a potential – at least transient – oligomerization of E6AP in contrast to NEDD4 HECT domain which eluted as a monomeric protein **(Figure 12C)** in the preparative SEC. The tendency to oligomerize might also arise from the very high protein concentrations which were obtained for the different E6AP constructs (~30 mg/ml) compared to the moderate protein yields of NEDD4 proteins (~10 mg/ml). The oligomerization behavior of E6AP HECT domain will be investigated in section **4.2**. For all other experiments, the monomeric protein eluting in the second peak was used solely.

The ubiquitin variants and the different E2 enzymes were purified as described elsewhere [47, 198, 233].

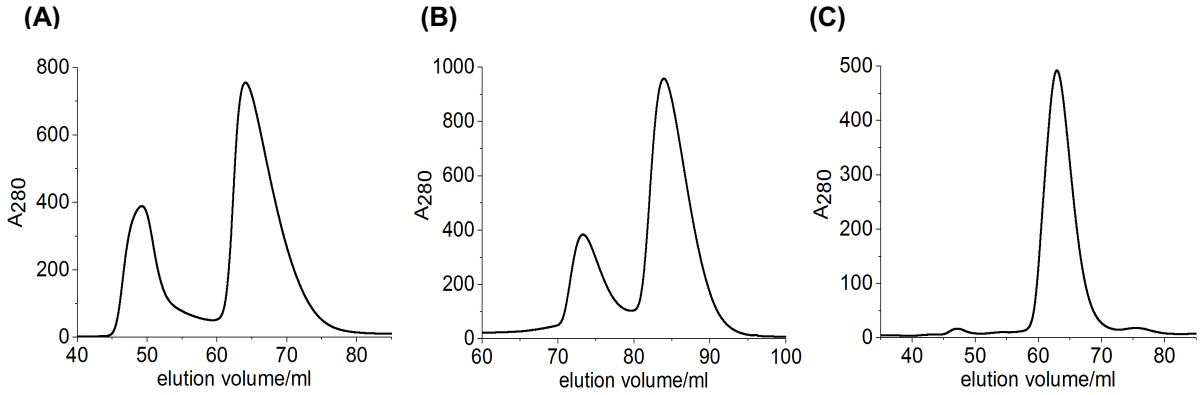

Figure 12: SEC of different E6AP constructs and NEDD4 HECT domain. (A) SEC elution profile of E6AP N-lobe, **(B)** E6AP C-lobe, **(C)** NEDD4 HECT domain. All SEC runs were performed with a HiLoad SD 16/600 75 pg at 4 °C. **(A)** and (**B)** were performed in 50 mM Tris/HCl, pH 7.5, 75 mM NaCl, 2 mM DTT and **(C)** in 100 mM HEPES, pH 7.5, 300 mM NaCl, 2 mM DTT.

4.2 Oligomerization behavior of the E6AP HECT domain

4.2.1 The isolated E6AP HECT domain is monomeric in solution

To figure out whether the observed transient interaction between untagged and tagged HECT domain reflects an oligomerization of E6AP HECT domain, I pooled the fractions from the first peak (fraction 1 to 5, **Figure 11E**) and from the second peak (fraction 9 to 11, **Figure 11E**), individually, concentrated them to 5 mg/ml and applied both samples to multi-angle light scattering (MALS) to determine the molecular weight of both samples in solution **(Figure 13A, B)**. The molecular mass (M_W) of the protein eluting in the first peak was 70.6 ± 15.4 kDa **(Figure 13A)** and 45.0 ± 2.2 kDa for the protein eluting in the second peak **(Figure 13B)**. Thus, the SEC-MALS experiments revealed that while the protein deriving from the second peak behaved as a monomer (M_W of monomeric E6AP HECT domain without His_6-tag): 42.07 kDa), the protein eluting in the first peak might exhibit mixed populations of monomers and dimers between the His_6-tagged and untagged version of E6AP HECT domain (M_W of monomeric E6AP HECT domain with His_6-tag: 44.22 kDa). Since different higher oligomers eluted prior to the protein deriving from the first peak **(Figure 13A)**, the determined molecular mass is influenced by those, as indicated by the constantly decreasing mass distribution across the protein peak. This would be in line with more His_6-tagged protein behaving as a monomer rather than forming a dimer with the untagged HECT domain.

To exclude the effect of different salt concentration potentially altering the oligomeric state of the HECT domain of E6AP, the monomeric protein was dialyzed in the presence of various salt concentrations (ranging from 50 mM to 1 M NaCl) at 4 °C overnight. Then the different samples were applied to aSEC **(Figure 13C)**. These experiments showed no significant shift of one of the samples with different salt concentrations. Running a protein standard in parallel revealed an elution volume corresponding to a 44 kDa globular protein, confirming the monomeric state of all samples. This result implies that the salt concentration did not influence the oligomerization behavior of the E6AP HECT domain. In addition, I could not detect a concentration dependent oligomerization of the E6AP HECT domain. At twice the concentration, the E6AP HECT domain showed the same elution profile, but with higher absorption values **(Figure 13D)**.

Thus, it seems that the used construct of isolated E6AP HECT domain does not have a tendency to oligomerize in solution under the tested conditions. The observed co-elution of tagged and untagged protein during purification might have been due to the very high protein concentrations promoting transient oligomerization rather than having a role for E6AP at moderate concentrations.

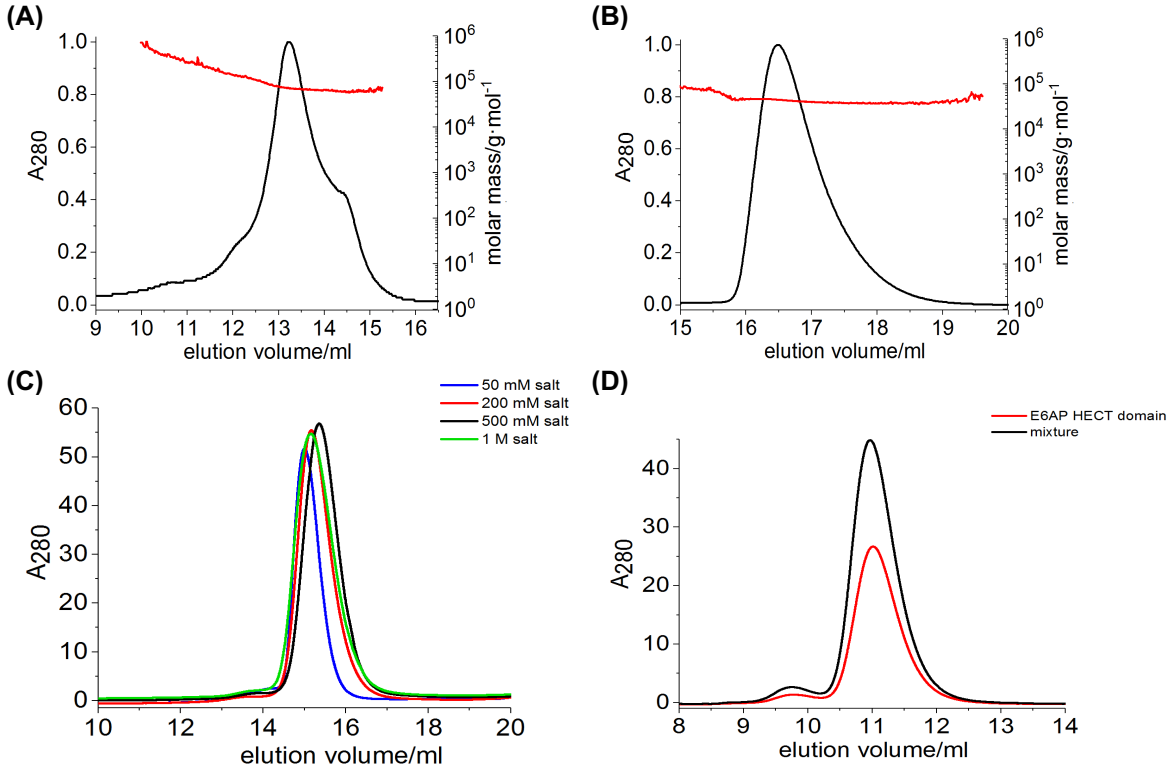

Figure 13: The isolated E6AP HECT domain is monomeric in solution. SEC-MALS elution profiles of 5 mg/ml protein **(A)** eluting in the first peak or **(B)** in the second peak of the preparative SEC of E6AP HECT domain WT **(Figure 11D)** with a HiLoad SD 200 10/300 GL in 50 mM Tris/HCl, pH 7.5, 200 mM NaCl, 2 mM DTT at RT. The RI signal (red line) indicates homogenous protein with an apparent M_W of **(A)** 70.6 ± 15.4 kDa and **(B)** 45.0 ± 2.2 kDa. **(C)** aSEC experiments of 80 μM monomeric protein sample dialyzed in different salt concentrations as indicated. aSEC experiments were performed with a HiLoad SD 200 10/300 GL in 50 mM Tris/HCl, pH 7.5, 0.05 M to 1 M NaCl, 2 mM DTT. **(D)** aSEC experiments of 25 μM E6AP HECT domain WT mixed with 25 μM E6AP HECT domain WT at RT for 1 h and loaded onto a HiLoad SD 75 10/300 GL in 50 mM Tris/HCl, pH 7.5, 200 mM NaCl, 2 mM DTT.

4.2.2 Influence of the α1'-helix

Apart from E6AP, all available structures of HECT domains contain a region N-terminal to the HECT domain, which was truncated in the E6AP HECT domain used for the original crystallization [85]. In the crystal structure it forms a trimer, which differs from the arrangements seen in other HECT domain crystal lattices. It is controversial if the crystallographic E6AP trimer is a crystallization artifact or a functionally relevant state. In fact, the trimerization interface in the crystal structure of E6AP involves the N-terminal region of the construct and would be incompatible with the presence of an N-terminal extension (if positioned in a similar manner as in other HECT ligases, **Figure 10B**). The residues of the N-terminal helix are conserved in over 20 HECT domain sequences analyzed thus far including E6AP, suggesting that this helix is a common structural feature of HECT domains. But the structural role of the helix during interactions with target proteins remains so far largely unknown. To obtain structural information for this helix of E6AP and to unravel the oligomeric state of E6AP in its presence, I generated different N-terminally extended E6AP HECT

domain constructs guided by secondary structure predictions using Phyre^2 [104]. Since flexible and unstructured regions within the protein are unfavorable for protein expression, the different designed constructs started in the vicinity of predicted α-helical regions (construct 2-5) or included the identified interaction module of the Hepatitis C virus (HCV) core protein, a known E6AP substrate (construct 1) **(Figure 14)**.

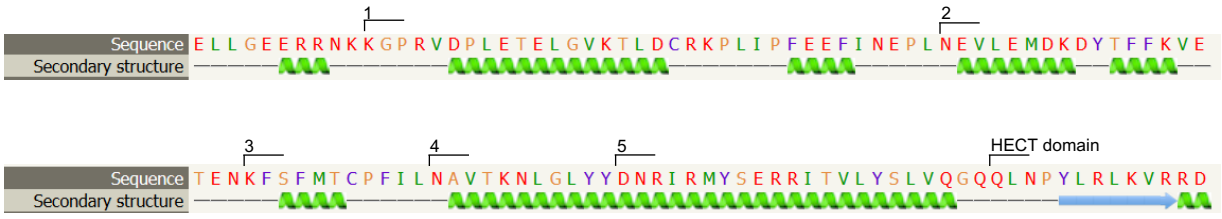

Figure 14: N-terminally extended expression constructs of the E6AP HECT domain. Secondary structure prediction of the region N-terminal to the HECT domain using Phyre^2 [104]. Construct no. 1 starts at aa 403, no. 2 at aa 432, no. 3 at aa 451, no. 4 at aa 462 aa, and no. 5 at aa 471 (according to the N-terminal extended HUWE1 construct [169]). The N-terminal border of the crystallized E6AP HECT domain (PDB ID: 1C4Z [85]) is also shown.

Extensive expression trials with the five N-terminally extended constructs in different *E. coli* cell lines, in different expression vectors, and with different solubility tags were performed. In **Table 10** the different expression combinations are summarized. While most constructs were found to be insoluble, a SUMO-tagged version of construct no. 5 was soluble, but eluted in the void volume in the preparative SEC. This indicates that the protein is in the form of a higher oligomer or aggregate. Screening for suitable buffer conditions using thermofluor did not give any hits. Also, the introduction of the autism mutation T485A (and the phospho-mimetic variant T485E) in the context of the His_6-SMT3 construct no. 5 led to soluble protein, but it eluted also in the void volume in SEC. Using the DrawCoil 1.0 program [75] to create a diagram of the predicted helix, which is formed by the α1'-helix region of E6AP (ranging from residue Asp473 to Val491), a very hydrophobic region including residues Tyr479 and Val486 is formed **(Figure 15A)**. Based on these findings, I introduced a glutamate residue at position 479 (Y479E) to make this coiled region possibly more stable. Indeed, this single point mutation improved the solubility of the N-terminally extended E6AP HECT construct drastically. Construct no. 5 Y479E with only a His_6-tag eluted as a monomer in SEC, but the yield was very low. After upscaling of the expression, sufficient protein for crystallization trials could be obtained. The purification of His_6-SMT3-tagged construct no. 5 Y479E without removal of the His-SUMO tag (since removal of the tag decreased the solubility drastically) yielded a high amount of pure protein in a monomeric state (60 mg; **Figure 15B-D**). Thermofluor analyses of the cleaved protein were performed to screen for better buffer conditions but did not reveal appropriate conditions to stabilize the protein. Extensive

crystallization trials with either of the two differentially tagged constructs and the Y479E substitution were unsuccessful.

Table 10: List of the expression trials

construct no. (starting residue)	vector, purification-tag, aa mutation	*E. coli* cell line	soluble protein
construct 1 (aa 403)	pSKB2 His_6	Rosetta pLysS	✗
	pCDF His_6-SMT3	Rosetta pLysS	✗
	pCDF His_6-SMT3 Y479E	Rosetta pLysS	✗
construct 2 (aa 432)	pSKB2 His_6	Rosetta pLysS	✗
	pCDF His_6-SMT3	Rosetta pLysS	✗
	pCDF His_6-TXR	Rosetta pLysS	✗
construct 3 (aa 451)	pSKB2 His_6	Rosetta pLysS	✗
		ArcticExpress (DE3)	✗
		BL21 (DE3) Gro7/KJE*	✗
	pCDF His_6-SMT3	Rosetta pLysS	✗
	pCDF His_6-TXR	Rosetta pLysS	✗
construct 4 (aa 462)	pSKB2 His_6	Rosetta pLysS	✗
		ArcticExpress (DE3)	✗
		BL21 (DE3) Gro7/KJE*	✗
	pCDF His_6-SMT3	Rosetta pLysS	✗
	pCDF His_6-TXR	Rosetta pLysS	✗
construct 5 (aa 471)	pSKB2 His_6	Rosetta pLysS	✗
		JM109 (DE3)	✗
		BL21 (DE3) Gro7/KJE*	✗
	pSKB2 His_6 Y479E	Rosetta pLysS	✓
	pCDF His_6-TXR	Rosetta pLysS	✗
	pCDF His_6-SMT3	Rosetta pLysS	✓
		BL21 SolBL	✓
	pCDF His_6-SMT3 Y479E	Rosetta pLysS	✓
	pCDF His_6-SMT3 T485A	Rosetta pLysS	✓
	pCDF His_6-SMT3 T485E	Rosetta pLysS	✓

Table 10 summarizes all constructs cloned in the respective expression vector with different purification tags, in different tested *E. coli* cell lines, and with additional amino acid substitutions (soluble protein: check; insoluble protein: cross). **E. coli* cell line which carries in addition a chaperone (KJE7 or Gro7) encoding vector (kindly provided by Prof. Andreas Martin, UC Berkeley, USA).

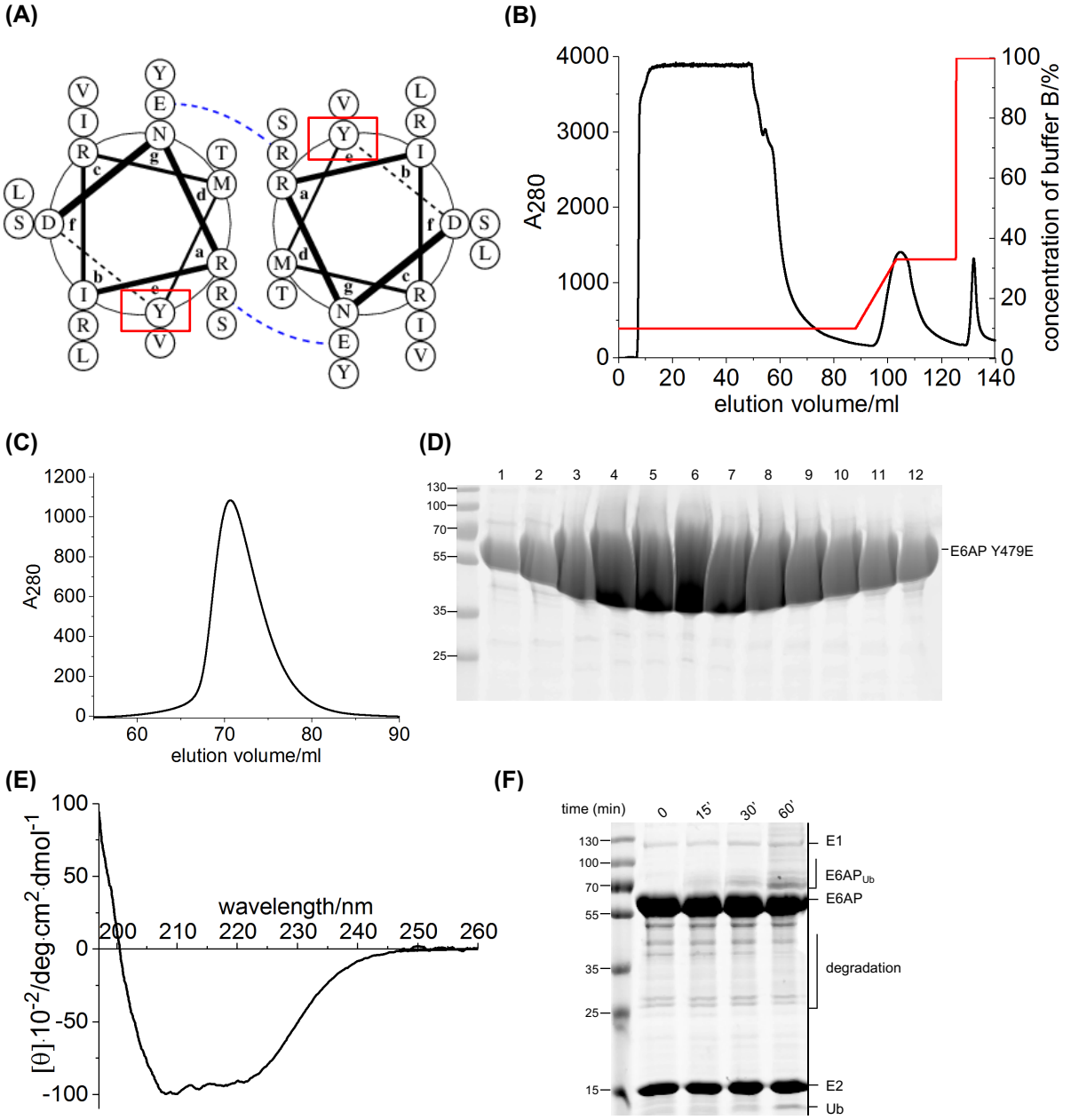

Figure 15: His$_6$-SMT3-tagged construct no. 5 Y479E is soluble, folded and active. (A) Helical wheel diagram generated with DrawCoil 1.0 [75] for the coiled coil domain of the predicted α1'-helix N-terminal to the E6AP HECT domain (starting with Asp473 to Val491). Tyr479 is highlighted. **(B)** Ni-NTA chromatography of His$_6$-SMT3-E6AP HECT domain construct no. 5 Y479E. **(C)** SEC with a HiLoad SD 16/600 200 pg in 50 mM Tris/HCl, pH 7.5, 75 mM NaCl, 2 mM DTT and **(D)** SDS-PAGE of the peak fractions (every 2 ml fraction from 68 to 80 ml). **(E)** CD spectrum of 4 μm of the His$_6$-SMT3-tagged construct no. 5 Y479E**.** The spectrum was recorded in 10 mM sodium phosphate, pH 7.4 at 10 °C. The resolution was 0.1 nm and the speed 50 nm/min. The bandwidth was 1 nm and the attenuation was 2 s (10 accumulations). **(F)** *In vitro* activity assay: 50 μM His$_6$-SMT3-tagged construct no. 5 Y479E was mixed with 1 μM UBA1, 50 μM UBE2L3 and 500 μM Ub in 50 mM Tris/HCl, pH 7.5, 200 mM NaCl, 2 mM DTT, 2 mM ATP, 5 mM $MgCl_2$ at 30 °C for 1 h monitored by SDS-PAGE and Coomassie staining.

To test whether the N-terminally extended construct is properly folded, a far-UV CD spectrum was recorded **(Figure 15E)**. Circular dichroism (CD) provides information of the unequal absorption of right- and left-circularly polarized light at asymmetric optical centers depending

on protein secondary structure elements/content [203]. In the far UV range from 170 nm to 260 nm, the signal is dominated by the contributions of the peptide bonds of the chiral amino acids (except for glycine). CD spectra with a maximum at 195 nm and minima at about 208 nm and 222 nm are characteristic of α-helical structures. The CD signal of a β-sheet is small and varies with its length and twist, and usually shows positive signals in the range of 190 nm to 200 nm. Minima near 196 nm point to unfolded or disordered structures (random coil) [203]. The deconvolution of a CD spectrum of a protein can theoretically yield the contributions of the individual secondary structure elements [20]. The spectrum of construct no. 5 Y479E has minima at about 208 nm and 222 nm. These minima point to a high fraction of α-helical structures. The signal below 200 nm is exclusively in the positive range, indicating that the protein is well ordered.

To find out whether the His_6-SMT3-tagged construct no. 5 Y479E is active I performed an isopeptide bond formation assay **(Figure 15F)**: The Y479E protein is active with respect to both auto-ubiquitination and free di-ubiquitin chain formation after a lag phase of 30 min. However, the protein heavily degraded under the tested conditions which might have also affected its ligase activity **(Figure 15F)**.

Taken together, these studies demonstrate that the N-terminally extended variants of the HECT domain either fused to the His_6- or His_6-SMT3-tag with the substitution Y479E eluted as a folded, active monomer. The prevalent aggregation during purification and the degradation in the activity assay imply that the hydrophobic, N-terminal extension of E6AP may be surface exposed. Possibly, it needs additional N-terminal regions to adopt its native conformation within the structure of the HECT domain. Thus, it remains unclear whether the α1'-helix plays a role for E6AP regulation, as it was shown for other HECT ligases [8, 169].

4.3 Mechanism of ubiquitin chain formation by E6AP

4.3.1 E6AP HECT domain auto-ubiquitinates *in vitro*

To obtain a comprehensive understanding of the structural mechanism of ubiquitin chain formation by E6AP *in vitro* activity assays were conducted. In the presence of the E1 (UBA1), the E2 UBE2L3 and ubiquitin, purified E6AP HECT domain can auto-conjugate ubiquitin to one or more of its lysine residues in the absence of a substrate and the N-terminal substrate binding region **(Figure 16A)**. The formed conjugates are stable to reducing agent, indicating that the isolated HECT domain can auto-ubiquitinate. Di-ubiquitin was the major free chain product, whereas longer Lys48-linked DTT-resistant chains were formed on lysine residues of E6AP HECT domain, as indicated by the disappearance of these chains using a K48R ubiquitin variant **(Figure 16A)**. E6AP HECT domain strongly prefers to build Lys48-linked ubiquitin chains as chain formation of free di-ubiquitin entities was significantly slower in the presence of ubiquitin K48R. In line with higher linkage specificity at lower pH value, unspecific free chain formation was almost completely prevented at pH values below 7 and shorter time points (as shown in **4.4.6**). Mutating the active site cysteine residue to an alanine eliminated the conjugation activities of E6AP, making it catalytically inactive (data not shown).

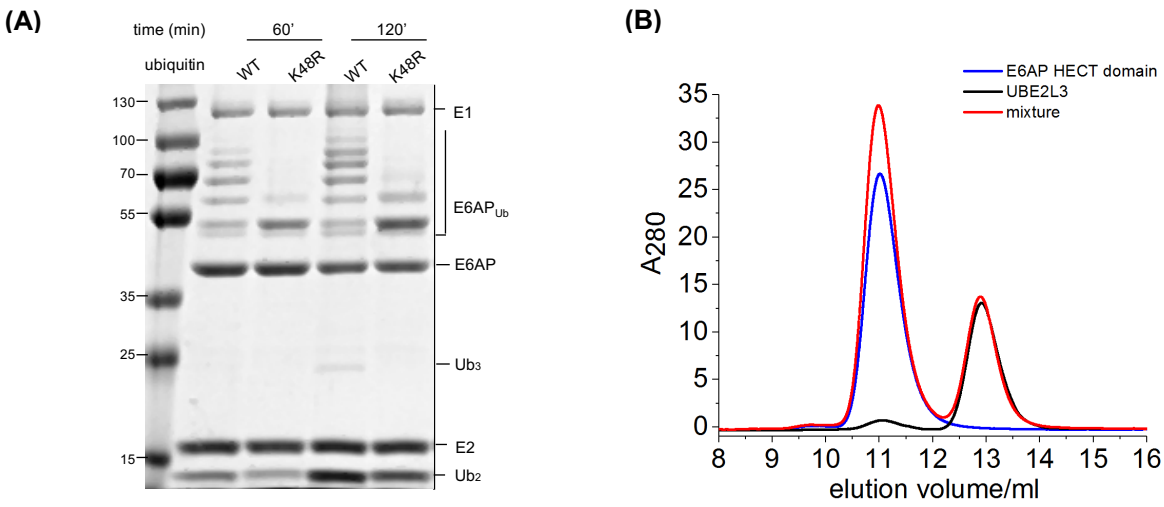

Figure 16: E6AP HECT domain functions with UBE2L3. (A) *In vitro* activity assay of 50 μM E6AP HECT domain WT with 1 μM UBA1, 50 μM UBE2L3 and 500 μM Ub WT or K48R in 50 mM Tris/HCl, pH 7.5, 200 mM NaCl, 2 mM DTT, 2 mM ATP, 10 mM $MgCl_2$ at 30 °C for 2 h monitored by SDS-PAGE and Coomassie staining. **(B)** aSEC elution profile of a 1:1 mixture of 200 μM E6AP HECT domain WT with 200 μM UBE2L3 (SD 75 10/300 GL in 50 mM Tris/HCl, pH 7.5, 200 mM NaCl, 2 mM DTT).

Using the isolated N-lobe or C-lobe respectively, neither auto-ubiquitination nor free ubiquitin chain formation could be observed with the E2 UBE2L3 (data not shown). Without the N-lobe, the E2-ubiquitin complex cannot be recruited to E6AP, thus no trans-thioesterification from the catalytic cysteine of the E2 enzyme to the catalytic cysteine of the E6AP C-lobe can

occur. Using the E2 enzyme UBE2D3 the isolated N-lobe became ubiquitinated after two hours. Since the N-lobe lacks the active site cysteine of the E3 enzyme, the N-lobe was apparently ubiquitinated directly by UBE2D3 (data not shown).

This agrees with the activity and thus the auto-ubiquitination of E6AP being dependent on the nature of the E2 enzyme. In contrast to the UBCH5 family (UBE2D1-3 and UBE2E1), UBE2L3 and UBE2L6, which were proposed to be the physiological E2 enzymes for E6AP [119], lack intrinsic, E3-independent reactivity with lysine residues [232]. Thus, it makes it unlikely that ubiquitin is transferred directly to a lysine residue of E6AP unless the binding to E6AP reprograms the E2 enzyme. UBE2D1-3 or UBE2E1 can react with either cysteines or lysine residues and therefore they can, in principle, transfer ubiquitin directly to a lysine residue within the HECT domain and of the isolated N-lobe of E6AP.

The dissociation constant for the interaction between E6AP and UBE2L3 was determined in the micromolar range by isothermal titration calorimetry (ITC; K_D = 2.2 µM) and fluorescence polarization assays (FP; K_D = 5.0 µM) [56, 57, 181]. However, I could not isolate a non-covalent complex with either the isolated N-lobe or the whole HECT domain and UBE2L3 by SEC **(Figure 16B)**. In the cell, however, co-localization of the two binding partners might favor such low-affinity protein complexes and thus ensure efficiency and directionality in the ubiquitination of substrates.

4.3.2 Auto-ubiquitination sites of the E6AP HECT domain

The E6AP HECT domain contains 24 lysine residues. With mass spec analyses seven auto-ubiquitination sites within the HECT domain of E6AP were identified **(Table 11)** (mass spec analysis were performed by the groups of Prof. Andreas Schlosser (RVZ, Würzburg) and Prof. Henning Urlaub, (MPI Göttingen)). Since the ubiquitination assays were performed with the E2 UBE2L3, which lacks intrinsic Lys reactivity [232], these lysine residues were ubiquitinated by E6AP itself.

Table 11: Auto-ubiquitination sites of the HECT domain of E6AP

mixture	ubiquitinated lysine residues
E6AP WT + UBE2L3 + ubiquitin K48R	Lys529, Lys530, Lys688, Lys799, Lys801, Lys806, Lys847

Table 11: Mass spec analysis were performed by the group of Prof. Schlosser (RVZ, Würzburg) and Prof. Urlaub (MPI Göttingen). After tryptic digest of the desired protein band extracted from the SDS-PAGE, peptides containing an additional di-glycine motif derived from ubiquitin were searched.

To analyze the effect of the auto-ubiquitination of E6AP, which could be crucial to modulate the catalytic activity of E6AP, individual substitutions of the seven lysine residues by arginine were performed. The variants were then subjected to *in vitro* activity assays. Seven of these eight Lys-to-Arg substitutions had no significant effect on auto-ubiquitination and free di-ubiquitin chain formation (data not shown). The variant K847R, however, showed a significant increase in activity, both in auto-ubiquitination of E6AP and in the formation of free ubiquitin chains **(Figure 17A)**. The same effect was detected for the substitution of Lys549 to Arg **(Figure 17A)**, which had not been found as an auto-ubiquitination site by mass spec. This could have been due to the tryptic peptide being too large for mass spec detection under the conditions applied. Since Lys549 is located within the N-lobe in immediate vicinity of the active site cysteine, it is conceivable that ubiquitination of this residue could occur readily *in cis*. It is also possible that a potential auto-ubiquitination of this lysine residue interferes with E6AP activity, for instance by hindering the C-lobe mobility.

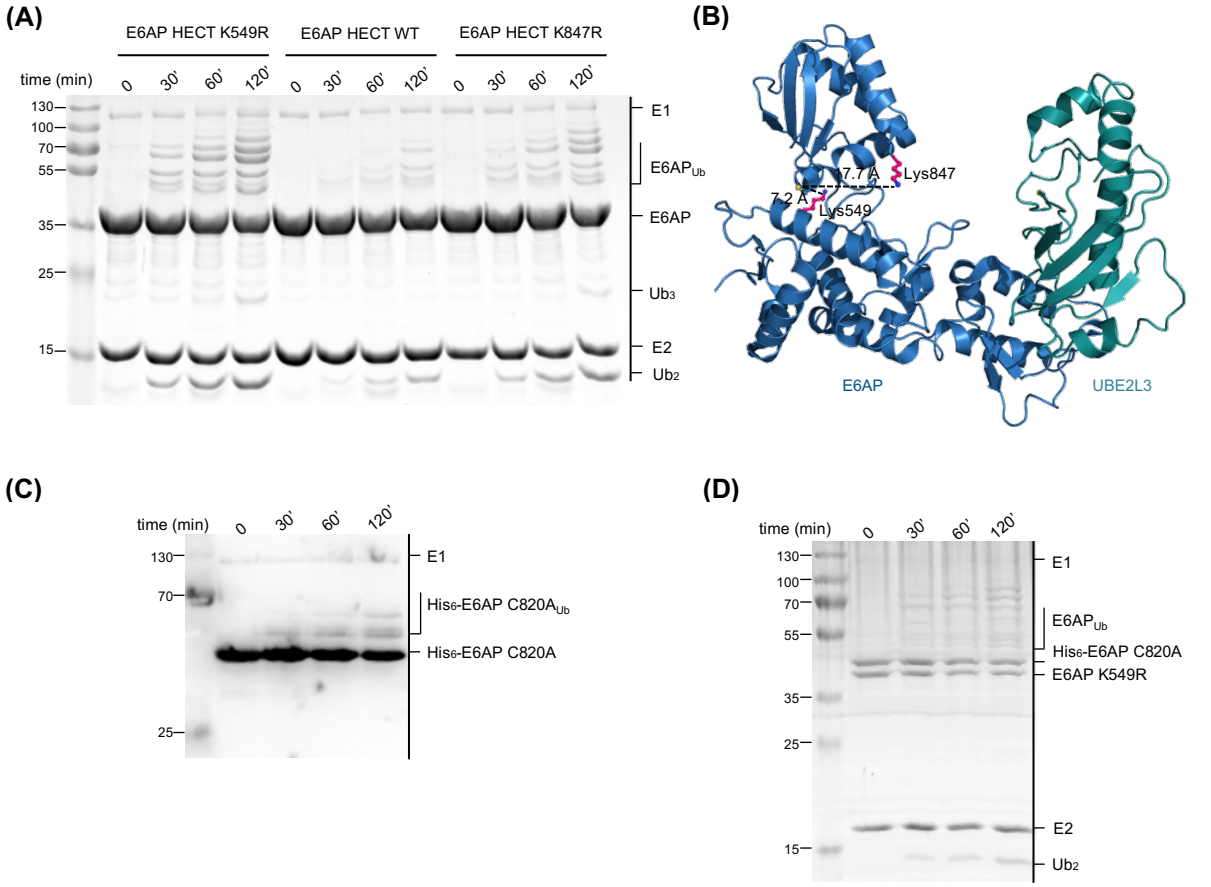

Figure 17: Auto-ubiquitination of E6AP HECT domain can occur *in trans*. (A) *In vitro* activity assay of E6AP HECT domain WT compared to K549R or K847R variant, respectively. The assay was performed with 1 μM UBA1, 50 μM UBE2L3, 50 μM E6AP HECT domain variant, 500 μM Ub in 50 mM HEPES, pH 7.5, 200 mM NaCl, 2 mM DTT, 2 mM ATP and 5 mM $MgCl_2$ at 30 °C for 2 h monitored by SDS-PAGE and Coomassie staining. **(B)** E6AP HECT domain-UBE2L3 complex shown in ribbon representation. The side chains of Lys549, Lys847 (modelled onto the C-terminus) and the active site cysteine residues are shown as balls and sticks. The distances between the lysine side chains and the active site of E6AP are highlighted (PDB ID: 1C4Z [85]). **(C)**, **(D)** Activity assay: 0.5 μM UBA1, 20 μM UBE2L3, 200 μM Ub were mixed with 10 μM E6AP K549R and 10 μM E6AP C820A in 50 mM HEPES, pH 7.5, 200 mM NaCl, 2 mM DTT, 2 mM ATP, 5 mM $MgCl_2$ at 30 °C for 2 h monitored by SDS-PAGE and **(C)** anti-His Western Blotting or **(D)** Coomassie staining.

Lys847 is located near the C-terminus of the HECT domain **(Figure 17B)** and may be ubiquitinated *in trans*. Krist and colleagues showed recently that the mutation K847A impairs both free ubiquitin chain formation and E6AP auto-ubiquitination [115]. The substitution to an arginine restores E6AP activity and makes it even more active **(Figure 17A)**. In line with the C-terminal tail playing a role in promoting ubiquitin chain formation as will be shown later (**4.4.6**), the ubiquitination at Lys847 might restrict an optimal orientation or interfere with donor binding. The substitution to an arginine or alanine might alter the chemical environment of the surface involved in ubiquitin binding, and thus promote (in case of K847R) or prevent (K847A) the optimal positioning of ubiquitin.

Different mechanisms for auto-ubiquitination are conceivable. A lysine residue on the E3 enzyme receiving the first ubiquitin moiety needs to be close to the active site of the E3. In the conformation of crystallized E6AP HECT domain (PDB ID: 1C4Z [85], **Figure 17B**), Lys549 is close to the active site, and a direct ubiquitin transfer thus seems feasible.

In case of the ubiquitination of Lys847, one might argue that chains on lysine residues are formed sequentially with ubiquitin being delivered from the E2 active site. But as pointed out above, only some E2 enzymes are able to transfer ubiquitin to lysine residues independent of the E3 enzyme [177]. E6AP was shown to bind and function predominantly with UBE2L3 and UBE2L6, which lack such lysine reactivity [119, 232]. Thus, this mechanism is unlikely for E6AP unless the E2 enzyme is reprogrammed through the interaction with the HECT ligase.

Alternatively, ubiquitination of Lys847 might occur through a transient oligomer of E6AP. To distinguish between intra- and intermolecular ubiquitination of the lysine residues of E6AP, the variant E6AP K549R, which is more active than the WT enzyme, and His-tagged E6AP C820A, which is catalytically inactive and thus cannot auto-ubiquitinate, were mixed **(Figure 17C, D)**. By anti-His Western blotting, I could detect ubiquitination of His-tagged E6AP C820A variant in the presence of the active variant E6AP K549R **(Figure 17C)**. This rules out that auto-ubiquitination occurs exclusively *in cis* and shows that E6AP self-ubiquitination can result through an E6AP multimer.

Taken together and in line with previous studies, I could identify a lysine residue, Lys847, within the E6AP HECT domain, which was auto-ubiquitinated and its substitution by an arginine residue enhanced the activity of E6AP [115]. A second lysine residue, Lys549, was identified whose substitution to an arginine residue also led to an increased activity. With its close proximity to the active site, this residue might also represent an auto-ubiquitination site, but this needs to be verified with different mass spec techniques.

4.3.3 Ubiquitin chain formation by the E6AP HECT domain does not occur on the active site

Several models for the synthesis of ubiquitin chains by HECT ligases have been reported. One model suggests that HECT ligases assemble ubiquitin chains on a protein in a sequential fashion, transferring one ubiquitin molecule at a time to the target protein (sequential model) [107, 225]. An alternative model posits that ubiquitin chains are pre-assembled on the E3 active site and then transferred *en bloc* to the target ('indexation' model) [225]. A direct visualization of the 'indexation' mechanism has been hampered by the susceptibility of the native thioester bond that should link a pre-assembled ubiquitin chain to the catalytic cysteine of the E3 enzyme in this model [225]. Evidence of either of these models within the NEDD4-type family has been presented [66, 213, 214].

In lieu of the labile thioester, I generated a stable complex between donor ubiquitin and the E6AP HECT domain through the enzymatic formation of an isopeptide bond between the ubiquitin and a lysine residue that substituted the catalytic cysteine of the E6AP HECT domain. UBE2L3 did not show a detectable reaction with this variant (**Figure 18A**, right). UBE2D3, however, was active with E6AP C820K (**Figure 18A**, left). Mass spec analysis (performed by the group of Prof. Schlosser and Prof. Urlaub) revealed that UBE2D3 predominantly transfers its thioester-linked ubiquitin to the active site lysine of the E6AP HECT domain. It could also conjugate ubiquitin independent of the E3 enzyme to lysine residues which are in proximity to the E2-binding site within the N-lobe of the E6AP HECT domain (Lys679, Lys688, Lys705) or at the flexible C-terminus of E6AP (Lys841, Lys847). Within 6 h mainly mono-ubiquitinated E6AP species was formed. No ubiquitin chain was built on the active site lysine residue C820K with ubiquitin being delivered from the E2 enzyme UBE2D3 (**Figure 18A**, left)**.** The presence of only a mono-ubiquitinated E6AP species would exclude that ubiquitin chain transfer occurs through an E2/E3 complex in which the lysine side chain of the acceptor ubiquitin bound to the E3 active site attacks the C-terminus of ubiquitin in the E2~ubiquitin thioester intermediate. Attesting to the fact that UBE2L3, the physiological E2 enzyme of E6AP, cannot discharge onto lysine residues (**Figure 18A**, right), this provides evidence that chain formation does not occur at the active site under these conditions.

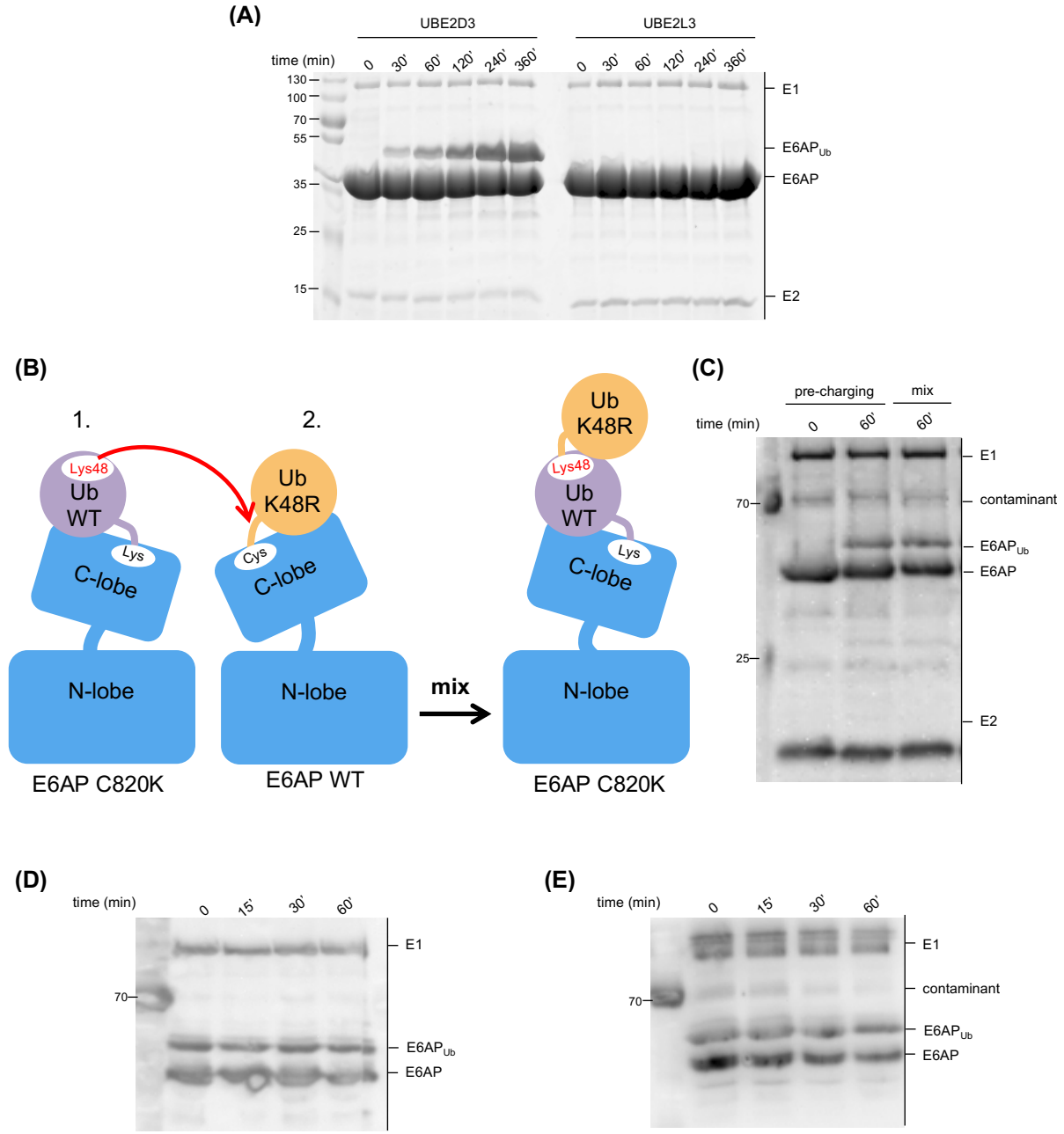

Figure 18: Ubiquitin chains are not formed on the active site of E6AP. (A) *In vitro* activity assay of 1 μM UBA1, 50 μM UBE2D3 or UBE2L3, 50 μM E6AP HECT domain C820K and 500 μM Ub in 50 mM HEPES, pH 7.5, 200 mM NaCl, 2 mM DTT, 2 mM ATP, 5 mM $MgCl_2$ at 30 °C for 6 h monitored by SDS-PAGE and Coomassie staining. **(B)** Schematic of a single-turnover experiment to test the 'indexation' model. If this mechanism applied, ubiquitin K48R thioester-linked to E6AP HECT domain WT should be transferred to E6AP HECT domain C820K pre-charged with ubiquitin WT, thus a reaction product with di-ubiquitin stably attached to the E3 active site lysine (C820K) should be formed. **(C)** His_6-E6AP HECT domain C820K is efficiently pre-charged after 1 h with Ub. Mixing this conjugate with a thioester intermediate of E6AP HECT domain WT~Ub K48R did not result in a transfer of Ub K48R to the E6AP C820K-Ub complex after 1 h (same conditions as in **(A)**) as monitored by SDS-PAGE and anti-His Western Blotting. **(D)** Pre-charged His_6-E6AP HECT domain C820K-Ub WT mixed with thioester intermediate of E6AP HECT domain K549R K688R K847R~Ub K48R did not result in a transfer of ubiquitin to the E6AP C820K-Ub after 1 h (same conditions as in **(A)**) as monitored by SDS-PAGE and anti-His Western Blotting. **(E)** Pre-charged His_6-E6AP HECT domain C820S-Ub WT mixed with thioester intermediate of E6AP HECT domain WT~Ub K48R did not result in a transfer of ubiquitin to the E6AP C820S-Ub after 1 h (same conditions as in **(A)**) as monitored by SDS-PAGE and anti-His Western Blotting.

Therefore, two separate pre-charging approaches were initiated in parallel: In the first approach, E6AP WT was charged with ubiquitin K48R (solely acts as a donor) by the E2 UBE2L3, which can solely transfer ubiquitin to the active site cysteine residue. In the second approach, the His-tagged lysine variant E6AP C820K was isopeptide-linked to ubiquitin WT (solely acts as an acceptor) with UBE2D3, which can transfer ubiquitin to the active site lysine of E6AP. After mixing both ubiquitin-loaded complexes, I could not detect a di-ubiquitinated His-tagged E6AP C820K by anti-His Western blotting **(Figure 18C)**. This would have been expected if ubiquitin K48R would have been transferred from E6AP WT to Lys48 of ubiquitin WT that is stably isopeptide-linked to E6AP C820K **(Figure 18B, C)**. Thus, indicating that E6AP was unable to assemble chains on its active site.

To rule out the possibility that ubiquitin-charged E6AP WT transfers its ubiquitin too rapidly to one of its own auto-ubiquitination lysine sites the assay was repeated with an E6AP variant in which potential auto-ubiquitination sites are substituted by arginine residues (K549R K688R K847R). However, no ubiquitin transfer could be detected **(Figure 18D)**.

To examine whether a lysine-linked ubiquitin-E6AP complex might be a poor ubiquitin acceptor or the C820K mutation causes any artifacts, I replaced the active site cysteine by serine (C820S). Serine is shorter than lysine, and the oxyester formed between ubiquitin and E6AP sterically matches the natural thioester more closely than the isopeptide linkage to lysine, but still ubiquitin transfer failed to appear in this assay **(Figure 18E)**.

My results thus strongly suggest that E6AP does not assemble chains on the active site position under the conditions used here.

4.4 Structural determinants for donor ubiquitin recognition by E6AP

Central parts outlined in this section have been originally presented in the publication of Ries et al. [184]. In parts, textual descriptions and figures have been adopted directly from the publication.

4.4.1 The E6AP C-lobe recognizes ubiquitin *in trans*

The HECT C-lobes interact *in trans* with both donor ubiquitin, as seen in a crystal structure of the *pre-trans*-thioesterification state of NEDD4L with a ubiquitin-loaded E2 enzyme [99], and acceptor ubiquitin, as required for linkage-specific ubiquitin chain formation [107]. Donor ubiquitin binding occupies the same site in the available structures of the NEDD4 family and HUWE1, whose HECT domain is closely related to the NEDD4 subfamily [94, 98, 99, 144]. For E6AP, it is yet unknown how the donor binds and whether the donor interface is conserved in the HECT family.

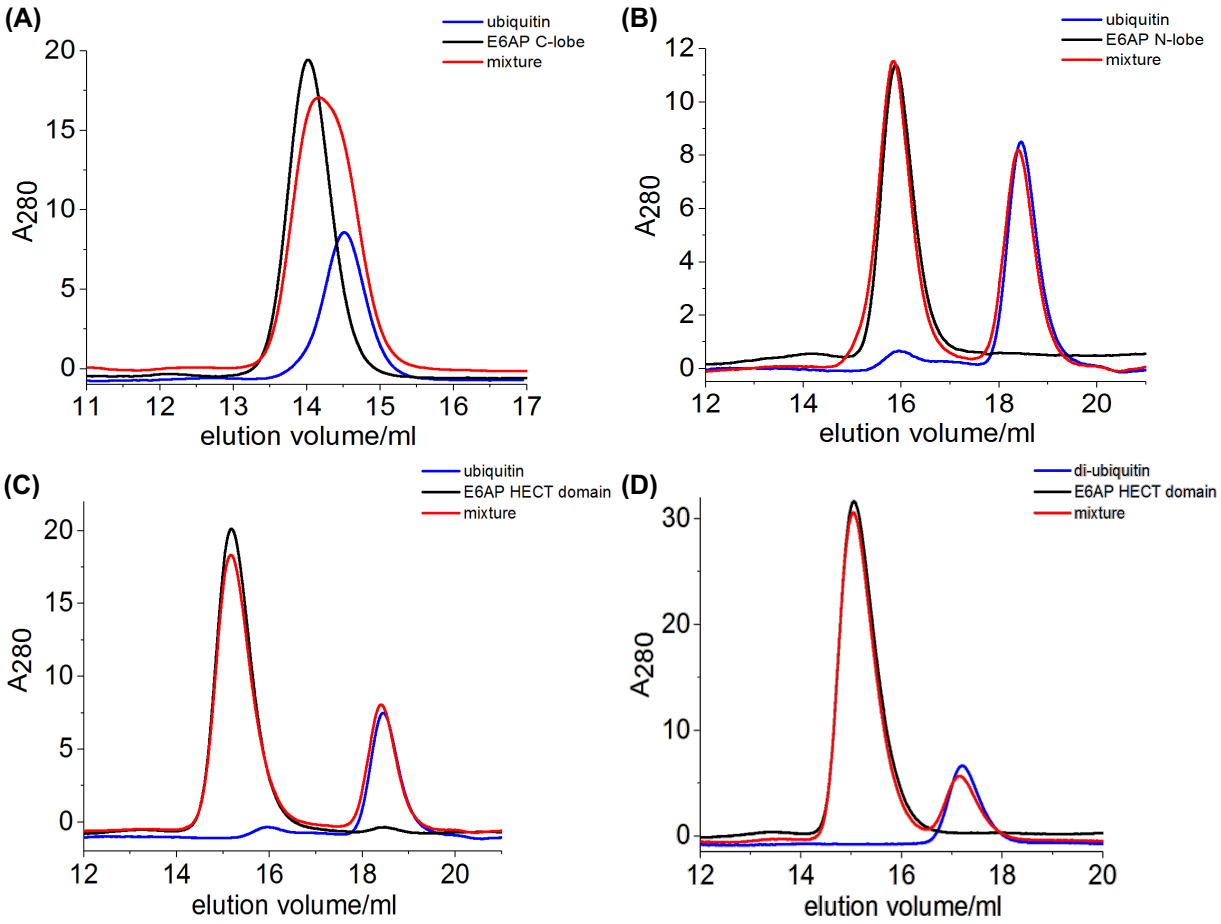

Figure 19: E6AP does not co-elute with ubiquitin by SEC. aSEC experiments were performed in 50 mM Tris/HCl, pH 7.5, 200 mM NaCl, 2 mM DTT with a SD 75 **(A)** or 200 **(B, C, D)** 10/300 GL. **(A)** 50 µM E6AP C-lobe mixed with 200 µM ubiquitin. **(B)** 20 µM E6AP N-lobe mixed with 200 µM ubiquitin. **(C)** 20 µM E6AP HECT domain mixed with 200 µM ubiquitin. **(D)** 40 µM E6AP HECT domain mixed with 80 µM di-ubiquitin.

Due to their transient nature, however, interactions between ubiquitin and HECT C-lobes might have escaped detection by pull-down experiments [67, 99, 107]. SEC experiments with different E6AP constructs mixed with a high excess of ubiquitin showed that the two proteins migrate independently of each other through the column, suggesting that they do not form a stable complex under the conditions and concentrations employed in the SEC experiments **(Figure 19A-C)**. Also, a Lys48-linked di-ubiquitin chain (Supplementary Data **Figure 44**: assembly of Lys48-linked ubiquitin chains) did not bind either to the HECT domain **(Figure 19D)** nor the isolated C-lobe (data not shown).

I employed NMR to uncover potential weak interactions between the C-lobe of E6AP and ubiquitin. Indeed, binding-induced chemical shift perturbations in ^{1}H-^{15}N-HSQC spectra of the E6AP C-lobe upon addition of ubiquitin and *vice versa* could be observed, indicating a specific interaction **(Figure 20A, B)**. The affected resonances map to mostly continuous surface areas on the two binding partners. On ubiquitin, this area includes several hydrophobic residues (Val5, Ile13, Ile36, Leu69, and Leu71) as well as residues in the flexible C-terminal tail (Arg72 and Arg74) **(Figure 20C)**. Perturbed resonances of E6AP map primarily to residues in the active site region surrounding the catalytic cysteine (Cys820), such as His818, Thr819, Phe821, Asn822, Val823, and Leu824, with additional resonance perturbations seen for Gly755, Lys801, Ile803, and Ala805 **(Figure 20C)**. All perturbed resonances showed similar titrations curves reaching saturation at ~10 mM ubiquitin, and could be fitted globally with a single-site model, indicating that the chemical shift perturbations reflect a single binding event **(Figure 20D)**. The NMR-derived dissociation constant for the interaction amounts to 1.5 +/- 0.1 mM **(Figure 20D)**. Based on FP measurements (performed by Dr. Bodo Sander) with fluorophore-labeled ubiquitin, an apparent dissociation constant, K_D, of 400 +/- 20 µM for the C-lobe-ubiquitin interaction was determined **(Figure 20E)**. The differences in the K_D-values might be due to the different techniques used. For the NMR measurements concentrations of up to 10 mM ubiquitin were needed to reach saturation and the protein samples were kept at RT for some time, which might have led to aggregation. FP measurements required less time and generally lower concentrations. Also, the physical properties measured are different: FP detects “tumbling” while I recorded changes in the chemical environment in the NMR experiments.

This rather weak affinities determined by two individually techniques explain why the interaction had not been directly detected in aSEC experiments, which were performed below the determined K_D-values **(Figure 19)**. Moreover, it is reminiscent of the interactions between isolated E2 enzymes and donor and acceptor ubiquitin, respectively, that typically fall into a near-millimolar K_D-range, as well, despite being functionally critical [153, 233].

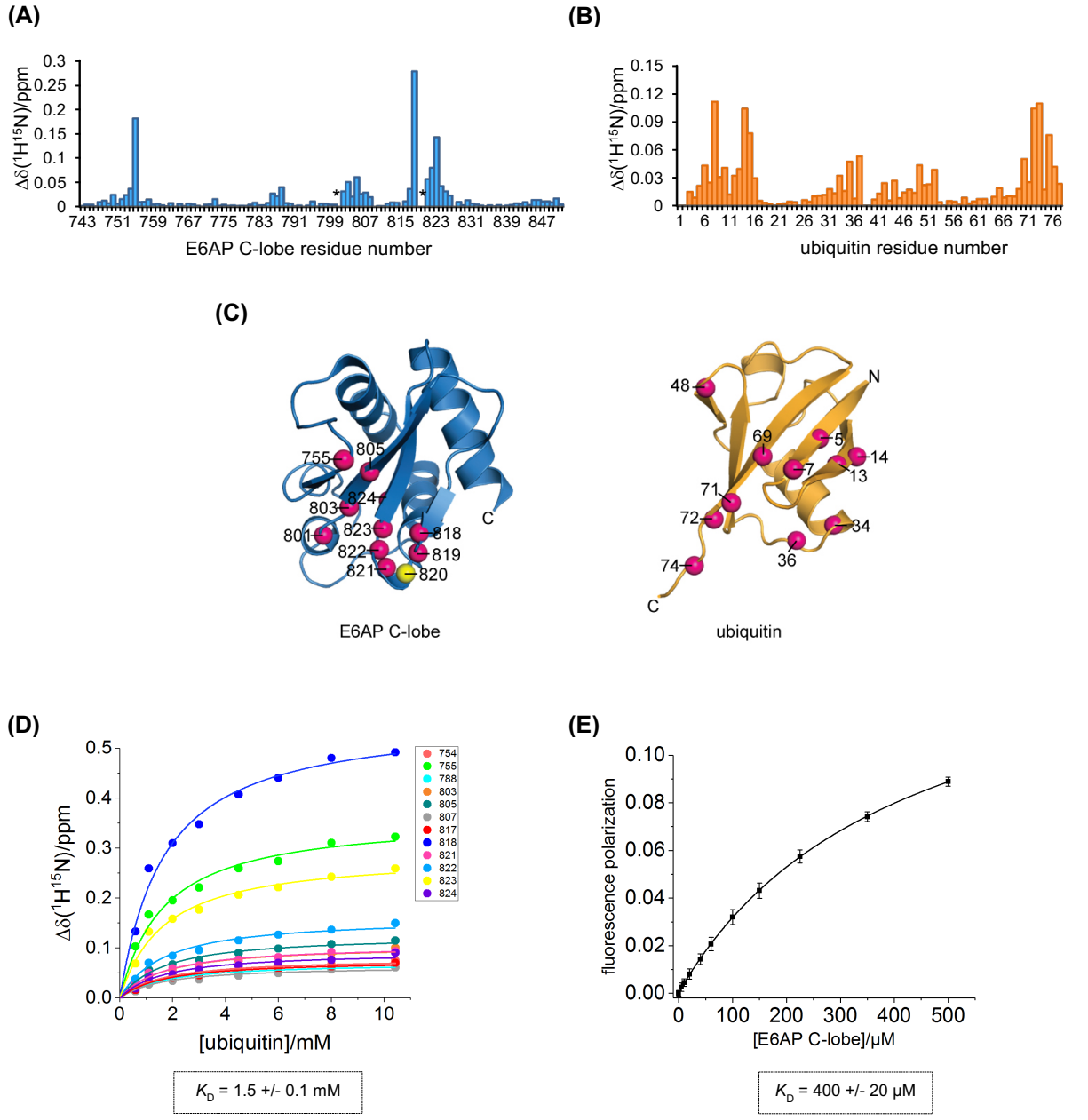

Figure 20: The E6AP C-lobe interacts with ubiquitin *in trans*. (A) Weighted, combined chemical shift perturbations, $\Delta\delta(^1H^{15}N)$, of E6AP C-lobe resonances induced by a 12.5-fold molar excess of ubiquitin, plotted over the E6AP residue number. Resonances that undergo line broadening (Lys801 and Thr819) are marked by an asterisk. **(B)** Weighted, combined chemical shift perturbations of ubiquitin resonances induced by a 12.5-fold molar excess of the E6AP C-lobe, plotted over the ubiquitin residue number. **(C)** Structures of the E6AP C-lobe (extracted from PDB ID: 1C4Z [85]) and ubiquitin (PDB ID: 1UBQ [221]), shown in ribbon representation. The nitrogen atoms of backbone amide groups whose resonances display binding-induced shift perturbations, $\Delta\delta(^1H^{15}N)>0.04$, or undergo line broadening (Lys801 and Thr819 of E6AP) are highlighted as balls (magenta). The side chain of the catalytic cysteine, Cys820, is also displayed. The figure was generated using PyMOL Molecular Graphics System, Version 2.0 Schrödinger, LLC. **(D)** NMR-based determination of the dissociation constant, K_D, for the interaction between the E6AP C-lobe and ubiquitin. Chemical shift perturbations ($\Delta\delta(^1H^{15}N)>0.06$ ppm in the presence of the maximal excess of ubiquitin) of E6AP resonances are plotted over the ubiquitin concentration and fitted globally to a single-site model. **(E)** Determination of an apparent dissociation constant, K_D, for the C-lobe-ubiquitin interaction based on FP measurements (performed by Dr. Bodo Sander). The mean FP signal and standard deviations from 3 independent experiments using a fluorophore-labeled ubiquitin variant were plotted as a function of the C-lobe concentration and fitted to a single-site binding model.

4.4.2 E6AP forms a NEDD4-type interface with the donor ubiquitin during thioester formation

To interrogate the functional significance of the identified E6AP-ubiquitin interaction individual alanine mutations were introduced at those positions that displayed the largest binding-induced chemical shift perturbations in the NMR analyses. Those include Ile803, His818, Thr819, Phe821, and Val823 of E6AP (Gly755 was not mutated for structural reasons; nor Lys801, Asn822 and Leu824, due to their side chains being buried); and Thr14, Glu34, Ile36, Leu71, and Arg74 of ubiquitin. The purified HECT domain variants were tested for their ability to receive the donor ubiquitin from the cognate E2 (UBE2L3) in thioester transfer reactions **(Figure 21A, B)**. Based on time course-experiments monitoring both the formation of the thioester-linked HECT domain-ubiquitin conjugate ('E6AP~Ub') and the concomitant loss of the E2-ubiquitin conjugate ('UBE2L3~Ub'), the mutations I803A, H818A, and T819A in E6AP were found not to impair thioester transfer **(Figure 21A, left)**. In contrast, the F821A substitution adjacent to the catalytic cysteine causes a strong defect, as seen from a delay in the formation of the E6AP~Ub product and prolonged presence of the UBE2L3~Ub precursor; the V823A variant is also compromised in thioester transfer, albeit to a smaller degree than F821A **(Figure 21A, right)**.

With the exception of T14A, all tested mutations in ubiquitin markedly suppress thioester transfer to the E6AP HECT domain **(Figure 21B)**. Notably, these defects are specific to the transfer of ubiquitin from the E2 to the E3, since the preceding reaction step, as monitored by the E1-mediated formation of UBE2L3~Ub, is unaffected by the mutations **(Figure 22)**, in line with previous analyses [156].

Interestingly, the residues required in ubiquitin for thioester transfer to E6AP coincide with a surface of the donor ubiquitin that engages the C-lobe of NEDD4-type ligases [94, 98, 99, 144]. I thus speculated that E6AP associates with the donor ubiquitin in a similar manner. To test this hypothesis mutations known to interfere with donor ubiquitin recognition by NEDD4-type ligases were introduced at the homologous positions in E6AP: Leu814 (homologous to Leu861 and Leu916 of NEDD4 and NEDD4L, respectively) [98, 99]; and Ala842 (homologous to Ala889 and Ala944 of NEDD4 and NEDD4L, respectively) [94, 144]. Another mutation reported to inhibit thioester transfer to NEDD4L (F881A, homologous to F785A in E6AP) [99] was also introduced into E6AP, but could not be studied further, since it reduced the stability of the HECT domain.

In line with the notion that donor ubiquitin recognition by E6AP follows a NEDD4-type mechanism, I found that the L814A and A842I HECT domain variants are impaired in

thioester formation with ubiquitin compared to the wildtype HECT domain of E6AP **(Figure 21C)**.

Consistently, thioester formation is also delayed upon mutation of Gln40 in ubiquitin (Q40A), which makes key contacts at the NEDD4-type donor ubiquitin interface **(Figure 21C)**. However, Gln40 is not required for thioester transfer of ubiquitin from the E1 (UBA1) to the E2 (UBE2L3) **(Figure 22)**.

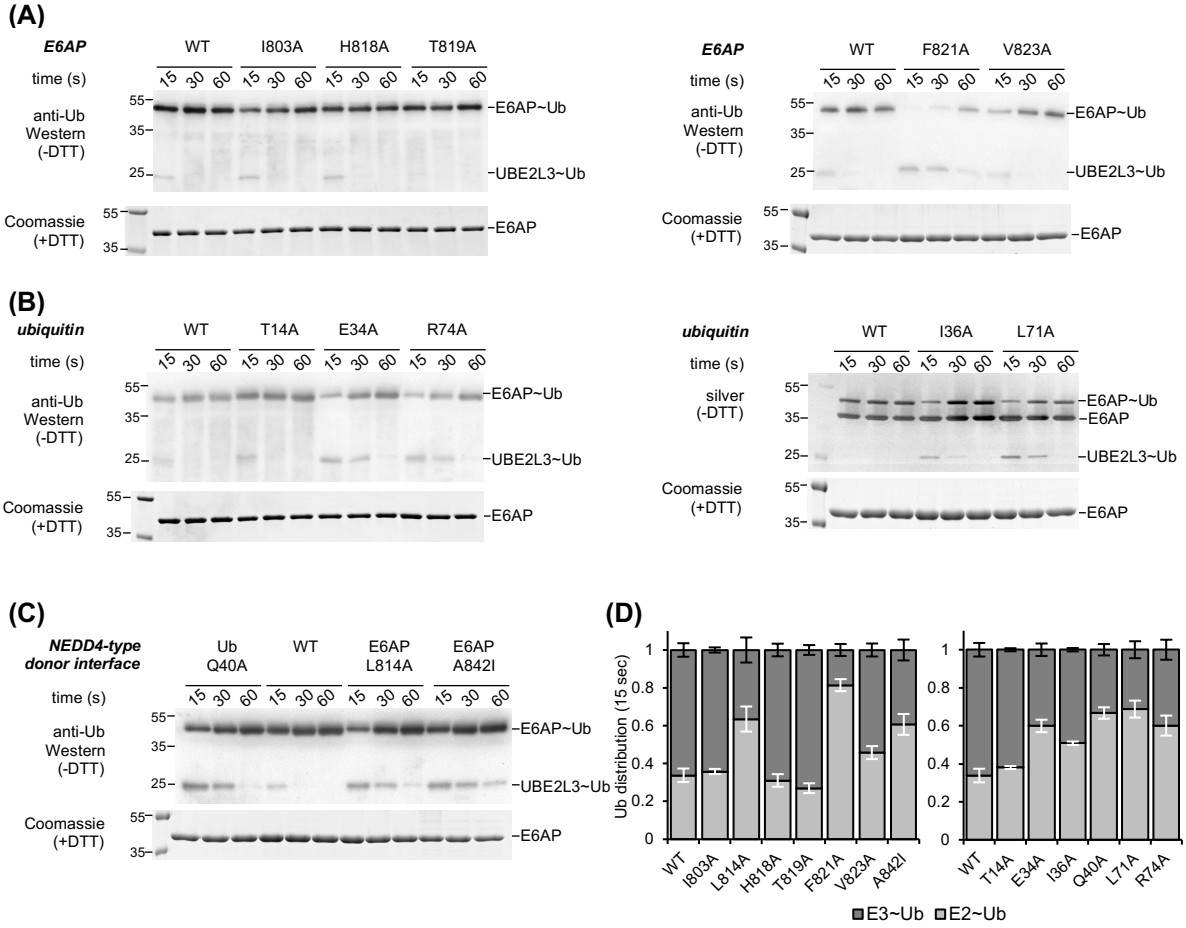

Figure 21: Thioester transfer of ubiquitin requires similar residues in E6AP and NEDD4-type ligases. (A) Thioester transfer of ubiquitin from the E2 (UBE2L3) to the E6AP HECT domain, followed in single-turnover, pulse-chase assays at 3 time points, as indicated, and monitored by non-reducing SDS-PAGE and anti-ubiquitin Western blotting. The thioester-linked HECT domain-ubiquitin conjugate ('E6AP~Ub') and, in some cases, the thioester-linked E2-ubiquitin precursor ('UBE2L3~Ub') are visible. The input amount of HECT domain ('E6AP') is monitored by reducing SDS-PAGE and Coomassie staining. Note that no auto-ubiquitination of the HECT domain occurs within the tested time range. **(B)** Analogous assays as in **(A)**, monitoring the effect of mutations in ubiquitin on thioester transfer to the E6AP HECT domain. For the I36A and L71A variants, silver staining (right) was used in lieu of anti-ubiquitin Western blotting (left), since these variants are not detected well by the antibody (P4D1) used here. **(C)** Analogous assays as in **(A)**, interrogating additional variants of ubiquitin (Q40A) and E6AP (L814A and A842I). The mutation sites are homologous to critical residues in the donor interface of NEDD4-type ligases [94, 99, 143, 144]. **(D)** The amounts of E6AP~Ub and UBE2L3~Ub from the experiments shown in **Figure (A)-(C)** were quantified and normalized to the input amount of E6AP (left: E6AP variants; right: Ub variants). Quantifications are based on 3 independent experiments; the means and standard deviations were plotted for the 15-sec time point.

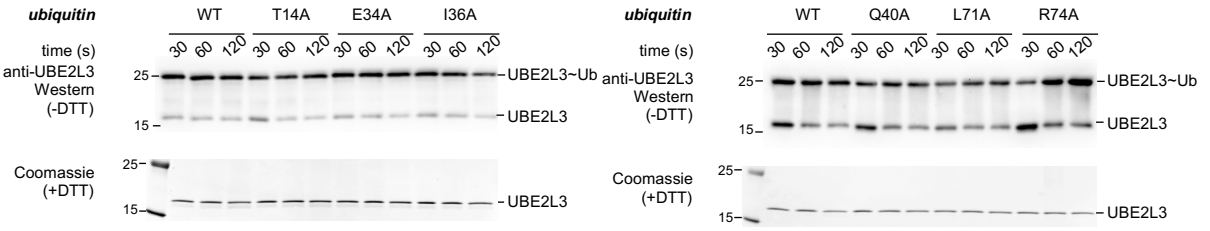

Figure 22: The NMR-derived mutations in ubiquitin variants do not disrupt thioester formation with UBE2L3. Thioester transfer of ubiquitin variants from the E1 (UBA1) to the E2 (UBE2L3), followed in single-turnover, pulse-chase assays at 3 time points, as indicated, and monitored by non-reducing SDS-PAGE and anti-UBE2L3 Western blotting. The formation of thioester-linked E2-ubiquitin conjugates ('UBE2L3~Ub') were monitored. The input amount of E2 ('UBE2L3') is monitored by reducing SDS-PAGE and Coomassie staining.

Next, I studied the functional significance of those residues of E6AP that displayed significant ubiquitin–induced chemical shift perturbations in the NMR experiments but are not required for thioester transfer of ubiquitin (Ile803, His818, Thr819; see **Figure 21A**). To this end, the second step in the catalytic cycle of HECT ligases – isopeptide bond formation – by virtue of auto-ubiquitination ('E6AP$_{Ub}$') and di-ubiquitin formation ('Ub$_2$') was monitored **(Figure 23A)**. These studies show that the mutation of residues in close proximity to the catalytic cysteine (H818A and T819A) causes defects in isopeptide bond formation compared to the WT. In contrast, Ile803, which borders a strand of the β-sheet flanking the active site region, has similar activity to the WT. These observations are consistent with the notion that the ubiquitin-induced chemical shift perturbations of E6AP backbone amide resonances report on both, direct contacts with ubiquitin, which occur predominantly at the active site region, and conformational changes propagated to the nearby β-sheet. Similarly, solution studies of donor ubiquitin conjugated to the C-lobe of SMURF2 or of HUWE1 showed conformational changes in the C-lobes that are remote from the canonical crystallographic donor interface [94]. However, it cannot be ruled out that the NMR data reflect more than one binding mode between the E6AP C-lobe and ubiquitin *in trans*. Taken together, the C-lobe of E6AP relies on similar contacts with ubiquitin as NEDD4-type ligases for thioester formation [94, 98, 99, 143, 144]. A structural model featuring the functionally validated residues, as well as those backbone amide groups that either experience propagated structural perturbations or are involved in alternate, yet uncharacterized interactions modes shown in **Figure 23B**.

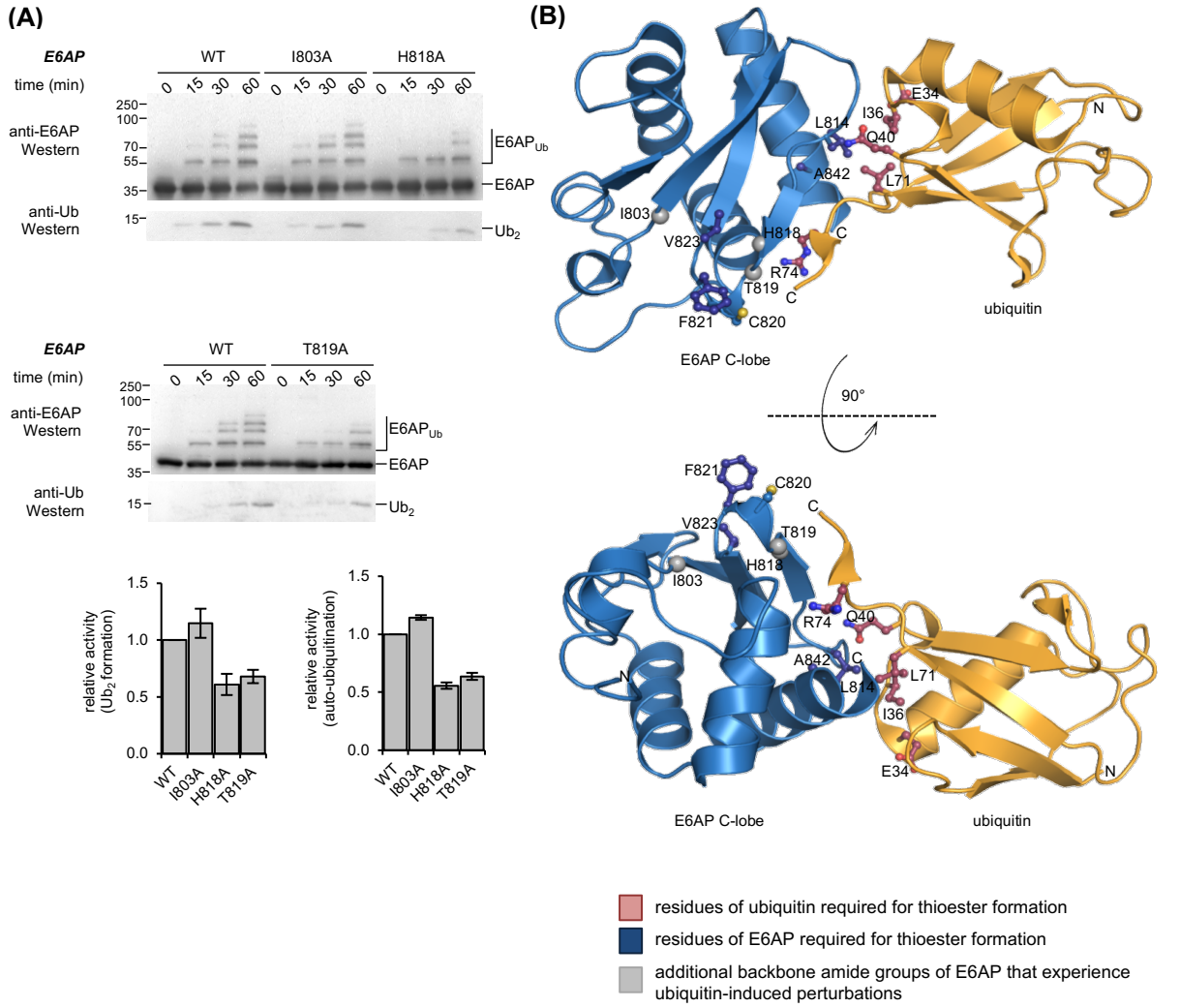

Figure 23: Interactions between the donor ubiquitin and NEDD4-type ligases are conserved in E6AP. (A) Isopeptide bond formation assays comparing the activities of the E6AP HECT domain WT and those variants tested in **Figure 21A** that do not display defects in thioester formation. Activities are monitored at 3 time points, as indicated, by reducing SDS-PAGE and Western blotting against E6AP (HECT domain auto-ubiquitination marked as 'E6AP$_{Ub}$') and ubiquitin (di-ubiquitin reaction product marked as 'Ub$_2$'), respectively. Time point zero denotes samples before ATP addition. The amounts of Ub$_2$ and E6AP$_{Ub}$ were quantified and normalized to the input amount of E6AP. Quantifications are based on 3 independent experiments; the means and standard deviations were plotted for the 60-min time point. The assay was performed at 30 °C with 0.2 μM UBA1, 2 μM UBE2L3, 2 μM E6AP HECT domain variant, 200 μM Ub in 50 mM Tris/HCl, pH 7.0, 75 mM NaCl, 2 mM DTT, 2 mM ATP and 10 mM $MgCl_2$ for 1 h. **(B)** Model of a 'NEDD4-type' complex of the E6AP C-lobe and donor ubiquitin. Ubiquitin was modeled by structural superposition of the C-lobe of the ubiquitin-bound HECT domain of NEDD4 (PDB ID: 4BBN, chain A [144]) with the C-lobe of the HECT domain of E6AP (extracted from PDB ID: 1C4Z, chain A [85]) Ubiquitin and the E6AP C-lobe are displayed in ribbon representation; the side chains of residues relevant for thioester formation are displayed as balls and sticks. The side chain of the catalytic cysteine, Cys820, is also displayed. The backbone nitrogen atoms of additional residues that experience perturbations upon ubiquitin addition are marked as spheres.

To test whether the different variants were folded properly and whether the introduced mutation affects the secondary structure far-UV CD spectra were recorded in comparison of the corresponding spectrum of the wild-type protein **(Figure 24)**. The substitutions have practically no influence on the secondary structure of the protein. The spectra of the E6AP

variants have minima at about 208 nm and 222 nm whereas the CD spectra of the ubiquitin variants show minima at 208 nm and 225 nm. These minima reflect the fraction of α-helical structures. The minor differences in signal intensities of the individual variants are presumably due to slight inaccuracies in the protein concentrations. Also, changes in the environment of aromatic residues exert influence on the CD signal. The signal-to-noise ratio is more pronounced in case of the ubiquitin variants (**Figure 24B** compared to **Figure 24A**) which reflects the lower secondary structure content of ubiquitin compared to the E6AP HECT domain.

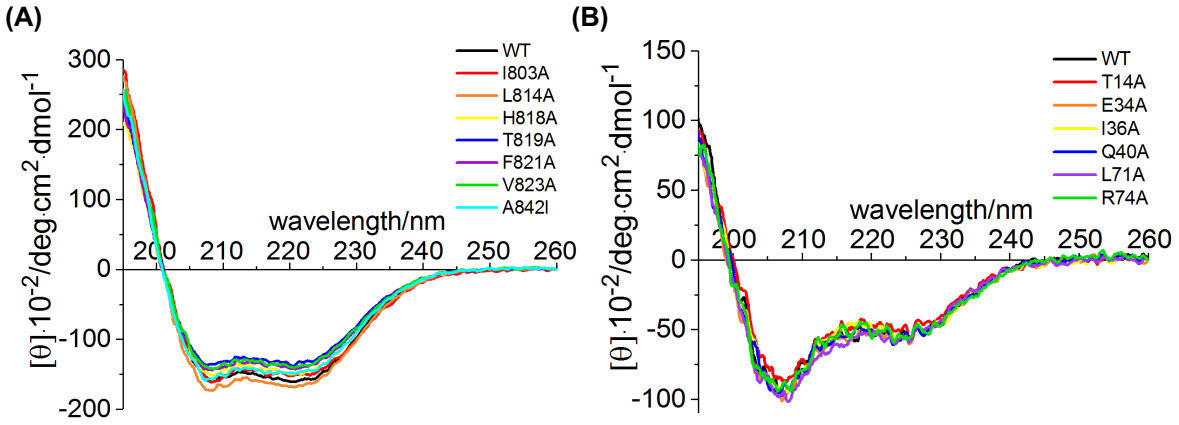

Figure 24: The structural integrity of the mutated variants of E6AP and ubiquitin is preserved compared to WT. Superposition of CD spectra of 4 μM of the indicated variants of the HECT domain of E6AP **(A)** and of 8 μM of the different ubiquitin variants **(B)**. The spectra were recorded in 10 mM sodium phosphate, pH 7.4 at 10 °C. The resolution was 0.1 nm and the speed 50 nm/min. The bandwidth was 1 nm and the attenuation was 2 s (10 accumulations).

4.4.3 Generation of E6AP-donor ubiquitin complexes

4.4.3.1 Covalently crosslinking of E6AP C-lobe to ubiquitin with Ellman's reagent

I next set out to analyze the interaction of the E6AP C-lobe with the donor ubiquitin in the context of different covalently linked intermediates structurally. Therefore, I established strategies to covalently link the donor ubiquitin to the C-lobe or the whole HECT domain of E6AP. In one approach, a stable mimic of the conjugate was prepared by replacing the native thioester with a disulfide bond, through an engineered cysteine residue at the C-terminus of ubiquitin (either G75C or G76C). This resulting disulfide bond (denoted as '~') is stable in the absence of reducing agent. The crosslinking was performed through the specific activation of ubiquitin with Ellman's reagent (DTNB). After removing excess of Ellman's reagent, crosslinking was initiated by mixing the ubiquitin species with the activated Cys residue at its C-terminus with E6AP C-lobe. The disulfide-linked conjugate was separated by cation exchange chromatography from unmodified ubiquitin, C-lobe and crosslinked C-lobe~C-lobe dimers using a salt gradient from 0 to 200 mM NaCl **(Figure 25A, B)**. The conjugate containing fractions were pooled and concentrated. The yield was ~2 mg of pure complex per 2 ml approach.

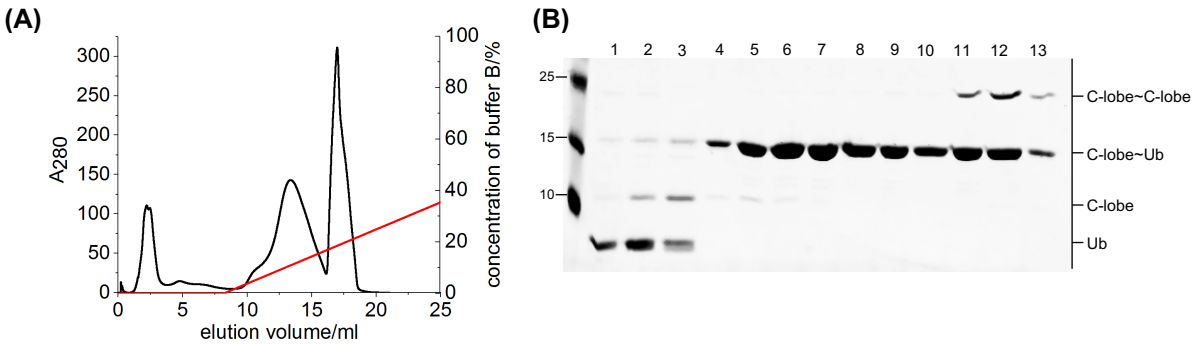

Figure 25: Crosslinking of E6AP C-lobe with ubiquitin G75C. (A) CIEX with a Mono S 4.6/100 PE in 25 mM Tris/HCl, pH 6.5, 1 mM EDTA, 0 to 500 mM NaCl and **(B)** corresponding SDS-PAGE (1-3: every 0.5 ml fraction from 2.5 ml to 4 ml; 4-13: every 1 ml fraction from 10 ml to 20 ml).

The complex was then subjected to crystallization trials. Different temperatures, additive screens and different protein concentrations (3 to 10 mg/ml) were tested. This led to the growth of several thin plate shaped protein crystals after one week in different conditions (1.0 M LiCl, 0.1 M Citric Acid pH 4.0/0.1 M HEPES pH 7.0, 20% PEG6000; 0.4 M KCl/1.0 M $LiNO_3$, 23% PEG4000; 0.2 M Calcium Acetate, 0.1 M HEPES pH 7.5, 18% PEG4000; 1.9 M Sodium malonat pH 5.0; 0.2 M NaCl, 0.1 M Tris pH 7.0, 30% PEG3000; 0.1 M Sodium citrate tribasic dehydrate pH 5.6, 20% 2-Propanol, 20% PEG4000; 0.1 M Citric Acid pH 4.0, 2 M NaCl; 0.5 M NaBr, 23% PEG4000). The crystals could be harvested in different cryogenic protectants (20% ethylene glycole, 20% glycerol) and were flash-frozen in liquid nitrogen. The

best crystals diffracted to a resolution of 3.8 Å at a wavelength of 0.9182 Å at BESSY II Berlin. Data processing was conducted with XDS/XSCALE [97]. Using the PDB entry for ubiquitin (PDB ID: 1UBQ [221]) and E6AP C-lobe (extracted from PDB ID: 1C4Z [85]), the structure could be solved by molecular replacement with Phaser within the CCP4 suite [148]. Only ubiquitin could be found, but E6AP C-lobe was not present. The structure of ubiquitin was solved in space group C121. The structural arrangement closely resembles a structure of Lys11-linked di-ubiquitin published by Prag and colleagues (PDB ID: 4Z9S) [127]. Washing these crystals and analyzing them via SDS-PAGE and silver staining did not show any E6AP C-lobe (data not shown). Interestingly, all ubiquitin crystals formed under conditions with the common feature of a low pH value, which probably led to the cleavage of the disulfide bridge.

To analyze the properties of the disulfide-linked ubiquitin~C-lobe conjugate in solution SEC analysis were performed **(Figure 26A-C)**. The conjugate does not interact detectably with a 5-fold excess of free ubiquitin **(Figure 26A)**, consistent with the previous finding that stable binding to ubiquitin could not be detected neither for the isolated HECT domain nor for the single lobes by SEC **(Figure 19)**. Upon mixing free desalted E6AP C-lobe with disulfide-linked ubiquitin~C-lobe conjugate, a shoulder eluting prior to the conjugate **(Figure 26B)** appeared. By SDS-PAGE, I could show that evidently a thiol/disulfide exchange reaction occurred **(Figure 26C)**: The disulfide bond between ubiquitin and the E6AP C-lobe was attacked by the reactive catalytic cysteine of the free E6AP C-lobe to liberate free ubiquitin, and thus a disulfide-linked C-lobe dimer was formed **(Figure 26C)**. This disulfide exchange reaction likely occurred because the catalytic cysteine in the free C-lobe is more reactive than Cys75 of ubiquitin, which thus became the leaving group. However, the underlying interaction must be transient and weak, since no binding of a C-lobe with an acetylated cysteine to the disulfide-linked conjugate could be detected **(Figure 26D)**. Native PAGE revealed at least two separate species for the C-lobe: one prominent species displaying the monomeric protein and a weaker species with a higher electrophoretic mobility, representing probably a dimeric fraction of E6AP C-lobe **(Figure 26E)**. Mixing the disulfide-linked complex with ubiquitin or free C-lobe did not show any significant complex formation, probably due to half of the concentration used for native PAGE **(Figure 26E)**.

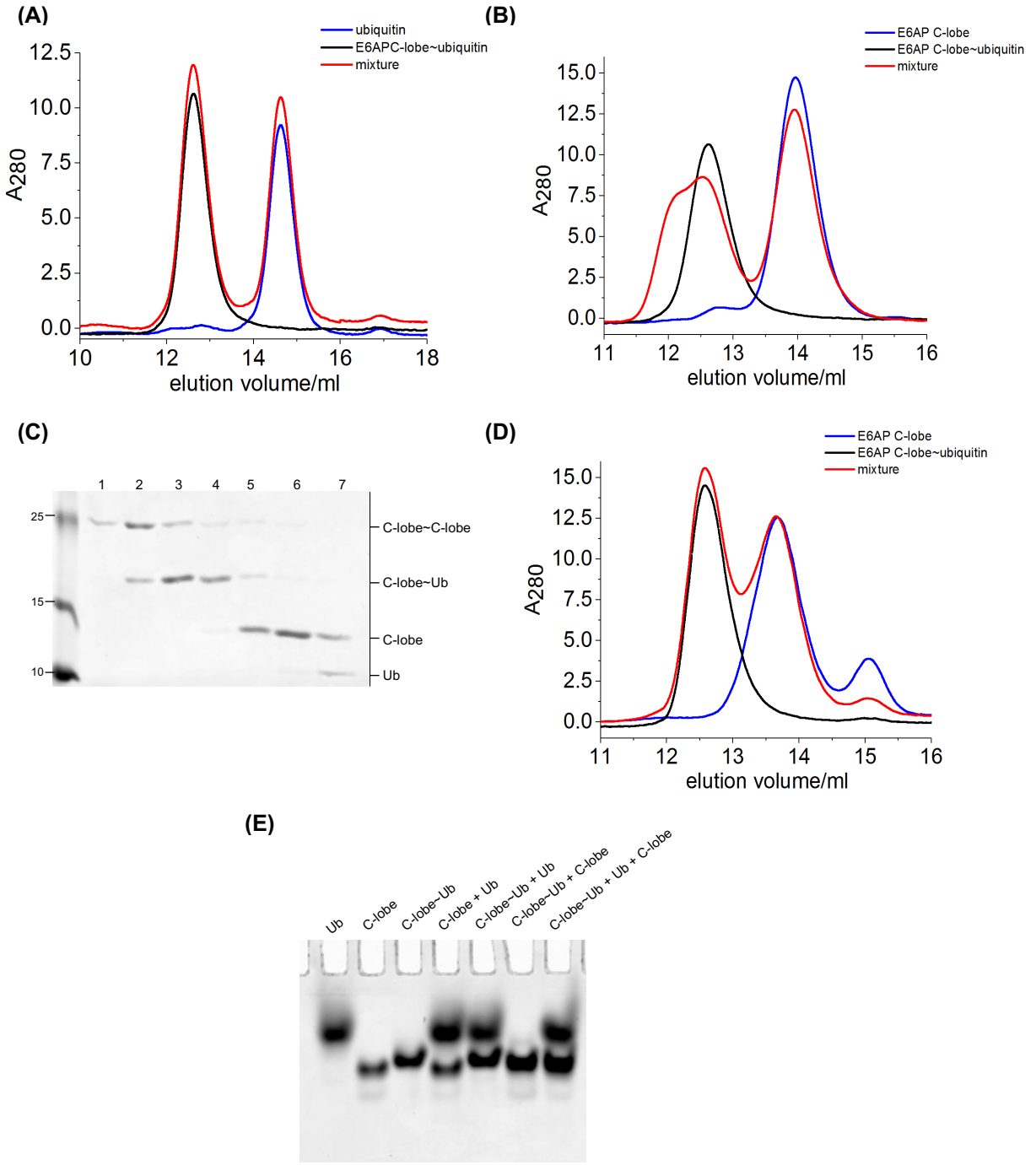

Figure 26: E6AP C-lobe~ubiquitin exchanges with free C-lobe. (A), **(B)** and **(D)**: aSEC with a HiLoad SD 75 10/300 GL in 50 mM Tris/HCl, pH 7.5, 200 mM NaCl, 2 mM DTT. **(A)** 50 μM E6AP C-lobe~Ub mixed with 250 μM Ub. **(B)** 50 μM E6AP C-lobe~Ub mixed with 50 μM E6AP C-lobe and **(C)** monitored by SDS-PAGE (1-10: every fraction from 11.5 ml to 15.0 ml). **(D)** 50 μM E6AP C-lobe~Ub mixed with 50 μM E6AP C-lobe pre-treated with 20 μM NEM for 30 min. **(E)** Native PAGE: 20 μM E6AP C-lobe~Ub mixed with 20 μM E6AP C-lobe and/or 100 μM Ub.

Next, substitutions in the donor interface required for thioester formation were tested to interfere with the tendency of E6AP C-lobe to be trapped by the disulfide linkage. Therefore, I mutated ubiquitin Ile36, or Leu71 to alanine in the context of ubiquitin G75C and crosslinked these variants to E6AP C-lobe using Ellman's reagent. The crosslinking efficiencies were comparable to ubiquitin WT and aSEC experiments showed that the variants recruited free C-lobe to the same extent and supported subsequent C-lobe dimerization **(Figure 27)**. The formation of the disulfide-linked C-lobe dimers is thus likely dominated by the chemical reactivity of the attacking cysteine and not influenced by the C-lobe-donor ubiquitin interface.

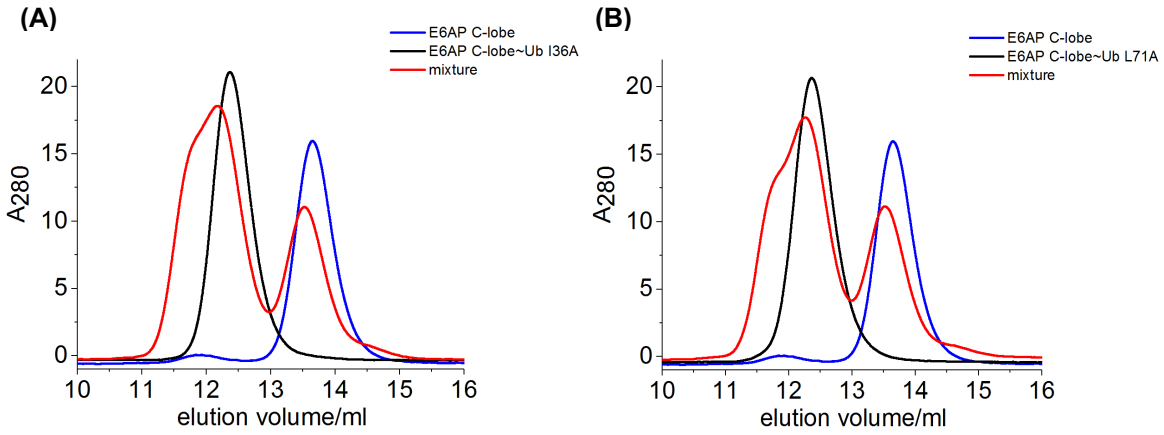

Figure 27: The alteration of the E6AP C-lobe-donor ubiquitin interface does not affect the exchange with free C-lobe. aSEC with a HiLoad SD 75 10/300 GL in 50 mM Tris/HCl, pH 7.5, 200 mM NaCl, 2 mM DTT. 50 μM E6AP C-lobe WT mixed with **(A)** 50 μM E6AP C-lobe~Ub I36A and **(B)** 50 μM E6AP C-lobe~Ub L71A.

4.4.3.2 Covalently crosslinking of E6AP C-lobe to ubiquitin with DCA

As an alternative strategy, His-tagged ubiquitin G76C was covalently linked via the sulfhydryl group with the bifunctional, thiol-specific reagent dichloroacetone (DCA) to the active site cysteine of E6AP C-lobe to generate a double non-hydrolyzable chloromethyl-thioether C-lobe-ubiquitin complex [234, 245]. After mixing ubiquitin G76C and C-lobe, DCA was added to the mixture. The reaction was then stopped by the addition of β-ME and Ni-NTA chromatography was performed. His-tagged ubiquitin-C-lobe complex could be thereby separated from unmodified C-lobe and crosslinked C-lobe dimer, which eluted in the flow-through **(Figure 28A, B)**. A final SEC step was used to separate the complex from free ubiquitin **(Figure 28C, D)**. From a 1 ml reaction volume 0.5 mg of the covalently linked complex was obtained. The complex was employed for crystallization trials at a concentration of 2 mg/ml, but crystals could not be obtained.

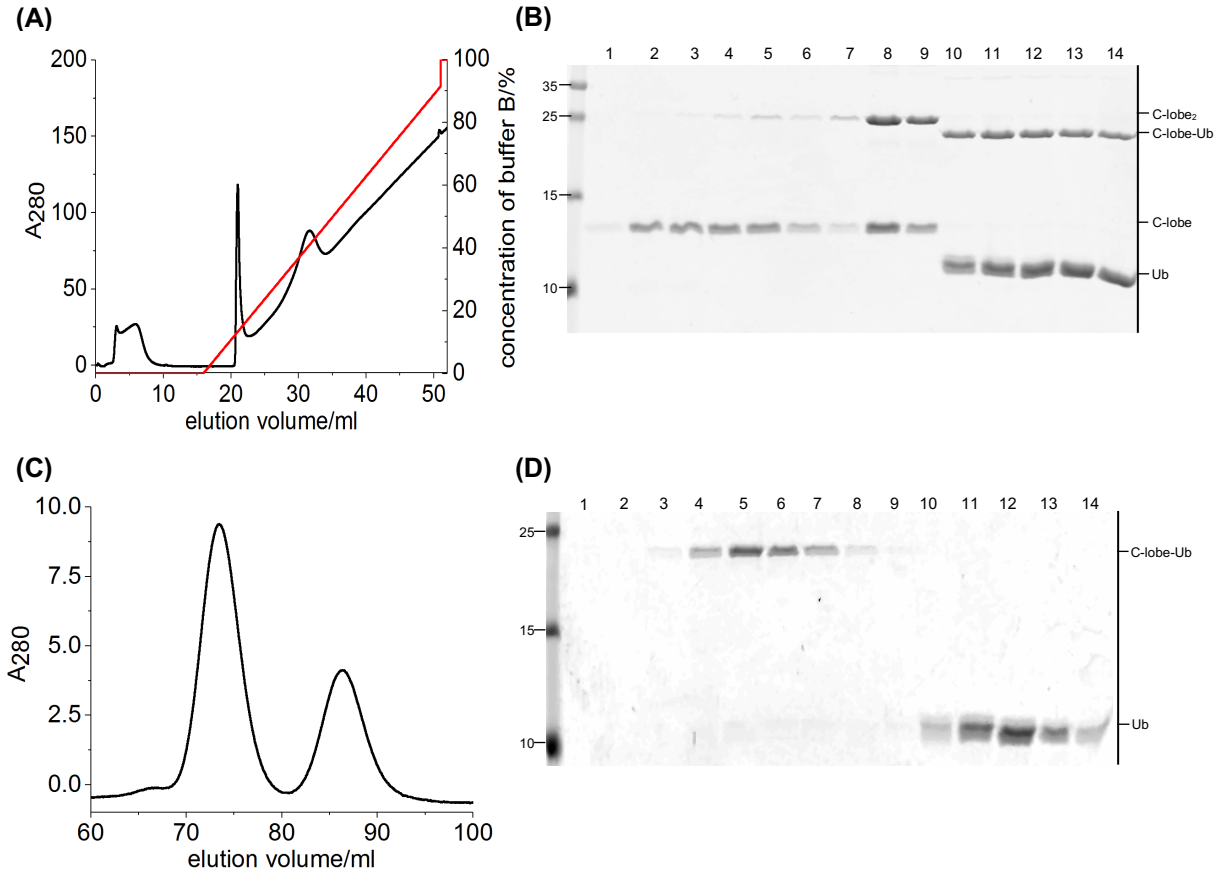

Figure 28: Purification of a non-hydrolyzable crosslinked ubiquitin G76C-E6AP C-lobe complex. (A) Ni-NTA chromatography with a HisTrap HP 1 ml column in 50 mM Tris/HCl, pH 7.5, 400 mM NaCl, 8 mM β-ME and **(B)** monitored by SDS-PAGE (1-6: every 1 ml fraction from 2 ml to 7 ml; 7-9: every 1 ml fraction from 21 ml to 23 ml; 10-14: every 1 ml fraction from 30 ml to 34 ml). **(C)** SEC with a HiLoad SD 75 16/600 pg in 50 mM Tris/HCl, pH 7.5, 200 mM NaCl, 1 mM EDTA and **(D)** monitored by SDS-PAGE (1-14: every second 1 ml fraction from 65 ml to 91 ml).

4.4.3.3 Crosslinking of the entire E6AP HECT domain to ubiquitin with Ellman's reagent

The disulfide crosslinking approach was used to extend the studies on the entire HECT domain rather than the isolated C-lobe, to investigate, for example, whether the donor ubiquitin affects the relative orientation of both lobes with respect to each other. To render the disulfide crosslinking specific I replaced the two additional Cys residues of the HECT domain by serines. The resulting single-cysteine variant C604S C737S is named 'CCSS' in the following. During preparative SEC this variant was prone to aggregation, and the yield of soluble protein was small. Thermofluor assays with the CCSS variant did not reveal suitable buffer conditions for improved stability and solubility. The activity of the CCSS variant was also reduced in comparison to the wild-type protein **(Figure 29A)**. The tendency to aggregate during purification and the reduced activity were also observed for the two variants with single cysteine-to-serine substitutions. This pronounced effect can be due to potential loss of proper folding of the protein or a contribution of the substituted cysteine residues to the catalysis of E6AP. Yet, the structural integrity of the CCSS variant could be validated by CD spectroscopy compared to E6AP WT **(Figure 29B)**.

However, crosslinking of the CCSS variant to ubiquitin G75C with Ellman's reagent was successful **(Figure 29C, D)**. The E6AP HECT CCSS~ubiquitin conjugate could be separated efficiently from the unmodified HECT domain and free ubiquitin by anion exchange chromatography **(Figure 29C, D)**. The yield was 2 mg pure complex.

I subjected the complex to aSEC, native PAGE analysis and crystallization trials. There was no transient trapping of the active site cysteine of E6AP CCSS in the disulfide-linked HECT domain~ubiquitin complex neither by free E6AP C-lobe nor by the free E6AP HECT domain (data not shown). In context of the whole HECT domain, the N-lobe might restrict the C-lobe to dimerize. Thus, the dimerization potential of E6AP C-lobe could only represent an inherent property of the isolated C-lobe as it will be shown in **4.4.4**. In native PAGE analysis, I could not detect non-covalent interactions of the covalently linked complex with ubiquitin, the E6AP C-lobe nor the HECT domain **(Figure 29E)**. Attempts to crystallize the conjugate were unsuccessful. In most conditions the complex precipitated which might be due to the low stability of the disulfide-linked complex. Therefore, the stability to thermal unfolding of E6AP HECT CCSS with or without bound ubiquitin in comparison to E6AP WT was investigated by the temperature-dependent change of the CD signal at 222 nm **(Figure 29F)**. The normalized thermal transitions show that the two cysteine-to-serine substitutions led to a significant decrease of the overall stability of the HECT domain.

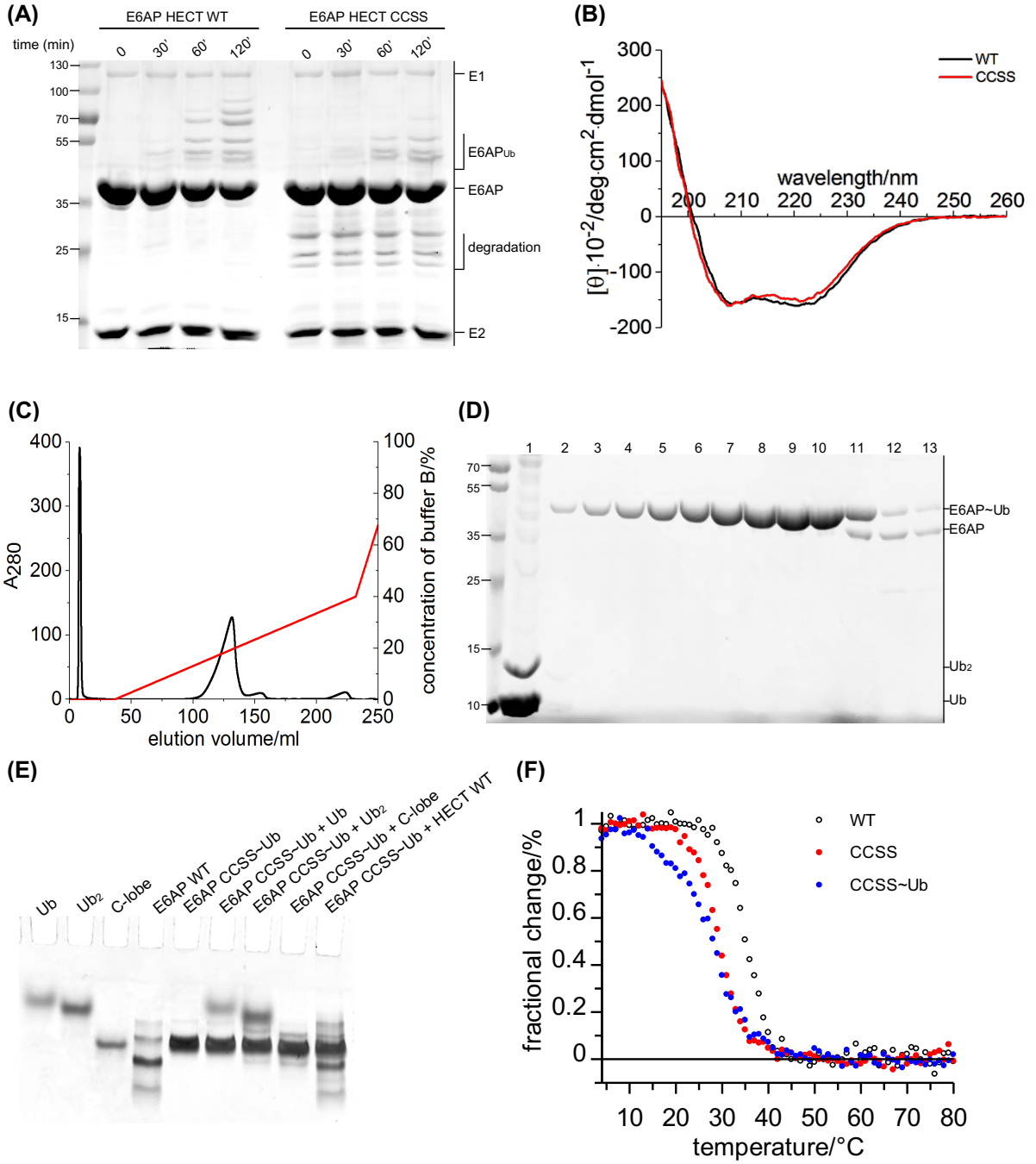

Figure 29: Crosslinking of ubiquitin G75C to the E6AP HECT domain CCSS. (A) *In vitro* activity assay of E6AP HECT domain WT compared to CCSS. The assay was performed at 30 °C with 1 μM UBA1, 50 μM UBE2L3, 50 μM E6AP HECT domain variant, 500 μM Ub in 50 mM HEPES, pH 7.5, 200 mM NaCl, 2 mM DTT, 2 mM ATP and 5 mM $MgCl_2$ for 2 h and monitored by SDS-PAGE and Coomassie staining. **(B)** CD spectra of E6AP HECT domain WT compared to E6AP HECT domain CCSS. The spectra were recorded with 4 μM protein in 10 mM sodium phosphate, pH 7.4 at 10 °C. The resolution was 0.1 nm and the speed 50 nm/min, bandwidth 1 nm, attenuation 2 s (10 accumulations). **(C)** AIEX of crosslinked E6AP HECT domain CCSS~Ub G75C and **(D)** corresponding SDS-PAGE (25 mM Tris/HCl, pH 6.5, 1 mM EDTA, 0 to 500 mM NaCl with a Mono Q 10/100 GL (1: pooled flow-through, 2-12: every second fraction from 105 ml to 150 ml). **(E)** Native PAGE of 20 μM E6AP HECT CCSS~Ub mixed with 100 μM Ub, 50 μM Ub_2, 20 μM E6AP C-lobe or 20 μM E6AP HECT domain WT at 4 °C after 30 min incubation prior to the run. **(F)** Normalized thermal induced transitions of E6AP WT, E6AP CCSS and E6AP CCSS~Ub complex, representing the fractional change in signal as a function of temperature. 4 μM protein in 10 mM NaPi, pH 7.4 from 10 °C to 80 °C with a heating rate of 60 K/h, a resolution of 0.2 K, a bandwidth of 1 nm and an attenuation of 8 s on a Jasco J-810 with PTC 348 WI Peltier element.

The apparent T_M is shifted from 35.1 °C for the wild-type protein to 29.6 °C for the CCSS variant, respectively. The crosslinking to ubiquitin led to a further decrease of the stability of the protein, and the T_M decreased by additional 2 degrees (T_M = 27.8 °C). The T_M values below 30 °C explain the degradation observed in the *in vitro* activity assays and also explain the high propensity for precipitation in the crystallization experiments at 20 °C. Repeating the crystallization trials at 4 °C led to less precipitate, but still failed to form crystals.

I also tried to crosslink ubiquitin G75C to the more stable wild-type HECT domain of E6AP with Ellman's reagent. In fact, a mixture of three different species, corresponding to ubiquitin being bound to either one of the three cysteine residues, was generated. Since I was not able to separate these species from each other, I abandoned this strategy.

4.4.3.4 Generation of an isopeptide-linked donor ubiquitin-E6AP HECT domain complex

An alternative strategy to generate a stably linked complex of the donor ubiquitin and the HECT domain relies on the enzymatic formation of an isopeptide bond between the donor ubiquitin and a lysine residue that is substituted for the catalytic cysteine at the active site of the E6AP HECT domain (**4.3.3**).

The auto-ubiquitination of E6AP C820K with ubiquitin was initially monitored for at least 6 h **(Figure 30A)**, showing the predominant formation of a covalent 1:1 complex between E6AP C820K and ubiquitin being isopeptide-linked to the active site lysine residue (as confirmed by mass spec, **4.3.3**). Since a prominent di-ubiquitinated E6AP species arose within 60 min, the assay was conducted only for 30 min in the following. The reaction mixture was then loaded onto a SD 16/600 75 pg column **(Figure 30B, C)**. Similar to the co-elution of tagged and untagged protein during E6AP purification **(Figure 11D)**, isopeptide-linked complex could not be separated from the unmodified E6AP HECT domain. The fractions containing the isopeptide-linked complex were pooled and dialyzed overnight. The dialysate was then subjected to an anion exchange chromatography **(Figure 30D, E)**. Using a very shallow salt gradient, the E6AP C820K-ubiquitin complex could be separated from unmodified E6AP HECT domain and from the complex with two bound ubiquitin molecules **(Figure 30D, E)**. Since there was a weak band of UBA1 co-eluting with the isopeptide-linked complex **(Figure 30E)**, I performed a final SEC with a SD 75 10/300 GL column **(Figure 30F, G)**. ~3 mg of pure protein was obtained after pooling the complex-containing fractions. This highly pure complex was subjected to extensive crystallization trials, which were not successful.

Taken together, I was able to prepare different covalently and stably-linked donor ubiquitin-HECT domain/C-lobe complexes through various approaches, chemically or enzymatically. Yet, crystals could not be produced.

Figure 30: Purification of isopeptide-linked donor ubiquitin-E6AP HECT domain C820K complex. (A) *In vitro* activity assay with 1 μM UBA1, 50 μM UBE2D3, 50 μM E6AP HECT domain C820K, 500 μM Ub in 50 mM Tris/HCl, pH 7.5, 200 mM NaCl, 2 mM DTT, 2 mM ATP, 5 mM $MgCl_2$ at 30 °C for 6 h monitored by SDS-PAGE and Coomassie staining. **(B)** SEC and **(C)** corresponding SDS-PAGE (HiLoad SD 16/600 75 pg in 50 mM Tris/HCl, pH 7.5, 200 mM NaCl, 2 mM DTT); every third fraction was loaded (from 52 ml to 85 ml). **(D)** AIEX of the complex and **(E)** corresponding SDS-PAGE (Mono Q 4.6/100 PE in 50 mM Tris/HCl, pH 6.5, 1 mM EDTA and 0 to 500 mM NaCl; every 1 ml fraction from 23 ml to 34 ml). (**F)** aSEC and **(G)** corresponding SDS-PAGE (SD 200 10/300 GL in 50 mM Tris/HCl, pH 7.5, 200 mM NaCl, 2 mM DTT; every 0.75 ml fraction from 12 ml to 16 ml).

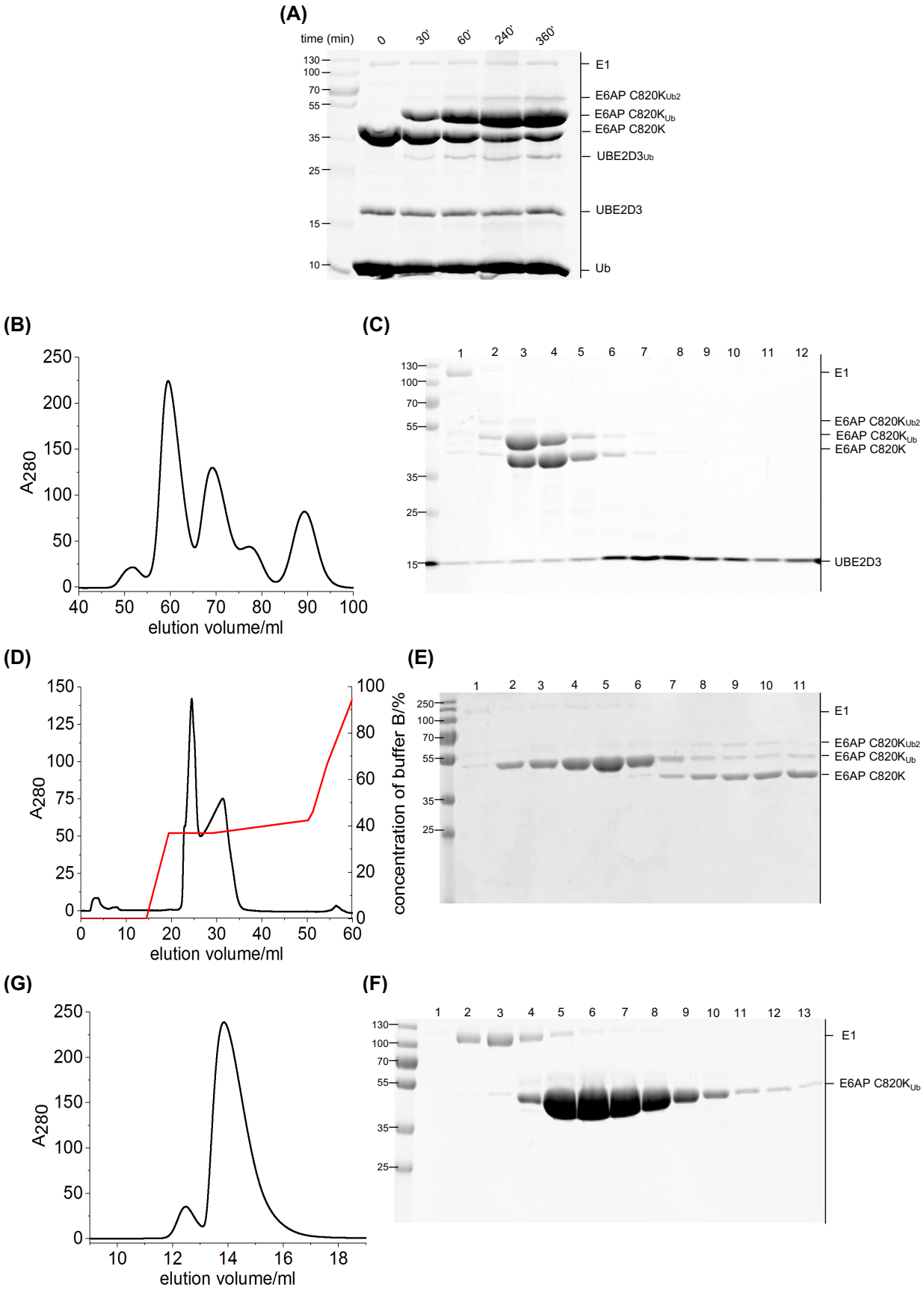
(A)
time (min)
0
30'
60'
240'
360'
130
100
70
55
35
25
15
10
E1
E6AP C820K$_{Ub2}$
E6AP C820K$_{Ub}$
E6AP C820K
UBE2D3$_{Ub}$
UBE2D3
Ub
(B)
A280
elution volume/ml
(C)
1 2 3 4 5 6 7 8 9 10 11 12
E1
E6AP C820K$_{Ub2}$
E6AP C820K$_{Ub}$
E6AP C820K
UBE2D3
(D)
A280
concentration of buffer B/%
elution volume/ml
(E)
1 2 3 4 5 6 7 8 9 10 11
E1
E6AP C820K$_{Ub2}$
E6AP C820K$_{Ub}$
E6AP C820K
(G)
A280
elution volume/ml
(F)
1 2 3 4 5 6 7 8 9 10 11 12 13
E1
E6AP C820K$_{Ub}$

4.4.4 E6AP C-lobe undergoes domain swapping at high concentrations

Based on the assumption that the E6AP C-lobe can promote transient dimerization of E6AP **(Figure 26B, C)**, I studied this behavior by aSEC-MALS experiments and NMR amide proton relaxation experiments. I first performed aSEC-MALS of 10 mg/ml isolated C-lobe in the presence of 5 mM DTT which suggested a molecular mass of 13.3 ± 0.4 kDa which is consistent with a monomeric species (M_W of E6AP C-lobe: 13.4 kDa) **(Figure 31A)**. In the absence of DTT, a second species with a molecular mass of 26.8 ± 2.1 kDa eluted prior to the main peak of monomeric E6AP C-lobe **(Figure 31B)**. NMR relaxation experiments in the presence of reducing agent showed no significant concentration dependent changes for E6AP C-lobe between 200 µM and 1000 µm (data not shown). These results are consistent with the idea that the C-lobe dimerizes only at very high concentration driven by the chemical reactivity of the cysteine residues in the absence of reducing agent.

I was able to purify an E6AP C-lobe dimer by preparative SEC after extensively concentrating the dialyzed protein in the absence of reducing reagent **(Figure 31C)**. The dimer containing fractions were pooled, concentrated and analyzed by aSEC-MALS which was consistent with a dimeric species (M_W = 26.6 ± 3.5 kDa) **(Figure 31D)**. The protein was then subjected to crystallization trials at concentrations ranging from 30 to 60 mg/ml. After six months, single crystals of diamond shape grew in a variety of conditions at acidic pH (4.6 to 6.5) in different precipitants (0.2 M $MgCl_2$, 0.05 M Sodium Cacodylate pH 6.0, 2.5 M KCl; 0.2 M Zinc Acetate, 0.1 M Sodium Cacodylate pH 6.5, 10% Isopropanol; 0.2 M NaCl, 0.1 M BisTris pH 5.5, 25% PEG3350; 0.1 M CaCl, 0.1 M Sodiumacetat pH 4.6, 30% PEG400; 0.1 M MES pH 6.0, 20% PEG6000; 0.2 M CaCl, 20% PEG3350) **(Figure 31E)**. They were harvested, cryo-protected in a solution containing mother liquor supplemented with 20-25% ethylene glycol and flash-frozen in liquid nitrogen. Initial diffraction data analysis confirmed that all crystals belonged to the same space group with similar unit cell parameters. Native data were collected to a maximum resolution of 1.3 Å resolution at BESSY II Berlin. Data were integrated with XDS and scaled with XSCALE [97]. By molecular replacement using Phaser [148] (C-lobe extracted from PDB ID: 1C4Z [85]), the structure could be solved in space group I4222. The model was then manually built in COOT and individual coordinates and B-factors were refined with REFMAC5 [160] or PHENIX.refine [2]. Data collection and preliminary statistics for processing and refinement are summarized in **Table 12**. However, note that these statistics are not validated yet and require more work. **Figure 31F** shows a preliminary crystallographic model in which the C-lobe forms a swapped dimer with a symmetry mate. The swapped region comprises the C-terminal α-helix (H14) and adjacent β-strand (S10).

The composite fold resembles the structure of an isolated C-lobe (extracted from PDB ID: 1C4Z [85]) **(Figure 31F)**. In course of refinement I noticed that the data might be reprocessed in a space group of lower symmetry which is an ongoing work. Thus, the model in **Figure 31F** should be treated with cautious. Anyhow, this domain swap likely presents an artifact arising at very high protein concentrations.

Table 12: Initally processed data collection, phasing and preliminary refinement statistics of the domain swapped E6AP C-lobe

Data collection	
Space group	I 4 2 2
Cell dimensions	
	72.3
a, b, c (Å)	72.3
	99.0
α, β, γ (°)	90
Wavelength	0.91842
Resolution (Å)	30.01-1.30 (1.347-1.30)
R_{pim}	1.3 (50.2)
CC1/2	100 (67.6)
$I/\sigma I$	26.6 (1.5)
Completeness (%)	100 (99.7)
Redundancy	8.5 (8.1)
Refinement	
Resolution (Å)	30.0-1.3 (highest shell)
No. reflections (free)	32539 (3211)
R_{work}/R_{free}	16.0/19.0 (30.0/30.6)
No. atoms	1875
B-factors	18.0
Rms deviations	
Bonds (Å)	0.018
Angles (°)	2.07

Table 12 listed the parameters of data collection, phasing procedure and preliminary refinement statistics for the crystal structure of a domain swapped E6AP C-lobe. The data of the high resolution shell is given in parenthesis. R_{Pim}: precision indicating merging R-factor; $CC_{1/2}$: correlation coefficient factor ½; $I/\sigma I$: I/Sigma(I); Rms: root mean square.

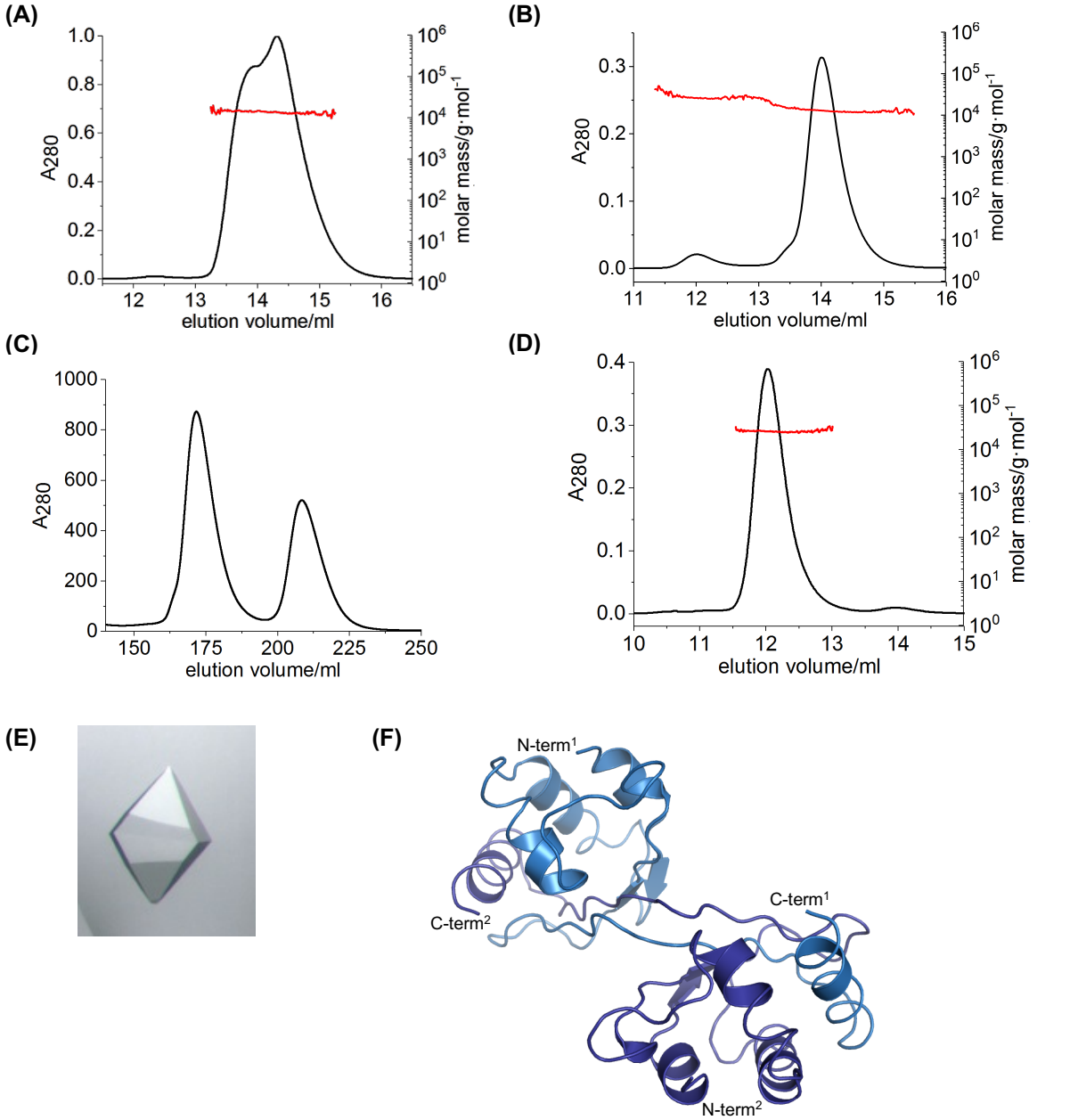

Figure 31: E6AP C-lobe tends to dimerize *in vitro* at high concentrations. aSEC-MALS analysis of E6AP C-lobe in 50 mM Tris/HCl, pH 7.5, 200 mM NaCl using a SD 75 10/300 GL column at RT with **(A)** 10 mg/ml E6AP C-lobe in the presence of 5 mM DTT, **(B)** 3.5 mg/ml E6AP C-lobe in the absence of DTT. The RI signal (red line) indicates homogenous protein with an apparent M_W of **(A)** 13.3 ± 0.4 kDa, **(B)** first peak 26.8 ± 2.1 kDa, second peak 13.0 ± 0.3 kDa. **(C)** SEC with a HiLoad SD 26/600 75 pg in 50 mM Tris/HCl, pH 7.5, 200 mM NaCl. **(D)** aSEC-MALS analysis with 4 mg/ml E6AP C-lobe dimer in 50 mM Tris/HCl, pH 7.5, 75 mM NaCl using a SD 75 10/300 GL column at RT. The RI signal indicates homogenous protein with an apparent M_W of 26.6 ± 3.5 kDa. **(E)** Best diffracting crystal from the initial screening condition (0.1 M Sodiumacetat, pH 4.6, 0.1 M CaCl, 30% PEG4000) of E6AP C-lobe. **(F)** Ribbon representation of the preliminary crystal structure of a domain swapped dimer between the E6AP C-lobe and a symmetry mate.

4.4.5 Canonical donor ubiquitin recognition by NEDD4

In a proof-of-principle experiment the crystal structure of ubiquitin G75C bound to the C-lobe of NEDD4 was solved following the crosslinking strategy with Ellman's reagent, which I used previously to link ubiquitin with E6AP **(Figure 25, 29)**. Crosslinking was followed by an anion exchange chromatography. Hereby, the disulfide linked NEDD4 C-lobe~ubiquitin complex could be separated from the non-crosslinked species **(Figure 32A, B)**. The conjugate was concentrated up to 10 mg/ml and initial crystal trials were set up at RT. After three days I obtained rod-shaped separated crystals in 0.1 M BisTris, pH 5.5, 0.2 M $MgCl_2$, 25% PEG3350 **(Figure 32C)**. They were harvested from the crystallization set-up, supplemented with 15% glycerol (v/v) as cryogenic protectant and flash-frozen in liquid nitrogen. The best-diffracting protein crystals exhibited a resolution maximum of about 1.9 Å when tested at the X-ray home source and about 1.6 Å at the synchrotron source at BESSY II Berlin. All data were processed with XDS/XSCALE [97]. The structure of the NEDD4 C-lobe~ubiquitin complex was solved by molecular replacement with Phaser within the CCP4 suite, using the PDB entry 4BBN [144, 148]. By iterative cycles of manual building in COOT and refinement with phenix.refine, the models were improved **(Table 13)** [2]. This structure confirmed that donor ubiquitin can form the same interface with the isolated C-lobe of NEDD4 as it does in the crystal structure containing the entire HECT domain [144, 148]. While this crystal structure showed interactions between the donor ubiquitin and the C-lobe *in trans* rather than *in cis*, the relevant interface between the two proteins is indeed conserved **(Figure 32D)**. This may be explained by the one amino acid shorter ubiquitin variant used in this approach (ubiquitin G75C instead of ubiquitin G76C which was used in the deposited structure [144]). Thus, the ubiquitin variant I used was probably too short for the ideal donor interaction taking place *in cis*. However, the interface is formed by the same hydrophobic residues of ubiquitin (Ile36, Leu71) and of the NEDD4 C-lobe (Leu861, Met888, Ala889) [144]. Furthermore, hydrogen bonds between Gln40 and the main chain of Leu861, as well as between the Asn892 and the Leu8 main chain are formed **(Figure 32E)**. The rmsd is only 0.52 Å compared to the crystal structure of the whole HECT domain interacting with donor ubiquitin deposited by Maspero and colleagues [144]. This crystal structure is thus consistent with the idea that the HECT N-lobe is dispensable for donor recognition by NEDD4.

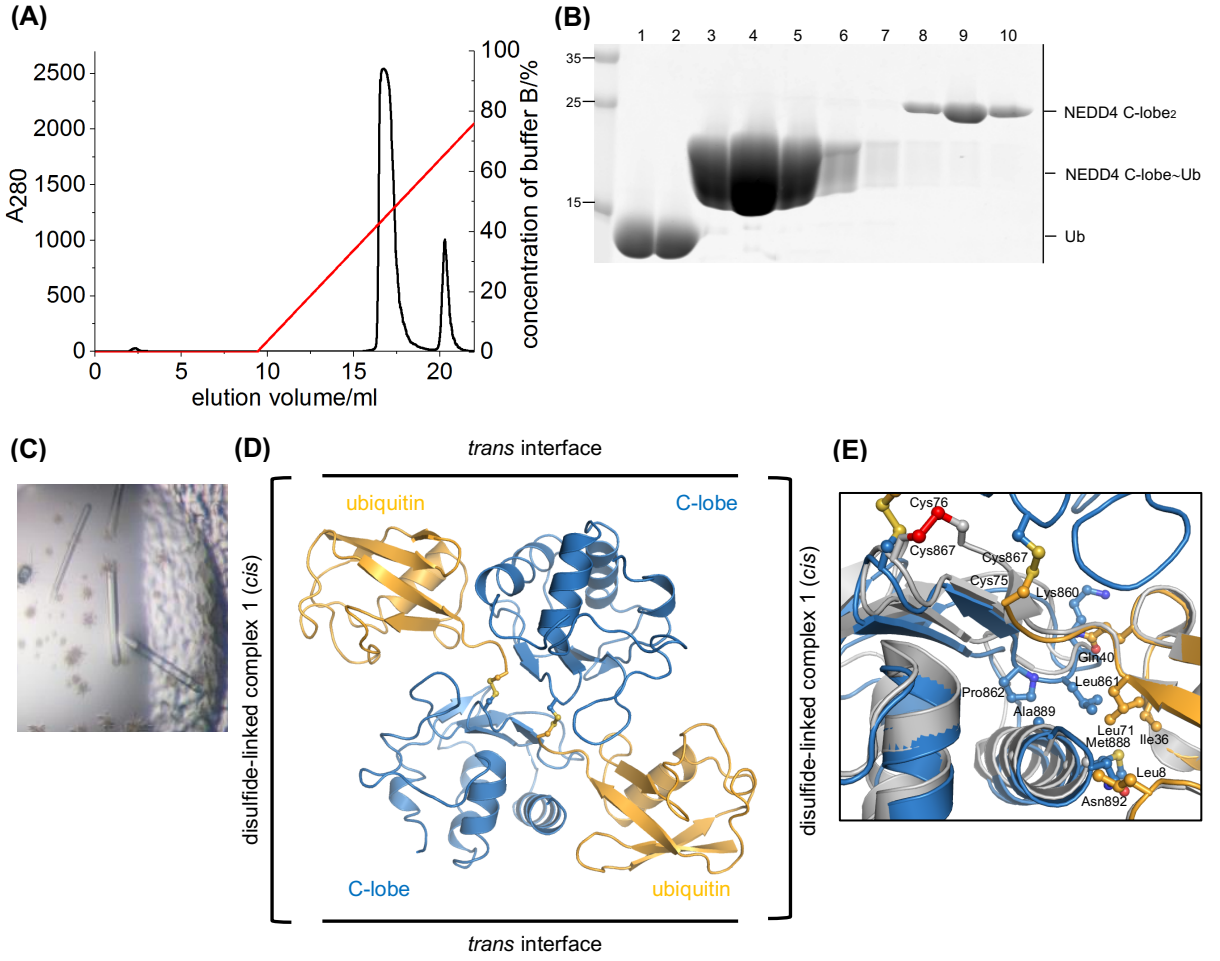

Figure 32: Ubiquitin recognition by the C-lobe of NEDD4. (A) AIEX of a disulfide-linked NEDD4 C-lobe~Ub G75C with a Mono Q 4.6/100 PE in 50 mM Tris/HCl, pH 8.0, 1 mM EDTA and 0 to 500 mM NaCl and **(B)** corresponding SDS-PAGE (1-2: every second 0.5 ml fraction from 2 ml to 3 ml; 3-10: every 0.5 ml fraction from 19 ml to 22.5 ml). **(C)** Best diffracting crystal from the initial screening condition (0.1 M BisTris, pH 5.5, 0.2 M $MgCl_2$, 25% PEG3350) of NEDD4 C-lobe~ubiquitin G75C. **(D)** Cartoon representation of two copies of the NEDD4 C-lobe~Ub G75C complex. The disulfide bonds are highlighted. In the crystal lattice the functionally relevant donor interface (shown as balls and sticks) between the C-lobe and Ub is formed *in trans*. **(E)** Structural superposition of the NEDD4 C-lobe~Ub G75C *trans* complex with the NEDD4 C-lobe~Ub G76C *cis* complex (grey; extracted from PDB ID: 4BBN [144]).

aSEC experiments were performed with the NEDD4 C-lobe~ubiquitin conjugate incubated with free NEDD4 C-lobe. Despite the high reactivity of the E6AP active site cysteine residue in context of the conjugate **(Figure 26B, C)**, free NEDD4 C-lobe was not able to be trapped by the disulfide linkage in NEDD C-lobe~ubiquitin (data not shown). Thus, NEDD4 C-lobe does not have the same tendency to dimerize in solution and this phenomenon does not represent a HECT specific feature, rather than an inherent E6AP propensity.

Table 13: Data collection, phasing and refinement statistics of the crystal structure of NEDD4 C-lobe~ubiquitin G75C

Data collection	
Space group	$P6_3$
Cell dimensions	
a, b, c (Å)	111.3 111.3 70.2
α, β, γ (°)	90 90 120
Wavelength	0.91842
Resolution (Å)	50-1.61 (1.64-1.61)
R_{pim}	3.3 (49.9)
CC1/2	99.9 (56.0)
$I/\sigma I$	16.2 (1.4)
Completeness (%)	99.8 (98.0)
Redundancy	8.0 (5.7)
Refinement	
Resolution (Å)	48.21-1.61 (highest shell)
No. reflections (free)	62385 (2096)
R_{work}/R_{free}	16.2/19.5 (27.2/30.3)
No. atoms	6678
B-factors	17.6
Rms deviations	
Bonds (Å)	0.012
Angles (°)	1.339

In **Table 13** all parameters of the data collection, the phasing procedure and the final refinement statistics for the crystal structure of the complex of NEDD4 C-lobe~ubiquitin G75C are summarized. Statistics for the highest resolution shell are given in parenthesis. R_{Pim}: precision indicating merging R-factor; $CC_{1/2}$: correlation coefficient factor ½; $I/\sigma I$: I/Sigma(I); Rms: root mean square.

4.4.6 The C-terminal tail of E6AP interacts with the donor ubiquitin and directs linkage specificity

Next, I wanted to analyze the interaction of the E6AP C-lobe with the donor ubiquitin in the context of the disulfide-linked C-lobe~ubiquitin intermediate using NMR (**Figure 33A**, left) and compare the pattern of chemical shift perturbations of C-lobe resonances induced by ubiquitin *in cis* with those seen *in trans* **(Figure 20A)**. In quantitative terms, this analysis yields overall rather similar chemical shift perturbations (**Figure 33A**, right). This is consistent with the FP-derived affinity for the interaction **(Figure 20E)**: At the given protein concentrations (200 μM C-lobe and a 12.5-fold molar access of ubiquitin) and a K_D-value of 400 μM, a complex saturation of ~85% is expected. However, the generally small amplitudes and limited number of chemical shift perturbations of E6AP resonances indicate that the donor ubiquitin retains considerable flexibility upon conjugation to the C-lobe.

Addition of high concentrations (up to 3 mM) of unlabeled ubiquitin to the conjugate results in a slight increase in the chemical shift perturbations of C-lobe resonances **(Figure 33B)**. This likely reflects an enhanced occupancy of the C-lobe-donor complex in the presence of added ubiquitin concentrations that approach the local concentrations of the covalently linked donor at the C-lobe. A defined second ubiquitin binding site on the C-lobe is not detected, indicating that interactions with the acceptor ubiquitin are extremely weak under these conditions and require additional components to be stabilized. As noted above, however, it is impossible to decide unequivocally whether the observed chemical shift perturbations result from a single or several dynamic binding modes.

In both *cis* and *trans*, major perturbations affect residues in the active site region (residues 818-823) and the rim of the flanking β-sheet (residues 755 and 802-807). Several resonances undergo pronounced chemical shift perturbations *in cis*; those correspond to Thr786, Thr787, Lys801, Met802, and Phe821, all of which are located in structural elements near the catalytic cysteine to which the C-terminal tail of ubiquitin is covalently attached; and Leu814 and Thr816, which fall into the canonical donor interface, in line with the model of thioester formation **(Figure 23B)**. Notably, specific chemical shift perturbations *in cis* are also observed in the C-terminal region of E6AP ('C-tail'; residues 845-852) **(Figure 33A, C)**, indicating that the C-tail contributes to interactions with the donor, once a covalent linkage between the C-lobe and ubiquitin has been established.

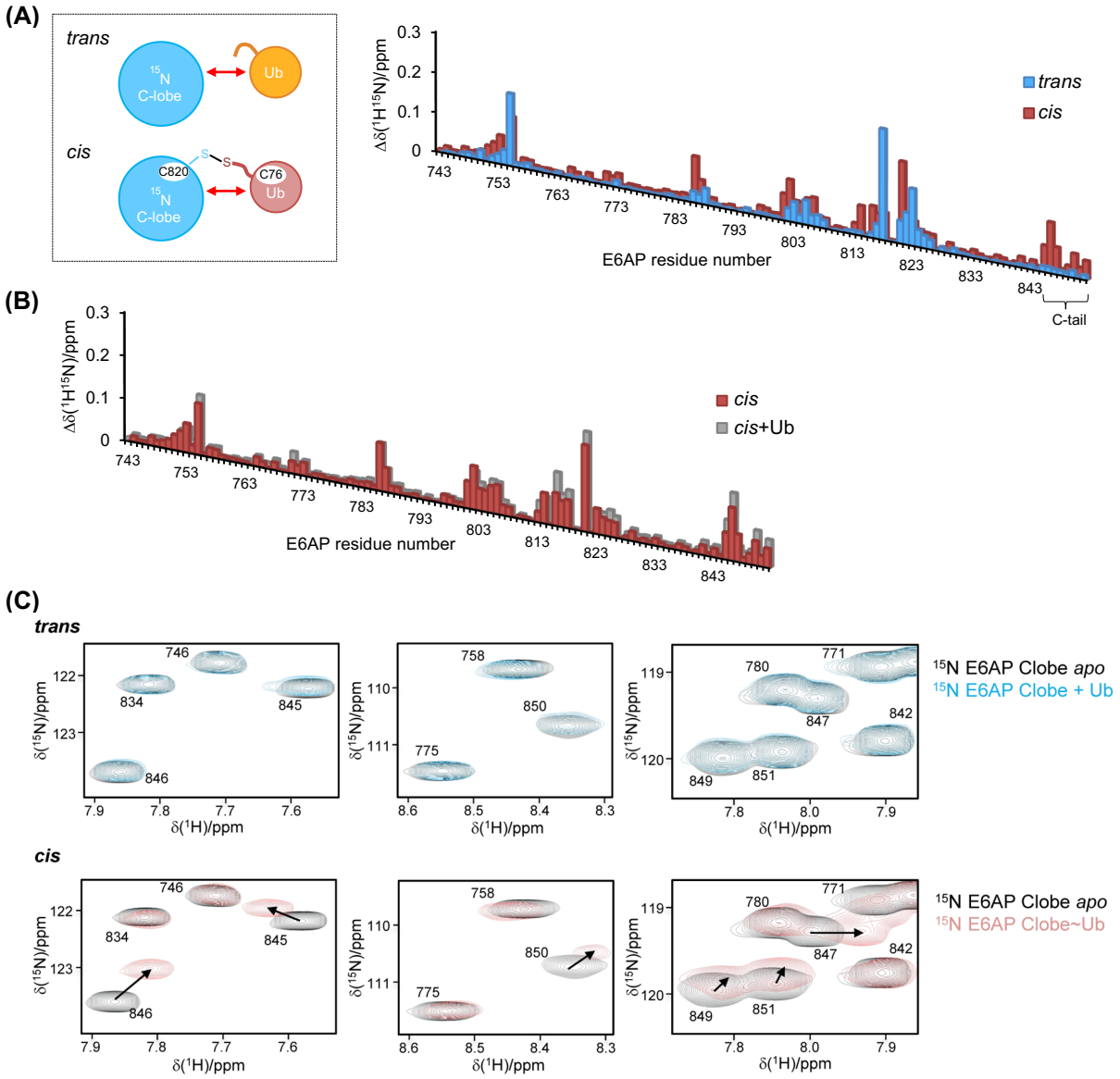

Figure 33: The C-terminal tail of E6AP interacts with the donor ubiquitin. (A) Schematic of the protein samples used to monitor the interactions of the ^{15}N-enriched C-lobe of E6AP and Ub *in trans* or in the context of a disulfide-linked complex containing Ub G76C (left). Weighted, combined chemical shift perturbations, $\Delta\delta(^1H^{15}N)$ of C-lobe resonances induced by ubiquitin *in trans* (12.5-fold molar excess) or *cis* plotted over the E6AP residue number (right). The functionally important 'C-tail' region is marked. **(B)** Weighted, combined chemical shift perturbations, $\Delta\delta(^1H^{15}N)$, of E6AP C-lobe resonances in the context of a covalent conjugate (*in cis*, see **(A)**) in the absence or presence of additional Ub (at 15-fold molar excess). **C)** Sections of the ^{1}H-^{15}N BEST-TROSY spectra (as analyzed in **(A)**) featuring resonances that originate from the C-tail. Each section shows a superposition of spectra in the presence (blue and rose, respectively) and absence (black) of Ub.

The C-terminal region of the C-lobe ('C-tail') of HECT ligases is an important element in these enzymes for catalysis, but its precise mechanistic role, however, has remained elusive [98, 144, 197, 220]. While the C-tail of E6AP is disordered in the available crystal structures [85], the last of the resolved residues is close to the catalytic site, and might thus affect both the donor and the acceptor ubiquitin. To dissect the function of the C-tail of E6AP variants of the

HECT domain were generated in which a conserved phenylalanine, Phe849, four residues from the C-terminus is replaced by alanine (F849A) or the four C-terminal residues are deleted ('Δ4'). Secondary structure analysis of the two tail mutants using CD spectroscopy revealed structural integrity in comparison to the wild-type protein **(Figure 34A)**. In line with previous mutational analyses, both variants promote thioester formation with the donor ubiquitin to a similar degree as the WT **(Figure 34B)** [190, 197].

With regards to isopeptide bond formation, both HECT domain variants form Ub_2 with similar efficiencies as the WT **(Figure 34C)**. However, they show slightly reduced activity in overall auto-ubiquitination, as quantified by the turnover of unmodified E6AP, and a pronounced defect in chain elongation during auto-ubiquitination **(Figure 34C)**.

These observations prompted me to examine whether the C-tail influences the recognition of the acceptor ubiquitin and linkage specificity of E6AP. Comparing the activities of the HECT domain variants (WT, F849A, Δ4) towards WT ubiquitin, individual Lys-to-Arg variants (K6R, K11R, K27R, K29R, K33R, K48R, and K63R), and a lysine-free variant ('K0'; all lysine residues replaced by arginine), respectively **(Figure 35A-C)** revealed that the C-tail variants promote Ub_2 formation with each of the single Lys-to-Arg variants of ubiquitin, including K48R. In contrast, the WT HECT domain is highly selective for the formation of Lys48-linkages, in line with previous studies [107, 109, 225]. Notably, K0 ubiquitin is a poor substrate for all three E6AP variants, indicating that linkage formation through the N-terminal amino group of ubiquitin is generally disfavored, regardless of the integrity of the C-tail **(Figure 35A-C)**.

To corroborate these findings, my collaboration partners Kirandeep Deol and Prof. Eric Strieter (University of Massachusetts, Amherst, MA/USA) analyzed the linkage composition of Ub_2 species assembled by the WT, F849A, and Δ4 HECT domain variants by AQUA MS (absolute quantification mass spectrometry) (**Figure 35D**, Supplementary Data **Figure 45**). These analyses confirm that the WT HECT domain is Lys48-specific. Alteration of the C-tail, however, results in a loss of specificity, as evidenced by the formation of Lys11- and Lys63-linkages. Notably, these data demonstrate also that studies on Lys-to-Arg variants of ubiquitin do not exactly mirror Ub-AQUA MS analyses (performed in the context of WT ubiquitin), consistent with previous reports, cautioning direct correlation of these two types of measurements [84].

Taken together, I conclude that the C-tail of E6AP, mediated by Phe849, contacts the donor ubiquitin in the covalently linked intermediate and contributes to Lys48-linkage specificity in chain formation by restricting the recognition of the acceptor ubiquitin.

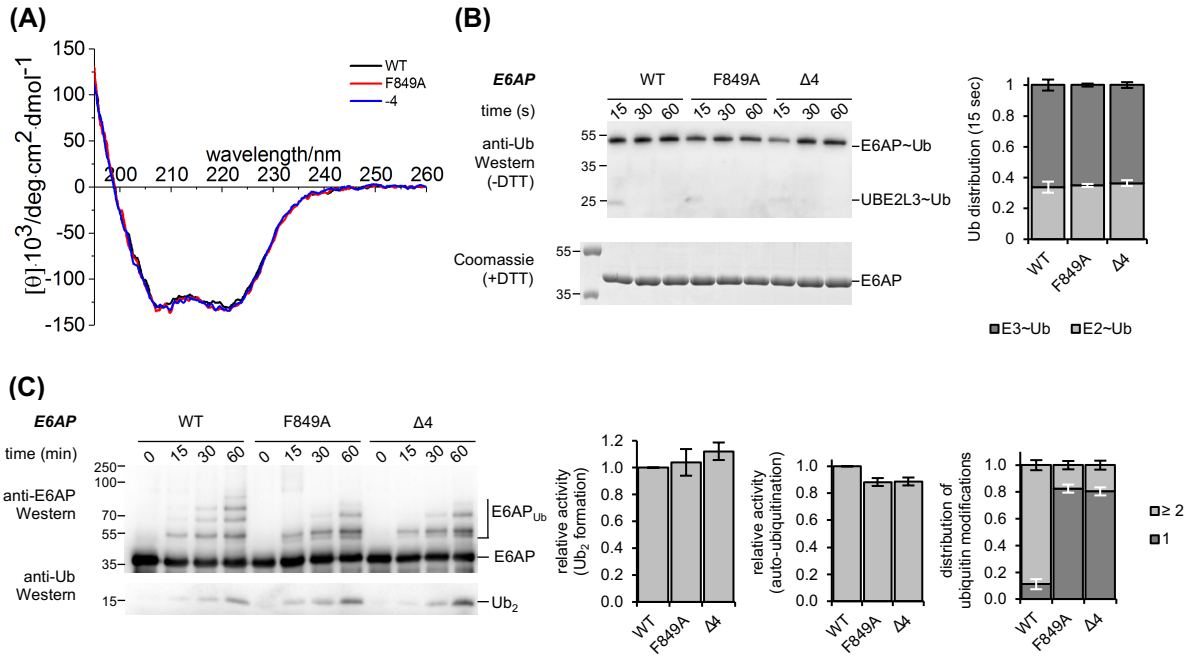

Figure 34: The C-terminal tail of E6AP does not impact thioester formation of the HECT domain with ubiquitin but has a pronounced defect in chain elongation during auto-ubiquitination. (A) CD spectra of E6AP HECT domain tail variants in comparison to WT. The spectra were recorded with 4 μM of protein in 10 mM sodium phosphate, pH 7.4. The resolution was 0.1 nm and the speed 50 nm/min, bandwidth 1 nm, attenuation 2 s (10 accumulations). **(B)** Thioester transfer of ubiquitin from the E2 (UBE2L3) to the E6AP HECT domain, followed in single-turnover, pulse-chase assays at 3 time points, as indicated, and monitored by non-reducing SDS-PAGE and anti-ubiquitin Western blotting. The thioester-linked HECT domain-ubiquitin conjugate ('E6AP~Ub') and, in some cases, the thioester-linked E2-ubiquitin precursor ('UBE2L3~Ub') are visible. The input amount of HECT domain ('E6AP') is monitored by reducing SDS-PAGE and Coomassie staining. The amounts of E6AP~Ub and UBE2L3~Ub were quantified and normalized to the input amount of E6AP. Quantifications are based on 3 independent experiments; the means and standard deviations were plotted for the 15-sec time point. **(C)** Isopeptide bond formation assays comparing the activities of the E6AP HECT domain WT and C-terminal tail variants. Activities are monitored at 3 time points, as indicated, by reducing SDS-PAGE and Western blotting against E6AP (HECT domain auto-ubiquitination marked as '$E6AP_{Ub}$') and ubiquitin (di-ubiquitin reaction product marked as 'Ub_2'), respectively. Time point zero denotes samples before ATP addition. The amounts of Ub_2 and unmodified E6AP were quantified and normalized to the input amount of E6AP. In addition, the contributions of mono-ubiquitination (1 ubiquitin moiety) and chain formation/multi-mono-ubiquitination (≥ 2 ubiquitin moieties) were quantified for each variant individually (with the total amount set to 1). Quantifications are based on 3 independent experiments; the means and standard deviations were plotted for the 60-min time point. The assay was performed at 30 °C with 0.2 μM UBA1, 2 μM UBE2L3, 2 μM E6AP HECT domain variant, 200 μM Ub in 50 mM Tris/HCl, pH 7.0, 75 mM NaCl, 2 mM DTT, 2 mM ATP and 10 mM $MgCl_2$ for 1 h.

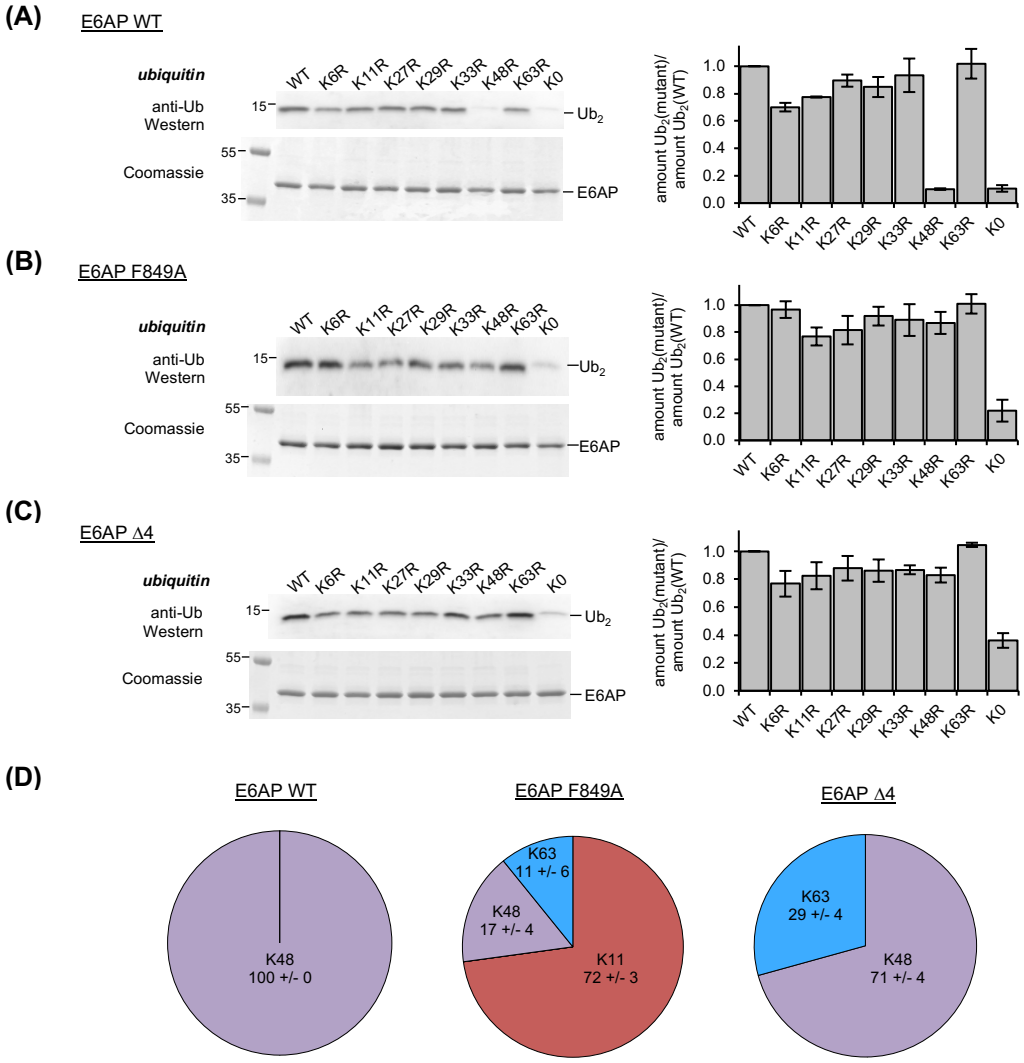

Figure 35: The C-terminal tail of E6AP directs Lys48-linkage specificity. (A-C) Assays monitoring the activities of the E6AP HECT domain WT and C-terminal tail variants towards Ub WT, single Lys-to-Arg variants, or a lysine-free ('K0') variant, respectively, by reducing SDS-PAGE and Western blotting against ubiquitin (di-ubiquitin reaction product marked as 'Ub_2'). Assays were conducted at 30 °C with 0.2 μM UBA1, 2 μM UBE2L3, 2 μM E6AP HECT domain variant and 200 μM Ub variant in 50 mM Tris/HCl, pH 7.0, 75 mM NaCl, 2 mM DTT, 2 mM ATP and 10 mM $MgCl_2$ for 15 min; the input amount of HECT domain ('E6AP') in the absence of ATP is monitored by reducing SDS-PAGE and Coomassie staining (left). The amount of Ub_2 was quantified and the ratio of the amounts of mutated Ub_2 to WT Ub_2 plotted. Quantifications are based on 3 independent experiments; the means and standard deviations were plotted for the 60-min time point (right). **(D)** AQUA mass spectrometric analysis of Ub_2 species formed by the E6AP HECT domain WT, F849A, and Δ4 variants performed by Kirandeep Deol and Prof. Eric Strieter. Results were normalized to the total amount of ubiquitin for each linkage type detected; the means and standard deviations from three replicates are shown. The corresponding data are provided in the Supplementary Data **Figure 45**.

4.4.7 A hydrophilic surface near Lys48 is critical for acceptor ubiquitin function with E6AP

To further decipher the requirements of acceptor ubiquitin recognition during E6AP-mediated ubiquitin linkage formation, I focused on an array of hydrophobic residues of ubiquitin (Leu8, Ile44, Val70), often referred to as the 'hydrophobic patch', that was reported to be critical for E6AP activity [156]. Since these residues do not fall into the canonical donor-C-lobe interface formed during thioester formation **(Figure 36A)**, I hypothesized that they may be required for additional interactions of the donor or, alternatively, for interactions of the acceptor ubiquitin. In addition, I decided to interrogate the functional significance of a series of hydrophilic residues of ubiquitin in proximity to the Lys48-acceptor site, including Arg42, Gln49, and Glu51 **(Figure 36A)**. Isopeptide bond formation assays, monitoring the activity of the E6AP HECT domain towards ubiquitin variants with individual alanine substitutions at the selected sites were performed. These studies confirm that residues in the hydrophobic patch of ubiquitin, as well as Arg42, and Gln49, are important for E6AP activity **(Figure 36B)**. Surprisingly, the E51A variant presents a better substrate for E6AP than WT ubiquitin **(Figure 36B)**. None of the tested mutations interfere with thioester transfer of ubiquitin to the E2 or E3 **(Figure 37A, B)**.

To understand the precise roles of the mutated, functionally important residues in ubiquitin for E6AP catalysis and discriminate donor from acceptor functions, a strategy previously used for the mechanistic analysis of E2-ubiquitin interactions was adopted [145, 233]. It involves a truncated ubiquitin variant, $Ub^{\Delta GG}$ (residues 1-74), which cannot be activated by the E1 and thus solely acts as an acceptor (**Figure 38A**, left). When supplied with a mixture of $Ub^{\Delta GG}$ and full-length ubiquitin, the E6AP HECT domain assembles two distinct Ub_2 species, which contain either two full-length ubiquitin molecules or a full-length ubiquitin molecule linked distally to a $Ub^{\Delta GG}$-variant. If one ubiquitin variant is employed with a His_6-tag, these alternate reaction products can be readily separated by SDS-PAGE and provide a selective read-out of mutational effects on the donor and acceptor functions. A proof-of-concept experiment is shown in **Figure 38A** (right). Using this set-up, I revealed that residues in the hydrophobic patch (Leu8, Ile44, and Leu70), as well as Gln49 are exclusively required by the donor ubiquitin during E6AP-mediated chain formation **(Figure 38B, C)**. Since these residues are dispensable for thioester formation, this implies that they mediate alternate interactions of the donor ubiquitin during isopeptide bond formation. Mutation of Arg42 interferes with both the donor and the acceptor ubiquitin functions **(Figure 38B, C)**. In contrast, mutation of Glu51 specifically promotes the function of the acceptor ubiquitin **(Figure 38B, C)**.

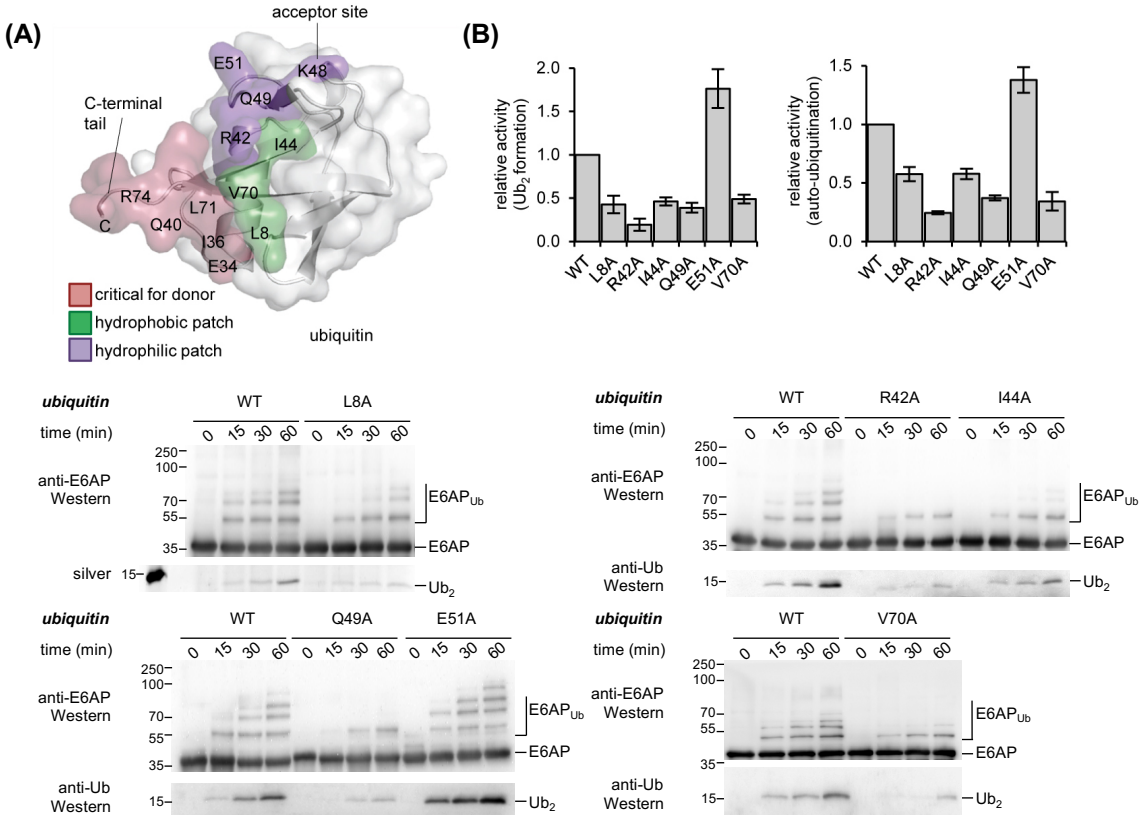

Figure 36: The hydrophobic patch and a hydrophilic region adjacent to Lys48 of ubiquitin are important for E6AP activity. (A) The structure of ubiquitin (PDB ID: 1UBQ [221]) is shown in ribbon and surface representation. The area of the donor ubiquitin, including the C-terminal tail, that contacts the HECT C-lobe in the canonical mode during thioester formation is colored rose; hydrophobic residues important for E6AP activity green [156]; and residues in proximity of the acceptor site, Lys48, as studied here, in purple. **(B)** Isopeptide bond formation assays comparing the activities of the E6AP HECT domain towards ubiquitin variants. Activities are monitored at 3 time points, as indicated, by reducing SDS-PAGE and Western blotting against E6AP (HECT domain auto-ubiquitination marked as '$E6AP_{Ub}$') and ubiquitin (di-ubiquitin reaction product marked as 'Ub_2'), respectively. For the L8A variant, silver staining was used in lieu of anti-ubiquitin Western blotting, since this variant is not detected well by the ubiquitin antibody (P4D1) used here. Time point zero denotes samples before ATP addition. The amounts of Ub_2 and $E6AP_{Ub}$ were quantified and normalized to the input amount of E6AP. Quantifications are based on 3 independent experiments; the means and standard deviations are plotted for the 60-min time point. The assay was performed at 30 °C with 0.2 μM UBA1, 2 μM UBE2L3, 2 μM E6AP HECT WT, 200 μM Ub variant in 50 mM Tris/HCl, pH 7.0, 75 mM NaCl, 2 mM DTT, 2 mM ATP and 10 mM $MgCl_2$ for 1 h.

Based on these observations, I speculated that the E51A mutation may alter the recognition of the acceptor ubiquitin by E6AP and allow for the formation of linkages other than Lys48. To test this idea, I analyzed the Ub_2 species assembled from WT and E51A ubiquitin by Western blotting using two anti-ubiquitin antibodies, which recognize all linkage types (P4D1) and Lys48-linkages (D9D5), respectively **(Figure 39D)**. Quantification of the relative amounts of Ub_2 detected by these antibodies suggests that the E51A mutation in ubiquitin triggers a loss in the Lys48-specificity of E6AP and enables the formation of alternate linkage types. Although my collaboration partners, Kirandeep Deol and Prof. Eric Strieter, could not accurately quantify the proportion of Lys48 linkages formed with the E51A variant due to the

impact of the mutation on the ionization, AQUA analysis reveals Lys11 as the alternative linkage (**Figure 38E**, Supplementary Data **Figure 46**). By contrast, Lys48 linkages are exclusively formed with WT ubiquitin **(Figure 35D, Figure 45A)**.

Taken together, these studies assign distinct roles to individual surfaces of ubiquitin during E6AP-mediated isopeptide bond formation: (i) The hydrophobic patch, along with Arg42 and Gln49, is required by the donor ubiquitin for interactions other than those formed with the C-lobe during thioester formation; these may involve interactions with the N-lobe, the acceptor ubiquitin, or alternate interaction modes with the C-lobe. (ii) A hydrophilic patch adjacent to Lys48 is utilized by the acceptor ubiquitin, with Glu51 making critical contributions to the Lys48-linkage specificity of E6AP.

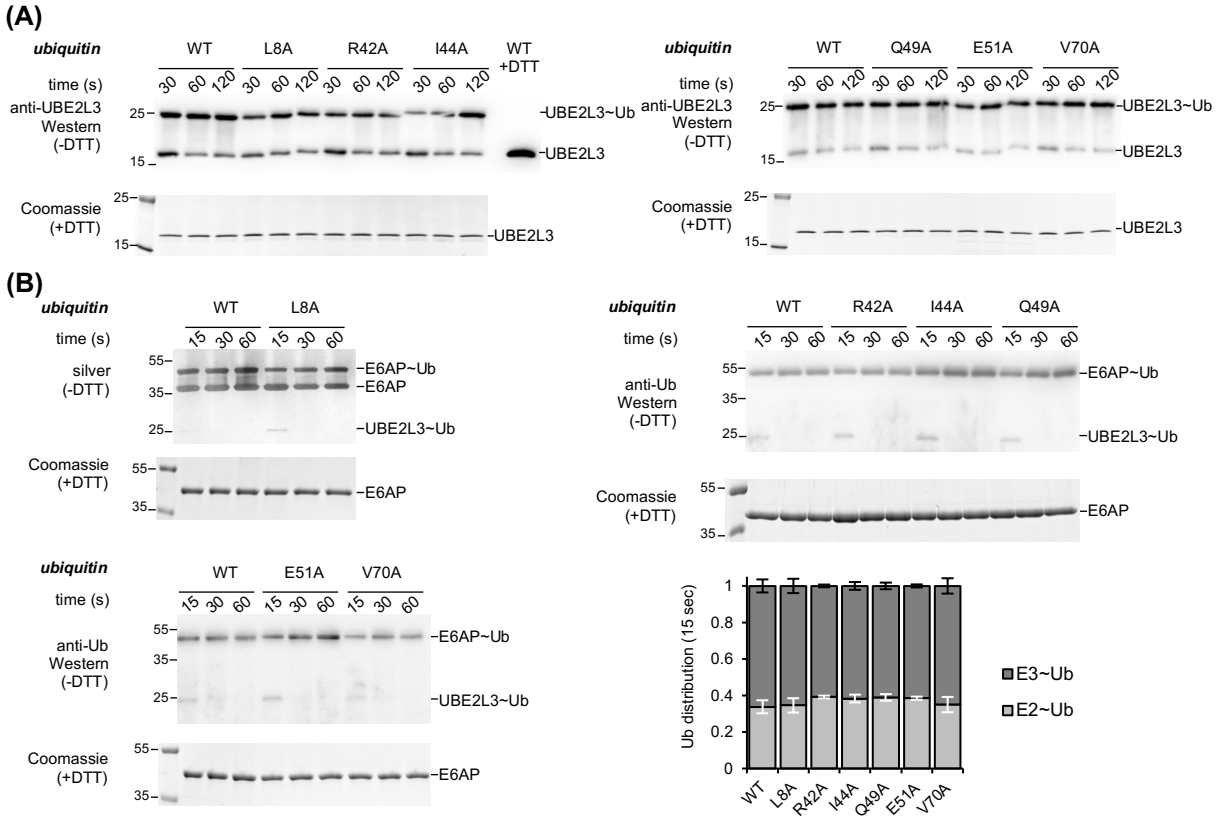

Figure 37: Mutations in the hydrophobic patch and in a hydrophilic region adjacent to Lys48 of ubiquitin do not disrupt thioester transfer of ubiquitin to UBE2L3 nor to E6AP. (A) Thioester transfer of ubiquitin variants from the E1 (UBA1) to the E2 (UBE2L3), followed in single-turnover, pulse-chase assays at 3 time points, as indicated, and monitored by non-reducing SDS-PAGE and anti-UBE2L3 Western blotting. The input amount of E2 ('UBE2L3') was monitored by reducing SDS-PAGE and Coomassie staining. **(B)** Thioester transfer of ubiquitin variants from the E2 (UBE2L3) to the E6AP HECT domain, followed in single-turnover, pulse-chase assays at 3 time points, as indicated, and monitored by non-reducing SDS-PAGE and anti-ubiquitin Western blotting. For the L8A variant, silver staining was used in lieu of anti-ubiquitin Western blotting, since this variant is not detected well by the ubiquitin antibody (P4D1) used here. The thioester-linked HECT domain-ubiquitin conjugate ('E6AP~Ub') and, in some cases, the thioester-linked E2-ubiquitin precursor ('UBE2L3~Ub') are visible. The input amount of HECT domain ('E6AP') is monitored by reducing SDS-PAGE and Coomassie staining. The amounts of E6AP~Ub and UBE2L3~Ub were quantified and normalized to the input amount of E6AP. Quantifications are based on 3 independent experiments; the means and standard deviations are plotted for the 15-sec time point.

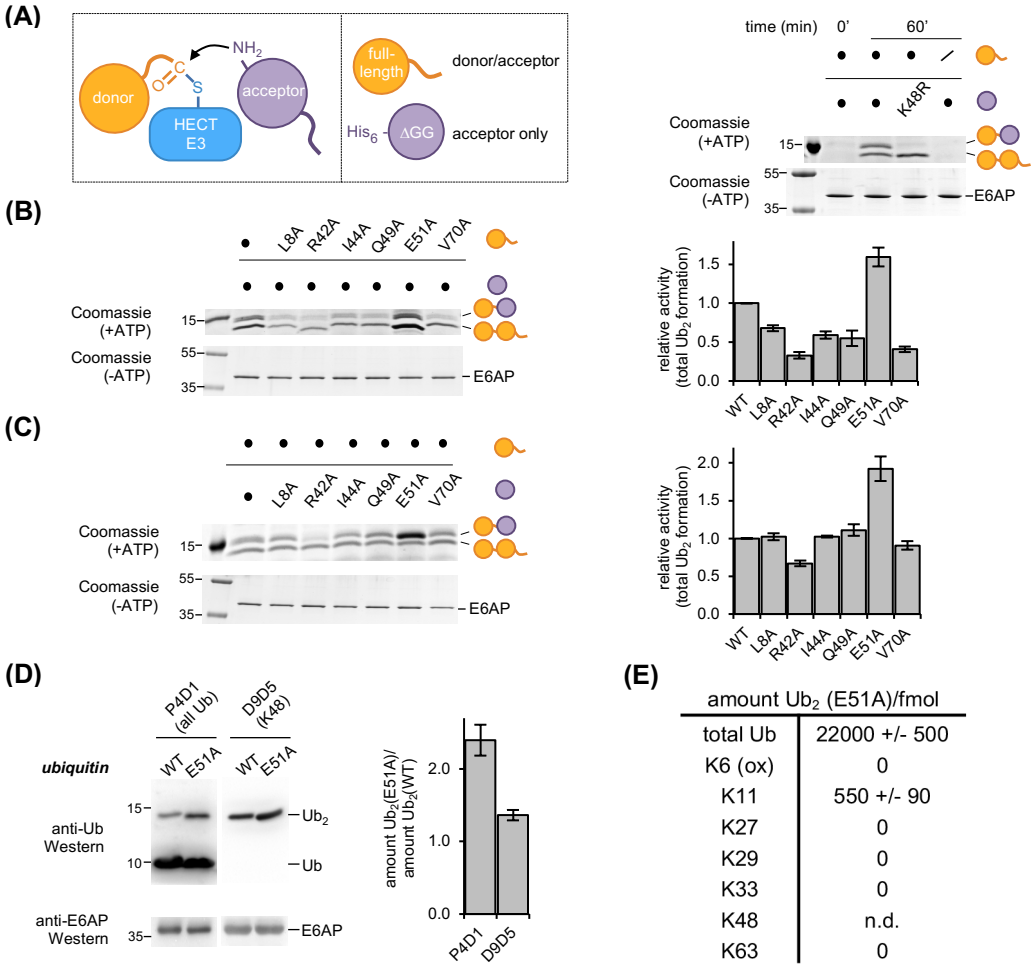

Figure 38: A hydrophilic region in proximity to Lys48 of ubiquitin is critical for acceptor recognition and linkage specificity. (A) Schematic of HECT ligase-mediated linkage formation between an enzyme-linked donor and an acceptor ubiquitin (left); and the two ubiquitin substrates employed in the 'ΔGG assay': WT ubiquitin and His_6-tagged, truncated ubiquitin (residues 1-74; '$Ub^{\Delta GG}$') (middle); validation of the assay using the E6AP HECT domain and equimolar mixtures of the indicated ubiquitin substrates. The Ub_2 reaction products were analyzed by reducing SDS-PAGE and Coomassie staining. The amount of E6AP in the absence of ATP serves as an input control. **(B, C)** ΔGG assay with ubiquitin variants, performed and analyzed as in **(A)**. The amount of both Ub_2 products combined were quantified, normalized to the amount of input E6AP, and the means and standard deviations from 3 independent experiments were plotted (right). **(D)** Comparison of the activity of the E6AP HECT domain towards ubiquitin WT and the E51A variant respectively, monitored by reducing SDS-PAGE and Western blotting. Two different anti-ubiquitin antibodies were used: P4D1 to monitor all ubiquitin modifications and D9D5 for Lys48-linkages. The amount of E6AP is shown as an input control, monitored by reducing SDS-PAGE and Western blotting against E6AP (left). The amounts of Ub_2 assembled from the WT and E51A ubiquitin variants were quantified after 30 min and the mean ratios and standard deviations from 3 independent experiments plotted (right). The assay was performed at 30 °C with 0.2 μM UBA1, 2 μM UBE2L3, 2 μM E6AP HECT WT, 200 μM Ub variant in 50 mM Tris/HCl, pH 7.0, 75 mM NaCl, 2 mM DTT, 2 mM ATP and 10 mM $MgCl_2$. **(E)** Amounts of Ub_2 species linked through individual lysine residues from reactions supplied with ubiquitin E51A, measured by AQUA MS (performed by Kirandeep Deol and Prof. Eric Strieter). The values reflect the means and standard deviations from 3 biological replicates. Note that Lys48-linkages could not be quantified reliably in this set-up, due to the E51A mutation impacting peptide ionization. The corresponding data are provided in the Supplementary Data **Figure 46** (corresponding data on Ub WT: **Figures 35D**, **Figure 45**).

4.4.8 The N-lobe of E6AP interacts with ubiquitin

To test for interactions between ubiquitin and the N-lobe of E6AP Dr. Bodo Sander performed FP experiments, analogous to the studies of the C-lobe. These data reveal that the isolated N-lobe binds to ubiquitin; the dissociation constant, 70 +/- 6 µM, is similar to the one measured for the full HECT domain (83 +/- 6 µM) **(Figure 39A)** and significantly tighter than the one he determined for the isolated C-lobe (400 +/- 20 µM; **Figure 20E**).

Since the N-lobe of several NEDD4-type enzymes was shown to recognize ubiquitin via a regulatory exosite [66, 67, 108, 143, 144, 167, 250] with comparable affinities in the micromolar range (~11 and between ~70 and 90 µM for the HECT domains of NEDD4 and RSP5, respectively [66, 108, 143]), I investigated whether E6AP also utilizes this site. Sequence and structural alignments of E6AP with NEDD4-type enzymes show that the exosite region is moderately conserved in E6AP **(Figure 40)**; for example, a particular helical linker (Asn621-Glu629 of NEDD4) that contains a functionally critical hydrophobic residue (Leu626 in NEDD4, corresponding to Phe583 in E6AP) is shortened in E6AP (Asn625 to Glu584). I introduced non-conservative mutations in E6AP at positions homologous to key residues in the exosite of NEDD4-type enzymes (Ile564, Phe583, and Phe665 of E6AP, corresponding to Tyr605, Leu626, and Phe707 of NEDD4; and Tyr516, Ile537, and Phe618 of RSP5, respectively [8, 67, 108, 143]) and Dr. Bodo Sander determined their affinities for ubiquitin by FP **(Figure 39B, C)**. Compared to the WT HECT domain, ubiquitin binding to the F665D and I564D/F583D variants is moderately weakened with K_D-values of 120 +/- 4 and 110 +/- 4 µM, respectively. In contrast, the equivalent mutations in NEDD4-type enzymes were reported to result in a drastic reduction in binding (e.g., K_D for NEDD4 F707A: 340 µM; Y605A: 87 µM [143]; RSP5 F618D and I537D: could not be determined [108]). However, the tested mutations in E6AP markedly reduce isopeptide bond formation by the HECT domain **(Figure 39D)**, while leaving thioester formation intact **(Figure 39E)**. These observations mirror the effect of the exosite in certain NEDD4-type ligases [101, 108, 143, 250], although recent studies using ubiquitin variant probes (UbVs) have indicated that the precise function of the exosite during catalysis varies across different HECT ligases [250]. Taken together, these observations indicate an important function of the exosite region of E6AP during isopeptide bond formation. Whether the newly identified interaction between the N-lobe in E6AP and ubiquitin occurs through a canonical or distinct mode of ubiquitin recognition, remains to be elucidated at a structural level.

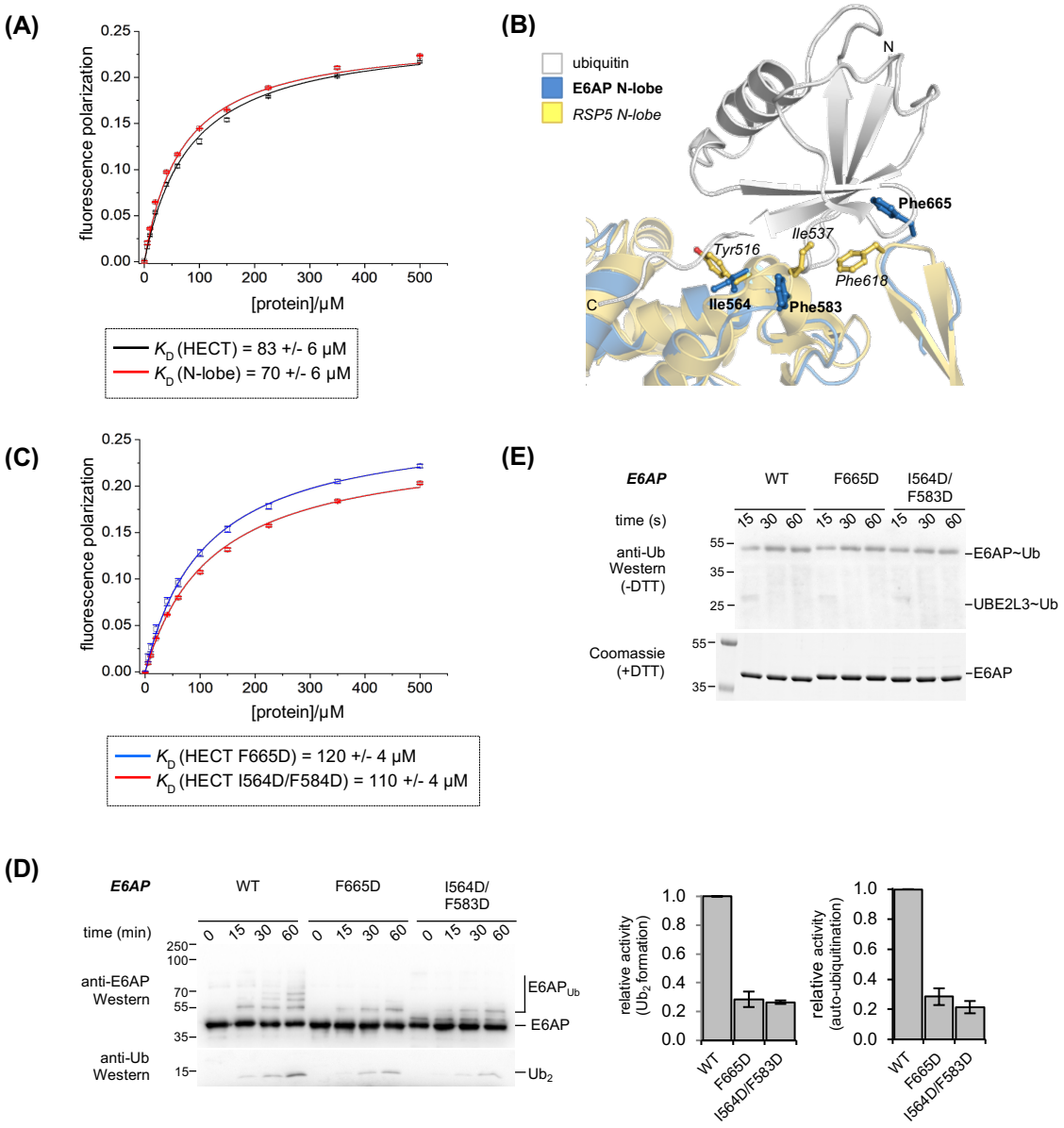

Figure 39: The N-lobe of E6AP interacts with ubiquitin, presumably in a manner that is distinct from canonical exosite interactions. (A) FP-based determination of an apparent dissociation constant, K_D, of the interaction of ubiquitin with the E6AP N-lobe and the HECT domain, respectively. The mean FP signal and standard deviations from 3 independent experiments were plotted and fitted to a single-site binding model (line). (performed by Dr. Bodo Sander). **(B)** Structural superposition of the E6AP N-lobe (extracted from PDB ID: 1C4Z [85]) with the ubiquitin-bound N-lobe of RSP5 (extracted from PDB ID: 3OLM [108]). Protein backbones are shown as ribbons, mutated residues as balls and sticks. **(C)** K_D-determination analogous to **(A)** using exosite variants of the E6AP HECT domain. **(D)** Isopeptide bond formation assays comparing the activities of E6AP HECT domain variants. Activities are monitored at 3 time points, as indicated, by SDS-PAGE and Western blotting against E6AP (HECT domain auto-ubiquitination marked as 'E6AP$_{Ub}$') and ubiquitin (di-ubiquitin reaction product marked as 'Ub$_2$'), respectively. Time point zero denotes samples before ATP addition. The amounts of Ub$_2$ and E6AP$_{Ub}$ at 60-min were quantified, normalized to the E6AP input, and the means and standard deviations from 3 independent experiments plotted. The assay was performed with 0.2 µM UBA1, 2 µM UBE2L3, 2 µM E6AP HECT variant, 200 µM Ub in 50 mM Tris/HCl, pH 7.0, 75 mM NaCl, 2 mM DTT, 2 mM ATP and 10 mM $MgCl_2$ at 30 °C for 1 h. **(E)** Thioester transfer of ubiquitin from the E2 (UBE2L3) to the E6AP HECT domain, followed in single-turnover, pulse-chase assays at 3 time points, as indicated, and monitored by non-reducing SDS-PAGE and anti-ubiquitin Western blotting. The input amount of HECT domain ('E6AP') is monitored by reducing SDS-PAGE and Coomassie staining.

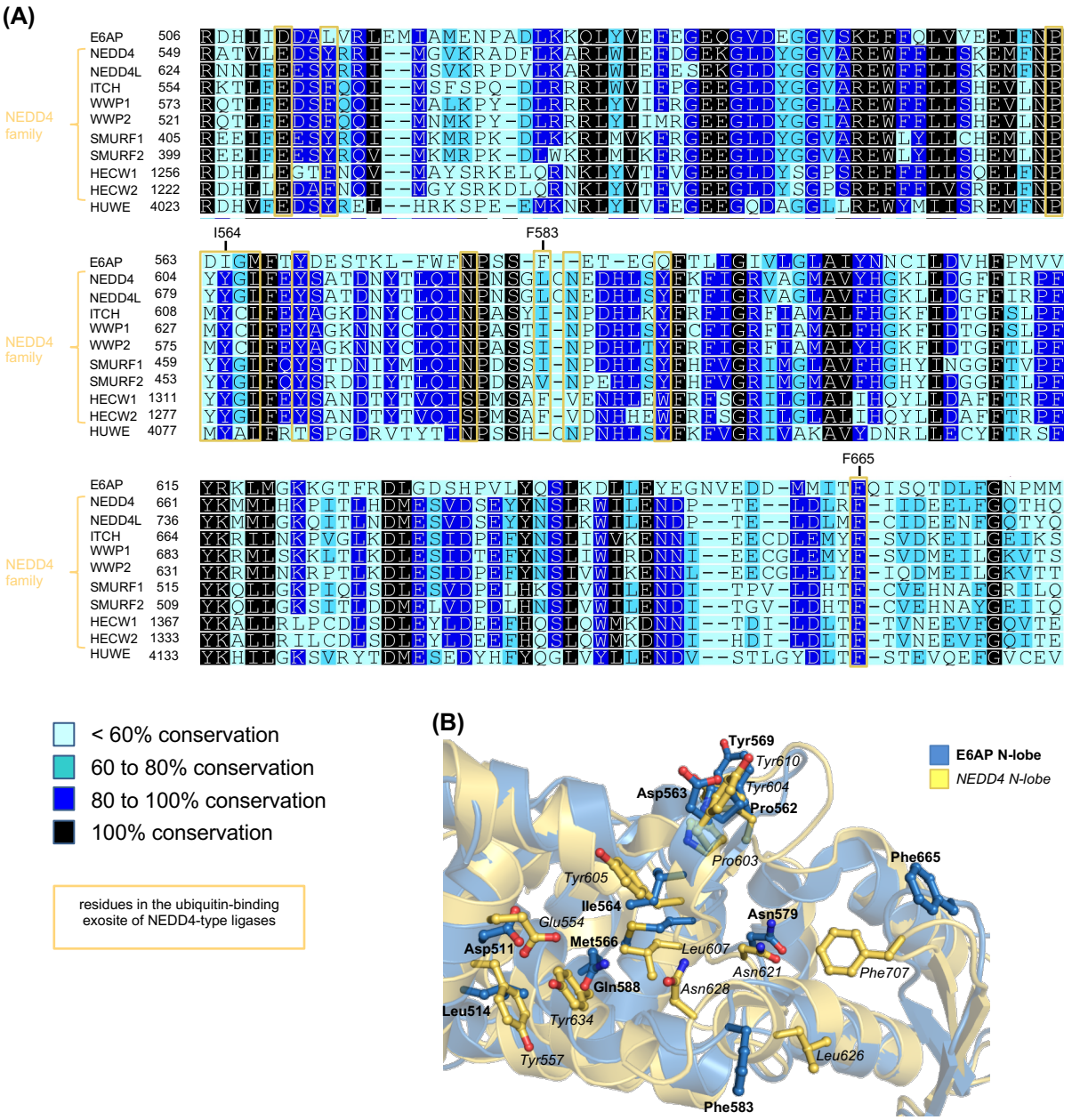

Figure 40: Residues in the ubiquitin-binding exosite of NEDD4-type ligases are partially conserved in E6AP. (A) Amino acid sequence alignment for the N-lobe of E6AP, the members of the NEDD4 subfamily (NEDD4 isoform 4, all others isoform 1), and HUWE1, as output by Clustal Omega (RRID:SCR_001591; http://www.ebi.ac.uk/Tools/msa/clustalo/) [207], illustrated with Geneious Basic (RRID:SCR_010519) [102] (generated by Dr. Bodo Sander). Residues in the exosite were defined based on the crystal structure of the ubiquitin-bound HECT domain of NEDD4 (PDB ID: 4BBN [144]) and a minimum surface burial upon complex formation of at least 50%, determined with the PISA server (http://www.ebi.ac.uk/ pdbe/prot_int/pistart.html) [114]. Residue numbers provided above the alignment refer to E6AP. **(B)** Structural superposition of the N-lobe of E6AP (extracted from PDB ID: 1C4Z [85]) and NEDD4 (extracted from PDB ID: 2XBB [143]); the C-lobes are not displayed for clarity. The proteins are shown in ribbon representation; the side chains of residues in the exosite (see **(A)**) are displayed in ball-and-stick mode (residue labels for E6AP in bolt and NEDD4 in italic).

5 Conclusion and future perspectives

HECT ligases are of major importance in medicine, given their immense functional range and the multitude of ways, in which these enzymes can malfunction in diseases and can deregulate critical signaling pathways in tumorigenesis [13, 200]. This is highlighted by the fact that many regulators of tumorigenesis are among their substrates. HECT ligases represent attractive targets for a therapeutic manipulation of specific signaling pathways in defined disease settings [30]. But still, most HECT ligases remain poorly characterized with regard to their structures and functions.

HECT ligases rely on combinatorial, weak interactions with ubiquitin, E2 enzymes, regulators and substrates to drive the conformational pathway towards their active form and thus to achieve catalytic efficiency and specificity in ubiquitin transfer. How these interactions contribute to the functional specialization of HECT E3 enzymes remain poorly understood. Here, I reported new insights into the molecular mechanism of ubiquitin recognition and ubiquitin chain formation by the HECT-type ubiquitin ligase E6AP, a key player in human papilloma virus-induced cervical carcinogenesis and several neurodevelopmental disorders. I further analyzed the oligomerization behavior of E6AP under various conditions and could uncover new features of E6AP compared to other HECT E3 enzymes. These results provide basic insights into the catalytic mechanism and functional specialization of E6AP and may generate avenues towards specific therapeutic applications.

5.1 The presence of the α1'-helix affects the solubility of the E6AP HECT domain

A tight control of HECT E3 activity contributes to ensure the required specificity and selectivity of the ubiquitination of their cognate substrates. For E6AP it was proposed that its activity is modulated by oligomerization of the HECT domain into a trimer through N-lobe-N-lobe interactions, as it was seen in a crystal structure [85, 189]. aSEC experiments in various buffer conditions revealed that the HECT domain of E6AP is monomeric in solution **(Figure 13C, D)**. In agreement with these data, MALS experiments also revealed a monomeric state **(Figure 13A, B)**, although the protein had the tendency to dimerize at excessive concentrations of around 30 mg/ml **(Figure 11D, E)**. A trimeric arrangement as seen in the crystal structure of the truncated HECT domain of E6AP is likely incompatible with the position of a predicted helix N-terminal to the HECT domain, if this region was oriented as in the NEDD4 family [8, 169]. However, the sequence of the α1'-helix of E6AP diverges from the other structurally defined HECT domains **(Figure 41)**. The α1'-helix of E6AP comprises in contrast to the other HECT ligases an additional stretch of several hydrophobic amino acids

flanked by two arginine residues **(Figure 41)**. Therefore, it should be analyzed how the α1'-helix is arranged structurally in different extended E6AP HECT domain constructs and whether its presence would preclude or allow for trimer formation. These studies should help to understand how the activity of E6AP might be modulated by oligomerization.

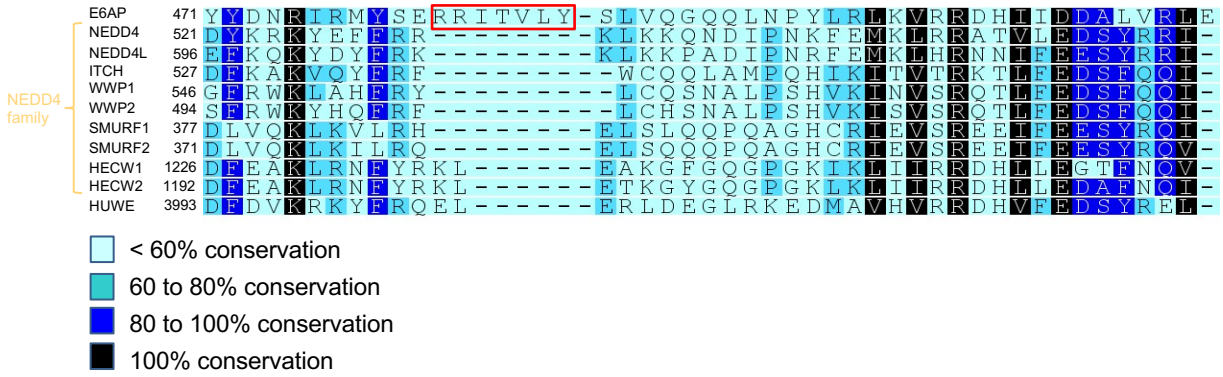

Figure 41: Multiple sequence alignment of the α1'-helix of different human HECT ligases. Amino acid sequence alignment of E6AP, the members of the NEDD4 subfamily, and HUWE1 (NEDD4 isoform 4, all others isoform 1), as output by Clustal Omega [207]. The residues of an additional seven amino acid long stretch of the α1'-helix of E6AP is highlighted. The illustration was prepared with Geneious Basic [102] by Dr. Bodo Sander.

My studies showed that the presence of the α1'-region drastically reduced the solubility of the HECT domain. Using different solubility tags and expression techniques, only one condition was found to yield soluble protein **(Table 10)**, yet it eluted in the void during SEC. The introduction of a negatively charged amino acid, Y479E, within the predicted helix yielded a soluble protein which was folded **(Figure 15E)** and was shown to be active as long as the tag was not removed **(Figure 15F)**. However, a structural picture of the HECT domain containing this helix could not be obtained. The difficulties in preparing N-terminally extended HECT domain constructs of E6AP support the notion that further N-terminal parts are needed to keep the very hydrophobic α1'-helix flanking the HECT domain protected towards the polar environment. It might also be that the α1'-helix holds the protein in a closed, inactive monomeric conformation which is relieved through interactions with hydrophobic binding partners, thus allowing for oligomerization. Such a regulatory switch would represent an exquisite mechanism to ensure regulation and specificity as suggested for NEDD4 [8], but this remains to be tested. Taken together, important questions concerning the impact of the N-terminal extension of the HECT domain are yet to be unraveled: Does E6AP trimerize in the presence of the α1'-helix? Does the structural information give insightful explanations for the effect of the autism mutation T485A which was shown to induce E6AP self-association and hyper-activation [244]? And does the presence of the α1'-helix might explain how phosphorylation of the N-lobe by the tyrosine kinase c-ABL prevents E6AP oligomerization [26]?

5.2 E6AP can auto-ubiquitinate and does not form chains on its active site *in vitro*

The structural plasticity of the HECT domain, and potentially also oligomerization, has a functional role during catalysis. Domain movements may be implicated in the transient binding and release of E2 enzymes or the repositioning of incoming ubiquitin moieties and substrates. The interaction with E2 enzymes and ubiquitin mediates substrate binding and converts the enzyme to a catalytically competent state and thus – in case of E6AP – allows to preferentially assemble Lys48-linked ubiquitin chains **(35A,D)** [107, 109, 225]. Structural data are not available on how E6AP accomplishes this Lys48-specificity in ubiquitin chain formation.

In the absence of a substrate, the E6AP HECT domain can function as its own substrate. The initial E6AP~ubiquitin thioester is rapidly discharged through competing processes of hydrolysis and transfer to a lysine residue of the HECT domain to form ubiquitin chains **(Figure 16A)**. The defined architecture of the N- and the C-lobe of the HECT domain and its thioester-bound ubiquitin during ligation restricts the orientation of the two lobes relative to each other, thus limiting the accessibility of lysine residues within the HECT domain in the auto-ubiquitination reaction. I identified several lysine residues which are auto-ubiquitinated by mass spec **(Table 11)**. Surprisingly, the substitution to an arginine of one of these lysine residues (K847R) resulted in an increased activity with respect to auto-ubiquitination and free ubiquitin chain formation **(Figure 17A)**. The same effect could be observed for K549R **(Figure 17A)**. This lysine residue could not be detected as an auto-ubiquitination site by mass spec, but its close proximity to the catalytic cysteine residue makes it to a potential candidate to be auto-ubiquitinated **(Figure 17B)**. Attesting to the idea that inter-lobe flexibility is a critical component of E6AP ligase activity, a potential auto-ubiquitination of Lys549 could hold E6AP in a locked conformation to prevent uncontrolled ubiquitination activity of E6AP. Since the C-terminal tail of E6AP contributes to donor and acceptor recognition **(Figure 33A, C, Figure 35A, D)**, ubiquitination of Lys847 at the C-terminus might interfere with ubiquitin binding and thus inhibits E6AP activity. Collectively, these data showed two potential regulatory sites within the HECT domain that might control the intrinsic E6AP activity occurring through auto-ubiquitination.

While the potential ubiquitination of Lys549 may take place *in cis*, ubiquitination of Lys847 at the C-terminus of E6AP might occur *in trans*. The intermolecular transfer of ubiquitin from one molecule to another would require at least transient oligomerization of E6AP. I could confirm that a catalytic dead mutant of E6AP (C820A) was ubiquitinated by E6AP K549R **(Figure 17C, D)**. Thus, ubiquitin transfer can proceed *in trans* which might involve oligomerization.

Activity assays with the E6AP variant in which the active site cysteine is replaced by a lysine (C820K) provided a read-out of the mechanism of ubiquitin chain formation and allowed to distinguish between the distinct ubiquitin chain formation models **(Figure 18)**. In single-turnover assays using E6AP HECT domain C820K, I could not monitor ubiquitin chains growing on the active site lysine residue rather than a single ubiquitin molecule isopeptide-linked to the active site **(Figure 18C)**. This result is in contrast to mutational and kinetic analyses of E6AP employing a mechanism that chains are formed on the E3 active site [225] and which might involve two functionally distinct E2-ubiquitin binding sites on E6AP [188, 190, 213]. Based on enzyme kinetics Ronchi et al. suggested that a cryptic E2 binding site is required for thioester formation and a canonical site (as seen in the crystal structure of E6AP with UBE2L3 [85]) is responsible for ubiquitin chain formation. Here, the two sites function through a cyclic 'indexation' mechanism to assemble ubiquitin chains at the active site of E6AP prior to *en bloc* transfer of the chain to the target [188, 190, 213].

However, UBE2L3 (or UBE2L6) lack intrinsic lysine specificity and was suggested to be the physiological E2 enzyme of E6AP **(Figure 18A)** [119, 232]. This makes it unlikely that ubiquitin is loaded onto a growing ubiquitin chain tethered to the active site by UBE2L3 unless this E2 enzyme is reprogrammed by full-length E6AP in the cellular context.

My assays do not provide evidence that ubiquitin chains are built on the active site of E6AP. However, I cannot rule out that the cysteine to lysine substitution at the active site, and thus replacing the native thioester with an isopeptide bond, may cause any artifacts. The isopeptide-linked ubiquitin might be tethered to the C-lobe in such a conformation which sterically does not allow for binding of a second ubiquitin molecule. It could also alter the interaction with the E2~ubiquitin complex and thus, preventing efficient ubiquitin transfer. Since UBE2D3 was used to charge the active site lysine residue, C820K, ubiquitination of other lysine residues by UBE2D3 occurred, which might also have prevented E6AP-driven ubiquitin chain formation.

In the future additional studies will be needed to get a detailed structural and mechanistic understanding of ubiquitin chain formation and substrate ubiquitination by HECT ligases.

5.3 Ubiquitin recognition by E6AP

Ubiquitination enzymes rely on combinatorial weak interactions to achieve efficiency and specificity in ubiquitin transfer. Due to its transient nature, structural underpinnings of ubiquitin recognition by E6AP activity have remained largely elusive. The weak interaction between ubiquitin and different E6AP constructs escaped detection by aSEC experiments **(Figure 19)**, but by NMR and FP measurements we could monitor the interaction of E6AP C-lobe and

ubiquitin *in trans* and determine the corresponding binding affinities **(Figure 20D, E)**. The K_D-values for the complex between the E6AP C-lobe and ubiquitin obtained by FP measurements (400 ± 20 µM) or NMR (1.5 ± 0.1 mM) show that the complex is weak, which explains why it had previously escaped detection by less sensitive experimental techniques [107]. By NMR, I could also identify the binding sites on both the C-lobe and ubiquitin **(Figure 20A-C)**. I found that the activity of E6AP relies on a specific interface with the donor ubiquitin that is formed in addition to the linkage of the two proteins at the E3 active site during thioester formation **(Figure 23B)**. This interface *per se* is weak and presumably dynamic, reminiscent of the functionally critical, 'closed' conformation of donor ubiquitin with respect to E2s in RING E3-driven catalysis [233], in which the ubiquitin tail is conformationally locked. The same mechanism is employed in conjugation reactions of the ubiquitin-like modifier SUMO [25, 182, 211]. However, the covalent linkage between the two proteins strongly raises their effective concentrations, and thus the complex becomes sufficiently populated [174, 233]. Additional macromolecular interactions of the binding partners with adapter proteins or complexes can also contribute to the stabilization of inherently weak interactions. For example, RING ligases promote the closed orientation of the donor ubiquitin towards the E2 enzyme by simultaneously interacting with both proteins [22, 52, 178]. As a result, the inherently weak E2-donor interface becomes significantly occupied and important for catalysis. Additional macromolecular interactions of the binding partners with adapter proteins or in the context of higher-order complexes can also contribute to the stabilization of inherently weak interactions. For example, RING/U-box as well as ligases specific for particular ubiquitin-like modifiers (Ubls), such as SUMO and NEDD8, promote 'closed' orientations of the donor ubiquitin/Ubl towards an E2 by simultaneously interacting with both proteins [22, 25, 52, 53, 178, 180, 182, 204].

Moreover, the human anaphase-promoting complex (APC/C), a multi-component RING ligase, holds the acceptor ubiquitin in a Lys11-specific position towards the chain-elongating E2, UBE2S [18, 19, 105]; and the Lys63-specific E2 UBC13 relies on an associated UEV (ubiquitin E2 variant), MMS2, to orient the acceptor ubiquitin [17, 55]. Multiple protein interfaces were also shown to be involved in positioning substrates for modification with Ubls [211, 247]. It is likely that similar combinatorial mechanisms serve to stabilize critical interfaces of ubiquitin with HECT ligases. Enzymes in this family are characterized by extended regions flanking the C-terminal catalytic domain that recruit substrates and can impact ubiquitin recognition in several cases [8, 32, 198, 253].

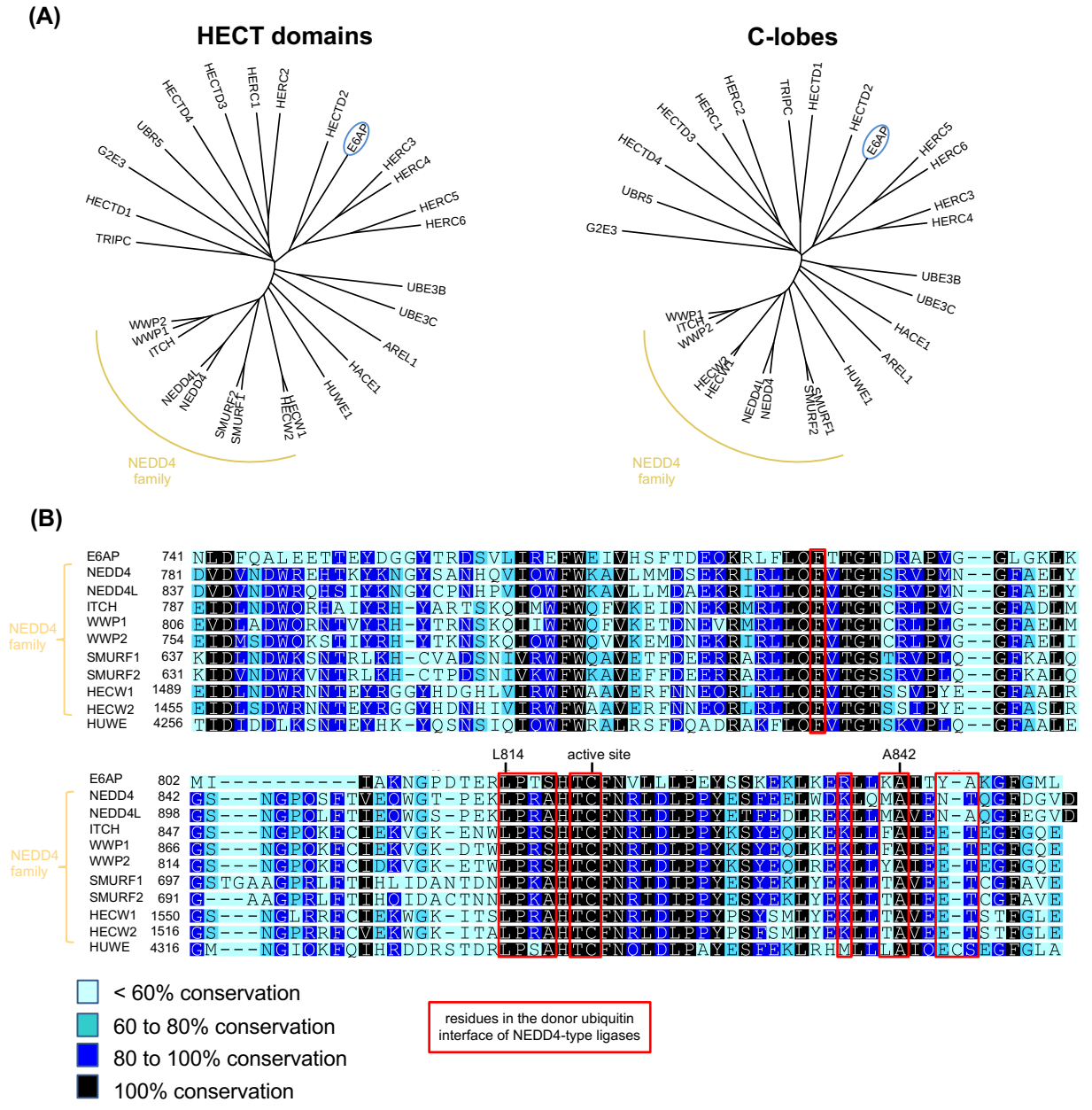

Figure 42: Phylogenetic analyses of the human HECT domains. (A) Phylogenetic trees for all human HECT domains (left) and C-lobes (right), generated with Clustal Omega [207] and the Interactive Tree of Life (iTOL) v3 server [126] by Dr. Sonja Lorenz. **(B)** Amino acid sequence alignment for the C-lobes of E6AP, the members of the NEDD4 subfamily, and HUWE1 (NEDD4 isoform 4, others isoform 1), as output by Clustal Omega [129, 149, 207] illustrated using Geneious Basic [102] generated by Dr. Bodo Sander. The catalytic cysteine and residues in the NEDD4-type interface with the donor ubiquitin are boxed. Interfacing residues were defined based on the crystal structure of the NEDD4 HECT domain-donor ubiquitin complex (PDB ID: 4BBN) [144] and a surface burial upon complex formation of at least 50%, as determined by the PISA server [114]. Residue numbers provided above the alignment refer to E6AP.

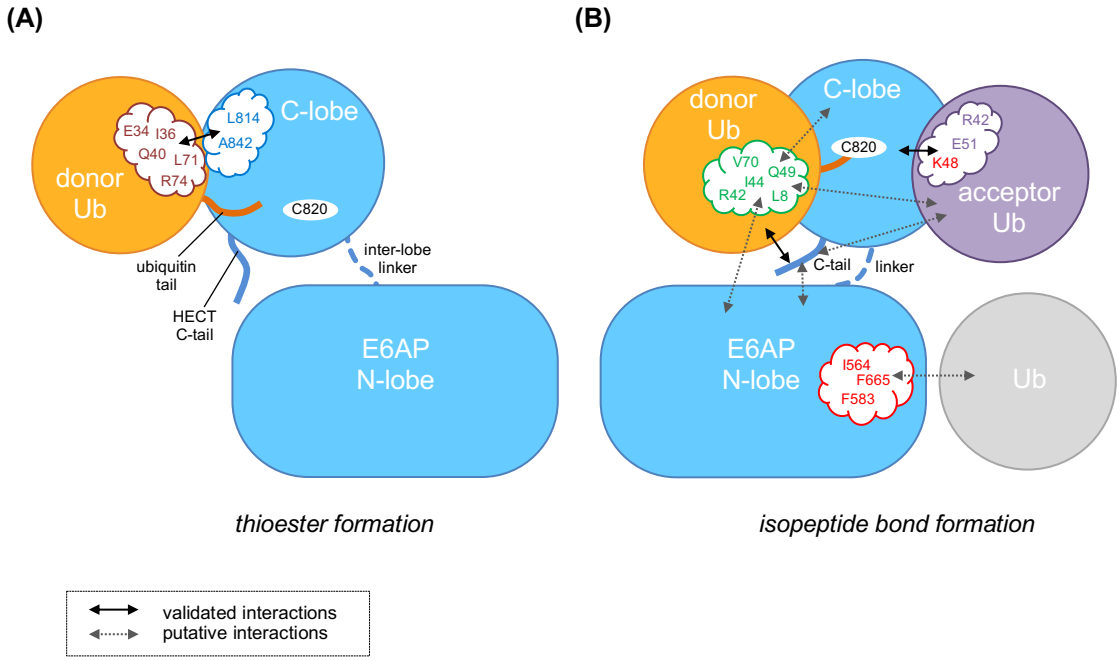

Figure 43: Interactions and surface patches critical during Lys48-linked ubiquitin chain formation by the E6AP HECT domain. (A) The C-lobe of E6AP utilizes canonical ('NEDD4-type') contacts with the donor ubiquitin during thioester transfer of ubiquitin from the E2 to the E3 enzyme. The C-terminal tail ('C-tail') of E6AP is not required for this step. **(B)** The 'hydrophobic patch' (green) is used by the donor ubiquitin for yet uncharacterized interactions with the N-lobe, the C-lobe, or the acceptor ubiquitin. The acceptor ubiquitin is critically dependent on a hydrophilic area around the acceptor residue, Lys48, including Glu51. The C-tail contacts the thioester-linked donor and confers linkage specificity during ubiquitin chain formation, possibly by additional contacts with the N-lobe or the acceptor ubiquitin. My studies further demonstrate that E6AP interacts with ubiquitin through its N-lobe and that the mutation of residues in the 'exosite' region weakens this interaction and reduce isopeptide bond formation; however, they do not affect thioester formation. Whether the N-lobe-ubiquitin interaction resembles the exosite-mediated ubiquitin binding mode seen in NEDD4-type enzymes remains awaits structural elucidation.

This study reveals that the catalytic domain of E6AP utilizes contacts with the donor ubiquitin for thioester formation that are equivalent to NEDD4-type ligases and HUWE1 (whose HECT domain is closely related to NEDD4-type ligases; **Figure 42A**) [94, 98, 99, 144]. Consistently, residues in the NEDD4-type donor interface are at least partially conserved in E6AP and functionally critical residues largely identical, despite the HECT domains being relatively distant in phylogenetic terms **(Figure 42A, B)**. Taken together, these observations support the notion that thioester transfer of ubiquitin from the E2 to the E3 occurs through a structurally conserved interface between ubiquitin and the C-lobe of HECT ligases **(Figure 43A)** [94].

I spent much effort on obtaining crystal structures of complexes mimicking the catalytic intermediate. My approaches to produce stable covalent adducts between the E6AP HECT domain or C-lobe with ubiquitin by various crosslinking strategies were successful and yielded mimics of the transient complex, but unfortunately none of them could be crystallized **(Figure 25, Figure 28-30)**. Still, the different covalent E6AP-ubiquitin complexes were instrumental for obtaining a molecular understanding of the interaction between E6AP and

ubiquitin. I could show that ubiquitin in a covalent complex with either the C-lobe or the HECT domain of E6AP did not promote non-covalent binding of additional free ubiquitin **(Figure 26A, Figure 29E)**.

I found that the disulfide linked C-lobe~ubiquitin complex tends to form a disulfide-linked C-lobe dimer upon a disulfide exchange reaction **(Figure 26B, C)**. In contrast this behavior was not observed for the whole HECT domain. This indicates a high reactivity of the active site cysteine in context of the isolated C-lobe **(Figure 26D)**. Interestingly, the catalytic cysteine of the NEDD4 C-lobe did not show such reactivity. Mutating residues of ubiquitin in the donor interface did not alter the C-lobe tendency to dimerize with E6AP C-lobe~ubiquitin **(Figure 27)**. At very high concentration, the C-lobe tended to dimerize **(Figure 31C, D)**. A preliminary crystal structure showed that the C-lobe swapped its C-terminal portion with one symmetry mate. Thereby, the same interface is formed as in its native state, yet in a dimeric arrangement **(Figure 31F)**. In context of the whole HECT domain, this reactivity is probably diminished because the N-lobe might restrict the interaction between two C-lobes and thus prevent domain swapping. I have no evidence that the propensity of the isolated E6AP C-lobe to dimerize is biologically meaningful.

In addition, I found out that the replacements of the two non-catalytic cysteine residues of the HECT domain by serine residues greatly decreased the stability of the HECT domain and decreased its ubiquitination activity **(Figure 29A, F)**. These cysteines are obviously important for the structural integrity of the HECT domain.

During isopeptide bond formation, E6AP requires the residues His818 and Thr819 next to the active site **(Figure 23A)** and the hydrophobic patch of ubiquitin **(Figure 36B)** [156]. My analyses pinpoint the significance of the hydrophobic patch to a function in the donor rather than the acceptor ubiquitin **(Figure 38)**. Since the hydrophobic patch is not part of the interface required during thioester transfer, several alternate models are conceivable: For example, the hydrophobic patch may be important for interactions of the donor with the N-lobe or the acceptor ubiquitin, with the donor adopting a canonical orientation towards the C-lobe **(Figure 43B)**. Alternatively, the hydrophobic patch may mediate alternate interactions of the donor with the C-lobe, following structural rearrangements in the course of isopeptide formation **(Figure 43B)**. Since the NMR data pointed to considerable flexibility within the donor-C-lobe conjugate **(Figure 33)** and the HECT domain harbors additional inter-lobe flexibility, such rearrangements may well occur, as the enzyme progresses from one sub-reaction to the next. In consequence, conformational variability in the orientation of both, the donor and the acceptor ubiquitin during isopeptide bond formation may provide the basis for

distinct linkage-specificities of individual ligases, despite a shared mode of ubiquitin recognition during thioester transfer.

To fully understand the conformational trajectory of the HECT domain of E6AP during catalysis it will be essential to structurally visualize the location of the acceptor ubiquitin or a substrate along with the donor-E3 conjugate – a yet unresolved problem in the field of HECT ligases.

Surprisingly, my studies identify a ubiquitin binding site on the N-lobe of E6AP **(Figure 39, 40)**, a feature thus far attributed primarily to NEDD4-type ligases [8, 66, 67, 108, 143, 144, 167, 250]. Whether ubiquitin recognition by the N-lobe of E6AP resembles a typical exosite interaction remains unclear, particularly since this site is moderately conserved and mutation of key residues weakens ubiquitin binding to the E6AP HECT domain only slightly **(Figure 39B, C)**. Yet, these residues are critical for isopeptide bond formation by E6AP **(Figure 39D)**. This latter observation mimics the function of the exosite region in NEDD4-type ligases, even though the specific function of this site in catalysis is enzyme-dependent [8, 66, 67, 108, 143, 144, 167, 250]. To unravel the precise function of the exosite during ubiquitin chain elongation by E6AP will require further investigation. On a broader scope, understanding how the exosite promotes chain elongation in different HECT ligases will likely also help to define the directionality of ubiquitin chain elongation, for which different models have been presented [66, 81, 101, 188, 190, 213, 225], as well as the functional consequences of oligomerization, which was associated with the exosite in certain cases [8, 189, 198, 214].

5.4 Determinants of Lys48-specificity of E6AP

Remarkably, these studies demonstrate that elements on both the ligase and ubiquitin are required. Consistent with previous studies identifying the C-terminal tail of HECT ligases as a sensitive element in catalysis and critical for the Lys63-linkage specificity of NEDD4 [94, 98, 144, 197], I found that the C-tail is essential for the Lys48-specificity of E6AP **(Figure 35)**. I further showed that the C-tail of E6AP interacts with the donor ubiquitin upon formation of the covalent linkage at the active site **(Figure 33)**, analogous to NEDD4-type ligases and HUWE1 [94]. These findings imply that the C-tail contributes to the orientation of the donor and/or the chemical environment at the active site in a manner that facilitates isopeptide bond formation [94, 144, 197]. In line with this notion, the C-terminal tail of RSP5, a NEDD4-orthologue from yeast, was suggested to mediate critical interactions between the N- and C-lobes as well as donor ubiquitin during substrate modification [98] and addition of a tail-derived peptide to E6AP was found to inhibit isopeptide bond formation non-competitively [190].

Interestingly, non-conservative amino acid substitutions and insertions occur in the C-tail of E6AP in Angelman's syndrome (missense: G850D; deletion/insertion: A842-T844/RCS; C-terminal insertion QNKIKQKKGRKKKEKI) [4, 123, 195] and certain cancer types (A842D, T844M) [65], likely causing E6AP malfunction in these settings. A molecular understanding of the role of the tail for isopeptide bond formation and for conferring linkage specificity will require a structural characterization of E6AP in complex with donor and acceptor ubiquitin or a target protein.

I also uncover a surface region on ubiquitin, adjacent to the Lys48, that is important for acceptor ubiquitin function with E6AP **(Figure 43B)**. Remarkably, exchange of single residue in this patch, Glu51, by alanine, diminishes the Lys48-linkage specificity of the E6AP HECT domain **(Figure 38D, E)**. It is thus tempting to speculate that isopeptide bond formation by E6AP is substrate-assisted – analogous to the mechanisms delineated for certain RING ligase-associated E2 enzymes [55, 187, 233]. In several of these cases, it is also an acidic residue near the acceptor site that confers linkage specificity. For example, the Lys11-linkage specificity of the human anaphase-promoting complex/cyclosome (APC/C)-associated E2, UBE2S, critically depends on Glu34 of the acceptor ubiquitin [233]; and UBE2N/UBE2V2 relies on Glu64 of the acceptor to form Lys63-linked chains [55]. Substrate-assisted catalysis has also been observed during the cleavage of ubiquitin linkages by DUBs [106, 151], suggesting it presents a common mechanism during ubiquitin chain assembly and disassembly.

Here, I have focused on the isolated HECT domain exclusively. How precisely the N-terminal regions adjacent to the HECT domain of E6AP influence Lys48-specificity remains to be elucidated. Interestingly, the N-terminal region of E6AP is unique and does not display homology to other HECT ligases, suggesting that E6AP utilizes distinct mechanisms of target recognition and ubiquitination.

5.5 Outlook

Ubiquitin ligases have emerged as powerful therapeutic targets. They select cellular substrates for modification and determine the types of ubiquitin modifications, and thus they provide specificity in ubiquitin signaling. Yet the structural basis of the activity and the specificity of ubiquitin ligases are incompletely understood.

This work provided novel conceptual insights into the catalytic mechanism and regulation of the HECT ligase E6AP. I uncovered the location of donor ubiquitin with respect to the C-lobe of the HECT domain during thioester formation, but still, a detailed molecular picture of how this E3 enzyme recognizes and orients the acceptor ubiquitin and how the Lys48-linkage

specificity is encoded, is missing. Since linkage specificity could be also influenced by the nature of the substrate or by interactions with additional factors, it is critical to study ubiquitin chain formation on substrates by several HECT ligases with distinct linkage type specificity. In the future, it will be also interesting to find out whether substrate levels affect the turnover of E6AP, and which additional binding partners affect E6AP stability, regulation and activity.

Several mechanisms have been suggested for how HECT E3 enzymes are regulated throughout their catalytic cycle, but structural insights are only beginning to emerge. They are required, however, to understand at the molecular level how HECT ligases achieve efficiency and directionality in the ubiquitination pathway. The new insights on E6AP regulation, ubiquitin recognition and ubiquitin chain formation gained in this study provide first steps to improve the understanding of E6AP catalysis. My results − along with recent descriptions of distinct auto-inhibitory states in HUWE1, ITCH, WWP1, and NEDD4 [8, 32, 198, 253] − highlight the remarkable diversity in the structural mechanisms of HECT ligases. This diversity holds the key to the functional specialization of these enzymes and the intriguing prospect of exploiting ligase-specific facets for therapeutic applications.

Bibliography

1. Adams, J. and M. Kauffman (2004). Development of the proteasome inhibitor Velcade (Bortezomib). *Cancer Invest*. **22**(2): p. 304-11.
2. Adams, P.D., et al. (2010). PHENIX: a comprehensive Python-based system for macromolecular structure solution. *Acta Crystallographica Section D-Biological Crystallography*. **66**: p. 213-221.
3. Adhikary, S., et al. (2005). The ubiquitin ligase HectH9 regulates transcriptional activation by Myc and is essential for tumor cell proliferation. *Cell*. **123**(3): p. 409-21.
4. Al-Maawali, A., et al. (2013). Angelman Syndrome Due to a Termination Codon Mutation of the UBE3A Gene. *Journal of Child Neurology*. **28**(3): p. 392-395.
5. Anan, T., et al. (1998). Human ubiquitin-protein ligase Nedd4: expression, subcellular localization and selective interaction with ubiquitin-conjugating enzymes. *Genes Cells*. **3**(11): p. 751-63.
6. Ansari, T., N. Brimer, and S.B. Vande Pol (2012). Peptide interactions stabilize and restructure human papillomavirus type 16 E6 to interact with p53. *J Virol*. **86**(20): p. 11386-91.
7. Artimo, P., et al. (2012). ExPASy: SIB bioinformatics resource portal. *Nucleic Acids Research*. **40**(Web Server issue): p. W597-603.
8. Attali, I., et al. (2017). Ubiquitylation-dependent oligomerization regulates activity of Nedd4 ligases. *EMBO J*. **36**(4): p. 425-440.
9. Bas, D.C., D.M. Rogers, and J.H. Jensen (2008). Very fast prediction and rationalization of pK(a) values for protein-ligand complexes. *Proteins-Structure Function and Bioinformatics*. **73**(3): p. 765-783.
10. Battye, T.G.G., et al. (2011). iMOSFLM: a new graphical interface for diffraction-image processing with MOSFLM. *Acta Crystallographica Section D-Biological Crystallography*. **67**: p. 271-281.
11. Beaudenon, S. and J.M. Huibregtse (2008). HPV E6, E6AP and cervical cancer. *BMC Biochem*. **9 Suppl 1**: p. S4.
12. Berman, H.M., et al. (2000). The Protein Data Bank. *Nucleic Acids Research*. **28**(1): p. 235-242.
13. Bernassola, F., et al. (2008). The HECT family of E3 ubiquitin ligases: Multiple players in cancer development. *Cancer Cell*. **14**(1): p. 10-21.
14. Blow, D.M. (2002). Rearrangement of Cruickshank's formulae for the diffraction-component precision index. *Acta Crystallogr D Biol Crystallogr*. **58**(Pt 5): p. 792-7.
15. Bond, S.R. and C.C. Naus (2012). RF-Cloning.org: an online tool for the design of restriction-free cloning projects. *Nucleic Acids Research*. **40**(W1): p. W209-W213.
16. Bosch, F.X., et al. (1995). Prevalence of human papillomavirus in cervical cancer: a worldwide perspective. International biological study on cervical cancer (IBSCC) Study Group. *J Natl Cancer Inst*. **87**(11): p. 796-802.
17. Branigan, E., et al. (2015). Structural basis for the RING-catalyzed synthesis of K63-linked ubiquitin chains. *Nat Struct Mol Biol*.
18. Brown, N.G., et al. (2016). Dual RING E3 Architectures Regulate Multiubiquitination and Ubiquitin Chain Elongation by APC/C. *Cell*. **165**(6): p. 1440-1453.
19. Brown, N.G., et al. (2014). Mechanism of Polyubiquitination by Human Anaphase-Promoting Complex: RING Repurposing for Ubiquitin Chain Assembly. *Molecular Cell*. **56**(2): p. 246-260.
20. Brown, S.B. (1980). An introduction to Spectroscopy for Biochemists. Chapter 2, Ultraviolet and Visible Spectroscopy. *Academic Press*.
21. Bruce, M.C., et al. (2008). Regulation of Nedd4-2 self-ubiquitination and stability by a PY motif located within its HECT-domain. *Biochem J*. **415**(1): p. 155-63.
22. Brzovic, P.S., et al. (2006). A UbcH5/ubiquitin noncovalent complex is required for processive BRCA1-directed ubiquitination. *Mol Cell*. **21**(6): p. 873-80.

23. Burette, A.C., et al. (2017). Subcellular organization of UBE3A in neurons. *J Comp Neurol*. **525**(2): p. 233-251.
24. Cai, J.B., et al. (2015). Ubiquitin-Specific Protease 7 Accelerates p14(ARF) Degradation by Deubiquitinating Thyroid Hormone Receptor-Interacting Protein 12 and Promotes Hepatocellular Carcinoma Progression. *Hepatology*. **61**(5): p. 1603-1614.
25. Cappadocia, L., A. Pichler, and C.D. Lima (2015). Structural basis for catalytic activation by the human ZNF451 SUMO E3 ligase. *Nat Struct Mol Biol*. **22**(12): p. 968-75.
26. Chan, A.L., et al. (2013). c-Abl phosphorylates E6AP and regulates its E3 ubiquitin ligase activity. *Biochemistry*. **52**(18): p. 3119-29.
27. Chau, V., et al. (1989). A multiubiquitin chain is confined to specific lysine in a targeted short-lived protein. *Science*. **243**(4898): p. 1576-83.
28. Chayen, N.E. and E. Saridakis (2008). Protein crystallization: from purified protein to diffraction-quality crystal. *Nature Methods*. **5**(2): p. 147-153.
29. Chen, D., C.L. Brooks, and W. Gu (2006). ARF-BP1 as a potential therapeutic target. *Br J Cancer*. **94**(11): p. 1555-8.
30. Chen, D., M. Gehringer, and S. Lorenz (2018). Developing Small-Molecule Inhibitors of HECT-Type Ubiquitin Ligases for Therapeutic Applications: Challenges and Opportunities. *Chembiochem*. **19**(20): p. 2123-2135.
31. Chen, V.B., et al. (2010). MolProbity: all-atom structure validation for macromolecular crystallography. *Acta Crystallogr D Biol Crystallogr*. **66**(Pt 1): p. 12-21.
32. Chen, Z., et al. (2017). A Tunable Brake for HECT Ubiquitin Ligases. *Molecular Cell*. **66**(3): p. 345-+.
33. Chen, Z. and C.M. Pickart (1990). A 25-kilodalton ubiquitin carrier protein (E2) catalyzes multi-ubiquitin chain synthesis via lysine 48 of ubiquitin. *Journal of Biological Chemistry*. **265**(35): p. 21835-42.
34. Chiu, Y.H., Q. Sun, and Z.J.J. Chen (2007). E1-L2 activates both ubiquitin and FAT10. *Molecular Cell*. **27**(6): p. 1014-1023.
35. Chong-Kopera, H., et al. (2006). TSC1 stabilizes TSC2 by inhibiting the interaction between TSC2 and the HERC1 ubiquitin ligase. *J Biol Chem*. **281**(13): p. 8313-6.
36. Chowdhury, S., et al. (2006). Arc/Arg3.1 interacts with the endocytic machinery to regulate AMPA receptor trafficking. *Neuron*. **52**(3): p. 445-59.
37. Clevers, H. (2006). Wnt/beta-catenin signaling in development and disease. *Cell*. **127**(3): p. 469-80.
38. Colas, D., et al. (2005). Sleep disturbances in Ube3a maternal-deficient mice modeling Angelman syndrome. *Neurobiol Dis*. **20**(2): p. 471-8.
39. Confalonieri, S., et al. (2009). Alterations of ubiquitin ligases in human cancer and their association with the natural history of the tumor. *Oncogene*. **28**(33): p. 2959-68.
40. Cook, E.H., Jr., et al. (1997). Autism or atypical autism in maternally but not paternally derived proximal 15q duplication. *Am J Hum Genet*. **60**(4): p. 928-34.
41. Corpet, F. (1988). Multiple sequence alignment with hierarchical clustering. *Nucleic Acids Research*. **16**(22): p. 10881-90.
42. Cummings, M.D., M.A. Farnum, and M.I. Nelen (2006). Universal screening methods and applications of ThermoFluor (R). *Journal of Biomolecular Screening*. **11**(7): p. 854-863.
43. Dagli, A., K. Buiting, and C.A. Williams (2012). Molecular and Clinical Aspects of Angelman Syndrome. *Mol Syndromol*. **2**(3-5): p. 100-112.
44. Dastur, A., et al. (2006). Herc5, an interferon-induced HECT E3 enzyme, is required for conjugation of ISG15 in human cells. *J Biol Chem*. **281**(7): p. 4334-8.
45. David, D., S.A. Nair, and M.R. Pillai (2013). Smurf E3 ubiquitin ligases at the cross roads of oncogenesis and tumor suppression. *Biochim Biophys Acta*. **1835**(1): p. 119-28.
46. de Bie, P. and A. Ciechanover (2011). Ubiquitination of E3 ligases: self-regulation of the ubiquitin system via proteolytic and non-proteolytic mechanisms. *Cell Death Differ*. **18**(9): p. 1393-402.
47. Deshaies, R.J. (2005). Methods on Enzymology - Ubiquitin and Protein Degradation. Vol. 399: *Elsevier*.

48. Deshaies, R.J. and C.A. Joazeiro (2009). RING domain E3 ubiquitin ligases. *Annu Rev Biochem*. **78**: p. 399-434.
49. Dhananjayan, S.C., et al. (2006). WW domain binding protein-2, an E6-associated protein interacting protein, acts as a coactivator of estrogen and progesterone receptors. *Molecular Endocrinology*. **20**(10): p. 2343-2354.
50. Diederichs, K. and P.A. Karplus (1997). Improved R-factors for diffraction data analysis in macromolecular crystallography. *Nat Struct Biol*. **4**(4): p. 269-75.
51. Doss, M. and A. Schmidt (1971). [Quantitative determination of delta-aminolevulinic acid and porphobilinogen in urine, using ion exchange chromatography columns]. *Z Klin Chem Klin Biochem*. **9**(2): p. 99-102.
52. Dou, H., et al. (2012). BIRC7-E2 ubiquitin conjugate structure reveals the mechanism of ubiquitin transfer by a RING dimer. *Nature Structural & Molecular Biology*. **19**(9): p. 876-883.
53. Dou, H., et al. (2013). Essentiality of a non-RING element in priming donor ubiquitin for catalysis by a monomeric E3. *Nat Struct Mol Biol*. **20**(8): p. 982-+.
54. Dubendorff, J.W. and F.W. Studier (1991). Controlling Basal Expression in an Inducible T7 Expression System by Blocking the Target T7 Promoter with Lac Repressor. *Journal of Molecular Biology*. **219**(1): p. 45-59.
55. Eddins, M.J., et al. (2006). Mms2-Ubc13 covalently bound to ubiquitin reveals the structural basis of linkage-specific polyubiquitin chain formation. *Nat Struct Mol Biol*. **13**(10): p. 915-20.
56. Eletr, Z.M., et al. (2005). E2 conjugating enzymes must disengage from their E1 enzymes before E3-dependent ubiquitin and ubiquitin-like transfer. *Nat Struct Mol Biol*. **12**(10): p. 933-934.
57. Eletr, Z.M. and B. Kuhlman (2007). Sequence determinants of E2-E6AP binding affinity and specificity. *J Mol Biol*. **369**(2): p. 419-28.
58. Ellman, G.L. (1959). Tissue sulfhydryl groups. *Arch Biochem Biophys*. **82**(1): p. 70-7.
59. Emsley, P. and K. Cowtan (2004). Coot: model-building tools for molecular graphics. *Acta Crystallographica Section D-Biological Crystallography*. **60**: p. 2126-2132.
60. Escobedo, A., et al. (2014). Structural Basis of the Activation and Degradation Mechanisms of the E3 Ubiquitin Ligase Nedd4L. *Structure*. **22**(10): p. 1446-1457.
61. Evans, P.R. (2011). An introduction to data reduction: space-group determination, scaling and intensity statistics. *Acta Crystallogr D Biol Crystallogr*. **67**(Pt 4): p. 282-92.
62. Fajner, V., E. Maspero, and S. Polo (2017). Targeting HECT-type E3 ligases: insights from catalysis, regulation and inhibitors. *FEBS Lett*.
63. Fang, P., et al. (1999). The spectrum of mutations in UBE3A causing Angelman syndrome. *Hum Mol Genet*. **8**(1): p. 129-35.
64. Favier, A. and B. Brutscher (2011). Recovering lost magnetization: polarization enhancement in biomolecular NMR. *J Biomol NMR*. **49**(1): p. 9-15.
65. Forbes, S.A., et al. (2017). COSMIC: somatic cancer genetics at high-resolution. *Nucleic Acids Research*. **45**(D1): p. D777-D783.
66. French, M.E., et al. (2017). Mechanism of Ubiquitin Chain Synthesis Employed by a HECT Ubiquitin Ligase. *J Biol Chem*.
67. French, M.E., B.R. Kretzmann, and L. Hicke (2009). Regulation of the RSP5 Ubiquitin Ligase by an Intrinsic Ubiquitin-binding Site. *Journal of Biological Chemistry*. **284**(18): p. 12071-12079.
68. Fulda, S., K. Rajalingam, and I. Dikic (2012). Ubiquitylation in immune disorders and cancer: from molecular mechanisms to therapeutic implications. *Embo Molecular Medicine*. **4**(7): p. 545-556.
69. Gabadinho, J., et al. (2010). MxCuBE: a synchrotron beamline control environment customized for macromolecular crystallography experiments. *J Synchrotron Radiat*. **17**(5): p. 700-7.
70. Gallagher, E., et al. (2006). Activation of the E3 ubiquitin ligase Itch through a phosphorylation-induced conformational change. *Proceedings of the National Academy of Sciences of the United States of America*. **103**(6): p. 1717-1722.

71. Gamell, C., et al. (2017). Reduced abundance of the E3 ubiquitin ligase E6AP contributes to decreased expression of the INK4/ARF locus in non-small cell lung cancer. *Sci Signal*. **10**(461).
72. Garcia-Gonzalo, F.R. and J.L. Rosa (2005). The HERC proteins: functional and evolutionary insights. *Cell Mol Life Sci*. **62**(16): p. 1826-38.
73. Gossan, N.C., et al. (2014). The E3 ubiquitin ligase UBE3A is an integral component of the molecular circadian clock through regulating the BMAL1 transcription factor. *Nucleic Acids Research*. **42**(9): p. 5765-5775.
74. Greer, P.L., et al. (2010). The Angelman Syndrome protein Ube3A regulates synapse development by ubiquitinating arc. *Cell*. **140**(5): p. 704-16.
75. Grigoryan, G. and A.E. Keating (2008). Structural specificity in coiled-coil interactions. *Curr Opin Struct Biol*. **18**(4): p. 477-83.
76. Haglund, K. and I. Dikic (2012). The role of ubiquitylation in receptor endocytosis and endosomal sorting. *J Cell Sci*. **125**(Pt 2): p. 265-75.
77. Handley, P.M., et al. (1991). Molecular cloning, sequence, and tissue distribution of the human ubiquitin-activating enzyme E1. *Proc Natl Acad Sci U S A*. **88**(1): p. 258-62.
78. Harper, J.W. and M.K.M. Tan (2012). Understanding Cullin-RING E3 Biology through Proteomics-based Substrate Identification. *Molecular & Cellular Proteomics*. **11**(12): p. 1541-1550.
79. Hershko, A. and A. Ciechanover (1992). The ubiquitin system for protein degradation. *Annu Rev Biochem*. **61**: p. 761-807.
80. Hershko, A. and A. Ciechanover (1998). The ubiquitin system. *Annu Rev Biochem*. **67**: p. 425-79.
81. Hochstrasser, M. (2006). Lingering mysteries of ubiquitin-chain assembly. *Cell*. **124**(1): p. 27-34.
82. Hoege, C., et al. (2002). RAD6-dependent DNA repair is linked to modification of PCNA by ubiquitin and SUMO. *Nature*. **419**(6903): p. 135-141.
83. Hogart, A., et al. (2010). The comorbidity of autism with the genomic disorders of chromosome 15q11.2-q13. *Neurobiol Dis*. **38**(2): p. 181-91.
84. Hong, J.H., et al. (2015). The use of ubiquitin lysine mutants to characterize E2-E3 linkage specificity: Mass spectrometry offers a cautionary "tail". *Proteomics*. **15**(17): p. 2910-2915.
85. Huang, L., et al. (1999). Structure of an E6AP-UbcH7 complex: Insights into ubiquitination by the E2-E3 enzyme cascade. *Science*. **286**(5443): p. 1321-1326.
86. Huang, X.D. and V.M. Dixit (2016). Drugging the undruggables: exploring the ubiquitin system for drug development. *Cell Research*. **26**(4): p. 484-498.
87. Huibregtse, J.M., et al. (1995). A Family of Proteins Structurally and Functionally Related to the E6-Ap Ubiquitin-Protein Ligase (Vol 92, Pg 2563, 1995). *Proceedings of the National Academy of Sciences of the United States of America*. **92**(11): p. 5249-5249.
88. Huibregtse, J.M., M. Scheffner, and P.M. Howley (1991). A cellular protein mediates association of p53 with the E6 oncoprotein of human papillomavirus types 16 or 18. *EMBO J*. **10**(13): p. 4129-35.
89. Huibregtse, J.M., M. Scheffner, and P.M. Howley (1993). Localization of the E6-Ap Regions That Direct Human Papillomavirus E6 Binding, Association with P53, and Ubiquitination of Associated Proteins. *Mol Cell Biol*. **13**(8): p. 4918-4927.
90. Iconomou, M. and D.N. Saunders (2016). Systematic approaches to identify E3 ligase substrates. *Biochemical Journal*. **473**: p. 4083-4101.
91. Ingham, R.J., G. Gish, and T. Pawson (2004). The Nedd4 family of E3 ubiquitin ligases: functional diversity within a common modular architecture. *Oncogene*. **23**(11): p. 1972-1984.
92. Inoue, S., et al. (2013). Mule/Huwe1/Arf-BP1 suppresses Ras-driven tumorigenesis by preventing c-Myc/Miz1-mediated down-regulation of p21 and p15. *Genes & Development*. **27**(10): p. 1101-1114.
93. Iossifov, I., et al. (2014). The contribution of de novo coding mutations to autism spectrum disorder. *Nature*. **515**(7526): p. 216-21.

94. Jackl, M., et al. (2018). beta-Sheet Augmentation Is a Conserved Mechanism of Priming HECT E3 Ligases for Ubiquitin Ligation. *J Mol Biol*. **430**(18 Pt B): p. 3218-3233.
95. Jiang, Y.H., et al. (1998). Mutation of the Angelman ubiquitin ligase in mice causes increased cytoplasmic p53 and deficits of contextual learning and long-term potentiation. *Neuron*. **21**(4): p. 799-811.
96. Jin, J., et al. (2007). Dual E1 activation systems for ubiquitin differentially regulate E2 enzyme charging. *Nature*. **447**(7148): p. 1135-8.
97. Kabsch, W. (2010). Xds. *Acta Crystallogr D Biol Crystallogr*. **66**(Pt 2): p. 125-32.
98. Kamadurai, H.B., et al. (2013). Mechanism of ubiquitin ligation and lysine prioritization by a HECT E3. *Elife*. **2**.
99. Kamadurai, H.B., et al. (2009). Insights into Ubiquitin Transfer Cascades from a Structure of a UbcH5B similar to Ubiauitin-HECTNEDD4L Complex. *Molecular Cell*. **36**(6): p. 1095-1102.
100. Kao, W.H., et al. (2000). Human papillomavirus type 16 E6 induces self-ubiquitination of the E6AP ubiquitin-protein ligase. *J Virol*. **74**(14): p. 6408-17.
101. Kathman, S.G., et al. (2015). A Small Molecule That Switches a Ubiquitin Ligase From a Processive to a Distributive Enzymatic Mechanism. *J Am Chem Soc*. **137**(39): p. 12442-5.
102. Kearse, M., et al. (2012). Geneious Basic: an integrated and extendable desktop software platform for the organization and analysis of sequence data. *Bioinformatics*. **28**(12): p. 1647-9.
103. Kee, Y., N. Lyon, and J.M. Huibregtse (2005). The Rsp5 ubiquitin ligase is coupled to and antagonized by the Ubp2 deubiquitinating enzyme. *EMBO J*. **24**(13): p. 2414-24.
104. Kelley, L.A., et al. (2015). The Phyre2 web portal for protein modeling, prediction and analysis. *Nature Protocols*. **10**(6): p. 845-858.
105. Kelly, A., et al. (2014). Ubiquitin Chain Elongation Requires E3-Dependent Tracking of the Emerging Conjugate. *Molecular Cell*. **56**(2): p. 232-245.
106. Keusekotten, K., et al. (2013). OTULIN antagonizes LUBAC signaling by specifically hydrolyzing Met1-linked polyubiquitin. *Cell*. **153**(6): p. 1312-26.
107. Kim, H.C. and J.M. Huibregtse (2009). Polyubiquitination by HECT E3s and the Determinants of Chain Type Specificity. *Mol Cell Biol*. **29**(12): p. 3307-3318.
108. Kim, H.C., et al. (2011). Structure and function of a HECT domain ubiquitin-binding site. *Embo Reports*. **12**(4): p. 334-341.
109. Kim, H.T., et al. (2007). Certain pairs of ubiquitin-conjugating enzymes (E2s) and ubiquitin-protein ligases (E3s) synthesize nondegradable forked ubiquitin chains containing all possible isopeptide linkages. *J Biol Chem*. **282**(24): p. 17375-86.
110. Kim, I.Y., et al. (2011). Role of Nonsteroidal Anti-inflammatory Drug-activated Gene-1 in Docetaxel-induced Cell Death of Human Colorectal Cancer Cells with Different p53 Status. *Archives of Pharmacal Research*. **34**(2): p. 323-330.
111. Kishino, T., M. Lalande, and J. Wagstaff (1997). UBE3A/E6-AP mutations cause Angelman syndrome. *Nat Genet*. **15**(1): p. 70-3.
112. Komander, D. and M. Rape (2012). The ubiquitin code. *Annu Rev Biochem*. **81**: p. 203-29.
113. Kozlov, G., et al. (2004). Structural basis of ligand recognition by PABC, a highly specific peptide-binding domain found in poly(A)-binding protein and a HECT ubiquitin ligase. *Embo Journal*. **23**(2): p. 272-281.
114. Krissinel, E. and K. Henrick (2007). Inference of macromolecular assemblies from crystalline state. *Journal of Molecular Biology*. **372**(3): p. 774-97.
115. Krist, D.T. and A.V. Statsyuk (2015). Catalytically Important Residues of E6AP Ubiquitin Ligase Identified Using Acid-Cleavable Photo-Cross-Linkers. *Biochemistry*. **54**(29): p. 4411-4.
116. Kuhne, C. and L. Banks (1998). E3-ubiquitin ligase/E6-AP links multicopy maintenance protein 7 to the ubiquitination pathway by a novel motif, the L2G box. *J Biol Chem*. **273**(51): p. 34302-9.
117. Kuhnle, S., et al. (2011). Physical and Functional Interaction of the HECT Ubiquitin-protein Ligases E6AP and HERC2. *Journal of Biological Chemistry*. **286**(22): p. 19410-19416.

118. Kulathu, Y. and D. Komander (2012). Atypical ubiquitylation - the unexplored world of polyubiquitin beyond Lys48 and Lys63 linkages. *Nat Rev Mol Cell Biol*. **13**(8): p. 508-23.
119. Kumar, S., W.H. Kao, and P.M. Howley (1997). Physical interaction between specific E2 and Hect E3 enzymes determines functional cooperativity. *Journal of Biological Chemistry*. **272**(21): p. 13548-13554.
120. Kumar, S., A.L. Talis, and P.M. Howley (1999). Identification of HHR23A as a substrate for E6-associated protein-mediated ubiquitination. *J Biol Chem*. **274**(26): p. 18785-92.
121. Kuslansky, Y., et al. (2016). Ubiquitin ligase E6AP mediates nonproteolytic polyubiquitylation of beta-catenin independent of the E6 oncoprotein. *J Gen Virol*. **97**(12): p. 3313-3330.
122. Laemmli, U.K. (1970). Cleavage of structural proteins during the assembly of the head of bacteriophage T4. *Nature*. **227**(5259): p. 680-5.
123. Landrum, M.J., et al. (2018). ClinVar: improving access to variant interpretations and supporting evidence. *Nucleic Acids Research*. **46**(D1): p. D1062-D1067.
124. Lee, K.A., et al. (2011). Ubiquitin Ligase Substrate Identification through Quantitative Proteomics at Both the Protein and Peptide Levels. *Journal of Biological Chemistry*. **286**(48): p. 41530-41538.
125. Leslie, A.G. (2006). The integration of macromolecular diffraction data. *Acta Crystallogr D Biol Crystallogr*. **62**(Pt 1): p. 48-57.
126. Letunic, I. and P. Bork (2016). Interactive tree of life (iTOL) v3: an online tool for the display and annotation of phylogenetic and other trees. *Nucleic Acids Research*. **44**(W1): p. W242-W245.
127. Levin-Kravets, O., N. Shohat, and G. Prag (2015). Tetrameric Assembly of Monoubiquitin Accurately Mimics the Lys11 Polyubiquitin Chain Structure. *Biochemistry*. **54**(30): p. 4704-10.
128. Li, W., et al. (2008). Genome-Wide and Functional Annotation of Human E3 Ubiquitin Ligases Identifies MULAN, a Mitochondrial E3 that Regulates the Organelle's Dynamics and Signaling. *Plos One*. **3**(1).
129. Li, W.Z., et al. (2015). The EMBL-EBI bioinformatics web and programmatic tools framework. *Nucleic Acids Research*. **43**(W1): p. W580-W584.
130. Liu, J., et al. (2014). SCF beta-TRCP-mediated degradation of NEDD4 inhibits tumorigenesis through modulating the PTEN/Akt signaling pathway. *Oncotarget*. **5**(4): p. 1026-1036.
131. Liu, P.Y., et al. (2013). The histone deacetylase SIRT2 stabilizes Myc oncoproteins. *Cell Death Differ*. **20**(3): p. 503-14.
132. Lorenz, S. (2018). Structural mechanisms of HECT-type ubiquitin ligases. *Biol Chem*. **399**(2): p. 127-145.
133. Lorenz, S., et al. (2016). Crystal Structure of a Ube2S-Ubiquitin Conjugate. *PLoS One*. **11**(2): p. e0147550.
134. Lorenz, S., et al. (2013). Macromolecular juggling by ubiquitylation enzymes. *BMC Biol*. **11**: p. 65.
135. Louria-Hayon, I., et al. (2009). E6AP promotes the degradation of the PML tumor suppressor. *Cell Death Differ*. **16**(8): p. 1156-66.
136. Lu, Z. (2011). PubMed and beyond: a survey of web tools for searching biomedical literature. *Database (Oxford)*. **2011**: p. baq036.
137. M. D. Abràmoff, P.J.M., S. J. Ram (2004). Image Processing with ImageJ. *Biophotonics International* **11**: p. 36-42.
138. Mani, A., et al. (2006). E6AP mediates regulated proteasomal degradation of the nuclear receptor coactivator amplified in breast cancer 1 in immortalized cells. *Cancer Res*. **66**(17): p. 8680-6.
139. Mari, S., et al. (2014). Structural and Functional Framework for the Autoinhibition of Nedd4-Family Ubiquitin Ligases. *Structure*. **22**(11): p. 1639-1649.
140. Martinez-Noel, G., et al. (2012). Identification and Proteomic Analysis of Distinct UBE3A/E6AP Protein Complexes. *Molecular and Cellular Biology*. **32**(15): p. 3095-3106.

141. Martinez-Noel, G., et al. (2018). Network Analysis of UBE3A/E6AP-Associated Proteins Provides Connections to Several Distinct Cellular Processes. *J Mol Biol*. **430**(7): p. 1024-1050.
142. Martinez-Zapien, D., et al. (2016). Structure of the E6/E6AP/p53 complex required for HPV-mediated degradation of p53. *Nature*.
143. Maspero, E., et al. (2011). Structure of the HECT:ubiquitin complex and its role in ubiquitin chain elongation. *Embo Reports*. **12**(4): p. 342-349.
144. Maspero, E., et al. (2013). Structure of a ubiquitin-loaded HECT ligase reveals the molecular basis for catalytic priming. *Nat Struct Mol Biol*. **20**(6): p. 696-+.
145. Mastrandrea, L.D., et al. (1999). E2/E3-mediated assembly of lysine 29-linked polyubiquitin chains. *J Biol Chem*. **274**(38): p. 27299-306.
146. Matta-Camacho, E., et al. (2012). Structure of the HECT C-lobe of the UBR5 E3 ubiquitin ligase. *Acta Crystallographica Section F-Structural Biology and Crystallization Communications*. **68**: p. 1158-1163.
147. Matthews, B.W. (1968). Solvent Content of Protein Crystals. *Journal of Molecular Biology*. **33**(2): p. 491-&.
148. Mccoy, A.J., et al. (2007). Phaser crystallographic software. *Journal of Applied Crystallography*. **40**: p. 658-674.
149. McWilliam, H., et al. (2013). Analysis Tool Web Services from the EMBL-EBI. *Nucleic Acids Research*. **41**(W1): p. W597-W600.
150. Meng, L., et al. (2015). Towards a therapy for Angelman syndrome by targeting a long non-coding RNA. *Nature*. **518**(7539): p. 409-12.
151. Mevissen, T.E.T., et al. (2016). Molecular basis of Lys11-polyubiquitin specificity in the deubiquitinase Cezanne. *Nature*. **538**(7625): p. 402-405.
152. Michelle, C., et al. (2009). What Was the Set of Ubiquitin and Ubiquitin-Like Conjugating Enzymes in the Eukaryote Common Ancestor? *Journal of Molecular Evolution*. **68**(6): p. 616-628.
153. Middleton, A.J., J.D. Wright, and C.L. Day (2017). Regulation of E2s: A Role for Additional Ubiquitin Binding Sites? *J Mol Biol*. **429**(22): p. 3430-3440.
154. Mishra, A., S.K. Godavarthi, and N.R. Jana (2009). UBE3A/E6-AP regulates cell proliferation by promoting proteasomal degradation of p27. *Neurobiol Dis*. **36**(1): p. 26-34.
155. Mori, S., et al. (1996). Improved sensitivity of HSQC spectra of exchanging protons at short interscan delays using a new fast HSQC (FHSQC) detection scheme that avoids water saturation (vol 108, pg 94, 1995). *Journal of Magnetic Resonance Series B*. **110**(3): p. 321-321.
156. Mortensen, F., et al. (2015). Role of ubiquitin and the HPV E6 oncoprotein in E6AP-mediated ubiquitination. *Proc Natl Acad Sci U S A*. **112**(32): p. 9872-7.
157. Mueller, U., et al. (2015). The macromolecular crystallography beamlines at BESSY II of the Helmholtz-Zentrum Berlin: Current status and perspectives. *European Physical Journal Plus*. **130**(7).
158. Mund, T., et al. (2015). Disinhibition of the HECT E3 ubiquitin ligase WWP2 by polymerized Dishevelled. *Open Biology*. **5**(12).
159. Munoz-Escobar, J., et al. (2015). The MLLE Domain of the Ubiquitin Ligase UBR5 Binds to Its Catalytic Domain to Regulate Substrate Binding. *Journal of Biological Chemistry*. **290**(37): p. 22841-22850.
160. Murshudov, G.N., et al. (2011). REFMAC5 for the refinement of macromolecular crystal structures. *Acta Crystallogr D Biol Crystallogr*. **67**(Pt 4): p. 355-67.
161. Myant, K.B., et al. (2017). HUWE1 is a critical colonic tumour suppressor gene that prevents MYC signalling, DNA damage accumulation and tumour initiation. *Embo Molecular Medicine*. **9**(2): p. 181-197.
162. Nicholls, R.D. and J.L. Knepper (2001). Genome organization, function, and imprinting in Prader-Willi and Angelman syndromes. *Annu Rev Genomics Hum Genet*. **2**: p. 153-75.
163. Nuber, U. and M. Scheffner (1999). Identification of determinants in E2 ubiquitin-conjugating enzymes required for hect E3 ubiquitin-protein ligase interaction. *J Biol Chem*. **274**(11): p. 7576-82.

164. Nuber, U., S.E. Schwarz, and M. Scheffner (1998). The ubiquitin-protein ligase E6-associated protein (E6-AP) serves as its own substrate. *European Journal of Biochemistry*. **254**(3): p. 643-649.
165. Oda, H., S. Kumar, and P.M. Howley (1999). Regulation of the Src family tyrosine kinase Blk through E6AP-mediated ubiquitination. *Proc Natl Acad Sci U S A*. **96**(17): p. 9557-62.
166. Ogunjimi, A.A., et al. (2005). Regulation of Smurf2 ubiquitin ligase activity by anchoring the E2 to the HECT domain. *Mol Cell*. **19**(3): p. 297-308.
167. Ogunjimi, A.A., et al. (2010). The ubiquitin binding region of the Smurf HECT domain facilitates polyubiquitylation and binding of ubiquitylated substrates. *J Biol Chem*. **285**(9): p. 6308-15.
168. Ozaki, T. and A. Nakagawara (2011). Role of p53 in Cell Death and Human Cancers. *Cancers (Basel)*. **3**(1): p. 994-1013.
169. Pandya, R.K., et al. (2010). A Structural Element within the HUWE1 HECT Domain Modulates Self-ubiquitination and Substrate Ubiquitination Activities. *Journal of Biological Chemistry*. **285**(8): p. 5664-5673.
170. Park, S., et al. (2012). Mechanism-Based Small Molecule Cross-Linkers of HECT E3 Ubiquitin Ligase-Substrate Pairs. *Biochemistry*. **51**(42): p. 8327-8329.
171. Pelzer, C., et al. (2007). UBE1L2, a novel E1 enzyme specific for ubiquitin. *J Biol Chem*. **282**(32): p. 23010-4.
172. Perry, W.L., et al. (1998). The itchy locus encodes a novel ubiquitin protein ligase that is disrupted in a18H mice. *Nat Genet*. **18**(2): p. 143-6.
173. Persaud, A., et al. (2014). Tyrosine phosphorylation of NEDD4 activates its ubiquitin ligase activity. *Science Signaling*. **7**(346).
174. Petroski, M.D. and R.J. Deshaies (2005). Mechanism of lysine 48-linked ubiquitin-chain synthesis by the cullin-RING ubiquitin-ligase complex SCF-Cdc34. *Cell*. **123**(6): p. 1107-1120.
175. Phu, L.L., et al. (2011). Improved Quantitative Mass Spectrometry Methods for Characterizing Complex Ubiquitin Signals. *Molecular & Cellular Proteomics*. **10**(5).
176. Pickart, C.M. and M.J. Eddins (2004). Ubiquitin: structures, functions, mechanisms. *Biochimica Et Biophysica Acta-Molecular Cell Research*. **1695**(1-3): p. 55-72.
177. Pickart, C.M. and I.A. Rose (1985). Functional heterogeneity of ubiquitin carrier proteins. *Prog Clin Biol Res*. **180**: p. 215.
178. Plechanovova, A., et al. (2012). Structure of a RING E3 ligase and ubiquitin-loaded E2 primed for catalysis. *Nature*. **489**(7414): p. 115-U135.
179. Porath, J. and P. Flodin (1959). Gel filtration: a method for desalting and group separation. *Nature*. **183**(4676): p. 1657-9.
180. Pruneda, J.N., et al. (2012). Structure of an E3:E2 similar to Ub Complex Reveals an Allosteric Mechanism Shared among RING/U-box Ligases. *Molecular Cell*. **47**(6): p. 933-942.
181. Purbeck, C., Z.M. Eletr, and B. Kuhlman (2010). Kinetics of the transfer of ubiquitin from UbcH7 to E6AP. *Biochemistry*. **49**(7): p. 1361-3.
182. Reverter, D. and C.D. Lima (2005). Insights into E3 ligase activity revealed by a SUMO-RanGAP1-Ubc9-Nup358 complex. *Nature*. **435**(7042): p. 687-692.
183. Rhodes, G. (2006). Crystallography made crystal clear : a guide for users of macromolecular models. Vol. 3. Boston: *Elsevier/Academic Press*.
184. Ries, L.K., et al. (2019). Analysis of ubiquitin recognition by the HECT ligase E6AP provides insight into its linkage specificity. *J Biol Chem*.
185. Riling, C., et al. (2015). Itch WW Domains Inhibit Its E3 Ubiquitin Ligase Activity by Blocking E2-E3 Ligase Trans-thiolation. *Journal of Biological Chemistry*. **290**(39): p. 23875-23887.
186. Robzyk, K., J. Recht, and M.A. Osley (2000). Rad6-dependent ubiquitination of histone H2B in yeast. *Science*. **287**(5452): p. 501-4.
187. Rodrigo-Brenni, M.C., S.A. Foster, and D.O. Morgan (2010). Catalysis of lysine 48-specific ubiquitin chain assembly by residues in E2 and ubiquitin. *Mol Cell*. **39**(4): p. 548-59.

188. Ronchi, V.P., et al. (2017). In silico modeling of the cryptic E2~ubiquitin binding site of E6-associated Protein (E6AP)/UBE3A reveals the mechanism of polyubiquitin chain assembly. *J Biol Chem*.
189. Ronchi, V.P., et al. (2014). The Active Form of E6-associated protein (E6AP)/UBE3A Ubiquitin Ligase Is an Oligomer. *Journal of Biological Chemistry*. **289**(2): p. 1033-1048.
190. Ronchi, V.P., J.M. Klein, and A.L. Haas (2013). E6AP/UBE3A ubiquitin ligase harbors two E2~ubiquitin binding sites. *Journal of Biological Chemistry*. **288**(15): p. 10349-60.
191. Rotin, D. and S. Kumar (2009). Physiological functions of the HECT family of ubiquitin ligases. *Nat Rev Mol Cell Biol*. **10**(6): p. 398-409.
192. Rougeulle, C., et al. (1998). An imprinted antisense RNA overlaps UBE3A and a second maternally expressed transcript. *Nat Genet*. **19**(1): p. 15-6.
193. Rougeulle, C., H. Glatt, and M. Lalande (1997). The Angelman syndrome candidate gene, UBE3A/E6-AP, is imprinted in brain. *Nat Genet*. **17**(1): p. 14-5.
194. Rupp, B. (2009). Biomolecular crystallography: principles, practice, and application to structural biology. New York: *Garland Science*.
195. Sadikovic, B., et al. (2014). Mutation Update for UBE3A Variants in Angelman Syndrome. *Human Mutation*. **35**(12): p. 1407-1417.
196. Sailer, C., et al. (2018). Structural dynamics of the E6AP/UBE3A-E6-p53 enzyme-substrate complex. *Nature Communications*. **9**.
197. Salvat, C., et al. (2004). The-4 phenylalanine is required for substrate ubiquitination catalyzed by HECT ubiquitin ligases. *Journal of Biological Chemistry*. **279**(18): p. 18935-18943.
198. Sander, B., et al. (2017). A conformational switch regulates the ubiquitin ligase HUWE1. *Elife*. **6**.
199. Scheffner, M., et al. (1993). The Hpv-16 E6 and E6-Ap Complex Functions as a Ubiquitin-Protein Ligase in the Ubiquitination of P53. *Cell*. **75**(3): p. 495-505.
200. Scheffner, M. and S. Kumar (2014). Mammalian HECT ubiquitin-protein ligases: Biological and pathophysiological aspects. *Biochimica Et Biophysica Acta-Molecular Cell Research*. **1843**(1): p. 61-74.
201. Scheffner, M., U. Nuber, and J.M. Huibregtse (1995). Protein Ubiquitination Involving an E1-E2-E3 Enzyme Ubiquitin Thioester Cascade. *Nature*. **373**(6509): p. 81-83.
202. Scheffner, M. and O. Staub (2007). HECT E3s and human disease. *BMC Biochem*. **8 Suppl 1**: p. S6.
203. Schmid, F.X. (1997). Optical spectroscopy to characterize protein conformation and conformational changes. Protein structure: a practical approach. , *T. E. Creighton. Oxford University Press*: Oxford. p. 261-298.
204. Scott, D.C., et al. (2014). Structure of a RING E3 Trapped in Action Reveals Ligation Mechanism for the Ubiquitin-like Protein NEDD8. *Cell*. **157**(7): p. 1671-1684.
205. Shi, S.Q., et al. (2015). Ube3a imprinting impairs circadian robustness in Angelman syndrome models. *Curr Biol*. **25**(5): p. 537-45.
206. Shiryev, S.A., et al. (2007). Improved BLAST searches using longer words for protein seeding. *Bioinformatics*. **23**(21): p. 2949-2951.
207. Sievers, F., et al. (2011). Fast, scalable generation of high-quality protein multiple sequence alignments using Clustal Omega. *Molecular Systems Biology*. **7**.
208. Sluimer, J. and B. Distel (2018). Regulating the human HECT E3 ligases. *Cellular and Molecular Life Sciences*. **75**(17): p. 3121-3141.
209. Smith, R.A., et al. (2006). Antisense oligonucleotide therapy for neurodegenerative disease. *J Clin Invest*. **116**(8): p. 2290-6.
210. Soss, S.E., R.E. Klevit, and W.J. Chazin (2013). Activation of UbcH5c similar to Ub Is the Result of a Shift in Interdomain Motions of the Conjugate Bound to U-Box E3 Ligase E4B. *Biochemistry*. **52**(17): p. 2991-2999.
211. Streich, F.C., Jr. and C.D. Lima (2016). Capturing a substrate in an activated RING E3/E2-SUMO complex. *Nature*. **536**(7616): p. 304-8.

212. Studier, F.W. and B.A. Moffatt (1986). Use of Bacteriophage-T7 Rna-Polymerase to Direct Selective High-Level Expression of Cloned Genes. *Journal of Molecular Biology*. **189**(1): p. 113-130.
213. Todaro, D.R., et al. (2017). The mechanism of neural precursor cell expressed developmentally down-regulated 4-2 (Nedd4-2)/NEDD4L-catalyzed polyubiquitin chain assembly. *J Biol Chem*. **292**(47): p. 19521-19536.
214. Todaro, D.R., et al. (2018). Oligomerization of the HECT ubiquitin ligase NEDD4-2/NEDD4L is essential for polyubiquitin chain assembly. *J Biol Chem*. **293**(47): p. 18192-18206.
215. Tomaic, V., et al. (2011). Regulation of the human papillomavirus type 18 E6/E6AP ubiquitin ligase complex by the HECT domain-containing protein EDD. *J Virol*. **85**(7): p. 3120-7.
216. Tompkins, E.R. and S.W. Mayer (1947). Ion Exchange as a Separations Method .3. Equilibrium Studies of the Reactions of Rare Earth Complexes with Synthetic Ion Exchange Resins. *Journal of the American Chemical Society*. **69**(11): p. 2859-2865.
217. Towbin, H., T. Staehelin, and J. Gordon (1979). Electrophoretic Transfer of Proteins from Polyacrylamide Gels to Nitrocellulose Sheets - Procedure and Some Applications. *Proceedings of the National Academy of Sciences of the United States of America*. **76**(9): p. 4350-4354.
218. Ulrich, E.L., et al. (2008). BioMagResBank. *Nucleic Acids Research*. **36**(Database issue): p. D402-8.
219. van den Ent, F. and J. Lowe (2006). RF cloning: A restriction-free method for inserting target genes into plasmids. *Journal of Biochemical and Biophysical Methods*. **67**(1): p. 67-74.
220. Verdecia, M.A., et al. (2003). Conformational flexibility underlies ubiquitin ligation mediated by the WWP1 HECT domain E3 ligase. *Mol Cell*. **11**(1): p. 249-59.
221. Vijay-Kumar, S., C.E. Bugg, and W.J. Cook (1987). Structure of ubiquitin refined at 1.8 A resolution. *J Mol Biol*. **194**(3): p. 531-44.
222. Wang, C., et al. (2001). TAK1 is a ubiquitin-dependent kinase of MKK and IKK. *Nature*. **412**(6844): p. 346-351.
223. Wang, J., et al. (2010). Calcium activates Nedd4 E3 ubiquitin ligases by releasing the C2 domain-mediated auto-inhibition. *J Biol Chem*. **285**(16): p. 12279-88.
224. Wang, M., et al. (2006). Molecular determinants of polyubiquitin linkage selection by an HECT ubiquitin ligase. *EMBO J*. **25**(8): p. 1710-9.
225. Wang, M. and C.M. Pickart (2005). Different HECT domain ubiquitin ligases employ distinct mechanisms of polyubiquitin chain synthesis. *EMBO J*. **24**(24): p. 4324-33.
226. Wang, X., et al. (2007). NEDD4-1 is a proto-oncogenic ubiquitin ligase for PTEN. *Cell*. **128**(1): p. 129-39.
227. Wang, Y., et al. (2017). Identifying the ubiquitination targets of E6AP by orthogonal ubiquitin transfer. *Nat Commun*. **8**(1): p. 2232.
228. Weiss, M.S. (2001). Global indicators of X-ray data quality. *Journal of Applied Crystallography*. **34**: p. 130-135.
229. Weiss, M.S. and R. Hilgenfeld (1997). On the use of the merging R factor as a quality indicator for X-ray data. *Journal of Applied Crystallography*. **30**: p. 203-205.
230. Wen, J., T. Arakawa, and J.S. Philo (1996). Size-exclusion chromatography with on-line light-scattering, absorbance, and refractive index detectors for studying proteins and their interactions. *Anal Biochem*. **240**(2): p. 155-166.
231. Wenzel, D.M. and R.E. Klevit (2012). Following Ariadne's thread: a new perspective on RBR ubiquitin ligases. *BMC Biol*. **10**: p. 24.
232. Wenzel, D.M., et al. (2011). UBCH7 reactivity profile reveals parkin and HHARI to be RING/HECT hybrids. *Nature*. **474**(7349): p. 105-U136.
233. Wickliffe, K.E., et al. (2011). The mechanism of linkage-specific ubiquitin chain elongation by a single-subunit E2. *Cell*. **144**(5): p. 769-81.
234. Wiener, R., et al. (2012). The mechanism of OTUB1-mediated inhibition of ubiquitination. *Nature*. **483**(7391): p. 618-22.

235. Wiesner, S., et al. (2007). Autoinhibition of the HECT-type ubiquitin ligase Smurf2 through its C2 domain. *Cell*. **130**(4): p. 651-62.
236. Wilkinson, K.D. (1997). Regulation of ubiquitin-dependent processes by deubiquitinating enzymes. *FASEB J*. **11**(14): p. 1245-56.
237. Winn, M.D., et al. (2011). Overview of the CCP4 suite and current developments. *Acta Crystallographica Section D-Biological Crystallography*. **67**: p. 235-242.
238. Wolyniec, K., et al. (2013). The E6AP E3 ubiquitin ligase regulates the cellular response to oxidative stress. *Oncogene*. **32**(30): p. 3510-3519.
239. Wong, J.J.Y., et al. (2006). HERC5 is an IFN-induced HECT-type E3 protein ligase that mediates type I IFN-induced ISGylation of protein targets. *Proceedings of the National Academy of Sciences of the United States of America*. **103**(28): p. 10735-10740.
240. Wu, Y.S. and P.J. Domaille (2001). 1H, 15N and 13C assignments of the catalytic domain of E6-associated protein (E6AP). *J Biomol NMR*. **21**(3): p. 285-6.
241. Yamamoto, Y., J.M. Huibregtse, and P.M. Howley (1997). The human E6-AP gene (UBE3A) encodes three potential protein isoforms generated by differential splicing. *Genomics*. **41**(2): p. 263-6.
242. Yang, B., et al. (2008). Nedd4 augments the adaptive immune response by promoting ubiquitin-mediated degradation of Cbl-b in activated T cells. *Nat Immunol*. **9**(12): p. 1356-63.
243. Yi, J.J., et al. (2015). An Autism-Linked Mutation Disables Phosphorylation Control of UBE3A. *Cell*. **162**(4): p. 795-807.
244. Yi, J.J., et al. (2017). The autism-linked UBE3A T485A mutant E3 ubiquitin ligase activates the Wnt/beta-catenin pathway by inhibiting the proteasome. *J Biol Chem*. **292**(30): p. 12503-12515.
245. Yin, L., et al. (2000). Nonhydrolyzable diubiquitin analogues are inhibitors of ubiquitin conjugation and deconjugation. *Biochemistry*. **39**(32): p. 10001-10.
246. Yip, T.T. and T.W. Hutchens (1992). Immobilized metal ion affinity chromatography. *Methods Mol Biol*. **11**: p. 17-31.
247. Yunus, A.A. and C.D. Lima (2006). Lysine activation and functional analysis of E2-mediated conjugation in the SUMO pathway. *Nat Struct Mol Biol*. **13**(6): p. 491-499.
248. Zaaroor-Regev, D., et al. (2010). Regulation of the polycomb protein Ring1B by self-ubiquitination or by E6-AP may have implications to the pathogenesis of Angelman syndrome. *Proc Natl Acad Sci U S A*. **107**(15): p. 6788-93.
249. Zanier, K., et al. (2013). Structural Basis for Hijacking of Cellular LxxLL Motifs by Papillomavirus E6 Oncoproteins. *Science*. **339**(6120): p. 694-698.
250. Zhang, W., et al. (2016). System-Wide Modulation of HECT E3 Ligases with Selective Ubiquitin Variant Probes. *Molecular Cell*. **62**(1): p. 121-136.
251. Zhao, H.Y., P.H. Brown, and P. Schuckt (2011). On the Distribution of Protein Refractive Index Increments. *Biophysical Journal*. **100**(9): p. 2309-2317.
252. Zhi, X. and C. Chen (2012). WWP1: a versatile ubiquitin E3 ligase in signaling and diseases. *Cell Mol Life Sci*. **69**(9): p. 1425-34.
253. Zhu, K., et al. (2017). Allosteric auto-inhibition and activation of the Nedd4 family E3 ligase Itch. *EMBO Rep*. **18**(9): p. 1618-1630.

Appendix

Abbreviations

Prefixes

µ	micro
m	milli
k	kilo

Units

°	degree
A	ampere
Å	Ångström
Da	Dalton
g	gram
h	hour
J	Joule
K	Kelvin
l	liter
m	meter
min	minute
M	molar (mol/l)
OD	optical density
rpm	revolutions per minute
s	second
v/v	volume per volume
w/v	weight per volume
°C	degree Celsius

Further abbreviation

a	analytical
α	anti
A	adenine
A	Alanine, Ala
A	anion
A_{280}	measured by absorbance at 280 nm
aa	amino acid
ADP	Adenosine-5'-diphosphate
Amp	Ampicillin

AMP	Adenosine-5’-monophosphate
APS	ammoniumpersulfate
AQUA	absolute quantification
AR	Ankyrin repeat
ARC	Activity-regulated cytoskeleton-associated protein
ARM	Armadillo type
AS	Angelman syndrome
ASD	Autism spectrum disorders
ASO	Antisense oligonucleotide
ATP	adenosine-5’-triphosphate
ATS	antisense transcript
BCL-2	B-cell lymphoma 2
BESSY	Berliner Elektronenspeicherring-Gesellschaft für Synchrotronstrahlung
bp	base pairs
BH3	BCL-2 homology region 3
BMRB	Biological Magnetic Resonance Bank
BSA	bovine serum albumine
c	concentration
C	cytosine
C	cysteine, Cys
C	cation
c-ABL	Abelson murine leukemia
CC1/2	correlation coefficient 1/2
CCC	Comprehensive Cancer Center
CCP4	Collaborative Computational Project, Number 4, 1994
CD	circular dichroism
CV	column volume
Cyt-B5	Cytochrome B5-like heme/steroid binding
D	aspartic acid, Asp
ddH_2O	bidestilled water
DMF	dimethylformamide
DMSO	dimethylsulfoxide
DNA	desoxyribonucleic acid
DNase	desoxyribunucelase
dNTP	desoxyribonucleoside-5’-triphosphate (dATP, dCTP, dGTP, dTTP)
DUB	deubiquitinase
DTNB	5,5′-Dithiobis-2-nitrobenzoic acid (Ellman’s reagent)
DTT	dithiothreitol
E	glutamic acid, Glu

E1	ubiquitin activating enzyme
E2	ubiquitin conjugating enzyme
E3	ubiquitin ligase
E6AP	E6-associated protein
E6TP1	E6 targeted protein 1
E. coli	*Escherichia coli*
ECL	enhanced chemoluminescence
EDTA	ethylendiamintetraacetate desoxyribonucleic acid
F	phenylalanine, Phe
F	forward
FL	full-length
FP	fluorescence polarization
FPLC	fast protein liquid chromatography
G	guanine
G	glycine, Gly
GEF	guanine nucleotide-exchange factor
GST	gluatathione-S-transferase
GTP	guanosine-5'-triphosphate
H	histidine, His
H_2O	water
HA	human influenza hemagglutinin
HCV	Hepatitis C virus
heclin	HECT ligase inhibitor
HeLa	Human cervic carcinoma cell line taken from Henrietta Lacks
HF	high fidelity
His_6	hexahistidine
HECT	homologous to E6AP C-Terminus
HEPES	2-[4-(2-hydroxyethyl)piperazin-1-yl]ethanesulfonic acid
HERC	HECT and RCC1-like domains
HPSF	high purity salt free
HPV	human papilloma virus
HRP	horseradish peroxiase
HUWE1	HECT, UBA and WWE domain-containing protein 1
I	isoleucine, Ile
IEX	ion exchange chromatography
IgG	Immunoglobulin
IMAC	immobilized metal affinity chromatography
IPTG	Isopropyl β-D-1-thiogalactopyranoside
ITC	isothermal titration calorimetry

K	lysine, Lys
Kan	Kanamycin
K_D	dissociation constant
L	leucine, Leu
LB	lysogeny broth
M	methionine, Met
MALS	multi-angle light scattering
mass spec	mass spectrometry
ME	Mercaptoethanol
MeOH	Methanol
MLLE	mademoiselle
MOPS	(3-(N-morpholino)propanesulfonic acid
MPI	Max-Planck-Institute
MR	molecular replacement
mRNA	messenger RNA
mTORC1	mammalian target of rapamycin complex 1
M_W	molecular weight
MWCO	molecular weight cut-off
N	asparagine, Asn
NEDD4	Neural precursor cell expressed developmentally down-regulated protein 4
NEM	N-ethylmaleimide
NF-κB	Nuclear factor kappa-light-chain-enhancer of activated B cells
NMR	Nuclear magnetic resonance
no.	number
NTA	nitrilotriacetic acid
OD_{600}	optical density (= absorbance) measured at a wavelength of 600 nm
p	phosphor
P	proline, Pro
PABC	poly(A)-binding protein C-terminus
PAGE	polyacrylamide gel electrophoresis
PAIP2	PABP-interacting protein 2
PCR	polymerase chain reaction
PDB	protein data bank
PDZ	**P**SD95/SAP90, septate-junction-protein **d**iscs large, tight junction-protein **z**onula occludens-1
PEG	polyethylene glycol
pI	isolelectric point
PGR	Progesterone receptor
PKA	Protein kinase A

PML	promyelocytic leukemia
PRC	Polycomb repressive complex
PSD	post synaptic density
PTEN	Phosphatase and Tensin homolog
PTPH1	protein tyrosine phosphatase H1
PVDF	polyvinylidene difluoride
R	arginine, Arg
R	reverse
RBR	RING-between-RING E3 enzyme
RCC1	regulator of chromosome condensation 1
RF	restriction free
RI	refractive index
RING	Really Interesting New Gene
RLD	regulator of chromosome condensation 1-like domains
rmsd	root-mean-square deviation
RNA	ribonucleic acid
ROS	reactive oxygen species
R_{Pim}	precision indicating merging R-factor
RSP5	Reverses SPT-phenotype protein 5
RT	room temperature
RVZ	Rudolf Virchow Zentrum
S	serine, Ser
SD	Superdex
SDS	sodium dodecyl sulfate
SEC	size-exclusion chromatography
SGC	Structural Genomics Consortium
SMT3	Suppressor of mif two 3
SMURF	Smad ubiquitin reculatory factors
Spec	Spectinomycine
SPRY	SPIA and RYanodine Receptor
Src	sarcoma
STR	short tandem repeats
SUMO	Small ubiquitin-related modifier
T	thymine
T	threonine, Thr
TB	Terrific Broth
TBS(-T)	Tris-buffered saline (with tween-20)
TEMED	N,N,N',N'-tetramethylethylendiamine
TEV	Tobacco Etch Virus

TFB	transformation buffer
T_M	melting temperature
Tris	Tris-(hydroxymethyl)-aminomethan
TXN	Thioredoxine
U	Uridine
UBA1	ubiquitin-activating protein 1
UBA	ubiquitin-associated domain
UBCH	ubiquitin-conjugating enzyme H
Ub	ubiquitin
UBM	ubiquitin-binding motif
ULP1	ubiquitin-like-specific protease 1
USP	ubiquitin-specific protease
UbV	ubiquitin variant probe
V	valine, Val
W	tryptophane, Trp
Wnt	wingless-type MMTV integration site family member
WT	wild-type
x	fold
Y	tyrosine, Tyr
YNB	yeast nitrogen base
ZNF	zinc finger

Additional Tables

Table 14: List of primers

Construct		Primer sequence (5'-3')
pET28a/pET30a_Ub (ΔGG) L8A	F	GCAGATTTTCGTGAAAACCGCGACGGGGAAGACCATCACCC
	R	GGGTGATGGTCTTCCCCGTCGCGGTTTTCACGAAAATCTGC
pET30a_Ub T14A	F	TTACGGGGAAGACCATCGCGCTCGAGGTTGAACCCTC
	R	GAGGGTTCAACCTCGAGCGCGATGGTCTTCCCCGTAA
pET30a_Ub E34A	F	GCCAAGATCCAGGATAAGGCGGGAATTCCTCCTGATCAGC
	R	GCTGATCAGGAGGAATTCCCGCCTTATCCTGGATCTTGGC
pET30a_Ub I36A	F	GATCCAGGATAAGGAAGGAGCACCTCCTGATCAGCAGAGAC
	R	GTCTCTGCTGATCAGGAGGTGCTCCTTCCTTATCCTGGATC
pET30a_Ub Q40A	F	GAAGGAATTCCTCCTGATGCGCAGAGACTGATCTTTGC
	R	GCAAAGATCAGTCTCTGCGCATCAGGAGGAATTCCTTC
pET28a/pET30a_Ub (ΔGG) R42A	F	GGAATTCCTCCTGATCAGCAGGCGCTGATCTTTGCTGGCAAGCAG
	R	CTGCTTGCCAGCAAAGATCAGCGCCTGCTGATCAGGAGGAATTCC
pET28a/pET30a_Ub (ΔGG) I44A	F	CCTGATCAGCAGAGACTGGCGTTTGCTGGCAAGCAGCTG
	R	CAGCTGCTTGCCAGCAAACGCCAGTCTCTGCTGATCAGG
pET28a/pET30a_Ub K48R	F	GACTGATCTTTGCTGGCCGTCAGCTGGAAGATGGACG
	R	CGTCCATCTTCCAGCTGACGGCCAGCAAAGATCAGTC
pET28a/pET30a_Ub (ΔGG) Q49A	F	CTGATCTTTGCTGGCAAGGCGCTGGAAGATGGACGTAC
	R	GTACGTCCATCTTCCAGCGCCTTGCCAGCAAAGATCAG
pET28a/pET30a_Ub (ΔGG) E51A	F	CTTTGCTGGCAAGCAGCTGGCGGATGGACGTACTTTGTCTG
	R	CAGACAAAGTACGTCCATCCGCCAGCTGCTTGCCAGCAAAG
pET30a_Ub K63R	F	GTCTGACTACAATATTCAACGTGAGTCTACTCTTCATCTTG
	R	CAAGATGAAGAGTAGACTCACGTTGAATATTGTAGTCAGAC
pET28a_Ub ΔGG V70A	F	GTCTACTCTTCATCTTGCGTTGAGACTTCGTTAAG
	R	CTTAACGAAGTCTCAACGCAAGATGAAGAGTAGAC
pET30a_Ub V70A	F	GTCTACTCTTCATCTTGCGTTGAGACTTCGTGGTG
	R	CACCACGAAGTCTCAACGCAAGATGAAGAGTAGAC
pET30a_Ub L71A	F	CTTCATCTTGTGGCGAGACTTAGAGGTGGTTAATG
	R	CATTAACCACCTCTAAGTCTCGCCACAAGATGAAG
pET30a_Ub R74A	F	CTTCATCTTGTGTTGAGACTTGCGGGTGGTTAATGAAAGCTTGCG
	R	CGCAAGCTTTCATTAACCACCCGCAAGTCTCAACACAAGATGAAG
pET28a_Ub G76C	F	CTTGTGTTGAGACTTCGTGGTTGCTAAGGCGCGCCATCGAGC
	R	GCTCGATGGCGCGCCTTAGCAACCACGAAGTCTCAACACAAG
pET28a_Ub ΔGG	F	CTTGTGTTGAGACTTCGTTAAGGTTAAGGCGCGCCATCGAGC
	R	GCTCGATGGCGCGCCTTAACCTTAACGAAGTCTCAACACAAG
pET28a_E6AP HECT domain K529R K530R	F	CGCTATGGAAAATCCTGCAGACTTGAGGAGGCAGTTGTA TGTGGAATTTGAAGGAGA
	R	TCTCCTTCAAATTCCACATACAACTGCCTCCTCAAGTCTGCAGGATT TTCCATAGCG
pET28a_E6AP HECT domain K549R	F	GTTGATGAGGGAGGTGTTTCCCGTGAATTTTTTCAGCTGGTTGTG
	R	CACAACCAGCTGAAAAAATTCACGGGAAACACCTCCCTCATCAAC
pET28a_E6AP HECT domain I564D	F	GTGGAGGAAATCTTCAATCCAGATGATGGTATGTTCACATACGATGA ATC
	R	GATTCATCGTATGTGAACATACCATCATCTGGATTGAAGATTTCCTC CAC
pET28a_E6AP HECT domain F583D	F	GGTTTAATCCATCTTCTGATGAAACTGAGGGTCAG
	R	CTGACCCTCAGTTTCATCAGAAGATGGATTAAACC
pET28a_E6AP HECT domain C604S	F	GGCTATTTACAATAACAGCATACTGGATGTACATTTTCC
	R	GGAAAATGTACATCCAGTATGCTGTTATTGTAAATAGCC
pET28a_E6AP HECT domain K688R	F	CAATTACAAATGAAAACAGGCGTGAATTTGTCAATCTTTATTC
	R	GAATAAAGATTGACAAATTCACGCCTGTTTTCATTTGTAATTG
pET28a_E6AP HECT domain F665D	F	CAGATATCACAGACAGATCTTGATGGTAACCCAATGATGTATG
	R	CATACATCATTGGGTTACCATCAAGATCTGTCTGTGATATCTG
pET28a_E6AP HECT domain C737S	F	GAAATTGAATTGCTTATAAGCGGAAGCCGGAATCTAG
	R	CTAGATTCCGGCTTCCGCTTATAAGCAATTCAATTTC

pET28a_E6AP HECT domain	F	GAAAAGACTCTTCTTGCAGGCGACAACGGGCACAGACAGAG
F785A	R	CTCTGTCTGTGCCCGTTGTCGCCTGCAAGAAGAGTCTTTTC
pET28a_E6AP HECT domain	F	CCTGTGGGAGGACTAGGACGTTTAAAGATGATTATAGCC
K799R	R	GGCTATAATCATCTTTAAACGTCCTAGTCCTCCCACAGG
pET28a_E6AP HECT domain	F	GTGGGAGGACTAGGAAAATTACGTATGATTATAGCCAAAAATGGC
K801R	R	GCCATTTTTGGCTATAATCATACGTAATTTTCCTAGTCCTCCCAC
pET28a_E6AP HECT domain	F	GGACTAGGAAAATTAAAGATGGCGATAGCCAAAAATGGCCCAGAC
I803A	R	GTCTGGGCCATTTTTGGCTATCGCCATCTTTAATTTTCCTAGTCC
pET28a_E6AP HECT domain	F	AAAGATGATTATAGCCCGTAATGGCCCAGACACAG
K806R	R	CTGTGTCTGGGCCATTACGGGCTATAATCATCTTT
pET28a_E6AP HECT domain	F	GGCCCAGACACAGAAAGGGCGCCTACATCTCATACTTGC
L814A	R	GCAAGTATGAGATGTAGGCGCCCTTTCTGTGTCTGGGCC
pET28a_E6AP HECT domain	F	GAAAGGTTACCTACATCTGCGACTTGCTTTAATGTGCTT
H818A	R	AAGCACATTAAAGCAAGTCGCAGATGTAGGTAACCTTTC
pET28a_E6AP HECT domain	F	AAGGTTACCTACATCTCATGCGTGCTTTAATGTGCTTTTAC
T819A	R	GTAAAAGCACATTAAAGCACGCATGAGATGTAGGTAACCTT
pET28a_E6AP HECT domain	F	CCTACATCTCATACTTGCGCGAATGTGCTTTTACTTCCG
F821A	R	CGGAAGTAAAAGCACATTCGCGCAAGTATGAGATGTAGG
pET28a_E6AP HECT domain	F	GGTTACCTACATCTCATACTGCGTTTAATGTGCTTTTACTTCCG
C820A	R	CGGAAGTAAAAGCACATTAAACGCAGTATGAGATGTAGGTAACC
pET28a_E6AP HECT domain	F	GGTTACCTACATCTCATACTAGCTTTAATGTGCTTTTACTTC
C820S	R	GAAGTAAAAGCACATTAAAGCTAGTATGAGATGTAGGTAACC
pET28a_E6AP HECT domain	F	CATCTCATACTTGCTTTAATGCGCTTTTACTTCCGGAATACTC
V823A	R	GAGTATTCCGGAAGTAAAAGCGCATTAAAGCAAGTATGAGATG
pET28a_E6AP HECT domain	F	CTTAAAGAGAGATTGTTGCGTGCCATCACGTATGCCAAAG
K841R	R	CTTTGGCATACGTGATGGCACGCAACAATCTCTCTTTAAG
pET28a_E6AP HECT domain	F	AAGAGAGATTGTTGAAGATTATCACGTATGCCAAAGG
A842I	R	CCTTTGGCATACGTGATAATCTTCAACAATCTCTCTT
pET28a_E6AP HECT domain	F	GGCCATCACGTATGCCCGAGGATTTGGCATGCTG
K847R	R	CAGCATGCCAAATCCTCGGGCATACGTGATGGCC
pET28a_E6AP HECT domain	F	GTATGCCAAAGGAGCGGGCATGCTGTAA
F849A	R	TTACAGCATGCCCGCTCCTTTGGCATAC
pET28a_E6AP HECT domain Δ4	F	CACGTATGCCAAAGGATAATAAGAATTCGAGCTCCG
	R	CGGAGCTCGAATTCTTATTATCCTTTGGCATACGTG
pET28a_E6AP N-Helix 1_aa 398	F	GGAAGTTCTGTTCCAGGGGCCCAAAGGTCCTCGAGTGGACC
pET28a_E6AP N-Helix 2_aa 432	F	GGAAGTTCTGTTCCAGGGGCCCAATGAGGTTCTAGAAATGGATAAAG
pET28a_E6AP N-Helix 3_aa 451	F	GGAAGTTCTGTTCCAGGGGCCCAAATTCTCTTTTATGACATGTCCCT
pET28a_E6AP N-Helix 4_aa 462	F	GGAAGTTCTGTTCCAGGGGCCCAATGCTGTCACAAAGAATTTGGG
pET28a_E6AP N-Helix 5_aa 471 Y471D	F	GGAAGTTCTGTTCCAGGGGCCCGATTATGACAATAGAATTCGCATGT
pET28a_E6AP N-Helix reverse primer	R	TGTCCACCAGTCATGCTAGCCATATGTTACAGCATGCCAAATCCTTTG
pET28a_E6AP N-Helix 5 Y479E	F	GACAATAGAATTCGCATGGAAAGTGAACGAAGAATCAC
	R	GTGATTCTTCGTTCACTTTCCATGCGAATTCTATTGTC
pET28_E6AP N-Helix 5 T485A	F	GTACAGTGAACGAAGAATCGCGGTTCTCTACAGCTTAGTTC
	R	GAACTAAGCTGTAGAGAACCGCGATTCTTCGTTCACTGTAC
pET28a_E6AP N-Helix 5 T485E	F	GTACAGTGAACGAAGAATCGAAGTTCTCTACAGCTTAGTTC
	R	GAACTAAGCTGTAGAGAACTTCGATTCTTCGTTCACTGTAC
T7-Promotor	F	TAATACGACTCACTATAGGG
T7-Terminator	R	GCTAGTTATTGCTCAGCGG

The vectors pET30a_Ub K6R/K11R/K27R/K29R/K33R/K0/G75C/G76C were kindly provided by Anna Liess, Julia Haubenreißer and Dr. Sonja Lorenz (RVZ, Würzburg).

Table 15: Composition of the thermofluor advanced buffer screen

well			Buffer [M]		well			Buffer [M]	
A1					E1	0.25	NaCl		
A2			0.1	citric acid pH 4.0	E2	0.25	NaCl	0.1	citric acid pH 4.0
A3			0.1	NaCOOH pH 4.5	E3	0.25	NaCl	0.1	Na acetate pH 4.5
A4			0.1	citric acid pH 5.0	E4	0.25	NaCl	0.1	citric acid pH 5.0
A5			0.1	mes pH 6.0	E5	0.25	NaCl	0.1	mes pH 6.0
A6			0.1	KP pH 6.0	E6	0.25	NaCl	0.1	KP pH 6.0
A7			0.1	citric acid pH 6.0	E7	0.25	NaCl	0.1	citric acid pH 6.0
A8			0.1	bis-tris pH 6.5	E8	0.25	NaCl	0.1	bis-tris pH 6.5
A9			0.1	Na cacodylate pH 6.5	E9	0.25	NaCl	0.1	Na cacodylate pH 6.5
A10			0.1	NaP pH 7.0	E10	0.25	NaCl	0.1	NaP pH 7.0
A11			0.1	KP pH 7.0	E11	0.25	NaCl	0.1	KP pH 7.0
A12			0.1	hepes pH 7.0	E12	0.25	NaCl	0.1	hepes pH 7.0
B1			0.1	mops pH 7.0	F1	0.25	NaCl	0.1	mops pH 7.0
B2			0.1	NH_4COOH pH 7.3	F2	0.25	NaCl	0.1	NH_4COOH pH 7.3
B3			0.1	tris pH 7.5	F3	0.25	NaCl	0.1	tris pH 7.5
B4			0.1	NaP pH 7.5	F4	0.25	NaCl	0.1	NaP pH 7.5
B5			0.1	imidazole pH 8.0	F5	0.25	NaCl	0.1	imidazole pH 8.0
B6			0.1	hepes pH 8.0	F6	0.25	NaCl	0.1	hepes pH 8.0
B7			0.1	tris pH 8.0	F7	0.25	NaCl	0.1	tris pH 8.0
B8			0.1	tricine pH 8.0	F8	0.25	NaCl	0.1	tricine pH 8.0
B9			0.1	bicine pH 8.0	F9	0.25	NaCl	0.1	bicine pH 8.0
B10			0.1	bicine pH 8.5	F10	0.25	NaCl	0.1	bicine pH 8.5
B11			0.1	tris pH 8.5	F11	0.25	NaCl	0.1	tris pH 8.5
B12			0.1	bicine pH 9.0	F12	0.25	NaCl	0.1	bicine pH 9.0
C1	0.15	NaCl			G1			0.02	hepes pH 7.5
C2	0.15	NaCl	0.1	citric acid pH 4.0	G2			0.05	hepes pH 7.5
C3	0.15	NaCl	0.1	NaCOOH pH 4.5	G3			0.1	hepes pH 7.5
C4	0.15	NaCl	0.1	citric acid pH 5.0	G4			0.25	hepes pH 7.5
C5	0.15	NaCl	0.1	mes pH 6.0	G5			0.02	NaP pH 7.5
C6	0.15	NaCl	0.1	KP pH 6.0	G6			0.05	NaP pH 7.5
C7	0.15	NaCl	0.1	citric acid pH 6.0	G7			0.1	NaP pH 7.5
C8	0.15	NaCl	0.1	bis-tris pH 6.5	G8			0.2	NaP pH 7.5
C9	0.15	NaCl	0.1	Na cacodylate pH 6.5	G9			0.02	tris pH 8.0
C10	0.15	NaCl	0.1	NaP pH 7.0	G10			0.05	tris pH 8.0
C11	0.15	NaCl	0.1	KP pH 7.0	G11			0.1	tris pH 8.0
C12	0.15	NaCl	0.1	hepes pH 7.0	G12			0.25	tris pH 8.0
D1	0.15	NaCl	0.1	mops pH 7.0	H1	0.05	NaCl	0.05	hepes pH 7.5
D2	0.15	NaCl	0.1	NH_4COOH pH 7.3	H2	0.125	NaCl	0.05	hepes pH 7.5
D3	0.15	NaCl	0.1	tris pH 7.5	H3	0.25	NaCl	0.05	hepes pH 7.5
D4	0.15	NaCl	0.1	NaP pH 7.5	H4	0.5	NaCl	0.05	hepes pH 7.5
D5	0.15	NaCl	0.1	imidazole pH 8.0	H5	0.75	NaCl	0.05	hepes pH 7.5
D6	0.15	NaCl	0.1	hepes pH 8.0	H6	1	NaCl	0.05	hepes pH 7.5
D7	0.15	NaCl	0.1	tris pH 8.0	H7	0.05	NaCl	0.05	tris pH 8.0
D8	0.15	NaCl	0.1	tricine pH 8.0	H8	0.125	NaCl	0.05	tris pH 8.0
D9	0.15	NaCl	0.1	bicine pH 8.0	H9	0.25	NaCl	0.05	tris pH 8.0
D10	0.15	NaCl	0.1	bicine pH 8.5	H10	0.5	NaCl	0.05	tris pH 8.0
D11	0.15	NaCl	0.1	tris pH 8.5	H11	0.75	NaCl	0.05	tris pH 8.0
D12	0.15	NaCl	0.1	bicine pH 9.0	H12	1	NaCl	0.05	tris pH 8.0

Supplementary Data

Assembly of Lys48-linked ubiquitin chains

The production of Lys48-linked ubiquitin chains was performed according to the protocol through the enzymatic reaction of UBA1 and CDC34A with wild-type ubiquitin at 37 °C overnight [33]. The Lys48-linked ubiquitin chains were separated from the reaction mixture by CIEX. With a linear gradient from 0 to 500 mM salt the ubiquitin chains of different length could be eluted and separated from each other **(Figure 44A)**. The purity of the chains was visualized via SDS-PAGE and Coomassie staining **(Figure 44B)**.

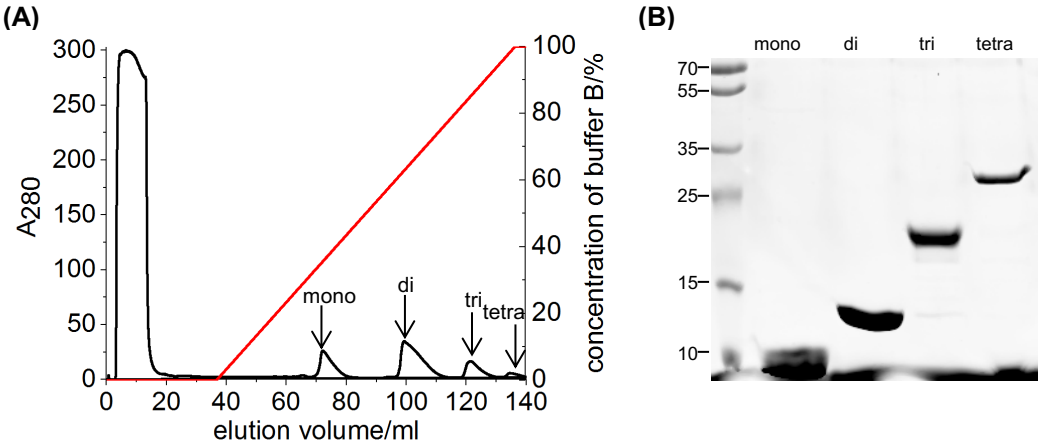

Figure 44: Enzymatically production of Lys48-linked ubiquitin chains. (A) CIEX with a Mono S 4.6/100 PE column in 50 mM NH_4COOH and a NaCl gradient from 0 to 500 mM. **(B)** SDS-PAGE of the purified ubiquitin species.

AQUA Mass Spec Trace

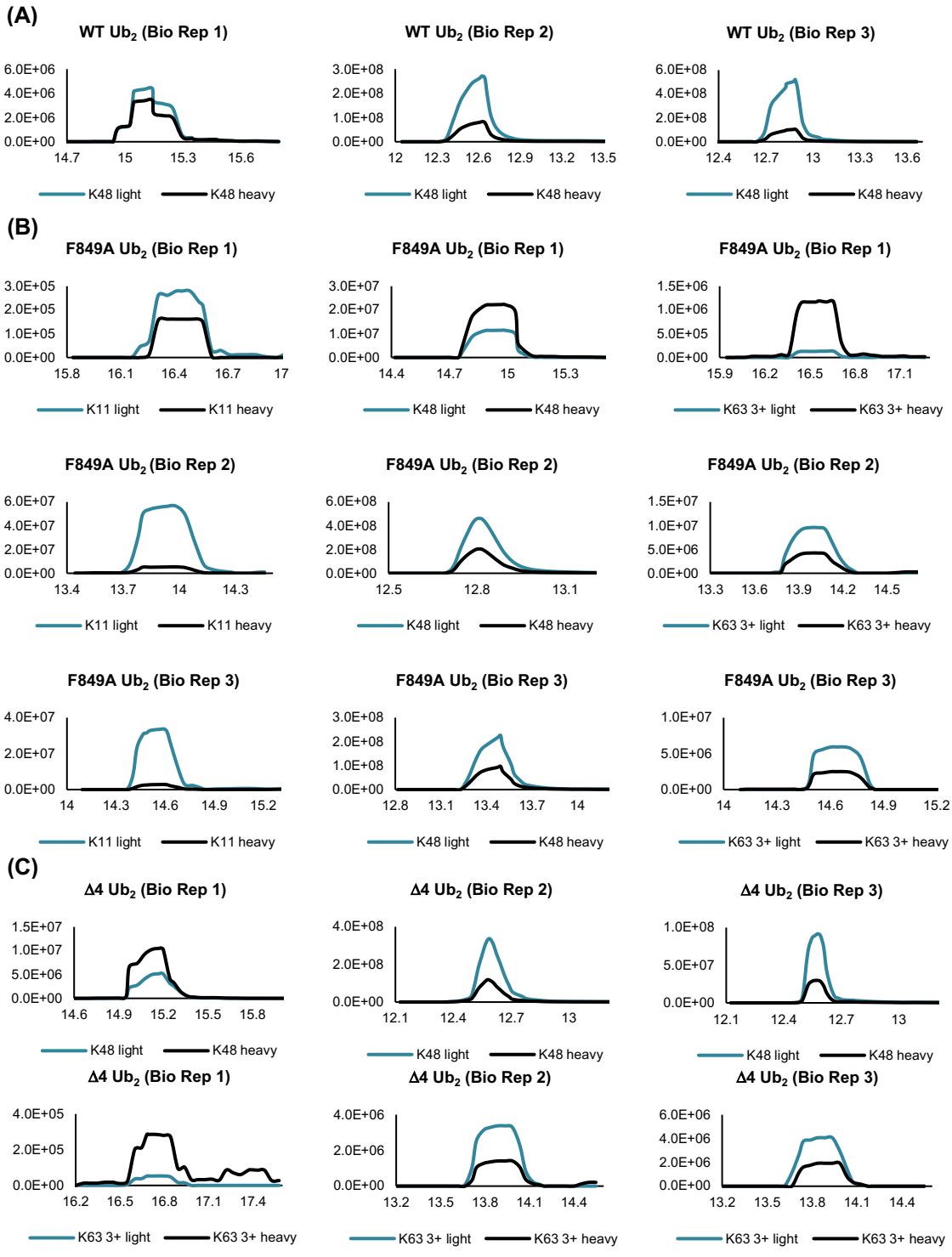

Figure 45: AQUA mass spectrometric analysis of Ub_2-linkage types formed by different E6AP HECT domain variants. The di-ubiquitin (Ub_2) reaction products formed by the E6AP HECT domain WT **(A)**, F849A **(B)**, and Δ4 **(C)**, respectively, were analyzed; extracted ion chromatograms are shown; pairs of the co-eluting light and heavy peaks are displayed on the same relative abundance scale (y-axis) as a function of the retention time (x-axis, in min). AQUA mass spectrometry was performed by Kirandeep Deol and Prof. Eric Strieter.

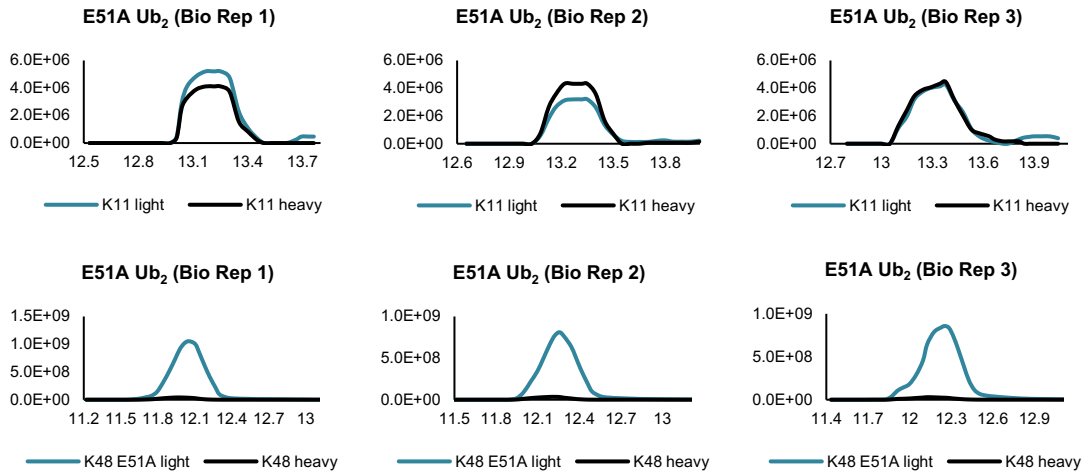

Figure 46: AQUA mass spectrometric analysis of Ub_2-linkage types formed by the E6AP HECT domain with E51A ubiquitin. Extracted ion chromatograms are shown; pairs of the co-eluting light and heavy peaks are displayed on the same relative abundance scale (y-axis) as a function of the retention time (x-axis, in min). AQUA mass spectrometry was performed by Kirandeep Deol and Prof. Eric Strieter.

Sequences

E6AP isoform 1

MKRAAAKHLIERYYHQLTEGCGNEACTNEFCASCPTFLRMDNNAAAIKALELYKINAKLCDPHPSKKGASSAYLE
NSKGAPNNSCSEIKMNKKGARIDFKDVTYLTEEKVYEILELCREREDYSPLIRVIGRVFSSAEALVQSFRKVKQH
TKEELKSLQAKDEDKDEDEKEKAACSAAAMEEDSEASSSRIGDSSQGDNNLQKLGPDDVSVDIDAIRRVYTRLLS
NEKIETAFLNALVYLSPNVECDLTYHNVYSRDPNYLNLFIIVMENRNLHSPEYLEMALPLFCKAMSKLPLAAQGK
LIRLWSKYNADQIRRMMETFQQLITYKVISNEFNSRNLVNDDDAIVAASKCLKMVYYANVVGGEVDTNHNEEDDE
EPIPESSELTLQELLGEERRNKKGPRVDPLETELGVKTLDCRKPLIPFEEFINEPLNEVLEMDKDYTFFKVETEN
KFSFMTCPFILNAVTKNLGLYYDNRIRMYSERRITVLYSLVQGQQLNPYLRLKVRRDHIIDDALVRLEMIAMENP
ADLKKQLYVEFEGEQGVDEGGVSKEFFQLVVEEIFNPDIGMFTYDESTKLFWFNPSSFETEGQFTLIGIVLGLAI
YNNCILDVHFPMVVYRKLMGKKGTFRDLGDSHPVLYQSLKDLLEYEGNVEDDMMITFQISQTDLFGNPMMYDLKE
NGDKIPITNENRKEFVNLYSDYILNKSVEKQFKAFRRGFHMVTNESPLKYLFRPEEIELLICGSRNLDFQALEET
TEYDGGYTRDSVLIREFWEIVHSFTDEQKRLFLQFTTGTDRAPVGGLGKLKMIIAKNGPDTERLPTSHTCFNVLL
LPEYSSKEKLKERLLKAITYAKGFGML

Pink: start of N-terminally extended HECT domain constructs 1-5

Yellow: start of HECT domain/N-lobe; cyan: start of C-lobe

NEDD4 isoform 4

MATCAVEVFGLLEDEENSRIVRVRVIAGIGLAKKDILGASDPYVRVTLYDPMNGVLTSVQTKTIKKSLNPKWNEE
ILFRVHPQQHRLLFEVFDENRLTRDDFLGQVDVPLYPLPTENPRLERPYTFKDFVLHPRSHKSRVKGYLRLKMTY
LPKTSGSEDDNAEQAEELEPGWVVLDQPDAACHLQQQQEPSPLPPGWEERQDILGRTYYVNHESRRTQWKRPTPQ
DNLTDAENGNIQLQAQRAFTTRRQISEETESVDNRESSENWEIIREDEATMYSNQAFPSPPPSSNLDVPTHLAEE
LNARLTIFGNSAVSQPASSSNHSSRRGSLQAYTFEEQPTLPVLLPTSSGLPPGWEEKQDERGRSYYVDHNSRTTT
WTKPTVQATVETSQLTSSQSSAGPQSQASTSDSGQQVTQPSEIEQGFLPKGWEVRHAPNGRPFFIDHNTKTTTWE
DPRLKIPAHLRGKTSLDTSNDLGPLPPGWEERTHTDGRIFYINHNIKRTQWEDPRLENVAITGPAVPYSRDYKRK
YEFFRRKLKKQNDIPNKFEMKLRRATVLEDSYRRIMGVKRADFLKARLWIEFDGEKGLDYGGVAREWFFLISKEM
FNPYYGLFEYSATDNYTLQINPNSGLCNEDHLSYFKFIGRVAGMAVYHGKLLDGFFIRPFYKMMLHKPITLHDME
SVDSEYYNSLRWILENDPTELDLRFIIDEELFGQTHQHELKNGGSEIVVTNKNKKEYIYLVIQWRFVNRIQKQMA
AFKEGFFELIPQDLIKIFDENELELLMCGLGDVDVNDWREHTKYKNGYSANHQVIQWFWKAVLMMDSEKRIRLLQ
FVTGTSRVPMNGFAELYGSNGPQSFTVEQWGTPEKLPRAHTCFNRLDLPPYESFEELWDKLQMAIENTQGFDGVD

Yellow: start of HECT domain; cyan: start of C-lobe

Ubiquitin

MQIFVKTLTGKTITLEVEPSDTIENVKAKIQDKEGIPPDQQRLIFAGKQLEDGRTLSDYNIQKESTLHLVLRLRG
G

UBE2D3

MALKRINKELSDLARDPPAQCSAGPVGDDMFHWQATIMGPNDSPYQGGVFFLTIHFPTDYPFKPPKVAFTTRIYH
PNINSNGSICLDILRSQWSPALTISKVLLSICSLLCDPNPDDPLVPEIARIYKTDRDKYNRISREWTQKYAM

UBE2L3

MAASRRLMKELEEIRKCGMKNFRNIQVDEANLLTWQGLIVPDNPPYDKGAFRIEINFPAEYPFKPPKITFKTKIY
HPNIDEKGQVCLPVISAENWKPATKTDQVIQSLIALVNDPQPEHPLRADLAEEYSKDRKKFCKNAEEFTKKYGEK
RPVD

CDC34A

MARPLVPSSQKALLLELKGLQEEPVEGFRVTLVDEGDLYNWEVAIFGPPNTYYEGGYFKARLKFPIDYPYSPPAF
RFLTKMWHPNIYETGDVCISILHPPVDDPQSGELPSERWNPTQNVRTILLSVISLLNEPNTFSPANVDASVMYRK
WKESKGKDREYTDIIRKQVLGTKVDAERDGVKVPTTLAEYCVKTKAPAPDEGSDLFYDDYYEDGEVEEEADSCFG
DDEDDSGTEES

3C

GPSLDFALSLLRRNVRQVQTDQGHFTMLGVRDRLAVLPRHSQPGKTIWIEHKLVNVLDAVELVDEQGVNLELTLI
TLDTNEKFRDITKFIPENISTASDATLVINTEHMPSMFVPVGDVVQYGFLNLSGKPTHRTMMYNFPTKAGQCGGV
VTSVGKVIGIHIGGNGRQGFCAGLKRSYFASEQ

TEV

GHIVWPDYANILKEVFGGARMACVTSAHMAGANGSILKKAEETSRATMHKPVIFGEDYVTEADLPYTPLHLEVNA
EMERMYYLGRRALTHGKRRKVSVNNKRNRRRKVAKTYVGRDSIVEKIVVPHTERKVDTTTAVKDTCNEVSTQLVH
NSMPKRKKQKNFLPATSLSNVYAQTWSIVRKRHMQVEIISKKSVRAKVKRFEGSVQLFASVRHMYGERKRVDLRI
DNWQQKTLLDLAKRFKNERVDQSKLTFGSSGLVLRQGSYAPAHWYRHGMFIVRGRSDGMLVDARAKVTFAVCYSM
THY

ULP1

MSVEVDKHRNTLQYHKKNPYSPLFSPISTYRCYPRVLNNPSESRRSASFSGIYKKRTNTSRFNYLNDRRVLSMEE
SMKDGSDRASKAGFIGGIRETLWNSGKYLWHTFVKNEPRNFDGSEVEASGNSDVESRSSGSRSSDVPYGLRENYS
SDTRKHKFDTSTWALPNKRRRIESEGVGTPSTSPISSLASQKSNCDSDNSITFSRDPFGWNKWKTSAIGSNSENN
TSDQKNSYDRRQYGTAFIRKKKVAKQNINNTKLVSRAQSEEVTYLRQIFNGEYKVPKILKEERERQLKLMDMDKE
KDTGLKKSIIDLTEKIKTILIENNKNRLQTRNENDDDLVFVKEKKISSLERKHKDYLNQKLKFDRSILEFEKDFK
RYNEILNERKKIQEDLKKKKEQLAKKKLVPELNEKDDDQVQKALASRENTQLMNRDNIEITVRDFKTLAPRRWLN
DTIIEFFMKYIEKSTPNTVAFNSFFYTNLSERGYQGVRRWMKRKKTQIDKLDKIFTPINLNQSHWALGIIDLKKK
TIGYVDSLSNGPNAMSFAILTDLQKYVMEESKHTIGEDFDLIHLDCPQQPNGYDCGIYVCMNTLYGSADAPLDFD
YKDAIRMRRFIAHLILTDALK

List of Figures

List of Tables

Acknowledgments

At this point, I would like to express my sincerest gratitude to all those who accompanied and supported me on my way.

To be named first, my supervisor Dr. Sonja Lorenz for her constant scientific support, her patience and her great ideas, for many stimulating discussions about the wide world of the ubiquitin field and for always providing guidance and help.

I am grateful for Prof. Dr. Hermann Schindelin, Prof. Dr. Franz Xaver Schmid and Prof. Dr. Martin Eilers being my committee members and providing valuable suggestions and led me gain from their huge knowledge. I want to emphasize Prof. Schmid for his mentorship and his trust in me since I started to study biochemistry at the University of Bayreuth.

I also thank all current and past members of the Lorenz, Kisker and Schindelin group for creating such welcome working atmosphere, for countless discussions and support. Likewise, I want to point out Dr. Bodo Sander, Dr. Florian Sauer and Dr. Christian Feiler who always shared their enormous wealth of experience and gave invaluable input and helped me with all the troubles.

I want to acknowledge the technical support of Dr. Nikita Popov, Dr. Wenshan Xu and Xenia Popov from CCC Mainfranken, Dr. Kristian Schweimer from the University of Bayreuth and Prof. Dr. Henning Urlaub and Prof. Dr. Andreas Schlosser and their teams for performing mass spec experiments.

I want to thank Kirandeep Deol and Prof. Dr. Eric Strieter for their great collaboration.

I would like to thank for financial support the ‘Fonds der chemischen Industrie’ and the ‘Emmy Noether Foundation’.

Big thanks go to all of my friends and family, especially Basti, who believed in me, when I couldn’t myself, and stood by my side against all odds.

Lastly, my great appreciation goes to my parents for their endless love, encouragement and everlasting support throughout my whole life – especially for the last years. This cannot be sufficiently appreciated.

Publications

Ries, L. K., Sander, B., Deol, K. K., Letzelter, M.-A., Strieter, E. R. and Lorenz, S. (2019). Analysis of Ubiquitin Recognition by the HECT ligase E6AP provides insight into its linkage specificity. *JBC,* 2019 Feb 8. pii: jbc.RA118.007014. doi: 10.1074/jbc.RA118.007014. [Epub ahead of print].

Ries, L. K., Schmid, F. X., Schmidpeter, P. A. (2016). Incorporation of an Unnatural Amino Acid as a Domain-Specific Fluorescence Probe in a Two-Domain Protein. *Biochemistry*. **55**(49): p. 6739-6742.

Schmidpeter, P. A., Ries, L. K., Theer, T., Schmid, F. X. (2015). Long-Range Energetic Changes Triggered by a Proline Switch in the Signal Adapter Protein c-CrkII. *J Mol Biol.* **427**(24): p. 3908-20.

Curriculum vitae

Affidavit

I hereby confirm that my thesis entitled “From recognition to reaction: Mechanistic analysis of the interactions of the HECT ligase E6AP with ubiquitin” is the result of my own work. I did not receive any help or support from commercial consultants. All sources and/or materials are listed and specified in the thesis.

Furthermore, I confirm that this thesis has not yet been submitted as part of another examination process neither in identical nor in similar form.

Place, Date Signature

Eidesstattliche Erklärung

Hiermit erkläre ich an Eides statt, die Dissertation „Von der Erkennung bis zur Reaktion: Mechanistische Analyse der Wechselwirkungen der HECT-Ligase E6AP mit Ubiquitin“ eigenständig, d.h. insbesondere selbstständig und ohne Hilfe eines kommerziellen Promotionsberaters, angefertigt und keine anderen als die von mir angegebenen Quellen und Hilfsmittel verwendet zu haben.

Ich erkläre außerdem, dass die Dissertation weder in gleicher noch in ähnlicher Form bereits in einem anderen Prüfungsverfahren vorgelegen hat.

Ort, Datum Unterschrift